Subthreshold Membrane Resonance in Neocortical Neurons

BRUCE HUTCHEON, ROBERT M. MIURA, AND ERNEST PUIL
Department of Pharmacology and Therapeutics, Faculty of Medicine, Department of Mathematics, and Institute of Applied Mathematics, The University of British Columbia, Vancouver, British Columbia V6T 1Z3, Canada

SUMMARY AND CONCLUSIONS

1. Using whole cell recording techniques, we studied subthreshold and suprathreshold voltage responses to oscillatory current inputs in neurons from the sensorimotor cortex of juvenile rats.

2. Based on firing patterns, neurons were classified as regular spiking (RS), intrinsic bursting (IB), and fast spiking (FS). The subthreshold voltage-current relationships of RS and IB neurons were rectifying whereas FS neurons were almost ohmic near rest.

3. Frequency response curves (FRCs) for neurons were determined by analyzing the frequency content of inputs and outputs. The FRCs of most neurons were voltage dependent at frequencies below, but not above, 20 Hz. Approximately 60% of RS and IB neurons had a membrane resonance at their resting potential. Resonant frequencies were between 0.7 and 2.5 Hz (24–26°C) near −70 mV and usually increased with hyperpolarization and decreased with depolarization. The remaining RS and IB neurons and all FS neurons were nonresonant.

4. Resonant neurons near rest had a selective coupling between oscillatory inputs and firing. These neurons selectively fired action potentials when the frequency of the swept-sine-wave (ZAP) current input was near the resonant frequency. However, when these neurons were depolarized to −60 mV, spike firing was associated with many input frequencies rather than selectively near the resonant frequency.

5. We examined three subthreshold currents that could cause low-frequency resonance: I_H, a slow, hyperpolarization-activated cation current that was blocked by external Cs^+ but not Ba^{2+}; I_{IR}, an instantaneously activating, inwardly rectifying K^+ current that was blocked by both Cs^+ and Ba^{2+}; and I_{NaP}, an quickly activating, inwardly rectifying persistent Na^+ current that was blocked by tetrodotoxin (TTX). Voltage-clamp experiments defined the relative steady state activation ranges of these currents. I_{IR} (activates below −80 mV) and I_{NaP} (activates above −65 mV) are unlikely to interact with each other because their activation ranges never overlap. However, both currents may interact with I_H, which activated variably at potentials between −50 and −90 mV in different neurons.

6. We found that I_H produces subthreshold resonance. Consistent with this, subthreshold resonance was blocked by external Cs^+ but not Ba^{2+} or TTX. Application of Ba^{2+} enlarged FRCs and resonance at potentials below −80 mV, indicating that $I_{K,ir}$ normally attenuates resonance. Application of TTX greatly diminished resonance at potentials more depolarized than −65 mV, indicating that I_{NaP} normally amplifies resonance at these potentials.

7. The ZAP current input may be viewed as a model of oscillatory currents that arise in neocortical neurons during synchronized activity in the brain. We propose that the frequency selectivity endowed on neurons by I_H may contribute to their participation in synchronized firing. The voltage dependence of the frequency-selective coupling between oscillatory inputs and spikes may indicate a novel mechanism for controlling the extent of low-frequency synchronized activity in the neocortex.

INTRODUCTION

During certain states of coherent activity in the central nervous system, synaptic inputs to neurons can be oscillatory rather than transient (Steriade et al. 1993a). However, the responses of single neurons to oscillatory stimuli have received less attention than the responses to transient stimuli, such as current pulses or evoked synaptic volleys. Because coherent brain activity reflects the synchronized activities of neurons at characteristic frequencies, it would be useful for neurons to have mechanisms for tuning their responses to these biologically significant frequencies. In this paper, we ask whether neocortical neurons, held at subthreshold potentials, respond preferentially to oscillatory inputs at specific frequencies. Such preferences, where the voltage responses to injected oscillatory currents are largest in a narrow frequency band (cf. Koch 1984) ("bandpass behavior"), are called membrane resonances. They have been described in cortical (Gimbarzevsky et al. 1984; Gutfreund et al. 1995; Jahnsen and Karnup 1994; Ströhmann et al. 1995), thalamic (Hutcheon et al. 1994; Puil et al. 1994; Ströhmann et al. 1994), spinal (Moore and Christiansen 1985), and peripheral (Correia et al. 1989; Hunt and Wilkinson 1980; Puil et al. 1986, 1988, 1989) neurons. These resonances have disparate mechanisms; however, they always depend on an interaction between the passive properties of membranes and time-dependent ionic currents.

To search for and study subthreshold resonance in neocortical neurons, we applied the techniques of frequency-domain analysis (Puil et al. 1986, 1988). In this paper, we describe low-frequency (1–3 Hz) resonances found in the frequency-response curves (FRCs) of neocortical neurons. We also investigate the ionic basis of resonance, focusing on three noninactivating subthreshold currents that could shape resonant responses: an inwardly rectifying cation current (I_H) (Solomon and Nerbonne 1993a,b; Solomon et al. 1993; Spain et al. 1987); an inwardly rectifying K^+ current (I_{IR}) (Constanti and Galvan 1983; Sutor and Hablitz 1993); and a persistent Na^+ current (I_{NaP}) Alzheimer et al. 1993a,b; Stafstrom et al. 1985). In particular, I_H is of interest because of its involvement in structuring the responses of neocortical neurons to time-varying subthreshold inputs (Schwindt 1992; Solomon and Nerbonne 1993a) and in rhythmic activity of other excitable cells (DiFrancesco et al. 1986; McCormick and Pape 1990).

Finally, we show that the mechanism of resonance affects firing patterns because voltage responses to inputs that are not close to the resonant frequency are attenuated and so do not generate spikes. In a subsequent paper, we use a combination of mathematical modeling and experimentation to show that the observed time and voltage dependence of I_H is sufficient to produce the low-frequency resonance and the effects of resonance on firing patterns.

METHODS

We used rats (Sprague-Dawley) with ages that varied from postnatal day 4 (P4) to P19, although most recordings were made in

neurons from P6 to P14 rats. After decapitation, the brain was removed and submerged in 5–7°C artificial cerebrospinal fluid (ACSF). The brain was cut into blocks before being glued to the stage of a Vibroslicer and cut coronally into 350–400 μm slices. Brain slices containing sensorimotor cortex were incubated for 1–2 h at room temperature before submersion in a Perspex bath (volume 0.3 ml, flow rate 1–1.5 ml/min), which was mounted on the stage of a microscope equipped with Hoffman modulation contrast optics. The slices were thin enough to discern partially the cortical layers that we used as an initial guide for placing the electrode. The recordings were made at room temperature (24–26°C), and all neurons accepted for analysis had overshooting action potentials and resting potentials more negative than −55 mV. At the end of a session, we measured the distance of the recorded neuron from the cortical edge of the slice using a graticule in the eyepiece of the microscope and identified the recording site using the atlas of Paxinos et al. (1991).

Solutions

The ACSF contained (in mM) 124 NaCl, 4 KCl, 1.25 KH_2PO_4, 26 $NaHCO_3$, 10 dextrose, 2 $MgCl_2$, and 2 $CaCl_2$, which gave a measured osmolarity of 310 mosmol. ACSF solutions were maintained at a pH of 7.4 by continuous bubbling with 95% O_2-5% CO_2. Patch-clamp electrodes were pulled from thin-wall borosilicate glass tubing (1.5 mm OD) with a Narashige PP-83 puller and were filled with a solution containing (in mM) 140 K-gluconate, 15 NaCl, 11 ethylene glycol-bis(β-aminoethyl ether)N,N,N',N'-tetraacetic acid, 1 $CaCl_2$, 10 Na-(N-[2-hydroxyethyl]piperazine-N'-[2-ethanesulfonic acid]), 1 Mg adenosine 5'-triphosphate, and 0.3 Na guanosine 5'-triphosphate and was balanced to pH 7.2 with KOH and d-gluconic acid. Initial electrode resistance was 5–8 MΩ; seals to the cells were 1–11 GΩ before breakthrough (cells with seals <1 GΩ were discarded). To compensate for the junction potential formed between the ACSF and the electrode solution, 11 mV was subtracted from all membrane potentials (e.g., a recorded membrane potential of −60 mV corresponds to an actual potential of −71 mV) (see Zhang and Krnjević 1993).

Frequency-domain analysis

The frequency-domain analysis of neurons has been described previously (Puil et al. 1986, 1988). Briefly, a DC current was first used to hold neurons near a desired membrane potential, then a computer generated current waveform (I) was injected into the neurons, and the resulting voltage response (V) was recorded. For each holding potential, an impedance (Z) was calculated from the ratio of the fast Fourier transforms of the voltage response and the current input using the formula

$$Z = \frac{FFT(V)}{FFT(I)}$$

The magnitude of the complex-valued impedance was plotted against frequency to give a FRC. The measurement and analysis systems were calibrated by comparing the measured impedance of a parallel resistor-capacitor circuit with its theoretical impedance.

A proper interpretation of the frequency-domain analysis requires an approximately linear relationship between current inputs and voltage responses. Linearity was maintained during neuronal recordings as long as voltage responses were <20 mV peak-to-peak and action potentials were not evoked. A criterion used to assure approximate linearity was to change the amplitude of the current input while monitoring the FRCs for effects of nonlinearities. Using this criterion, we note that approximate linearity was maintained over larger peak-to-peak voltage responses in neocortical neurons than in thalamocortical neurons (cf. Fig. 1 of Ströhmann et al. 1994).

For the input waveform, we usually used a swept-sine-wave

TABLE 1. *Electrophysiological properties of neocortical neurons*

	RS*	IB	FS
Resting potential, mV	−66 ± 5	−72 ± 5	−66 ± 5
Membrane time constant, ms	47 ± 20	31 ± 10	50 ± 25
Input resistance, MΩ	373 ± 275	218 ± 107	450 ± 255
Number (total = 103)	75	16	12

Values, except Number, are means ± SD. RS, regular spiking; IB, intrinsic bursting; FS, fast spiking. * Firing pattern.

current (ZAP current input) (Puil et al. 1986) of finite duration, T, and with the formula

$$I(t) = a \sin(bt^3), \quad 0 \le t \le T$$

Here, a and b were adjustable parameters controlling, respectively, the amplitude and bandwidth of the input. In other cases, we used a sine wave input or a sum-of-sine-waves (SSW) input consisting of 128 superimposed sine-waves of equal amplitude and systematically varied frequency and phase.

Electrical recordings

To inject DC and oscillatory currents as well as measure voltage responses for frequency-domain analysis, we employed an Axoclamp 2A amplifier that was adjusted optimally in bridge mode to compensate for the electrode resistance and capacitance. For voltage-clamp studies, the same amplifier was used in the continuous single-electrode voltage-clamp mode. For digital data acquisition, a 40-kHz Labmaster A/D-D/A board was controlled with pClamp software or software written specifically for the purpose of acquisition and analysis of frequency-domain data. Voltage and current traces for time-domain recordings were filtered at 10 kHz and then stored on a computer disk or on video tape (Beta) using a PCM encoder (Sony) and a video recorder (Sony).

RESULTS

Electrical properties

The results described in this paper are based on recordings from 147 neurons in layers II–V of sensorimotor cortex. Most did not spontaneously fire action potentials. In cases where electrical recordings were made in control ACSF (103 of 147 neurons), the firing characteristics of neurons were similar to those previously described for juvenile rat neocortex (Kasper et al. 1994a,b; McCormick and Prince 1987). We identified regular spiking (RS), intrinsic bursting (IB), and fast spiking (FS) neurons by the properties of their action potentials and the firing patterns evoked by 1-s current pulses (Connors and Gutnick 1990; McCormick et al. 1985). Regular spiking neurons had broad spikes, prominent medium afterhyperpolarizations (AHPs), small or no fast AHPs, and adapting spike trains. Depolarizing afterpotentials (DAPs) occurred on the falling phase of spikes in 39 of 75 RS neurons. The presence of DAPs often led to the formation of high-frequency spike doublets or triplets at the beginning of a spike train. IB neurons could be recognized by stereotyped bursts of two or more spikes that occurred in an all-or-none fashion at the beginning of the response to a current pulse or reoccurred throughout the pulse. FS neurons had narrow action potentials with a ratio of <2 for the rates of depolarization to repolarization, prominent fast AHPs, and nonadapting spike trains. Table 1 gives some
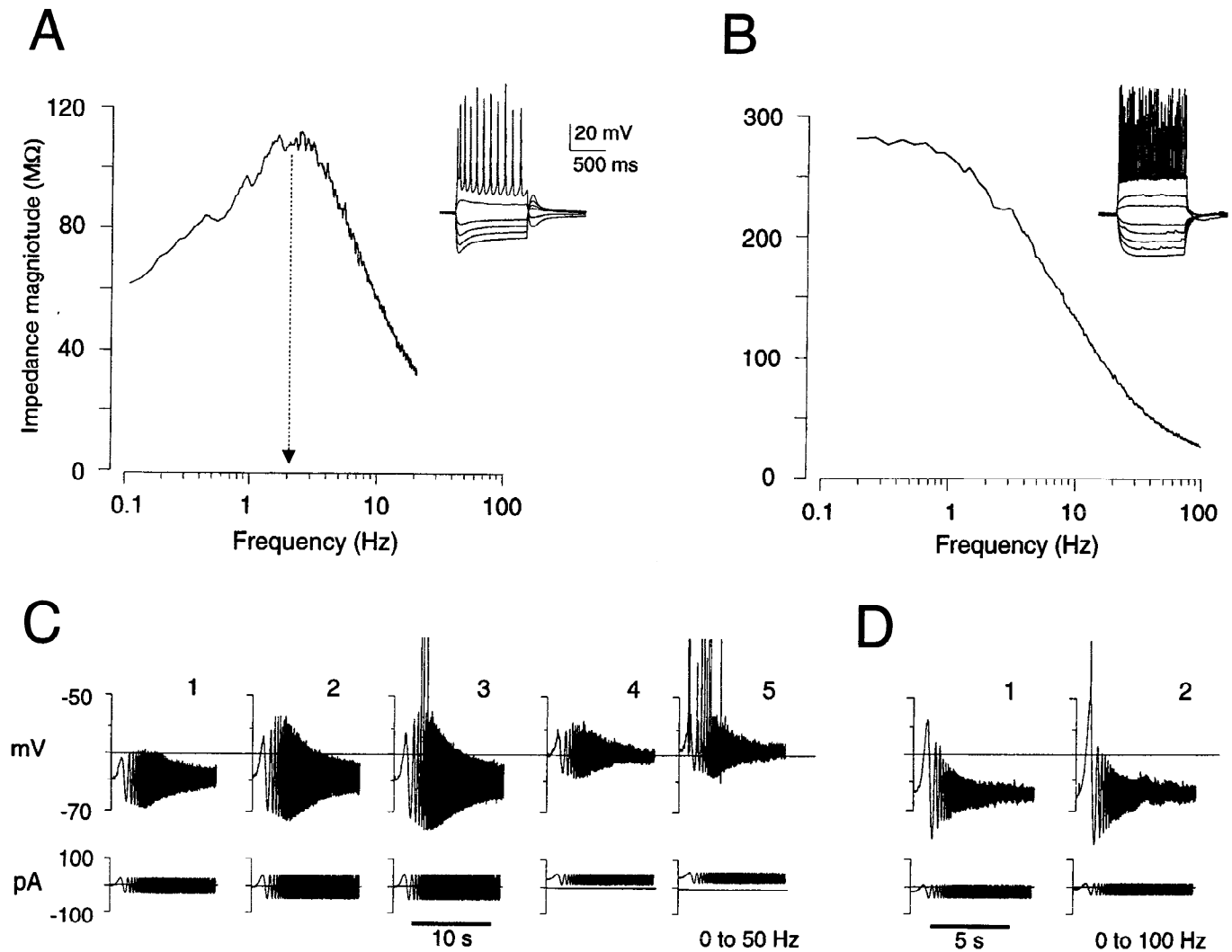
FIG. 1. Frequency- and time-domain responses of resonant and nonresonant neurons. A: in a regular spiking (RS) neuron (resting potential −65 mV), resonance appears as a hump in the frequency-response curve (FRC) with a peak at 2.1 Hz and a Q value (see text) of 1.8. Responses of same neuron to square current pulses are shown (*inset*); note sags and depolarizing rebounds, which are manifestations of resonance in time domain. B: in a fast spiking (FS) neuron (resting potential −67 mV), the FRC declined monotonically from a maximum at lowest frequency recorded. Voltage responses to square pulses do not show sags or rebounds (*inset*). C: swept-sine-wave (ZAP) current inputs (*bottom*) and corresponding voltage responses (*top*) in a resonant neuron demonstrate a voltage-dependent, selective coupling of inputs near resonant frequency and spikes. When neuron was initially held near −65 mV, subthreshold ZAP current inputs of different amplitudes resulted in spindle-shaped voltage responses with the largest part of the response near the resonant frequency ($C1$ and $C2$). When spikes were evoked by a sufficiently large ZAP current input, they were associated with resonant band of frequencies ($C3$). After depolarization (with DC injection) to near −60 mV, the neuron was still resonant ($C4$) but selective coupling had disappeared ($C5$). D: voltage responses of a nonresonant neuron to ZAP current inputs are wedge-shaped rather than spindle-shaped because largest responses were at lowest frequencies. For suprathreshold inputs ($D2$), action potentials arose first in response to lowest frequencies. In this and subsequent figures, action potentials are clipped.

electrophysiological properties of the different types of neurons.

Frequency-response curves

To investigate the frequency preferences of neurons, we determined their FRCs. Figure 1, A and B, shows the FRCs of RS and FS neurons near their respective resting potentials. The responses of the same neurons to current pulses are shown in the upper right of each figure. In these neurons, as in all neurons we studied, the smallest impedance magnitudes occurred at high frequencies. There were important

differences, however, in the low-frequency behavior of the FRCs in different neurons.

RESONANT NEURONS. Some neurons were resonant near their resting potentials. For the neuron of Fig. 1A, the FRC had a resonant hump that peaked near 2 Hz. In the same neuron, there were no other resonant peaks in the interval 2–500 Hz. Similarly, we could not resolve multiple humps in the FRCs of other neurons.

We quantified the resonance of a neuron by measuring its resonant frequency (f_{res}) and "Q value." The f_{res} of a neuron is defined as the frequency at the peak of the resonant hump in the FRC. The Q value is constructed by dividing the

TABLE 2.   *Resonant frequencies (f_{res}) and Q values for resonant neocortical neurons*

	RS	IB	FS
n^*	25/41	7/11	0/7
f_{res}, Hz	1.3 ± 0.4	1.3 ± 0.5	
Q	1.4 ± 0.3	1.3 ± 0.3	

Measured at -70 mV and 24–26°C, values given as proportion or means ± SD. For abbreviations, see Table 1. * Proportion of neurons with resonance.

magnitude of the impedance at f_{res} by the magnitude at the lowest recorded frequency (Koch 1984). The f_{res} of the neuron illustrated in Fig. 1A is 2.1 Hz. Its Q value, 1.8, was one of the largest we recorded. Table 2 gives the incidence of resonance and the values of f_{res} and Q at -70 mV in 59 neurons of different firing types. Approximately two-thirds of RS and IB neurons were resonant at -70 mV. All f_{res} values were between 0.7 and 2.5 Hz and most were between 1 and 2 Hz. There were no significant differences between RS and IB neurons with respect to their resonant properties at this membrane potential (2-tail t-tests). The total incidence of resonance among RS and IB neurons is underestimated in Table 2 because some neurons that were nonresonant at -70 mV were resonant at other potentials.

NONRESONANT NEURONS.   All of the FS neurons and some of the RS and IB neurons did not have resonant humps in their FRCs at the potentials we usually investigated (potentials more negative than -55 mV). We call the neurons that did not have resonant humps at these potentials "nonresonant"; however, we recognize that they may have had resonance at other potentials. Figure 1B shows a typical FRC for a nonresonant FS neuron together with its responses to current pulses. The value of the impedance magnitude decreased monotonically with frequency, resulting in an FRC with characteristics of a low-pass filter. Thus the Q value of the nonresonant FS neuron of Fig. 1B is equal to 1, as is the case for all nonresonant neurons.

Resonance does not depend on the input waveform

The relationship between small amplitude current inputs and voltage responses was almost linear in most neurons. This was evident in the FRCs that essentially were unchanged by increasing or decreasing the amplitude of the ZAP current input when the membrane potential was more negative than -60 mV. In resonant neurons, when this potential was not exceeded, changes in the magnitude of the input affected f_{res} weakly and left the Q value unaltered. Figure 2 shows, for a resonant neuron, the FRCs generated near -70 mV by SSW and ZAP inputs with similar frequency bands. The FRCs were nearly identical although the time courses, but not the frequency compositions, of the inputs were very different. We conclude the subthreshold resonance in the neurons we investigated is independent of the form of the input.

Coupling of oscillatory inputs to the firing of action potentials

The differences between resonant and nonresonant neurons were reflected in the time courses of their responses to

ZAP inputs. In the resonant RS neuron depicted in Fig. 1C, note the peak in its voltage response to a constant amplitude ZAP input (Fig. 1C, 1 and 2). Because of the systematic order in which the ZAP input sweeps through the frequencies, it is easy to see that this peak occurs at intermediate frequencies. This gives it a spindle shape that is characteristic of resonant neurons. In fact, the largest response was near f_{res}. In contrast, the voltage response of the nonresonant neuron in Fig. 1D1 is wedge-shaped because the largest response occurred at the lowest frequencies.

In both resonant and nonresonant neurons, large-amplitude ZAP stimuli evoked action potentials. However, there was a clear difference between resonant and nonresonant neurons in the stimulus frequencies that most readily evoked firing. In resonant neurons, action potentials were generated preferentially when the input frequencies were near f_{res} (e.g., Fig. 1C3). In nonresonant neurons, on the other hand, firing was associated with the lowest frequencies of the input (Fig. 1D2). This difference between resonant and nonresonant neurons was observed consistently. All resonant neurons tested with large-amplitude inputs fired action potentials as the input passed through the resonant band of frequencies ($n = 4$). In five of six nonresonant neurons, the spikes arose at the lowest injected frequencies. In summary, the frequency preference of resonant neurons resulted in a preferential coupling between inputs at frequencies near f_{res} and firing.

The selective coupling does not imply that action potentials will fire at the same frequency as an oscillatory input delivered near the resonant frequency. In trials using single-frequency sine-waves, we found that action potentials sometimes fired on every other cycle or in some more complicated pattern (cf. Fig. 1C5).

Selective coupling of oscillatory inputs with firing did not occur at all membrane potentials. Firing near the resonant frequency often was observed near -70 mV. When resonant neurons were depolarized above approximately -60 mV by DC current, firing occurred at all frequencies below 10 Hz (Fig. 1C5). The neurons, however, were still resonant at this potential (Fig. 1C4). Thus the ability of resonance to mediate coupling between oscillatory inputs and the firing of action potentials was voltage dependent.

Voltage dependence of frequency response curves

The FRCs of most neurons were voltage dependent over a 20-mV range near the resting potential. Figures 3 and 4 show the FRCs at different membrane potentials in two RS neurons treated with 300 nM tetrodotoxin (TTX). In the neuron of Fig. 3A, we used DC current injection to displace the membrane potential to values between -90 and -50 mV. The neuron was clearly resonant between -90 and -65 mV. As shown in Fig. 3B, the f_{res} and Q values were also voltage dependent. The value of f_{res} increases steadily from a minimum of 1.9 Hz at -65 mV to a maximum of 3.6 Hz at -90 mV. The Q values are near 1 at -60 mV or more depolarized potentials, increase to 1.5 by -77 mV and remain near 1.5 at more hyperpolarized potentials. The amplitudes of the FRCs in Fig. 3A also change with membrane potential. The largest impedance magnitudes are associated with the FRC taken at -72 mV (also see Fig. 3C). At more hyperpolarized or depolarized potentials, the FRCs have smaller peak values. The decreased amplitude of the FRCs
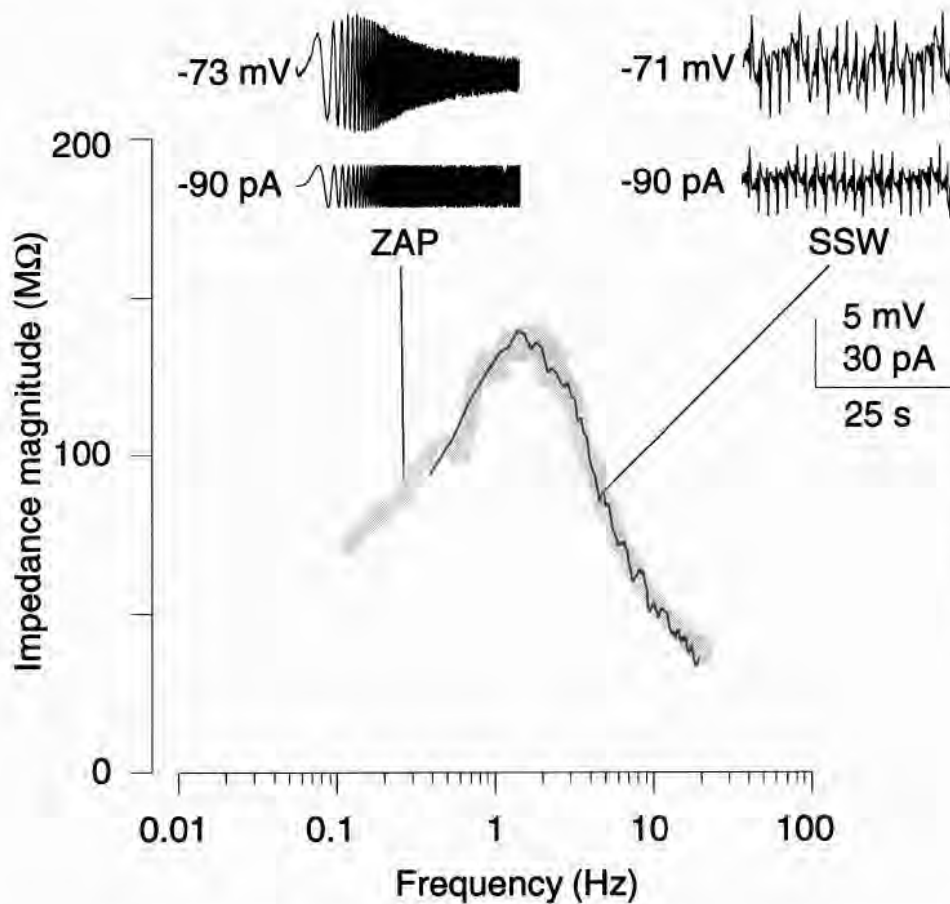
FIG. 2. Frequency and magnitude of subthreshold resonance is independent of time course of input current. FRC derived by the ZAP method (gray shading) is compared with the FRC derived from a sum-of-sine waves (SSW, black line) input consisting of 128 sine-waves with systematically varied phase and equal amplitude. Although bandwidth of SSW input was narrower than that of ZAP input, features of FRC do not change. Time-domain traces for inputs and their voltage responses also are shown (*right inset;* voltage responses shown *top*). Note that time scale indicated for ZAP response (25 s) is different for SSW response (5.2 s).

above −60 mV in Fig. 3*A* and in Figs. 4*A* and 10*A* may reflect the action of a depolarization-activated current, but this was not investigated. Above 10 Hz, the FRCs approached an asymptotic curve determined by the membrane time constant (dealt with in the companion paper).

The above description illustrates a pattern commonly seen in resonant neurons treated with TTX, that is, the value of f_{res} increases with hyperpolarization, the Q value is greater at hyperpolarized than at depolarized potentials, the largest impedance values lie between −65 and −75 mV, and the FRCs are independent of voltage at high frequencies. The last two points were also characteristic of the FRCs of nonresonant neurons treated with TTX. For example, as seen in Fig. 4, the FRCs at low frequencies were highly dependent on voltage with the largest amplitude FRC occurring between −65 and −75 mV and smaller amplitude FRCs at more depolarized and hyperpolarized voltages. In contrast, all FRCs were similar at high frequencies.

Subthreshold rectification in RS neurons

The voltage dependence of the FRCs in resonant and nonresonant neurons implies that the responses of these neurons to oscillatory inputs are shaped by voltage-dependent subthreshold currents. This also is suggested by the mechanisms of resonances found in neocortical and other neurons (Gutfreund et al. 1995; Hutcheon et al. 1994; Mauro et al. 1970). To characterize the currents that could be involved in the generation and modification of resonance in neocortical neu-

rons, we investigated their subthreshold rectifying properties.

We regularly encountered three forms of steady state, subthreshold rectification. These were identified tentatively as due to three noninactivating, voltage-dependent currents; I_H, I_{IR}, and I_{NaP} (see INTRODUCTION). Both I_H and I_{IR} activate with hyperpolarization whereas I_{NaP} activates on depolarization from rest. In the following sections, we describe the properties of these currents and, in particular, characterize their voltage dependencies and time courses so that they may be compared to the frequency-domain characteristics of RS neurons described above.

RECTIFICATIONS ACTIVATED BY HYPERPOLARIZATION.   *Current-clamp studies.* Figure 5 shows firing patterns and current-voltage (*I-V*) relations for RS (Fig. 5*A*), IB (Fig. 5*B*), and FS (Fig. 5*C*) neurons. Most *I-V* relations for RS and IB neurons showed a tendency to curve upward as the membrane was hyperpolarized from rest. This was not a prominent feature for FS neurons.

Current-clamp recordings from RS and IB neurons exhibited two hyperpolarization-activated rectifications that were distinguished on the basis of their voltage dependence, time course, and pharmacology. On hyperpolarization beyond −80 mV, some neurons showed a quickly developing rectification that decreased their input resistances (evident as decreased voltage responses to equally spaced current steps, see Fig. 6*A*) and shortened their membrane time constants (dotted line, Fig. 6*A*). This can result from the actions of
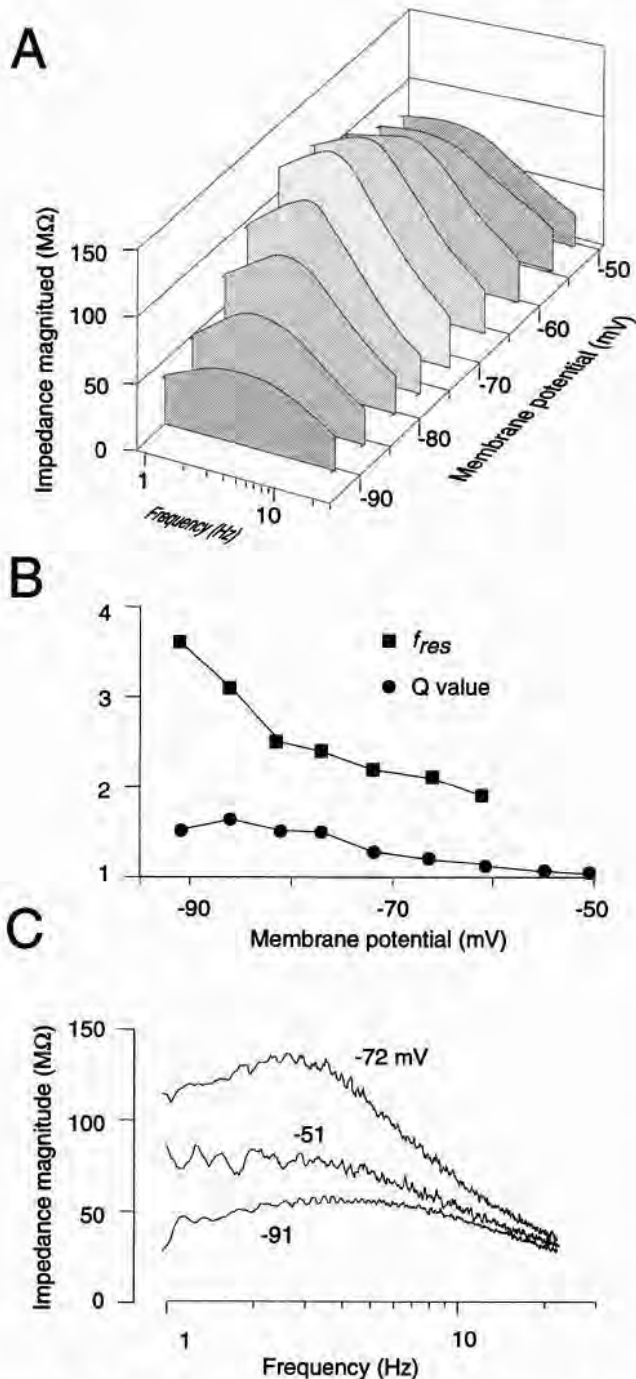
These effects of Ba^{2+} often were accompanied by a small depolarization of the resting potential (Fig. 9A) and are consistent with the blockade of I_{IR}.

Some neurons possessed a slowly developing rectification that was evident as sagging voltage responses to hyperpolarizing current pulses (Fig. 6, B and C1). Overshooting rebounds followed the sags on termination of the hyperpolarizing pulses. The sags and rebounds are the time-domain manifestations of resonance. This is seen by putting a waveform consisting of a single square pulse through a digital filter the properties of which are determined by the FRC of a resonant neuron. The output waveform from the filter had the same types of sags and rebounds as seen in the neuronal responses to square pulses (Fig. 8). When the same input was put through a filter based on a nonresonant FRC, the output has no sags or rebounds (not shown).

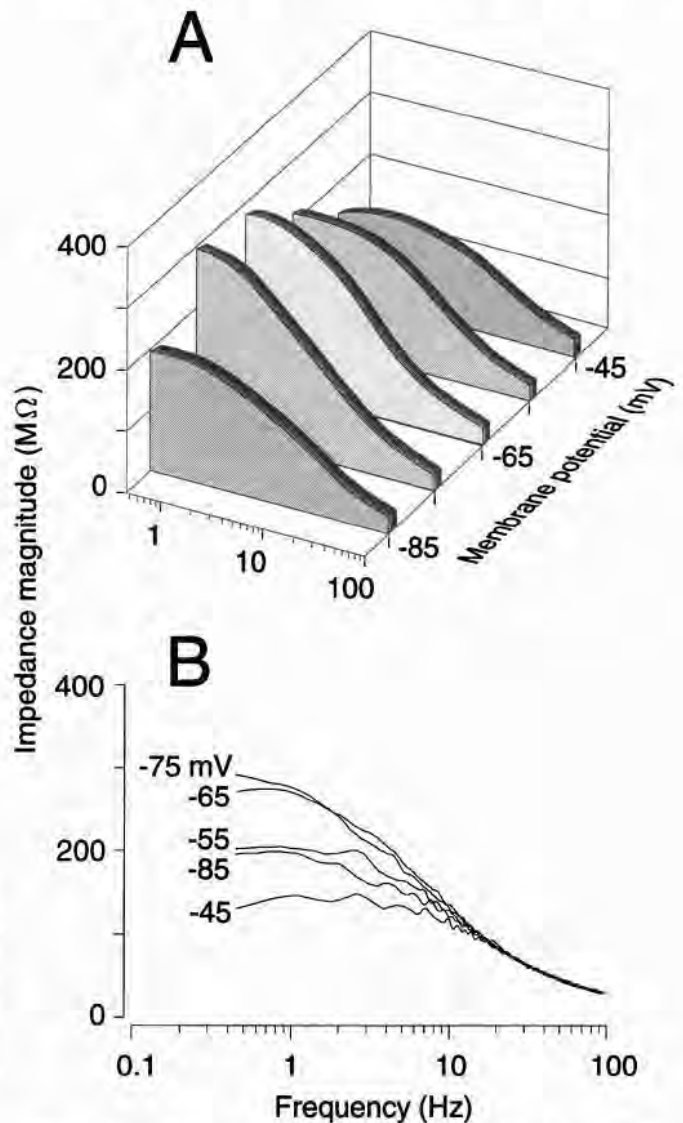The amplitudes of the rebounds after a 1-s hyperpolariza-

FIG. 3. Voltage dependence of FRCs of a resonant RS neuron [in presence of 300 nM tetrodotoxin (TTX), initial resting potential of −72 mV]. A: three-dimensional plot reveals overall relationship between FRCs and membrane voltage. FRCs shown here and in subsequent 3-dimensional plots are curves fitted by eye to data. B: values of Q and resonant frequency (f_{res}) are shown for same neuron as in A. Increase of f_{res} with hyperpolarization is typical of subthreshold resonances described in this paper. C: three of FRCs from A are superimposed on same axis. Holding potentials for each FRC are shown. Each curve is result of a 5-point moving average performed 3 times on data.

I_{IR}. External application of 0.2–3 mM Ba^{2+} ($n = 4$), a blocker of I_{IR} (Sutor and Hablitz 1993), increased the membrane time constant and greatly increased the apparent input resistance, especially in the hyperpolarizing direction (Fig. 7A, 1 and 2; note the different current command steps).

FIG. 4. Voltage dependence of FRC of a nonresonant RS neuron (in presence of 300 nM TTX). A: three-dimensional plot reveals overall relationship between FRCs and membrane voltage. B: same FRCs as in A, presented as a 2-dimensional plot of smoothed data. Note that voltage dependence is small at frequencies >20 Hz. Note shallow hump in FRC at −45 mV.
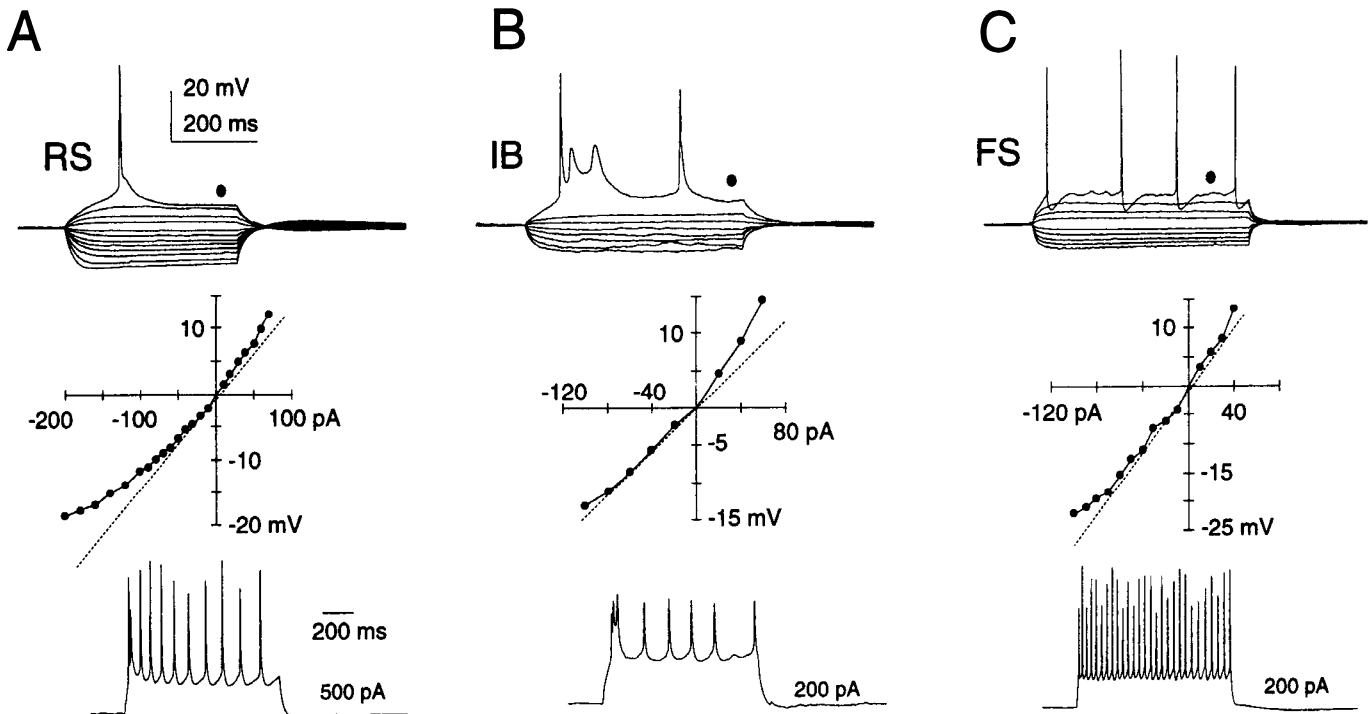
FIG. 5. Firing patterns and *I-V* relations for RS, intrinsic bursting (IB), and FS neurons (*A-C*). For each part of figure, responses of neurons to square current pulses are shown at *top* and *bottom* and *I-V* relation generated by these pulses in *middle*. Measurements for *I-V*s were taken at times indicated (■, *top*). At bottom, responses to large depolarizing current pulses (amplitudes shown to *right*) are shown on a different time scale to illustrate firing patterns. Note that both RS and IB neurons have an initial high-frequency burst of action potentials. Burst arises in an all-or-none fashion in IB but not RS neurons (compare the just-suprathreshold responses at top).

tion were correlated to the magnitudes and durations of the preceding sags (e.g., Figs. 6*C*). This is shown in Fig. 6*D*, which displays the relationship between sags and rebounds in 19 consecutively recorded RS neurons. The correlation depended on the holding potential. When neurons were held near −70 mV, the amplitudes of the sags and rebounds were correlated positively ($r^2 = 0.93$, Fig. 6*D1*), implying that the sags and rebounds rely on the same current, e.g., I_H. When neurons were held near −60 mV, on the other hand, the amplitudes of the rebounds had only a slight dependence on the magnitudes of the preceding sags ($r^2 = 0.47$, Fig. 6*D2*). Also, the firing of action potentials during rebounds after the termination of hyperpolarizing pulses was facilitated at −60 mV even though the sags were smaller than those evoked at −70 mV. Thus at −60 mV, the mechanisms underlying sags and rebounds appear to differ. This dissociation between sags and rebounds at −60 mV is reminiscent of the dissociation between resonance and frequency-preferential firing at the same potentials and could be due to the activation of currents other than I_H at potentials near −60 mV.

Application of external 0.5 mM Ba^{2+} did not reduce the sags or rebounds ($n = 5$, Fig. 7*A*). However, application of 3 mM external Cs^+ (a blocker of both I_{IR} and I_H) (Constanti and Galvan 1983; Foehring and Waters 1991; Spain et al. 1987) by itself or together with Ba^{2+} eliminated sags and reduced rebounds by >80% in seven of eight neurons (e.g., Fig. 7*A3*). This implies that I_H is the major current underlying the slow rectification.

We explored the possibility of a current other than I_H contributing to the rebounds. Rebounds often were blocked incompletely by Cs^+ whereas sags were eliminated totally. This may reflect a partial or voltage-dependent blockade of I_H by Cs^+ or may implicate other currents in the formation of rebounds. The latter possibility is highlighted in the case of four neurons where large rebounds occurred in the absence of sags during the preceding hyperpolarization. In two of these neurons, external application of 0.5 mM Ni^{2+} reduced the rebounds by 65% (Fig. 7*B*, *1-3*). In one of the neurons where Ni^{2+} reduced the rebounds, Cs^+ completely blocked the rebounds after small hyperpolarizations but failed to block rebounds after hyperpolarizations beyond −75 mV (Fig. 7*B*, *3* and *4*). These observations point to the involvement of a low-threshold Ca^{2+} current in some rebounds. We could not determine whether such a current plays a role in rebounds after sags because application of Ni^{2+} to four neurons with sags produced variable results.

Sags in the voltage responses to small hyperpolarizing currents were observed over a wide range of potentials. In some neurons, the sags were evoked by small hyperpolarizations from potentials ranging from threshold to −90 mV. In other neurons, sagging responses were seen only at potentials more negative that −80 mV. The thresholds at which sags could be evoked often appeared to drift to more negative values over the course of an experiment. In contrast, the membrane potential where fast rectification was first detected was consistently between −75 and −85 mV in most neurons and did not change over the course of an experiment. The fast and slow rectifications often coexisted in RS and IB neurons. However, FS neurons seldom had slow sags and rebounds (2 of 12 FS neurons), and, when present, they occurred at very negative potentials (e.g., below −90 mV).
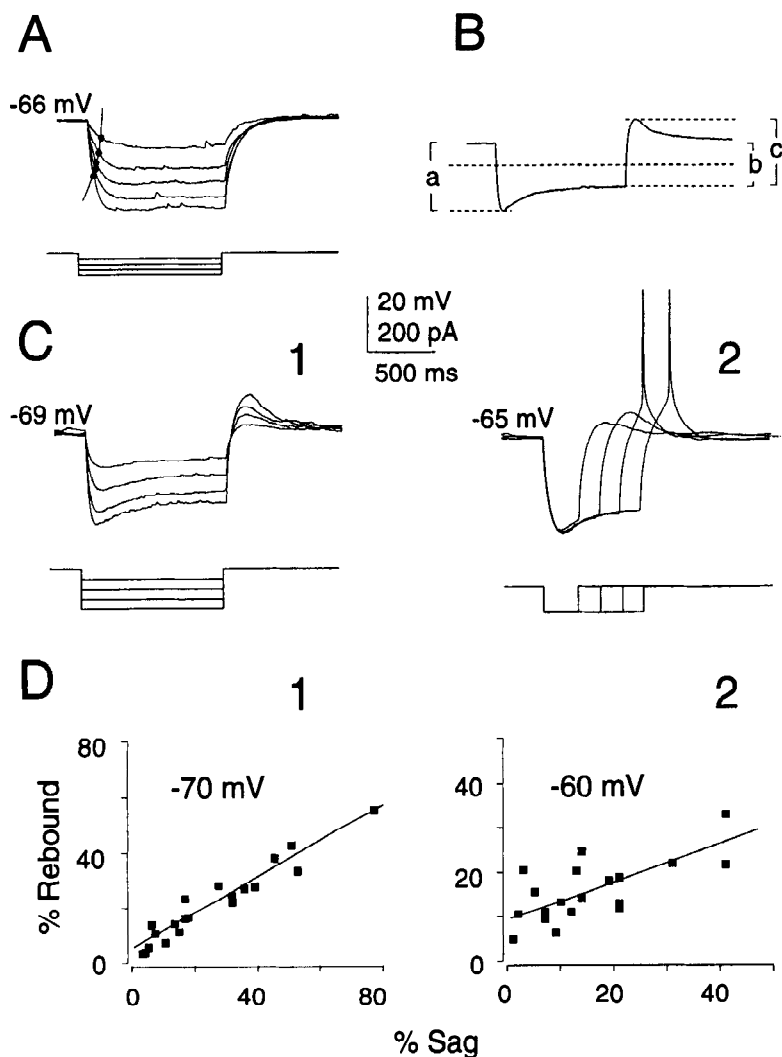
FIG. 6. Consequences of fast and slow rectification in neocortical neurons. *A*: in a nonresonant RS neuron, a fast hyperpolarization-activated inward current decreased apparent input resistance and membrane time constant during hyperpolarizing pulses. Time taken for each voltage response to fall to $1/e$ of its initial value (apparent time constant) is indicated ($\cdot$ – $\cdot$). *B*: quantification of sags and rebounds in resonant neurons. Lowercase letters: percent sag was defined as $100(1 - b/a)$ and percent rebound as $100(1 - c/a)$. *C, 1* and *2*: sags and rebounds in a resonant RS neuron depend on magnitude (*C1*) and duration (*C2*) of hyperpolarizing input. In *C2*, sufficiently large rebounds evoked spikes. Neurons in *A–C* were initially at their resting potentials. *D*: relationship between percent sags and rebounds at -70 (*D1*) and -60 mV (*D2*). Pooled data for 19 resonant and nonresonant neurons. When neurons were held near -70 mV, there was a high correlation between sags and rebounds but at -60 mV correlation was weaker. Linear regression lines are shown with the data.

In six of nine neurons tested, I_H contributed to the resting potential because 3 mM Cs$^+$ reversibly hyperpolarized the membrane potential [-3.1 ± 1.9 mV, (mean $\pm$ SD) range: 2–12 mV). In two of the remaining neurons, Cs$^+$ had no effect on the resting potential and, in a single neuron, evoked a 1.5-mV depolarization.

RECTIFICATIONS ACTIVATED BY HYPERPOLARIZATION. *Voltage-clamp studies.* We voltage clamped neurons to examine the currents underlying their fast and slow hyperpolarization-activated rectifications. When the membrane potential was held near -60 mV and then stepped to more hyperpolarized values (Fig. 9*A1*), the total evoked inward current could be resolved into a transient component due to the capacitance (arrow, Fig. 9*A2*), a quickly activating component, and a slowly activating component identified with I_H (Fig. 9*A2*). The slowly activating inward current was isolated during data analysis by fitting the total current with a sum of exponential terms and ignoring the components in the fit corresponding to the instantaneous and capacitive currents (Scroggs et al. 1994). The resulting fits of I_H (with a time constant, τ_H, as long as 4 s at -80 mV) are shown superimposed on the data in Fig. 9*A1*. Figure 9*B* (○) shows the voltage-current (*V-I*) relation of the slowly activating component (I_H) for the same neuron as Fig. 9*A*.

The quickly activating current derived from the fit of the total inward current is composed of a leak current, proportional to the magnitude of the applied voltage step, and an inwardly rectifying current. The fast activation and voltage dependence (*V-I* relation in Fig. 9*B*, filled symbols) of the rectifying current is consistent with the properties of an inwardly rectifying K$^+$ current that has been described in cortical neurons (Constanti and Galvan 1983; Sutor and Hablitz 1993; Womble and Moises 1993).

Application of 0.2–3 mM Ba^{2+} greatly reduced the rectifying component of the instantaneous current without blocking the slower components of the total inward current ($n = 2$). External application of 2 mM Cs$^+$ or its coapplication with Ba^{2+} resulted in the complete blockade of both hyperpolarization-activated rectifying currents ($n = 7$). These results confirm the identities of I_{IR} and I_H as the currents that underlie the fast and slow rectifications, respectively, and show that Ba^{2+} can be used in these neurons to block I_{IR} without blocking I_H.

The activation point of a current was defined as the first membrane potential where the current was >5 pA. A comparison of the *V-I* relations of I_H and I_{IR} in Fig. 9*B* shows that they are simultaneously active at membrane potentials more negative than -85 mV. This appears to be the only
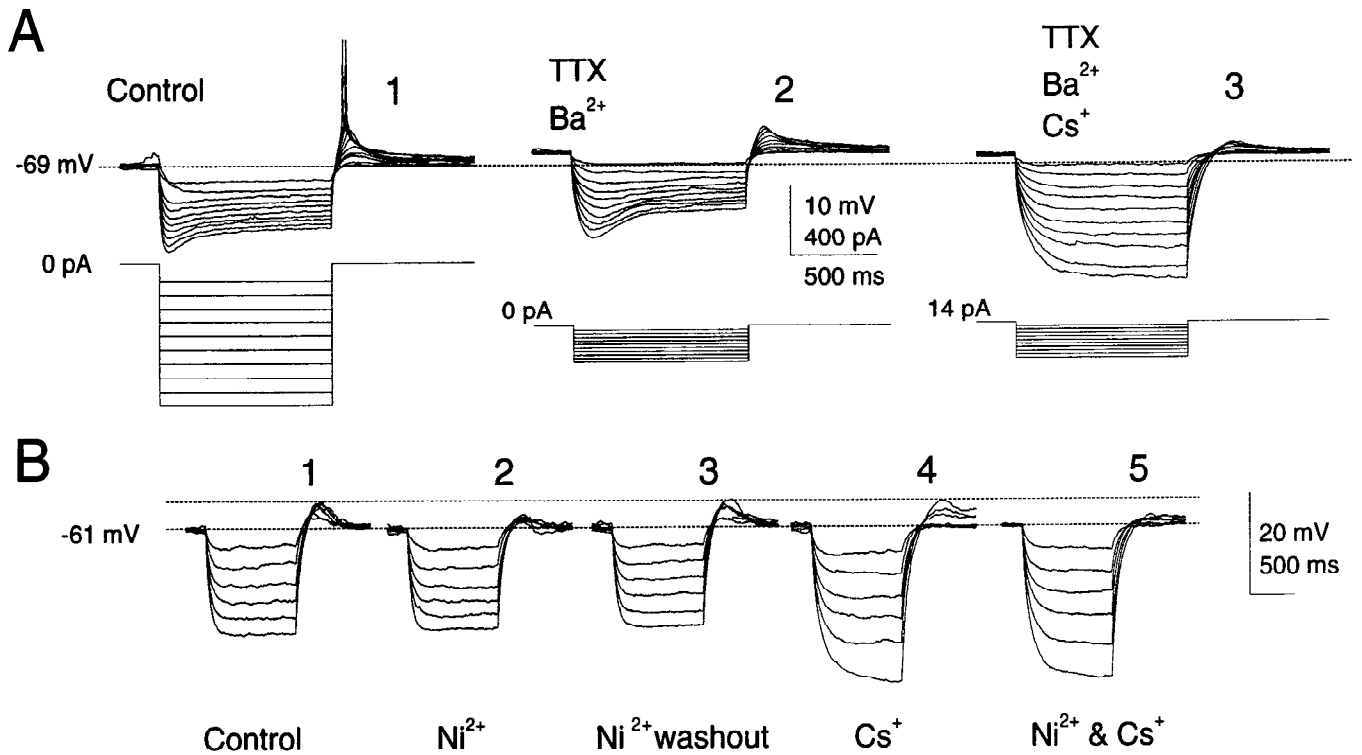
FIG. 7. Pharmacological blockade of voltage sags and overshooting rebounds evoked by hyperpolarizations in 2 RS neurons (A and B). A, 1 and 2: application of Ba^{2+} (0.5 mM, 2 min) increased input resistance but did not reduce sags or rebounds (note change in amplitude of current commands between A, 1 and 2). Small depolarization due to Ba^{2+} application is consistent with a block of a leak current. This also was observed in other neurons (mean depolarization = 1.3 ± 0.8 mV, $n = 4$). Action potentials were eliminated with 300 nM TTX. $A3$: additional application of 3 mM Cs^+ to same neuron eliminated sags and greatly reduced rebounds. Note that Cs^+ application hyperpolarized resting potential such that 14 pA of current were needed to hold neuron near same potential as in $A2$. B: a neuron where substantial rebounds were not preceded by sags ($B1$). Rebounds were 70% reduced by external application of 500 μM Ni^{2+} ($B2$) suggesting an involvement of a Ca^{2+} current in rebounds. In same neuron, Cs^+ blocked rebounds following small hyperpolarizations and increased duration of rebounds following large hyperpolarizations and ($B4$). Combination of Ni^{2+} and Cs^+ reduced rebounds by >90% ($B5$).

region along the voltage axis where they can interact in this neuron. We measured the activation points of I_H and I_{IR} in 27 RS neurons and assessed the possible regions of interaction of these currents. Figure 10 shows the activation points of I_H and I_{IR} in these neurons. The values for I_H (-73.4 ± 10.1 mV) were more depolarized and more variable than those for I_{IR} (-81.6 ± 3.3 mV). Thus because both currents are activated by hyperpolarization, the activation point of I_{IR}
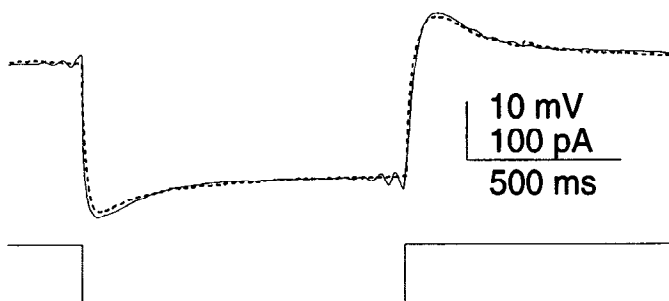

FIG. 8. Measured and reconstructed voltage responses of a RS neuron. A square current pulse (bottom, ———) caused a hyperpolarizing response (top, - - -) with a prominent sag and rebound. Same current pulse then was run through a digital filter constructed using resonant FRC of same neuron (together with simultaneously measured data on frequency-dependent phase changes). Reconstructed response (top, ———) fits response recorded from neuron. Wavelets appear at onset and offset of reconstructed response because FRC was measured over a narrower bandwidth than actual bandwidth of neuron.
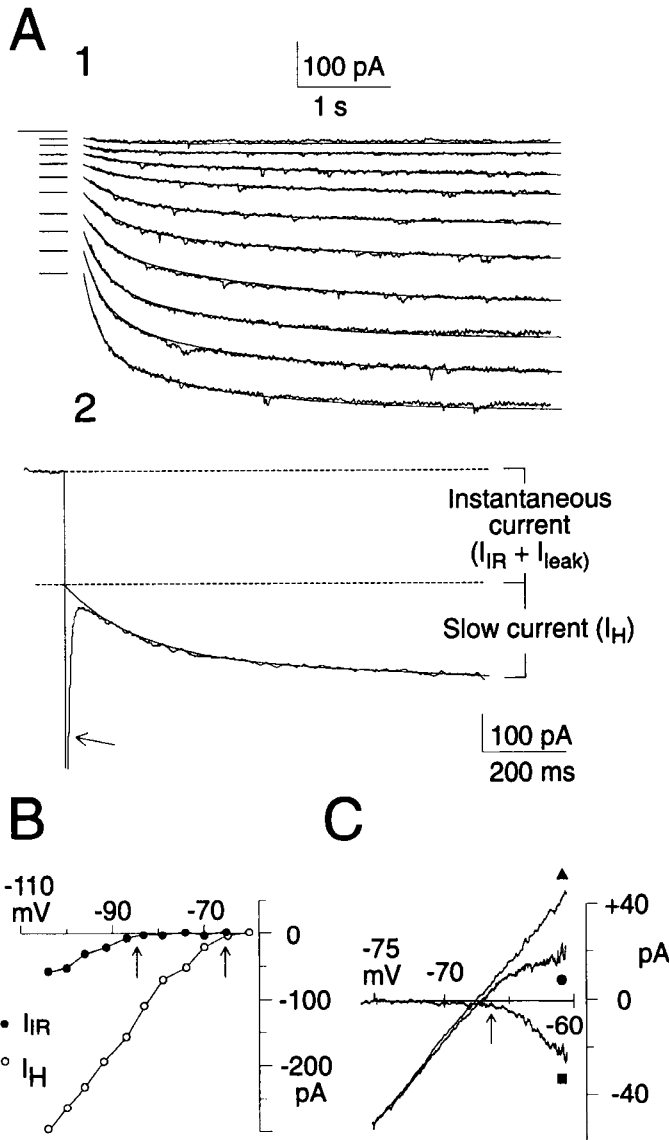
determines the range of interaction of I_H and I_{IR} in most neurons.

Rectification activated by depolarization

Most neurons were outwardly or inwardly rectifying (Fig. 5) between the resting membrane potential and the threshold for action potentials (generally near -55 mV). We voltage clamped neurons and used slowly ascending (10 mV/s) voltage ramps to acquire quasi-steady state V-I curves. The same procedure was repeated after application of 10–300 nM TTX. Subtracting the trace recorded in TTX from the control trace revealed a steady state inward current that activated with depolarization (Fig. 9C). Because of its voltage dependence, lack of inactivation, and blockade by TTX this inward current is likely the persistent Na^+ current, I_{NaP} (Alzheimer et al. 1993a,b; Stafstrom et al. 1985). In nine RS neurons, the activation points of I_{NaP} ranged between -68 and -56 mV. In Fig. 10, the mean value for the I_{NaP} activation points (-61.4 ± 4.1 mV) is indicated by a dashed horizontal line and the standard deviation by a gray region. Comparing the I_{NaP} activation range and the location of the I_H activation points shows that I_{NaP} and I_H are likely to interact in some RS neurons. In support of this, we found that TTX reduced the size of rebounds by 12–26% ($n = 5$). The separation between the distributions for the activation points of I_{NaP} and I_{IR} (Fig. 10) indicates that they will not interact.

slow time course of its activation kinetics are consistent with a possible role in generating low-frequency resonance.

In nonresonant neurons at membrane potentials more negative than -75 mV, Ba^{2+} application increased the amplitudes of FRCs and eliminated their low-frequency voltage dependence ($n = 2$, Fig. 11, cf. Fig 4A). Most of the increase in the FRCs occurred at frequencies <20 Hz (Fig. 4, A and B). At other potentials, Ba^{2+} either slightly increased the amplitudes of the FRCs or left them unaltered (the decreased FRC at -65 mV in Fig. 11A is anomalous). The effect of Ba^{2+} is therefore to enlarge FRCs over the same voltage range that it blocks I_{IR}. On this basis, we conclude that I_{IR} normally acts like a high-pass filter by attenuating the FRCs of neurons at frequencies <20 Hz.

This was confirmed in resonant neurons where Ba^{2+} application increased the amplitudes of the FRCs at low frequencies, enlarged their resonant humps, and shifted f_{res} to lower values ($n = 5$, Fig. 12). Application of Cs^+, together with Ba^{2+}, further increased the amplitudes of FRCs and either shifted their resonant peaks to very low frequencies or abolished resonance ($n = 3$, Fig. 12). This was similar to the effect of Cs^+ alone, which abolished resonance and increased the amplitudes of FRCs over a broad range of subthreshold potentials ($n = 4$). Like Ba^{2+}, the effects of Cs^+ were most evident at low frequencies (<10 Hz). Unlike Ba^{2+}, Cs^+ increased the impedance magnitudes of FRCs to a greater extent at frequencies below f_{res} than above it. During the application of Cs^+ the FRCs thus adopted the form of low-pass filters.

These results point to I_H as the mechanism of subthreshold resonance in these neurons. The action of I_H is to attenuate the responses of neurons at low frequencies that, in combination with the high-frequency attenuation of responses by the neuronal capacitance, forms a resonant peak in the FRC.

At membrane potentials more depolarized than -65 mV, I_{NaP} also affected the FRCs. In nonresonant and resonant neurons under control conditions, the amplitudes of the
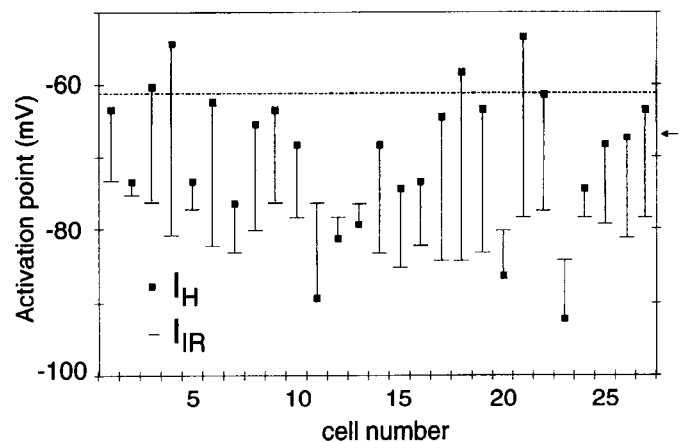
FIG. 9.   Hyperpolarization-evoked inward currents in a voltage-clamped RS neuron. $A1$: hyperpolarizing voltage steps from -60 mV in 5-mV increments evoked inward currents. Smooth lines though the data represent I_H as determined by exponential fits to total current (see text). Short horizontal lines on left indicate the instantaneous component of total current. Longer horizontal line on left indicates holding current before voltage steps. $A2$: details of first second of total current evoked by most negative voltage step in $A1$. Total current consists of a component proportional to capacitance of the neuron (truncated, ←), an instantaneously activated current, and a slow component due to I_H. Instantaneous component has an ohmic part due to I_{leak} and a rectifying part due to I_{IR}. B: steady state V-I plot generated for neuron in A. Contributions of I_H (○) and I_{IR} (●) are plotted separately, ignoring the contribution of leak current. Activation point for each current, defined as membrane potential where current first becomes >5 pA, is indicated (↑). C: in a different neuron, a slowly ascending voltage ramp was used to obtain a quasi-steady state V-I plot (●), which displays inward rectification between -67 and -60 mV. Application of 300 nM TTX abolished the inward rectification (▲). Subtracting TTX trace from control trace gives voltage dependence of persistent Na^+ current (I_{NaP}). An arrow indicates activation point for I_{NaP}.

Effect of ionic blockers on FRCs

Because I_{IR} and I_{NaP} rarely activate near rest (Fig. 10), they are unlikely to account for the resonances we observed there. On the other hand, the voltage range of I_H and the

FIG. 10.   Activation points for I_H, I_{NaP}, and I_{IR}. Activation points of I_H and I_{IR} are plotted for 27 RS neurons. Each solid vertical line indicates, for a single neuron, gap between the activation point of I_H (■) and that of I_{IR} (short horizontal line). Note that I_H usually activates at more depolarized voltages than I_{IR} and that dispersion of activation points for I_H is greater than that for I_{IR}. A horizontal dashed line shows mean activation point for I_{NaP}, determined in 9 additional neurons and the gray area is ±1 SD. In most cases, I_H turns on at potentials that are too hyperpolarized to provide a steady state interaction with I_{NaP}. Arrowhead on right indicates mean resting potential for RS neurons.
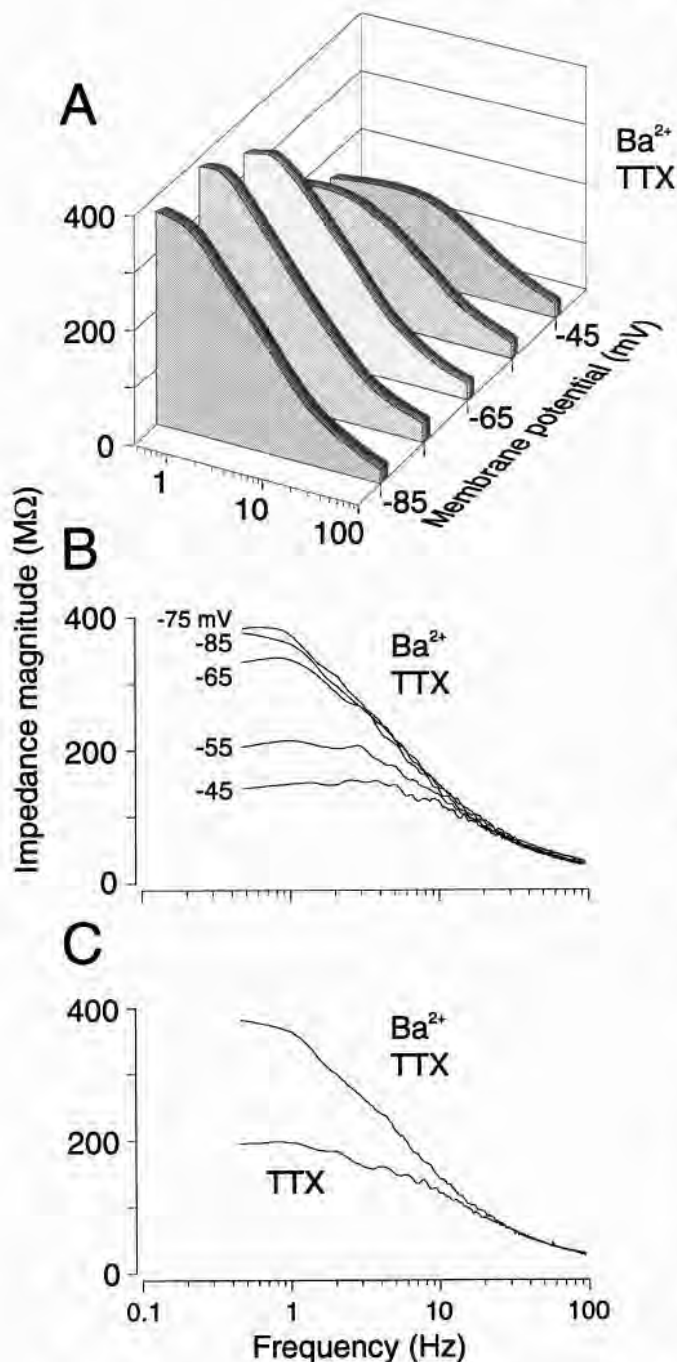
of TTX eliminated the voltage-dependent increase in the FRCs (Fig. 13*B*) and also resulted in smoother FRC plots ($n = 10$). In resonant neurons, TTX reduced the size of the hump in the FRC but did not eliminate resonance (Fig. 13*B*). These results imply that I_{NaP} is a low-frequency amplifier of FRCs and resonance, active when the membrane potential is near threshold.

DISCUSSION

The main findings of this investigation are that RS and IB, but not FS, neocortical neurons possess a subthreshold resonance at low frequencies. A hyperpolarization-activated cation current (I_H) produces this resonance, which mediates a selective coupling of oscillatory current inputs near the resonant frequency to the consequent firing of action potentials. The membrane resonance appears as a hump, with a nonzero peak frequency, in the frequency-response curve of neurons. When a swept-sine-wave ZAP current of constant amplitude is used as an input, resonance appears as a bulge in the oscillatory voltage response that is largest near the resonant frequency. The tuning of the neuronal frequency response by resonance has physiological significance if the ZAP input is viewed as a model of oscillatory currents that enter the soma from the dendrites during states of rhythmic synchronized activity in the brain.

ZAP method

The ZAP method is an organized approach to the study of the interactions of the passive and active electrical properties of neurons when they are stimulated by oscillatory currents (see METHODS). The ZAP current input repeatedly
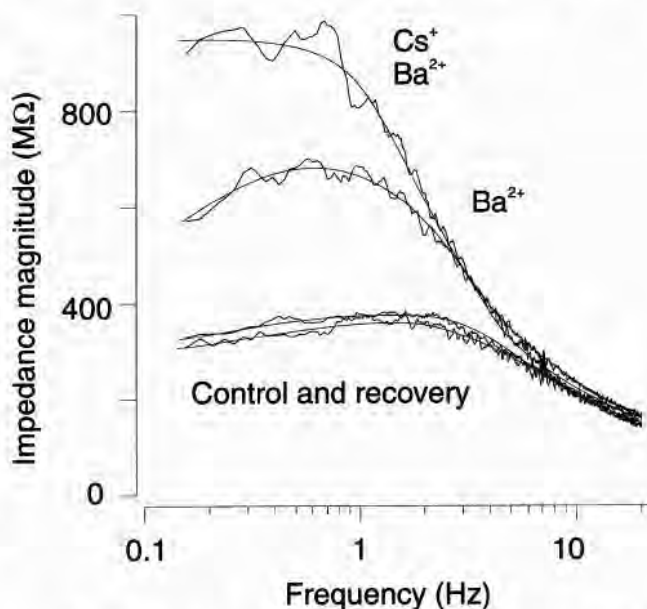
FIG. 11. Effects of external Ba^{2+} application on FRCs of a neuron with no resonance and no I_H (same neuron as in Fig. 4). All FRCs were measured in the presence of 300 nM TTX. *A*: application of Ba^{2+} (200 μM), a blocker of I_{IR}, results in high amplitude FRCs at potentials below -65 mV (cf. Fig. 4*A*). At these potentials FRCs are almost voltage independent. *B*: smoothed FRCs for same neuron as in *A* but replotted in a 2-dimensional format. Membrane potentials for each FRC is shown (*left*). *C*: comparison of FRCs at -85 mV (in presence of 300 nM TTX) before and after Ba^{2+} (control trace redrawn from Fig. 4*B*).

FRCs increased twofold or more as the membrane potential was depolarized from rest to near threshold. This voltage-dependent amplification of the FRCs was confined to frequencies <10 Hz. In resonant neurons, the amplification included a large increase in the Q value of the resonance did not have a large effect on f_{res} (Fig. 13*A*). Application

FIG. 12. Effects of ionic blockers on resonance in presence of 300 nM TTX. Under control conditions, FRC measured near -80 mV showed a broad resonant hump. Application of Ba^{2+} (200 μM, 3.5 min) increased amplitude of FRC and Q value of its resonant hump and decreased resonant frequency (*middle*). Additional application of Cs^+ (12 min later) greatly increased FRC amplitude and eliminated resonant hump. Washout of Cs^+ and Ba^{2+} shows that their effects were completely reversible. Smooth lines through data are fitted by eye.
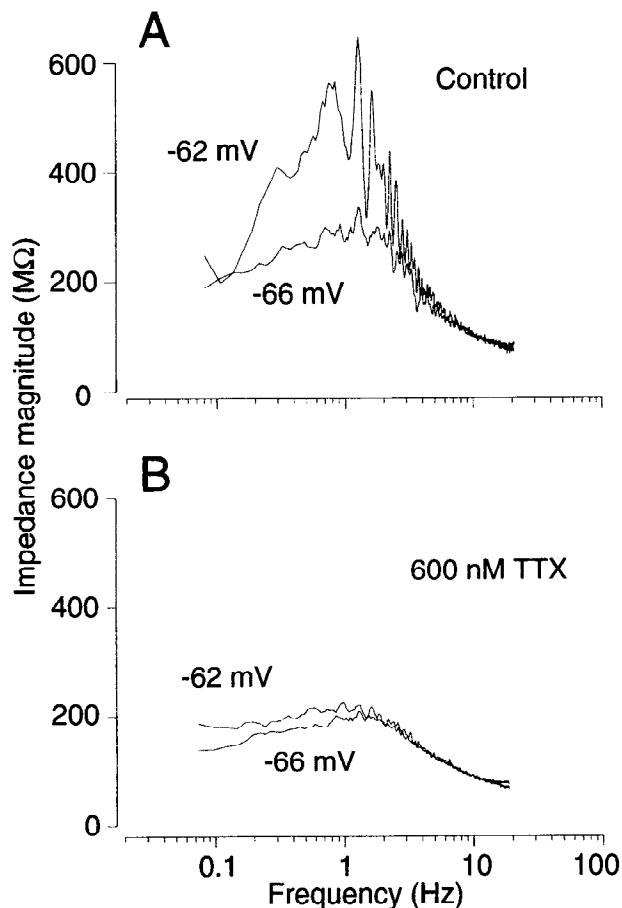
FIG. 13. Effects of TTX on resonance. A: in control artificial cerebrospinal fluid, FRCs of most neurons were larger between −65 and −55 mV than at more hyperpolarized potentials. In resonant RS neuron shown here, there was a substantial difference in FRC amplitudes and Q value of resonance, between −66 and −62 mV. B: application of 600 nM TTX (for 3.5 min) reduced FRC and Q value, but did not eliminate resonance. Resonant frequency, f_{res}, is approximately same before and after TTX.

charges and discharges the membrane and alters various ionic currents, thereby shaping the voltage output. In this paper, we used the ZAP method in two ways. First, we carried out a linear frequency analysis (see METHODS) to find the FRCs of neurons. This gave a frequency-domain description of the relationship between inputs and subthreshold voltage outputs and allowed us to quantify the resonance. The use of the ZAP input was convenient, but not essential, for this purpose because many other input waveforms could have been used with equal success in principle (e.g., sum of sine-waves, see Fig. 2, or white noise). However, the ZAP input has distinctive attributes when used for the study of nonlinear neuronal responses to oscillatory stimuli. Because the ZAP current is oscillatory, with monotonically increasing (or decreasing) frequency, its frequency distribution is evident in the time domain. Thus the input frequency associated with a feature of interest can be identified by its position within the response. An example is the bulge that indicates the resonant frequency in the voltage response to a ZAP current input (see Fig. 1C). We made use of this attribute to identify those frequencies that most readily evoked spikes as the amplitude of the ZAP current was increased. This would not be possible using white noise or sum-of-sine-wave inputs. The ability to combine a quantita-

tive frequency analysis with a simple qualitative assessment of nonlinear frequency selectivity is thus a distinctive attribute of the ZAP method.

Mechanism of I_H-dependent resonance

The resonance described in this paper likely is due to the hyperpolarization activated cation current, I_H. Many points of similarity between resonant neurons and neurons with I_H suggest this possibility: 1) resonance and I_H were both evident at subthreshold membrane potentials and had similar voltage dependencies. Moreover, when the activation point of I_H was outside its usual range (between −65 and −75 mV), the voltage dependence of resonance was shifted in the same direction; 2) neurons that did not have an I_H were nonresonant—an observation also made by Ströhmann et al. (1995) who used the ZAP method to investigate neurons of field L, the avian equivalent of the mammalian auditory neocortex; 3) in resonant neurons, Cs^+, but not Ba^{2+}, blocked both I_H and resonance; and 4) the slow time course of I_H activation was consistent with the resonant frequencies. These observations show that I_H is necessary for the subthreshold resonance. However, it is not clear from our experiments whether I_H is the only current required for the appearance of a resonant hump in the FRC.

To understand how I_H endows neurons with resonance, consider the consequences of I_H activation within a neuron. During a hyperpolarization, I_H slowly activates and contributes an inward current that partially counteracts the hyperpolarization. The opposite happens during a depolarization—I_H deactivates slowly and partially counteracts the depolarization. The net effect of I_H, therefore, is to resist voltage changes. For square-wave inputs, this produces the sags and rebounds. For oscillating inputs, I_H attempts to attenuate voltage responses when the input frequency is sufficiently low that the slow activation and deactivation processes of I_H can keep up. At slightly higher input frequencies, the kinetics of I_H are overwhelmed, relieving the attenuation. Finally, at still higher frequencies, the capacitive properties of the neuronal membrane again attenuate the responses. Thus the resonant hump is shaped by the attenuations at low frequencies due to I_H and at high frequencies due to the capacitance.

Control and modulation of resonance

The FRCs of resonant and nonresonant neurons were voltage dependent. For resonant neurons, both the resonant frequencies and the Q values of the FRCs changed with membrane potential. This suggests that a simple way of controlling the frequency response of resonant neocortical neurons is to change the resting membrane potential—possibly by the release of modulatory transmitters (McCormick et al. 1993). However, the subthreshold voltage dependence of resonant and nonresonant FRCs in this study extended only from 0 to ~20 Hz. Above 20 Hz, the FRCs of most neurons were almost voltage independent even though many neurons had strongly curved I-V relations at these potentials. This reflects the fact that conventional steady state I-V relations are related only to the DC components of FRCs (i.e., at 0 frequency). The functional implication of this finding is that the processing of low-frequency and not high-frequency

rhythmic inputs by neocortical neurons is susceptible to neuromodulation via control of the resting membrane potential.

Two voltage-dependent currents other than I_H affected the FRCs of neurons at potentials below -55 mV. According to our findings, these currents play opposite roles in shaping subthreshold responses to oscillatory stimuli. One of these currents, I_{NaP}, increases FRCs at potentials more positive than -65 mV. In contrast, I_{IR} reduces the amplitude of FRCs at potentials more negative than -80 mV. Both currents can coexist with I_H and either amplify (I_{NaP}) or attenuate (I_{IR}) resonance.

The physiological consequences of these interactions are unclear. On the one hand, I_{IR} attenuates FRCs at voltages outside the physiological range for the generation of action potentials. On the other hand, we observed a weak coupling between resonance and firing over much of the activation range of I_{NaP} (i.e., at potentials more depolarized than -60 mV, see Fig. 1B). Thus there may be only a narrow range of potentials between -65 and -60 mV where the amplification of resonance due to I_{NaP} might have a functional consequence. It is possible that, at potentials more positive than -60 mV, I_{NaP} has other functions such as the control of firing rate (Reyes and Fetz 1993; Stafstrom et al. 1984a,b). Note, that the magnitude and voltage range of the interaction between I_H and I_{NaP} may be different in vivo because they are subject to second messenger modulation (Ca^{2+}, Schwindt et al. 1992; adenosine 3',5'-cyclic monophosphate, Banks et al. 1993; Pape and Mager 1992).

Resonance mediates a frequency-selective coupling of inputs and firing

Resonant neurons had a selective coupling of frequency components of the current input to the firing of action potentials. This coupling was demonstrated for the case of ZAP current inputs when neurons fired most readily as the input was swept past the resonant frequency. A simple mechanism involving resonance near a firing threshold can account for these observations. Figure 14 demonstrates this schematically by comparing an idealized voltage response to a ZAP current input with the voltage threshold for the firing of action potentials (horizontal dashed line). Firing is expected where the response exceeds the threshold, as indicated (●). In this way, the spikes are associated with frequencies of the input near the resonant frequency, i.e., where the subthreshold response was largest. Inputs at other frequencies, in contrast, are attenuated relative to the resonant frequency and so less likely to result in spiking. Although this mechanism is highly simplified, it accounts for the elements of the coupling as can be seen by comparison with the voltage responses of a real neuron to ZAP current input (Fig. 14B).

It is necessary to emphasize that the occurrence of spikes due to the above mechanism not only depends on the frequency content but also on the amplitude and phase of each frequency component of the input. For instance, it is possible to drive the response corresponding to any frequency component of the input above threshold if the input is large enough. Thus as the amplitude of the ZAP current input increases, the spikes appear over a wider region (see Fig. 14B) because the amplitudes of some of the nonresonant frequencies in the input become large enough to evoke spikes. The notion of a selective coupling of input frequency components to

spikes best describes the situation when a resonant neuron responds to sinusoidal inputs with comparable amplitude, each at a different frequency.

A significant finding is that this coupling was voltage dependent. Resonant neurons held at potentials between -80 and -65 mV could be induced to fire preferentially in response to inputs near their resonant frequency. This was not the case, however, when the same neurons were held near -60 mV—despite the persistence of resonance at these potentials. The disruption of the frequency-selective coupling between inputs and firing may be due to currents other than I_H that activate near -60 mV. This is consistent with our finding that sags and rebounds were poorly correlated near -60 mV. On the other hand, the simple explanation proposed above to account for the frequency-selective coupling also may be sufficient to account for its voltage dependence. This is because the currents required to drive neurons past threshold from -60 mV may be too small to generate significant differences in the voltage responses to different frequencies (compare Fig. 1C, 2 and 4).

Whatever the mechanism, the voltage dependence of the coupling suggests the existence of two firing modes in neocortical neurons: a hyperpolarized mode in which the neuron is able to sense and respond selectively to synchronized, convergent inputs with frequencies in the neuron's resonant band and a more depolarized mode in which the firing does not couple preferentially to low-frequency inputs. Because many neuromodulators affect conductances that change the resting potential of neocortical neurons (McCormick et al. 1993), these firing modes could form a basis for the voltage-dependent modulation of low-frequency coherent activity by coupling and uncoupling I_H-generated resonance to spike production in the neocortex.

Comparison with other frequency-domain studies

Other studies also have found low-frequency resonances in central neurons. These include an I_H-resonance with resonant frequencies between 6 and 10 Hz (at 30°C) in neurons from the auditory thalamus of chicks (Ströhmann et al. 1994) and a 2–4 Hz (34°C) resonance generated by a low-threshold Ca^{2+} current in neurons from the mediodorsal thalamus of guinea pigs (Hutcheon et al. 1994; Puil et al. 1994).

Jahnsen and Karnup (1994) have plotted power spectra for guinea pig central neurons stimulated with white noise and found putative resonances in several areas of the CNS. One resonance, in hippocampal CA1 neurons, is probably due to I_H. Consistent with an I_H mechanism, the resonance is voltage dependent, blocked by Cs^+, and associated with sags and rebounds in the voltage responses to current pulses. The resonant frequency in these neurons was near 12 Hz (see Fig. 6F in Jahnsen and Karnup 1994), which is higher than the resonant frequencies reported here. This may reflect species- or tissue-specific differences in the properties of I_H but is more likely a result of the higher temperatures (35°C rather than 24–26°C) used in their experiments (Hutcheon et al. 1996). In neocortical neurons from the same study, Jahnsen and Karnup (1994) did not find a low-frequency resonance such as found here. However, the sample rates and bandwidths used to estimate the spectra do not allow good resolution of the 1- to 2-Hz band. It is unclear whether a narrow spike at 24 Hz in the spectra of spontaneously
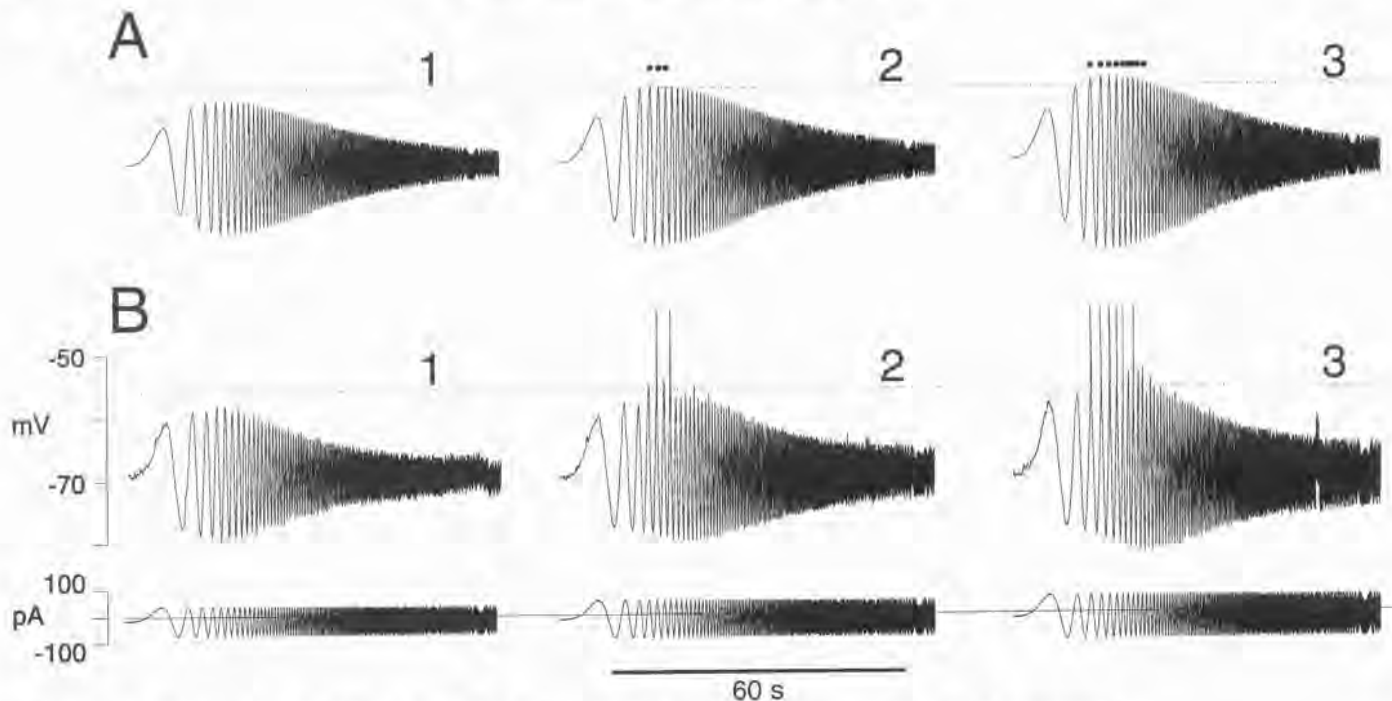
FIG. 14.   Possible mechanism for selective coupling between firing and near-resonant frequencies in input. *A*: combination of resonance and a threshold for firing (horizontal dotted line) implies selective coupling. This is shown for idealized responses to ZAP current inputs. In *A1*, subthreshold voltage responses are largest near resonant frequency. When a sufficiently large input is used, spikes appear where response exceeds threshold, near resonance (*A2*, ●). This mechanism also implies that frequency band over which input couples to spikes widens as ZAP input amplitude increases (*A3*, ●). *B*: relationship between firing threshold (· · ·) and voltage responses (*top*) to oscillatory ZAP current inputs (*bottom*) in an actual neuron is consistent with proposed mechanism.

oscillatory neocortical neurons (Fig. 10*B* in Jahnsen and Karnup 1994) is a resonance because it could be due to spontaneous activity rather than a response to stimulation.

Gutfreund et al. (1995) have identified a subthreshold resonance with a resonant frequency between 3 and 15 Hz (34°C) underlying spontaneous oscillations of the membrane potential in neurons of guinea pig frontal cortex. This resonance is prominent from −65 to −40 mV and has a resonant frequency that increases with depolarization, making it unlikely that it is due to an I_H mechanism. We occasionally observed a similar low-frequency resonance at depolarized potentials in rat cortical neurons. In Fig. 4*A*, for instance, the FRC shows a shallow resonant hump at −45 mV with a peak near 3 Hz. However, we did not systematically examine neurons for resonance at membrane potentials positive to −50 mV.

Physiological relevance

The resonance generated by I_H endows neurons with an enhanced sensitivity to oscillatory inputs near the resonant frequency. The physiological relevance of this enhancement may be seen when the oscillatory ZAP input is considered as a simplified model of the oscillatory current inputs that the soma of a neuron receives from the dendrites during coordinated rhythmic activity in the brain. Intracellular in vivo recordings from cortical neurons of anesthetized rat or cat, or cerveau isolé preparation, can show almost sinusoidal, low-frequency oscillations of the voltage caused by rhythmic sequences of synaptic inputs at characteristic frequencies (e.g., Cowan and Wilson 1994; Metherate and Ashe 1993; Steriade et al.

1993b,c). These oscillations are the cellular correlates of large-amplitude rhythmic patterns of the electroencephalogram reflecting the synchronous activity of large numbers of central neurons. Thus during some behavioral states, neurons are presented with inputs signaling the presence of synchronized activity at biologically important frequencies in brain circuits. Under these circumstances, resonance could contribute to the propagation and frequency-stabilization of synchronized firing. The use of the ZAP method to assess the frequency dependence of coupling between oscillatory inputs and action potentials therefore can be viewed as an investigation of mechanisms that might allow neurons to enter into patterns of coordinated activity in the cortex.

The resonance we have described here and its coupling to firing patterns leads us to speculate that I_H may play a role in coordinating rhythmic activity in the forebrain. Such a mechanism apparently would be limited to excitatory neurons because the putative inhibitory neurons we encountered (FS neurons) did not have resonance.

REFERENCES

ALZHEIMER, C., SCHWINDT, P. C., AND CRILL, W. E. Modal gating of Na$^+$ channels as a mechanism of persistent Na$^+$ current in pyramidal neurons from rat and cat sensorimotor cortex. *J. Neurosci.* 13: 660–673, 1993a.

ALZHEIMER, C., SCHWINDT, P. C., AND CRILL, W. E. Postnatal development of a persistent Na$^+$ current in pyramidal neurons from rat sensorimotor cortex. *J. Neurophysiol.* 69: 290–292, 1993b.

BANKS, M. I., PEARCE, R. A., AND SMITH, P. H. Hyperpolarization-activated cation current (I$_h$) in neurons of the medial nucleus of the trapezoid body: voltage-clamp analysis and enhancement by norepinephrine and cAMP suggest a modulatory mechanism in the auditory brain stem. *J. Neurophysiol.* 70: 1420–1432, 1993.

CONNORS, B. W. AND GUTNICK, M. J. Intrinsic firing patterns of diverse neocortical neurons. *Trends Neurosci.* 13: 99–104, 1990.

CONSTANTI, A. AND GALVAN, M. Fast-inward rectifying current accounts for anomalous rectification in olfactory cortex neurones. *J. Physiol. Lond.* 335: 153–178, 1983.

CORREIA, M. J., CHRISTENSEN, B. N., MOORE, L. E., AND LAND, D. G. Studies of solitary semicircular canal hair cells in the adult pigeon. I. Frequency- and time-domain analysis of active and passive membrane properties. *J. Neurophysiol.* 62: 924–934, 1989.

COWAN, R. L. AND WILSON, C. J. Spontaneous firing patterns and axonal projections of single corticostriatal neurons in the rat medial agranular cortex. *J. Neurophysiol.* 71: 17–32, 1994.

DIFRANCESCO, D., FERRONI, A., MAZZANTI, M., AND TROMBA, C. Properties of the hyperpolarizing-activated current (I$_f$) in cells isolated from the rabbit sinoatrial node. *J. Physiol. Lond.* 377: 61–88, 1986.

FOEHRING, R. C., LORENZON, N. M., HERRON, P., AND WILSON, C. J. Correlation of physiologically and morphologically identified neuronal types in human association cortex in vitro. *J. Neurophysiol.* 66: 1825–1837, 1991.

FOEHRING, R. C. AND WATERS, R. S. Contributions of low-threshold calcium current and anomalous rectifier (I$_h$) to slow depolarizations underlying burst firing in human neocortical neurons in vitro. *Neurosci. Lett.* 124: 17–21, 1991.

GIMBARZEVSKY, B., MIURA, R. M., AND PUIL, E. Impedance profiles of peripheral and central neurons. *Can. J. Physiol. Pharmacol.* 62: 460–462, 1984.

GUTFREUND, Y., YAROM, Y., AND SEGEV, I. Subthreshold oscillations and resonant frequency in guinea-pig cortical neurons: physiology and modelling. *J. Physiol. Lond.* 483: 621–640, 1995.

HUNT, C. C. AND WILKINSON, R. S. An analysis of receptor potential and tension of isolated cat muscle spindles in response to sinusoidal stretch. *J. Physiol. Lond.* 302: 241–262, 1980.

HUTCHEON, B., MIURA, R. M., AND PUIL, E. Models of subthreshold membrane resonance in neocortical neurons. *J. Neurophysiol.* 76: 698–714, 1996.

HUTCHEON, B., MIURA, R. M., YAROM, Y., AND PUIL, E. Low-threshold calcium current and resonance in thalamic neurons: a model of frequency preference. *J. Neurophysiol.* 71: 583–594, 1994.

JAHNSEN, H. AND KARNUP, S. A spectral analysis of the integration of artificial synaptic potentials in mammalian central neurons. *Brain Res.* 666: 9–20, 1994.

KASPER, E. M., LARKMAN, A. U., LUBKE, J., AND BLAKEMORE, C. Pyramidal neurons in layer 5 of the rat visual cortex. II. Development of electrophysiological properties. *J. Comp. Neurol.* 339: 475–494, 1994a.

KASPER, E. M., LUBKE, J., LARKMAN, A. U., AND BLAKEMORE, C. Pyramidal neurons in layer 5 of the rat visual cortex. III. Differential maturation of axon targeting, dendritic morphology, and electrophysiological properties. *J. Comp. Neurol.* 339: 495–518, 1994b.

KOCH, C. Cable theory in neurons with active, linearized membranes. *Biol. Cybern.* 50: 15–33, 1984.

MAURO, A., CONTI, F., DODGE, F., AND SCHOR, R. Subthreshold behavior and phenomenological impedance of the squid giant axon. *J. Gen. Physiol.* 55: 497–523, 1970.

MCCORMICK, D. A., CONNORS, B. W., LIGHTHALL, J. W., AND PRINCE, D. A. Comparative electrophysiology of pyramidal and sparsely spiny stellate neurons of the neocortex. *J. Neurophysiol.* 54: 782–806, 1985.

MCCORMICK, D. A. AND PAPE, H. C. Properties of a hyperpolarization-activated cation current and its role in rhythmic oscillation in thalamic relay neurones. *J. Physiol. Lond.* 431: 291–318, 1990.

MCCORMICK, D. A. AND PRINCE, D. A. Post-natal development of electrophysiological properties of rat cerebral cortical pyramidal neurones. *J. Physiol. Lond.* 393: 743–762, 1987.

MCCORMICK, D. A., WANG, Z., AND HUGUENARD, J. Neurotransmitter control of neocortical neuronal activity and excitability. *Cereb. Cortex* 3: 387–398, 1993.

METHERATE, R. AND ASHE, J. H. Ionic flux contributions to neocortical slow waves and nucleus basalis-mediated activation: whole-cell recordings in vivo. *J. Neurosci.* 13: 5312–5323, 1993.

MOORE, L. E. AND CHRISTENSEN, B. N. White noise analysis of cable properties of neuroblastoma cells and lamprey central neurons. *J. Neurophysiol.* 53: 636–651, 1985.

PAPE, H. C. AND MAGER, R. Nitric oxide controls oscillatory activity in thalamocortical neurons. *Neuron* 9: 441–448, 1992.

PAXINOS, G., TÖRK, I., TECOTT, L. H., AND VALENTINO, K. L. *Atlas of the Developing Rat Brain.* San Diego: Academic Press, 1991.

PUIL, E., GIMBARZEVSKY, B., AND MIURA, R. M. Quantification of membrane properties of trigeminal root ganglion neurons in guinea pigs. *J. Neurophysiol.* 55: 995–1016, 1986.

PUIL, E., GIMBARZEVSKY, B., AND SPIGELMAN, I. Primary involvement of K$^+$ conductances in membrane resonance of trigeminal root ganglion neurons. *J. Neurophysiol.* 59: 77–89, 1988.

PUIL, E., MIURA, R. M., AND SPIGELMAN, I. Consequences of 4-aminopyridine applications to trigeminal root ganglion neurons. *J. Neurophysiol.* 62: 810–820, 1989.

PUIL, E., MEIRI, H., AND YAROM, Y. Resonant behavior and frequency preferences of thalamic neurons. *J. Neurophysiol.* 71: 575–582, 1994.

REYES, A. D. AND FETZ, E. E. Two modes of interspike interval shortening by brief transient depolarizations in cat neocortical neurons. *J. Neurophysiol.* 69: 1661–1672, 1993.

SCHWINDT, P. C. Ionic currents governing input-output relations of Betz cells. In: *Single Neuron Computation*, edited by T. McKenna, J. Davis, and S. F. Zornetzer. Boston, MA: Academic, 1992, p. 235–258.

SCHWINDT, P. C., SPAIN, W. J., AND CRILL, W. E. Effects of intracellular calcium chelation on voltage-dependent and calcium-dependent currents in cat neocortical neurons. *Neuroscience* 47: 571–578, 1992.

SCROGGS, R. S., TODOROVIC, S. M., ANDERSON, E. G., AND FOX, A. P. Variation in I$_H$, I$_{IR}$, and I$_{LEAK}$ between acutely isolated adult rat dorsal root ganglion neurons of different size. *J. Neurophysiol.* 71: 271–279, 1994.

SOLOMON, J. S., DOYLE, J. F., BURKHALTER, H., AND NERBONNE, J. M. Differential expression of hyperpolarization-activated currents reveals distinct classes of visual cortical projection neurons. *J. Neurosci.* 13: 5082–5091, 1993.

SOLOMON, J. S. AND NERBONNE, J. M. Hyperpolarization-activated currents in isolated superior colliculus-projecting neurons from rat visual cortex. *J. Physiol. Lond.* 462: 393–420, 1993a.

SOLOMON, J. S. AND NERBONNE, J. M. Two kinetically distinct components of hyperpolarization-activated current in rat superior colliculus-projecting neurons. *J. Physiol. Lond.* 469: 291–313, 1993b.

SPAIN, W. J., SCHWINDT, P. C. AND CRILL, W. E. Anomalous rectification in neurons from cat sensorimotor cortex in vitro. *J. Neurophysiol.* 57: 1555–1576, 1987.

STAFSTROM, C. E., SCHWINDT, P. C., AND CRILL, W. E. Repetitive firing in layer V neurons from cat neocortex in vitro. *J. Neurophysiol.* 52: 264–277, 1984a.

STAFSTROM, C. E., SCHWINDT, P. C., CHUBB, M. C., AND CRILL, W. E. Properties of persistent sodium conductance and calcium conductance of layer V neurons from cat sensorimotor cortex in vitro. *J. Neurophysiol.* 53: 153–170, 1985.

STAFSTROM, C. E., SCHWINDT, P. C., FLATMAN, J. A., AND CRILL, W. E. Properties of subthreshold response and action potential recorded in layer V neurons from cat sensorimotor cortex in vitro. *J. Neurophysiol.* 52: 244–263, 1984b.

STERIADE, M., MCCORMICK, D. A., AND SEJNOWSKI, T. J. Thalamocortical oscillations in the sleeping and aroused brain. *Science Wash. DC* 262: 679–685, 1993a.

STERIADE, M., NUÑEZ, A., AND AMZICA, F. Intracellular analysis of relations between the slow (<1 Hz) neocortical oscillation and other sleep rhythms of the electroencephalogram. *J. Neurosci.* 13: 3266–3283, 1993b.

STERIADE, M., NUÑEZ, A., AND AMZICA, F. A novel slow (<1 Hz) oscillation of neocortical neurons in vivo: depolarizing and hyperpolarizing components. *J. Neurosci.* 13: 3252–3265, 1993c.

STRÖHMANN, B., SCHWARZ, D. W. F., AND PUIL, E. Subthreshold frequency selectivity in avian auditory thalamus. *J. Neurophysiol.* 71: 1361–1372, 1994.

STRÖHMANN, B., SCHWARZ, D. W. F., AND PUIL, E. Electrical resonances in central auditory neurons. *Acta Otolaryngol.* 115: 168–172, 1995.

SUTOR, B. AND HABLITZ, J. J. Influence of barium on rectification in rat neocortical neurons. *Neurosci. Lett.* 157: 62–66, 1993.

WOMBLE, M. D. AND MOISES, H. C. Hyperpolarization-activated currents in neurons of the rat basolateral amygdala. *J. Neurophysiol.* 70: 2056–2065, 1993.

ZHANG, L. AND KRNJEVIĆ, K. Whole-cell recording of anoxic effects on hippocampal neurons in slices. *J. Neurophysiol.* 69: 118–127, 1993.

45 Siesjö, B.K. (1980) Regional metabolic rates in the brain. In *Brain Energy Metabolism*, pp. 131–150, Wiley
46 Lutz, P.L. (1992) Mechanisms for anoxic survival in the vertebrate brain. *Annu. Rev. Physiol.* 54, 601–618
47 Sick, T.J. *et al.* (1992) Maintaining coupled metabolism and membrane function in anoxic brain: A comparison between turtle and rat. In *Surviving Hypoxia* (Hochachka, P. *et al.*, eds), pp. 351–363, CRC
48 Rice, M.E. and Cammack, J. (1991) Anoxia-resistant turtle brain maintains ascorbic acid content *in vitro*. *Neurosci. Lett.* 132, 141–145
49 Halliwell, B. (1996) Vitamin C: antioxidant or pro-oxidant *in vivo*. *Free Radic. Res.* 25, 439–454
50 Hillered, L. *et al.* (1988) Increased extracellular levels of ascorbate in striatum after middle cerebral artery occlusion in the rat monitored by intracerebral microdialysis. *Neurosci. Lett.* 95, 286–290
51 Lyrer, P. *et al.* (1991) Levels of low molecular weight scavengers in the rat brain during focal ischemia. *Brain Res.* 567, 317–320
52 Cao, W. *et al.* (1988) Oxygen free radical involvement in ischemia and reperfusion injury to brain. *Neurosci. Lett.* 88, 233–238
53 Sciamanna, M.A. and Lee, C.P. (1993) Ischemia/reperfusion-induced injury of forebrain mitochondria and protection by ascorbate. *Arch. Biochem. Biophys.* 305, 215–224
54 Ranjan, A. *et al.* (1993) Ascorbic acid and focal ischaemia in a primate model. *Acta Neurochir.* 123, 87–91
55 Henry, P.T. and Chandry, M.J. (1998) Effect of ascorbic acid on infarct size in experimental focal cerebral ischemia and reperfusion in a primate model. *Acta Neurochir.* 140, 977–980
56 Pérez-Pinzón, M.A. *et al.* (1997) *Brain Res.* 754, 163–170
57 Dykens, J.A. *et al.* (1987) Mechanism of kainate toxicity to cerebellar neurons *in vitro* is analogous to reperfusion tissue injury. *J. Neurochem.* 49, 1222–1228
58 Coyle, J.T. and Puttfarcken, P. (1993) Oxidative stress, glutamate, and neurodegenerative disorders. *Science* 262, 689–695
59 Lafon-Cazal, M. *et al.* (1993) NMDA-dependent superoxide production and neurotoxicity. *Nature* 354, 535–537
60 Prehn, J.H. (1998) Mitochondrial transmembrane potential and free radical production in excitotoxic neurodegeneration. *Naunyn-Schmiedebergs's Arch. Pharmacol.* 357, 316–322
61 Ciani, E. *et al.* (1996) Inhibition of free radical production or free radical scavenging protects from the excitotoxic cell death mediated by glutamate in cultures of cerebellar granule cells. *Brain Res.* 728, 1–6
62 Atlante, A. *et al.* (1997) Glutamate neurotoxicity in rat cerebellar granule cells: a major role for xanthine oxidase in oxygen radical formation. *J. Neurochem.* 68, 2038–2045
63 Brahma, B. *et al.* (2000) Ascorbate inhibits edema in brain slices. *J. Neurochem.* 74, 1263–1270
64 Sato, K. *et al.* (1993) Synergism of tocopherol and ascorbate on the survival of cultured neurones. *NeuroReport* 4, 1179–1182
65 Sharma, P. (1997) Consequences of hypoxia on the cell size of neuropeptide-Y neurons and the role of ascorbate in cultured neurons from chick embryo. *Neurochem. Int.* 30, 337–344
66 Majewska, M.D. *et al.* (1990) Regulation of the NMDA receptor by redox phenomena: inhibitory role of ascorbate. *Brain Res.* 537, 328–332
67 Buettner, G.R. (1993) The pecking order of free radicals and antioxidants: lipid peroxidation, α-tocopherol, and ascorbate. *Arch. Biochem. Biophys.* 300, 535–543
68 Kuo, C-H. *et al.* (1978) Subcellular distribution of ascorbic acid in rat brain. *Jpn. J. Pharmacol.* 28, 789–791
69 Glembotski, C.C. (1987) The role of ascorbic acid in the biosynthesis of the neuroendocrine peptides α-MSH and TRH. *Ann. New York Acad. Sci.* 498, 54–62
70 Miller, B.T. and Cicero, T.J. (1987) Ascorbate-induced release of LHRH: noradrenergic and opioid modulation. *Brain Res. Bull.* 19, 95–99
71 Eldridge, C.F. *et al.* (1987) Differentiation of axon-related Schwann cells *in vitro*. I. Ascorbic acid regulates basal lamina assembly and myelin formation. *J. Cell Biol.* 105, 1023–1034

Resonance, oscillation and the intrinsic frequency preferences of neurons

Bruce Hutcheon and Yosef Yarom

The realization that different behavioural and perceptual states of the brain are associated with different brain rhythms has sparked growing interest in the oscillatory behaviours of neurons. Recent research has uncovered a close association between electrical oscillations and resonance in neurons. Resonance is an easily measurable property that describes the ability of neurons to respond selectively to inputs at preferred frequencies. A variety of ionic mechanisms support resonance and oscillation in neurons. Understanding the basic principles involved in the production of resonance allows for a simplified classification of these mechanisms. The characterization of resonance and frequency preference captures those essential properties of neurons that can serve as a substrate for coordinating network activity around a particular frequency in the brain.

Bruce Hutcheon is at the Institute for Biological Science, National Research Council of Canada, Ottawa, Canada K1A 0R6, and Yosef Yarom is at the Dept of Neurobiology, and the Center for Neuronal Computation, Hebrew University, Jerusalem, Israel 91904.

THE WORKING BRAIN is characterized by the rhythmic activation of large numbers of its neurons on characteristic temporal and spatial scales. These modes of coherent activity appear as the various brain rhythms. A series of firmly established empirical associations with the behavioural states of organisms provides compelling evidence that brain rhythms reflect basic modes of dynamical organization in the brain[1]. However, the mechanisms that bind neurons into these rhythmical coherent ensembles are not well understood.

What determines the characteristic frequency range of each brain rhythm? Broadly speaking, there are two types of explanation. One invokes patterns of connectivity between neurons and the dynamic properties of the intervening synapses. For example, reverberating activity within re-entrant neural circuits could result in the rhythmic activation of fundamentally non-oscillatory neurons within well-defined frequency bands[2]. A different explanation states that network rhythmicity arises via the coupling of oscillatory sub-units, each of which possesses an intrinsically determined frequency preference[3]. These two explanations are not mutually exclusive (network connectivity could reinforce the patterns of excitation produced by coupled

Box 1. Hunting resonance in circuits and cells

Physicists and engineers have long used frequency-domain techniques to describe the wave-like existence of particles, the motions of electrons in atoms, or the movement of a pendulum. These methods regard oscillation as a fundamental mode of behaviour and frequency as its natural unit of measure. For neurons, frequency-domain techniques provide an alternative to time-based descriptions of activity: a simpler and more-natural one for neurons that spend much of their existence immersed in sea of rhythmic inputs. Measurement of the electrical impedance characterizes the input–output relationship of neurons in a frequency-dependent way. Resonance is a property of the impedance. To explain further, it helps to explore first the principles of impedance and resonance in electrical circuit caricatures of neuronal behaviour.

Impedance is the frequency-domain extension of the concept of resistance for electrical circuits. Like resistance, it is a relationship between voltage and current. Unlike resistance, impedance is a frequency-dependent relationship between the amplitudes (and phases)

of oscillatory signals. The impedance of a simple circuit can be determined by probing it with an input current and observing the voltage response at each frequency. Although any input that has a known frequency composition can be used, the process is illustrated in this case using a signal that sweeps through many frequencies over time (the so called 'ZAP' input[a]). This input is useful because it is poised almost equally between the time and frequency domains. Each frequency in the input is isolated briefly in time so that the frequency response can be judged by eye as well as by later analysis. For the experimentalist who is probing neuronal circuits this real-time feedback is valuable.

The simplest of impedance relationships occurs for the simplest of all circuits, a resistor connected to ground (see Fig. Ia). In this case, as in all others, the impedance is found by dividing the Fourier spectrum (calculated using the Fast Fourier Transform, or FFT) of the output by that of the input. In this example, the impedance is simply a constant with a value equal the resistance.

A slightly more-sophisticated circuit comprises a resistor and capacitor connected in parallel (Fig. Ib). This is a common model for the passive electrical properties of an isopotential neuron. In this case, the impedance is a more-complicated function, the decline in impedance with increasing frequency indicates that an oscillatory input current of unit amplitude produces a smaller and smaller voltage response as the frequency rises. This circuit, therefore, acts in a way that is similar to a low-pass filter, that is, current inputs arriving at low frequencies yield relatively large voltage responses but higher frequency inputs are attenuated or blocked. All neurons have some contribution from a low-pass mechanism such as this in their frequency response.

Finally, adding an inductive element to the circuit results in a qualitatively different impedance relation (Fig. Ic). A resonant peak appears so that instead of acting in the same way as a low-pass filter, the system responds like a bandpass. The meaning of this is seen in the time-domain response to the ZAP input. The system is activated preferentially as the input passes through the resonant frequencies. Thus, it exhibits a frequency preference: a frequency at which the response to inputs is best.

Like electrical circuits, neurons can exhibit resonance and therefore sustain a frequency preference (Fig. Id). Resonant neurons produce large responses when driven by inputs near their resonant frequency and smaller responses at other frequencies. Functionally, such resonances constrain neurons to respond most powerfully to inputs at biologically important frequencies such as those associated with brain rhythms.

| Input current | Circuit | Output voltage | Impedance |
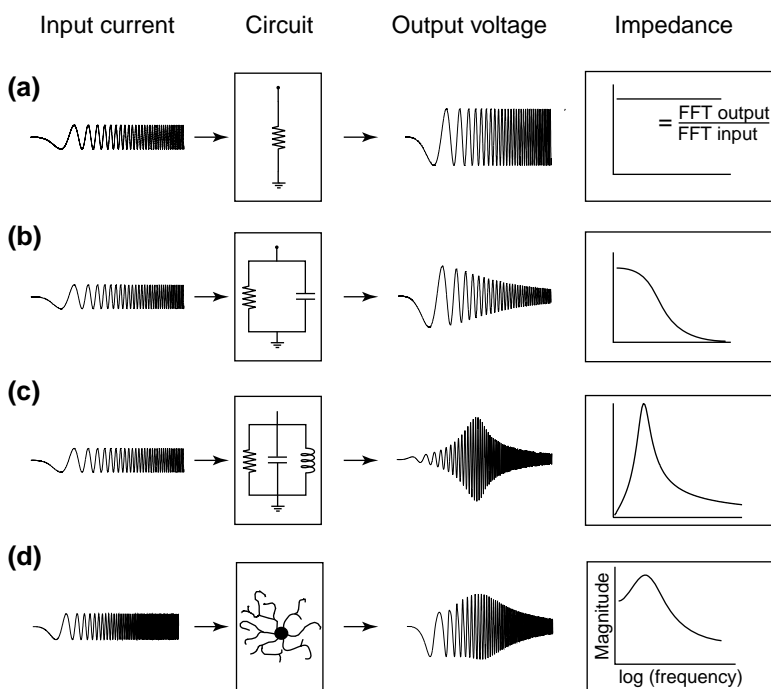
Fig. I. *Frequency-dependent properties of electronic circuits and neurons: detection and analysis. The relationship between the current input (first column) and the voltage output (third column) of electrical circuits or neurons (second column) enables the calculation of the impedance as a function of frequency (fourth column). The use of a ZAP input function concentrates the analysis within a specific range of frequencies.*
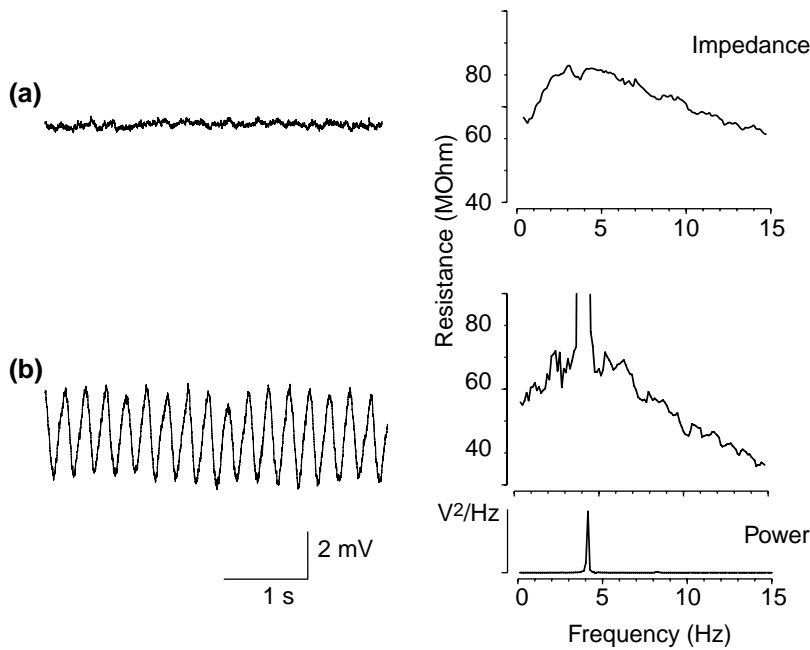
Reference
a Puil, E. *et al.* (1986) Quantification of membrane properties of trigemenal root ganglions in guinea pigs. *J. Neurophysiol.* 55, 995–1016

oscillators); however, at present, we have no clear example of a centrally produced rhythm that relies on patterns of connectivity to determine its frequency. On the other hand, we now have good evidence that individual neurons can have frequency preferences that enable them to either generate spontaneous membrane-voltage oscillations, or respond best to inputs within a narrow frequency window (see below). Such intrinsically defined properties of individual neurons will have a role in determining the dynamics of coherent brain activity.

This article discusses the possibility that there is a common element underlying the diverse mechanisms of frequency preference in neurons. Resonance, a property that characterizes the frequency at which neurons

respond best to inputs of injected current (Box 1), provides one means to describe the frequency-dependent properties of different neurons on a common basis. Although resonance measurements assess only the small-signal responses of neurons (thus ignoring, or only approximating, their strongly nonlinear properties) this is usually adequate for understanding how neurons process oscillatory inputs at subthreshold potentials. Using resonance to reveal the similarities between oscillatory mechanisms of different neurons should lead to basic insights regarding the development and modulation of rhythms in the brain; understanding their differences should yield specific new targets for drug action in disorders as diverse as epilepsy and insomnia.

Fig. 1. *Neurons of the inferior olive have an intrinsically determined frequency preference that is reflected in their network behaviour.* **(a)** *A whole-cell recording of an olivary neuron in vitro shows that it has a stable resting potential (left). The impedance profile of the same neuron (right) reveals a resonance at 4 Hz. The resonance is generated by the low-threshold Ca^{2+} current, I_T.* **(b)** *In a different olivary neuron, the membrane potential (left) oscillates steadily at 4 Hz as shown by the power spectrum (lower right). The impedance of this neuron also exhibits a resonance with a peak at the same frequency as the oscillations (the large truncated peak centered on the top of the resonance is due to the spontaneous oscillations). Oscillations in these neurons are partly intrinsic and partly caused by electrical coupling with other olivary neurons. Although the existence of oscillation is controlled by the strength of coupling and other modulatory factors such as the leak conductance, the frequency of the oscillations is determined by the resonance in the individual cells.*

Resonance as a probe of frequency preference

The use of frequency-response analysis for understanding neuronal function was pioneered by Cole[4], who used it, before the advent of voltage clamp techniques, to describe some of the basic events concerned with the generation of action potentials in the giant axon of the squid. Research using frequency-domain techniques was then carried forward by researchers who wished to study emergent electrical phenomena in single neurons by using Fourier techniques to tease apart the components of the response (for a review see Ref. 5). A distinctive property noted in some neurons using such techniques is a peak in the impedance curve, that is, a resonance (Box 1). The existence of a resonance in a neuron indicates that it is able to discriminate between its inputs, on the basis of their frequency content, so that oscillatory inputs near the resonant frequency produce the largest responses. Resonances have now been described in a number of excitable cell types such as cardiac cells[5], hair cells of the inner ear[6], and various peripheral[7] and central[8–14] neurons.

There are a few well-documented examples where frequency analysis has been used to demonstrate a close association between resonance and subthreshold oscillations of the membrane potential. In the neurons of the inferior olive, a coordinated subthreshold oscillation acts as a timing device to gate inputs[15,16]. These oscillations require the presence of the low-voltage activated Ca^{2+} current (I_T)[17]. In slice recordings, impedance measurements show that all olivary neurons display resonance even if they do not oscillate (Fig. 1a). In neurons

with subthreshold oscillations, the peak of the resonance and the frequency of the oscillations coincide (Fig. 1b). As evidence of their intimate relationship, both the oscillations and the resonance are eliminated by pharmacological block of I_T (Ref. 13). In thalamic neurons, a similar mechanism involving I_T is responsible for a resonance near the same frequencies[10,18].

Pyramidal neurons in the neocortex have two resonances with different voltage dependence. A 1–2 Hz resonance that occurs near the resting membrane potential requires activation of the hyperpolarization-activated cation current, I_H (Ref. 12), whereas a 5–20 Hz resonance (the exact frequency is voltage dependent) is seen at potentials that are more positive than −55 mV (Ref. 19). Two ionic conductances are implicated in the generation of the more-depolarized resonance because it is abolished by TEA (tetraethylammonium; a K$^+$ channel blocker), and strongly attenuated, but not altered in frequency, by TTX (tetrodotoxin; a Na$^+$ channel blocker). Furthermore, this resonance is associated with the sporadic occurrence of self-sustained subthreshold oscillations of the membrane potential near the resonant frequency. The oscillations require the full integrity of both of the currents involved in the resonance because either TEA or TTX abolishes them. The oscillations are interpreted as arising from an interaction between a TEA-sensitive mechanism that generates a resonance and a TTX-sensitive mechanism that is capable of amplifying the resonance strongly to produce oscillations.

The possible functional importance of the resonance and oscillations observed in thalamic and cortical neurons lies in the known participation of these neurons in various brain rhythms. The low-frequency resonances in the cortex and thalamus appear suited to support the thalamocortical delta-wave oscillations that are particularly prominent during deep sleep. The higher-frequency oscillatory behaviour and underlying resonance in pyramidal and inhibitory[20] neurons of the neocortex might have some involvement with higher-frequency rhythms that appear in the cortex during cognition[21].

How to make resonance: rules of thumb

The examples above show there are diverse ways to create resonance and oscillations in neurons. Fortunately, there are some simple regularities that govern these processes. In particular, as in the dual mechanism that underlies the depolarized resonance in neocortical cells, there is often a dissociation between the basic mechanisms responsible for the existence of resonance and the subsequent amplification of resonance to generate oscillations. This allows the study of these processes in relative isolation. The basic mechanisms that establish resonance and how resonance can be amplified and turned into oscillation will now be considered.

Resonances in central neurons always arise from an interplay between their active and passive properties. In fact, to generate resonance it is necessary to combine in a neuron two mechanisms that have specific frequency-domain properties: one that attenuates voltage responses to inputs that occur at high frequencies and another that attenuates responses to inputs arriving at low frequencies. The resulting combination of low- and high-pass filtering behaviour effectively creates a notch filter that is capable of rejecting inputs at frequencies outside the pass-band.

There is no difficulty in locating which properties of neurons result in low-pass filtering characteristics. The mechanism is well known and ubiquitous. It is a fundamental property of all cells that the parallel leak conductance and capacitance of the outer membrane forms the equivalent of a filter that attenuates responses to inputs at high frequencies. The mechanism that underlies low-frequency attenuation, however, is less well known. Such mechanisms arise from the operation of specific classes of voltage-gated currents. There are two elementary rules for deciding which voltage-gated currents will act as high-pass filters and will therefore be capable of combining with the passive properties of neurons to produce resonance.

(1) Currents that actively oppose changes in membrane voltage can produce resonance. In Fig. 2a, this is demonstrated using a simulation model of an isopotential neuron with a voltage-gated current (I_K) that has properties similar to a delayed rectifier. As can be seen by comparing parts a and b in Fig. 2a, the voltage changes in response to a current pulse are greatly reduced by the addition of I_K. By definition, all voltage-gated currents whose reversal potential falls near the base of their activation curve will act in the same way to oppose changes in membrane voltage actively. Examples of such currents are outwardly rectifying K^+ currents and inwardly rectifying I_H (see Fig. 3a). The ability to oppose voltage changes, however, is not yet sufficient to produce resonance. One more requirement must be met.

(2) To produce resonance, currents that meet the criterion above must, in addition, activate slowly relative to the membrane time constant. This is demonstrated once again for a model neuron with I_K (Fig. 2a, part b). The model shows the damped oscillations that occur at the onset and offset of the response to an injected current pulse as the slow kinetics of I_K force it to turn on and off with a lag relative to the passive charging of the membrane. The damped oscillations, often called 'sag' and 'rebound' in neurons, are the time-domain signature of resonance. The same basic phenomenon is seen in the response to a 'ZAP' (see Box 1) current input where the slow kinetics of I_K result in it being most effective in tracking and opposing low-frequency changes in membrane voltage. The net result is that I_K attenuates low frequencies and acts as a high-pass filter with a corner frequency set by its activation time constant (Fig 2b). In addition, the low-pass filter formed by the passive properties of the membrane has a corner frequency set by the RC time constant. Resonance arises at intermediate frequencies where inputs induce voltage changes at frequencies too high to be opposed by I_K and too low to be counteracted by the passive properties of the membrane. If there is not enough of a gap between these high- and low-frequency regions of attenuation, resonance will be eliminated. As a general rule, the activation time constant for the voltage-gated current should be slower than the membrane time constant in order to produce resonance. If this criterion is fulfilled, the resonant frequency lies between these two time constants.

To summarize, slowly activating currents that actively oppose changes in membrane voltage produce resonance. The approximate frequency of the resonance can be estimated when the values of the activation and passive membrane time constants are known. Given that the kinetics of resonant currents are voltage dependent, the resonant frequency will also be voltage dependent.
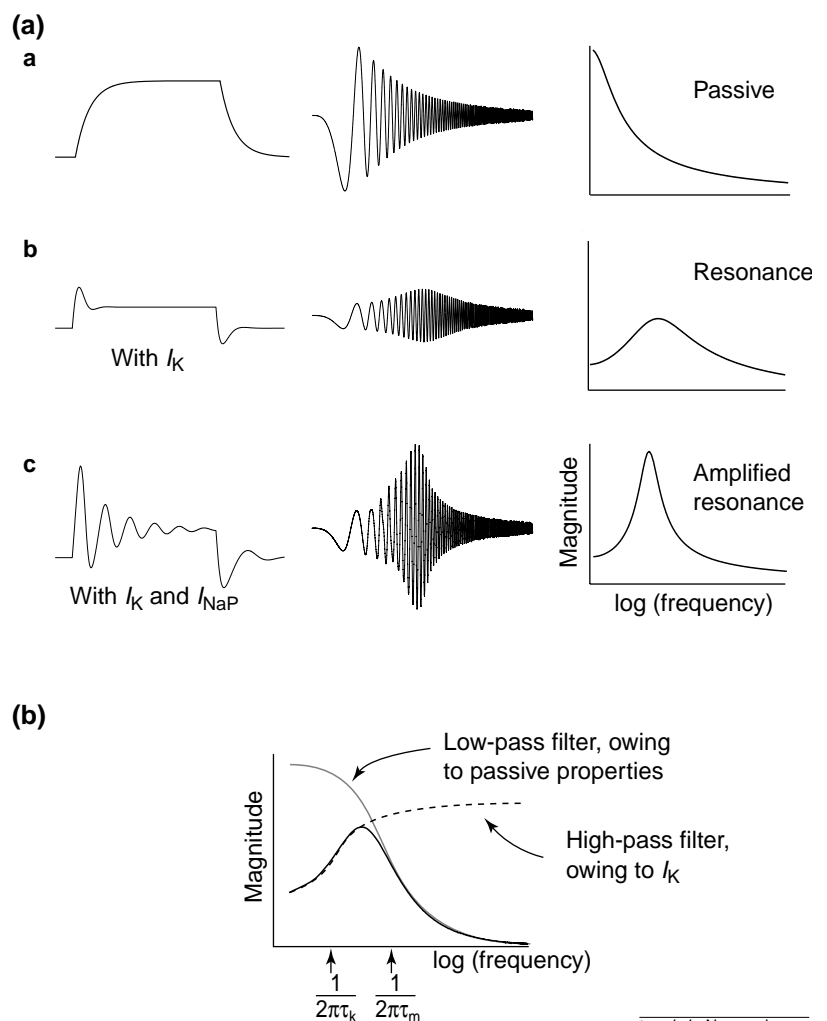

Fig. 2. Resonance is formed by the interaction of active and passive properties in a neuron. *(a) Properties of three models that have passive properties only (part a), passive properties plus a resonant current, I_K (part b), and passive properties, a resonant current and an additional amplifying current, I_{NaP} (part c). For each model, the response to a pulse of current is shown on the left, the response to a 'ZAP' input in the middle and the corresponding impedance magnitude on the right. The amplified resonance results in oscillations, and an enlargement and narrowing of the resonant peak in the impedance magnitude. If the conductance of the amplifying current is increased much beyond the value shown, the oscillations become self-sustaining and the model acts like a pacemaker. (b) Demonstration of the separate contributions of the resonant current and passive properties to resonance in the impedance (unbroken line). The broken line shows the contribution of the resonant current (I_K) to the impedance. At low frequencies, the effectiveness of I_K at countering voltage changes is high, resulting in a small impedance. This effect is reduced at frequencies above $1/2\pi\tau_k$, where τ_k is the time constant for activation of I_K. On the other hand, the passive properties of the membrane (gray line) dominate the impedance at frequencies above $1/2\pi\tau_m$ where τ_m is the membrane time constant. The resonant peak occurs between these frequencies.*

Amplifying currents, amplified resonance and oscillation

Although the rules for identifying resonant currents have been explained, the story is not yet complete. What is missing is the concept of an amplifying current. Such a current is essentially the inverse of a resonant current. Its reversal potential lies near the top, rather than the base, of its voltage-activation curve (Fig. 3); and it therefore actively potentiates, rather than opposes, voltage changes (cf. parts b and c in Fig. 2a). In addition, it activates quickly, rather than slowly, relative to the membrane time constant. Amplifying currents enhance voltage fluctuations through a weakly regenerative mechanism analogous to that responsible for the rising phase of action potentials. Examples of such
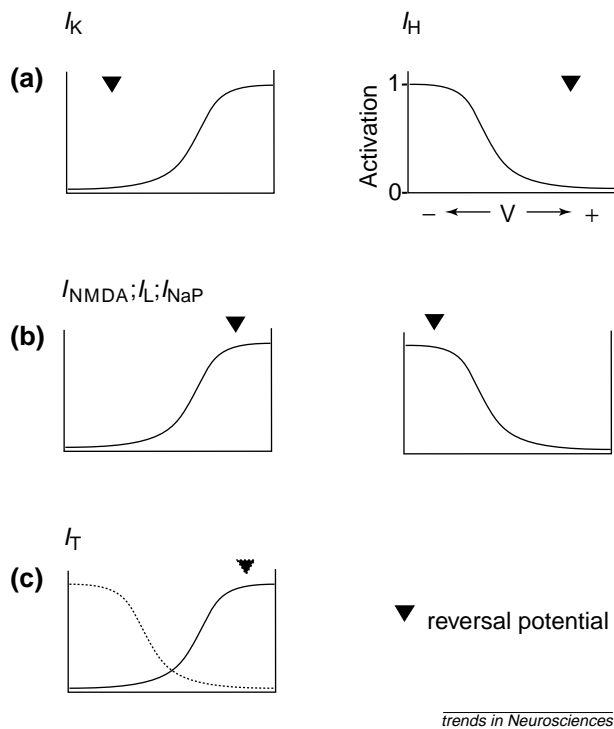
Fig. 3. *Classification of voltage-gated currents. Each panel shows, schematically, a possible arrangement of steady-state activation and reversal potential (arrowheads) that can lead to either resonant* **(a)** *or amplifying behaviour* **(b)**. *The horizontal axes shows arbitrarily scaled membrane voltage with depolarized values on the right.* (a) *Currents that have their reversal potential at the base of their activation curves can produce resonance. Resonance is strongest where the slope of the steady-state activation curve is steep. There are two possible arrangements depending on whether the current is activated by depolarization or hyperpolarization. Examples of each possibility are listed above each panel.* (b) *Currents with a reversal potential at the top of the activation curve are amplifying. Examples of such currents that activate with depolarization are the persistent Na^+ current (I_{NaP}) the L-type Ca^{2+} current (I_L) and the NMDA-receptor current (I_{NMDA}). To date, there is no clearcut example of an amplifying current that is activated upon hyperpolarization.* (c) *The low-threshold Ca^{2+} current produces an amplified resonance and can be understood as made up of two active mechanisms. The inactivation process (broken line) produces a resonance, whereas the activation process (unbroken line) is amplifying. Abbreviations: I_H, hyperpolarization-activated cation current; I_K, outwardly rectifying K^+ currents; I_T, low-threshold Ca^{2+} current.*

currents (Fig. 3) are the persistent Na^+ current, I_{NaP}, the current that flows through NMDA-receptor channels, I_{NMDA}, and the dihydropyridine-sensitive high-threshold Ca^{2+} current, I_L.

Amplifying currents interact with resonant currents to enhance resonance without greatly altering the resonant frequency. This is seen by comparing the ZAP responses or the impedance curves in parts b and c of Fig 2a. If the resulting mechanism were to be described in terms of electronic circuits, we would speak of a band-pass amplifier rather than a band-pass filter. Amplified resonance has been demonstrated empirically for the interaction between I_{NaP} and I_H in somatosensory neocortical neurons from rats[12], and again for I_{NaP} and a slowly activating K^+ current at depolarized potentials in neurons from the frontal cortex of guinea pigs[19].

When amplifying currents are of sufficient strength, they are capable of coupling resonance to self-sustained oscillations of the membrane potential. This can be shown theoretically using simulation models but has also been demonstrated empirically by Gutfreund

et al.[19] (see Box 2). In such systems, two distinct currents interact to produce emergent phenomena: amplified resonances or spontaneous oscillations, whose frequency is set by one partner and whose strength is set by the other.

The oscillations and resonance caused by I_T in olivary and thalamic neurons can now be understood in the framework of resonant and amplifier currents. In brief, I_T is a special case where the resonant and amplifying mechanisms have been packaged together in the same current (Fig. 3c). The inactivation process of I_T meets all the requirements for producing resonance, whereas its fast activation mechanism acts as an amplifier. The resulting amplified resonance or spontaneous oscillations occur at voltages that are centered on the region of overlap of the steady state activation and inactivation curves (that is, the region of the 'window' current[22]). The frequency is determined by the kinetics of I_T inactivation.

Concluding remarks

There are many different ways to construct a resonance or frequency preference in neurons. Despite the differences, however, an underlying theme emerges that allows a simple classification of the oscillatory characteristics of neurons. To summarize, there are three classes of frequency-dependent mechanism in central neurons: (1) solitary resonances caused by unaided resonant currents; (2) amplified resonances that arise from the interaction of resonant and amplifying mechanisms; and (3) spontaneous oscillations caused when a resonant current interacts so strongly with an amplifying current that the resting membrane potential becomes destabilized. Only in this last class is the frequency preference of the neuron overtly displayed as a pacemaker oscillation. In the first two classes the frequency preference of the neuron is latent and revealed only in the presence of inputs.

Given the large diversity of voltage-operated channels available, it is likely that every neuron in the brain has a resonance under some set of conditions and within some range of membrane voltages. A question therefore arises: are resonances used by neurons or are they simply epiphenomena?

A broad answer to this question is that, in nature, epiphenomena seldom remain epiphenomena for long; they are the raw material for evolutionary advances. It would be surprising to find that the brain has not found a use for a set of mechanisms capable of tuning neurons to specific frequencies, particularly in light of the prevalence of robust brain rhythms. On a more-specific level, it is obvious there are circumstances where strongly amplified resonances are used to coordinate the emergent pattern of network activity around a preferred frequency. This is the case in the inferior olive and it might also apply to the thalamic participation in delta- and spindle-wave generation[23,24]. In other brain regions, functions for the subthreshold oscillations that are observed have not yet been found. However, this research is still in its infancy. Finally, for the weaker resonances, it can be argued that the widespread possession of a resonance of whatever strength aids neurons in the integration of their inputs. In effect, the establishment of even a weak resonance makes a neuron a good listener for activity within a specialized frequency band. A host of good listeners, mutually connected, should tune networks to operate in frequency ranges of special biological meaning.

Box 2. From resonance, to oscillation and back via phase-plane analysis

As in the case of resonance, spontaneous oscillations in neurons arise from an interplay of voltage-dependent conductances[a,b], where they might have important roles in the timing and integration of neuronal inputs and outputs[c,d,e]. Moreover, resonance and spontaneous oscillations can coexist in the same system. A simple model, examined with the aid of tools developed for the branch of mathematical analysis known as dynamical systems theory, demonstrates that resonance and spontaneous oscillations are two aspects of the same basic phenomenon of frequency preference.

A mathematical model of an isopotential neuron with non-inactivating K^+ and Na^+ conductances (g_K and g_{Na}, respectively) is constructed according to the system of differential equations shown below. To simplify matters, a reduced system of parameters governing the kinetic and voltage behaviours of these conductances has been used. The Na^+ conductance, for example, is assumed to activate instantaneously, and the maximal conductances of both the voltage-operated conductances are normalized by the amount of passive leak conductance. Given such a system, one can ask whether different combinations of the parameters result in oscillations or stable behaviours. The results of such a stability analysis (found by integrating the equations forward in time for each parameter set or using an analytical equation) are encoded in a stability diagram such as that shown in Fig Ia. It can be seen that specific combinations of g_K and g_{Na} values result in a stable resting potential (blue), whereas others result in destabilization of the resting potential and the consequent appearance of spontaneous oscillations (red).

$$\frac{dv}{dt} = -\left[v - v_{leak}\right] - g_{Na}(v)\left[v - v_{Na}\right] - g_K n\left[v - v_K\right] \quad (1)$$

$$\frac{dn}{dt} = \frac{n - n_\infty(v)}{\tau_K} \quad (2)$$

A closer look at the behaviour of the system when it is in the blue region in Fig. I shows that, although there are no spontaneous oscillations, the system nonetheless retains a disposition towards oscillation. This is seen by viewing so-called phase-plane diagrams of the system. For any combination of parameters, the phase-plane portrait shows the joint evolution of two or more dynamic variables of the system following a perturbation. In this case, the variables are the instantaneous values of the membrane voltage (v) and activation level of the K^+ conductance (n). The arrowed lines in Fig. Ib represent trajectories or orbits the system might follow if the values of the variables were suddenly displaced and then released. The two phase-plane portraits on the left, which correspond to the parameter com-

binations at positions 1 and 2 in the stability diagram at the top, both show the system eventually approaching a stable point (the resting potential) after a perturbation. The spiral nature of these trajectories reveals that the return to resting potential is oscillatory in these systems. The more-pronounced spirals in the phase-plane portrait in the middle panel indicate that the system is strongly oscillatory owing to the interaction of the resonant conductance (g_K), and the amplifying conductance (g_{Na}) whose value is high relative to that of the system in the portrait on the left. Thus, even when the system is in the stable blue region in the stability diagram, the model neuron can be oscillatory to differing degrees. The intrinsic tendency to oscillate is revealed as damped oscillations in the response to inputs such as the modeled synaptic-like current inputs shown below each diagram. Equivalently, if these stable systems are probed with oscillatory inputs, a resonance is observed.

If the value of amplifying (g_{Na}) conductance is raised more, the system enters the red area of the stability diagram, the stability of the resting potential is lost, and any perturbation of the system variables eventually results in the system entering an orbit around a so-called limit cycle. The limit cycle, which corresponds to a spontaneous, self-sustained oscillation, is seen in the rightmost phase-plane diagram. The time-domain trace below the diagram shows that the oscillation has about the same frequency as the damped oscillations in the stable systems. Moreover, an oscillatory current input to this spontaneously active system will reveal a resonance near the frequency of the oscillation. Thus, damped and spontaneous oscillations are seen as arising from a single fundamental mechanism involving interactions between voltage-and time-dependent conductances. As resonance measurements are capable of probing such interactions independent of whether the system lies in the stable or unstable regions of the stability diagram (Fig Ia), they provide the most convenient way of investigating the frequency preferences of neurons on a common basis.

References

a White, J.A. et al. (1995) A bifurcation analysis of neuronal subthreshold oscillations. Biophys. J. 69, 1203–1217
b Wang, X-J. (1993) Ionic basis for intrinsic oscillations. NeuroReport 5, 221–224
c Alonso, A. et al. (1990) Postsynaptic Hebbian and non-Hebbian long-term potentiation of synaptic efficacy in the entorhinal cortex in slices and in the isolated adult guinea pig brain. Proc. Natl. Acad. Sci. U. S. A. 87, 9280–9284
d Llinás, R.R. (1988) The intrinsic electrophysiological properties of mammalian neurons: insights into central nervous system function. Science 242, 1654–1664
e Desmaisons, D. et al. (1999) Control of action potential timing by intrinsic subthreshold oscillations in olfactory bulb output neurons. J. Neuroscience 19, 10727–10737
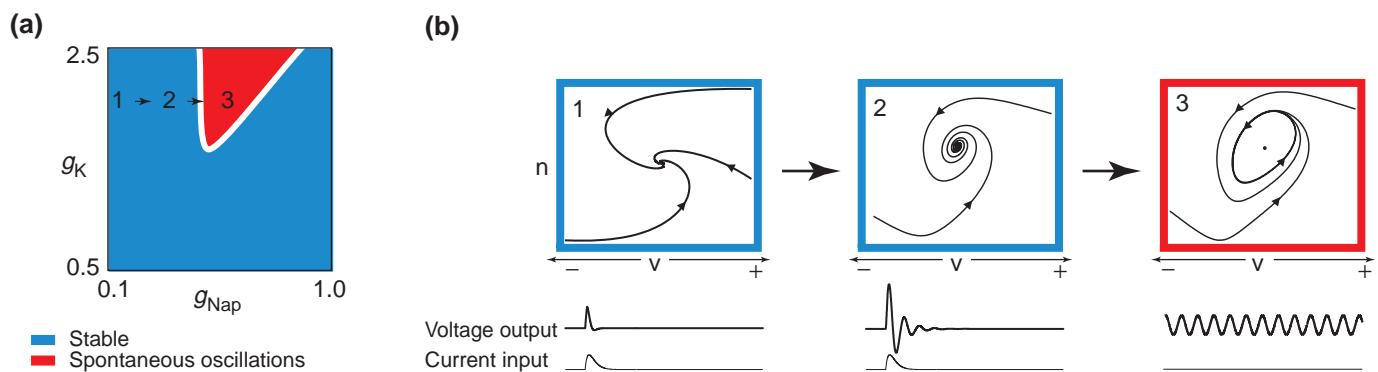
trends in Neurosciences

Fig. I. *Theoretical analysis of a resonant model neuron.* (a) *Stability diagram showing combinations of resonant (g_K) and amplifying (g_{NaP}) maximal conductance values where the system has a stable resting potential (blue) or exhibits spontaneous oscillations (red).* (b) *Phase-plane diagrams showing details of the system response at the three positions indicated by the numbers in the stability diagram at top. These diagrams show how a resonant system evolves continuously into a spontaneously oscillatory system as the amplifying conductance is increased. The frequency of the oscillations of resonance is set by the properties of the resonant conductance.*

Selected references

1 Steriade, M. *et al.* (1990) *Thalamic Oscillations and Signalling*, John Wiley and Sons
2 Traub, R.D. and Miles, R. (1991) *Neuronal Networks of the Hippocampus*, Cambridge University Press
3 Llinás, R. (1988) The intrinsic electrophysiological properties of mammalian neurons: insights into central nervous system function. *Science* 242, 1654–1664
4 Cole, K.S. (1941) Rectification and inductance in the squid giant axon. *J. Gen. Physiol.* 25, 29–51
5 DeFelice, L. (1981) *Introduction to Membrane Noise*, Plenum
6 Hudspeth, A. (1985) The cellular basis of hearing: the biophysics of hair cells. *Science* 230, 745–752
7 Puil, E. *et al.* (1986) Quantification of membrane properties of trigemenal root ganglions in guinea pigs. *J. Neurophysiol.* 55, 995–1016
8 Fishman, H.M. *et al.* (1977) K^+ conduction description from the low frequency impedance and admitance of the squid axon. *J. Memb. Biol.* 32, 255–290
9 Mauro, A. *et al.* (1970) Subthreshold behavior and phenomenological impedance of the squid giant axon. *J. Gen. Physiol.* 55, 497–523
10 Jahnsen, H. and Karnup, S. (1994). A spectral analysis of the integration of artificial synaptic potentials in mammalian central neurons. *Brain Research* 666, 9–20
11 Moore, L.E. and Christensen, B.N. (1985). White noise analysis of cable properties of neuroblastoma cells and lamprey central neurons. *J. Neurophysiol.* 53, 636–651
12 Hutcheon, B. *et al.* (1996). Subthreshold membrane resonance in neocortical neurons. *J. Neurophysiol.* 76, 683–697
13 Lampl, I. and Yarom, Y. (1997). Subthreshold oscillations and resonant behaviour: two manifestations of the same mechanism. *Neuroscience* 78, 325–341
14 Leung, L.S. and Yu, H-W. (1998). Theta-Frequency resonance in hippocampal CA1 neurons *in vitro* demonstrated by sinusoidal current injection. *J. Neurophysiol.* 79, 1592–1596
15 Lampl, I. and Yarom, Y. (1993). Subthreshold oscillations of the membrane potential: a functional synchronizing and timing device. *J. Neurophysiol.* 70, 2181–2186
16 De Zeeuw, C.I. *et al.* (1998). Microcircuitry and function of the inferior olive. *Trends Neurosci.* 21, 391–400
17 Llinás, R. and Yarom, Y. (1986). Oscillatory properties of guinea pig olivary neurons and their pharmacological modulation: an *in vitro* study. *J. Physiol.* 376, 163–182
18 Puil, E. *et al.* (1994). Resonant behavior and frequency preferences of thalamic neurons. *J. Neurophysiol.* 71, 575–582
19 Gutfreund, Y. *et al.* (1995). Subthreshold oscillations and resonant frequency in guinea pig cortical neurons: physiology and modeling *J. Physiol.* 483, 621–640
20 Llinás, R.R. *et al.* (1991). *In vitro* neurons in mammalian cortical layer 4 exhibit intrinsic oscillatory activity in the 10- to 50-Hz frequency range. *Proc. Natl. Acad. Sci. U. S. A.* 88, 897–901
21 Gray, C.M. *et al.* (1989). Oscillatory responses in cat visual cortex exhibit intercolumnar synchronization which relfects global stimulus properties. *Nature* 338, 334–340
22 Hutcheon, B. *et al.* (1994). Low-threshold calcium current and resonance in thalamic neurons: a model of frequency preference *J. Neurophysiol.* 76, 683–697
23 Dossi, R.C. *et al.* (1992). Electrophysiology of a slow (0.5–4 Hz) intrinsic oscillation of cat thalamocortical neurons in vivo. *J. Physiol.* 447, 215–234
24 Destexhe, A. *et al.* (1996). Ionic mechanisms underlying synchronized oscillations and propagating waves in a model of ferret thalamic slices. *J. Neurophysiol.* 76, 2049–2070

Calcium signaling in the ER: its role in neuronal plasticity and neurodegenerative disorders

Mark P. Mattson and Sic L. Chan are at the Laboratory of Neurosciences, National Institute on Aging, Baltimore, MD 21224, USA. Frank M. LaFerla and Malcolm A. Leissring are at the Laboratory of Molecular Neuropathogenesis, Dept of Neurobiology and Behavior, University of California at Irvine, CA 92697, USA. P. Nickolas Shepel and Jonathan D. Geiger are at the Dept of Pharmacology and Therapeutics, University of Manitoba Faculty of Medicine, Winnipeg, Manitoba, Canada.

Mark P. Mattson, Frank M. LaFerla, Sic L. Chan, Malcolm A. Leissring, P. Nickolas Shepel and Jonathan D. Geiger

Endoplasmic reticulum (ER) is a multifaceted organelle that regulates protein synthesis and trafficking, cellular responses to stress, and intracellular Ca^{2+} levels. In neurons, it is distributed between the cellular compartments that regulate plasticity and survival, which include axons, dendrites, growth cones and synaptic terminals. Intriguing communication networks between ER, mitochondria and plasma membrane are being revealed that provide mechanisms for the precise regulation of temporal and spatial aspects of Ca^{2+} signaling. Alterations in Ca^{2+} homeostasis in ER contribute to neuronal apoptosis and excitotoxicity, and are being linked to the pathogenesis of several different neurodegenerative disorders, including Alzheimer's disease and stroke.

Trends Neurosci. (2000) 23, 222–229

ENDOPLASMIC RETICULUM (ER) is widely distributed within neurons, being present in dendrites and dendritic spines, axons and presynaptic nerve terminals, and in growth cones (Fig. 1)[1–5]. It is highly motile, rapidly extending into and retracting from distal regions of growth cones[5], and congregating in stack-like structures within dendrites in response to stimulation of metabotropic glutamate receptors[6]. Microtubules and actin filaments appear to have key roles in controlling ER motility, as well as in its structure and function[7,8]. ER is continuous with the outer nuclear membrane and is often associated intimately with plasma membrane and mitochondria, which suggests functional coupling between these structures[9]. It is classically divided into two subtypes: 'rough' ER, which contains ribosomes and is responsible for protein synthesis, and 'smooth' ER, which can serve a particularly important role in Ca^{2+} signaling. Although smooth and rough ER coexist in neuronal cell bodies and proximal regions of axons and dendrites, the specialized endings of neurites (growth cones, axon terminals and dendritic spines) contain mainly smooth ER. Emerging evidence suggests that, by controlling levels of cytoplasmic free Ca^{2+} locally in growth cones and synaptic compartments, ER regulates functional and structural changes in nerve cell circuits in both the developing and adult nervous systems.

Intracellular Analysis of Relations between the Slow (<1 Hz) Neocortical Oscillation and Other Sleep Rhythms of the Electroencephalogram

M. Steriade, A. Nuñez, and F. Amzica

Laboratoire de Neurophysiologie, Faculté de Médecine, Université Laval, Quebec, Canada G1K 7P4

The newly described slow cortical rhythm (≈0.3 Hz), whose depolarizing–hyperpolarizing components are analyzed in the preceding article, is now investigated from the standpoint of its relations with delta (1–4 Hz) and spindle (7–14 Hz) rhythmicity.

Regular-spiking and intrinsically bursting cortical neurons were mostly recorded from association suprasylvian areas 5 and 7; fewer neurons were also recorded from pericruciate motor and posterolateral visual areas. Although most cells were investigated under various anesthetics, a similar slow cortical rhythm was found in animals with brainstem transection at the low- or high-collicular levels. These cerveau isolé (isolated forebrain) preparations display the major sleep rhythms of the EEG in the absence of general anesthetics.

In 38% of recorded cortical neurons (n = 105), the slow rhythm was combined with delta oscillation. Both cellular rhythms were phase locked to the slow and delta oscillations in the surface- and depth-recorded EEG. In a group of this cell sample (n = 47), delta activity occurred as stereotyped, clocklike action potentials during the interdepolarization lulls of the slow rhythm. In another neuronal subsample (n = 58), delta events were grouped in sequences superimposed upon the depolarizing envelope of the slow rhythm, with such sequences recurring rhythmically at ≈0.3–0.4 Hz. The associations between the two cellular and EEG rhythms (1–4 Hz and 0.3–0.4 Hz) were quantified by means of autocorrelograms, cross-correlograms, and spike-triggered averages.

In 26% of recorded neurons (n = 72), the slow rhythm was combined with spindle oscillations. Regular-spiking cortical neurons fully reflected the whole frequency range of thalamically generated spindles (7–14 Hz). However, during similar patterns of EEG spindling, intrinsically bursting cells fired grouped action potentials (with intraburst frequencies of 100–200 Hz) at only 2–4 Hz.

The dependence of the slow cortical oscillation upon the thalamus was studied by lesions and stimulation. The slow rhythm survived extensive ipsilateral thalamic destruction by means of electrolytic lesions or kainate-induced loss of perikarya in thalamic nuclei that were input sources to the recorded cortical neurons. To further prevent the possibility of a thalamic role in the genesis of the slow rhythm, through the contralateral thalamocortical systems and callosal projections, we also transected the corpus callosum in thalamically lesioned animals, and still recorded the slow rhythm in cortical neurons. These data indicate that the thalamus is not essentially implicated in the genesis of the slow rhythm. However, thalamocortical and callosal volleys (repeated pulse trains at 10 Hz) were able to alter the cortical rhythm and to transform it into faster oscillations. As a consequence of 10 Hz stimulation, some intrinsically bursting cortical neurons developed a self-sustained activity within the same frequency range and discharge patterns as in the final stage of stimulation.

These results demonstrate that cortical neurons integrate various sleep rhythms as a result of interactions between thalamic and cortical networks. The final article in this series (Steriade et al., 1993b) will describe the novel slow oscillation in reticular thalamic and thalamocortical cells and will discuss the reflection of slow thalamic oscillations back onto cortical neurons.

[Key words: slow rhythm, delta rhythm, spindle rhythm, sleep, EEG, neocortex, thalamus, intracellular recording]

In the first article of this series we described various components building up the slow (<1 Hz) depolarizing–hyperpolarizing oscillation of neocortical cells recorded from different cortical areas (Steriade et al., 1993a). We now analyze the relations between this slow cortical rhythm and other sleep patterns of the EEG. As global EEG activity reflects a variety of oscillations, generated in the thalamus and cerebral cortex, we attempted to study the association between the novel slow rhythm (mainly at ≈0.3 Hz) and the two other sleep patterns within the frequency range of delta waves (1–4 Hz) and spindles (7–14 Hz). The dramatic synchrony between cellular and EEG activities shown in the present article supports the data presented in the preceding article, reporting that 88% of cortical neurons recorded from sensory, motor, and associational areas display the slow oscillation. The fact that the slow neocortical rhythm coexists with the thalamically generated delta and spindle oscillations in both single cortical cells and large neuronal networks is indicative for the importance of traveling influxes in interacting thalamocortical networks. We will show that the slow cortical oscillation survives complete lesions of thalamic peri-

karya projecting to the recorded cortical areas, but that the thalamus potently modulates the cortical rhythmicity.

Materials and Methods

Data reported in this article resulted from the same experiments on adult cats as presented in the preceding article. Details on different anesthetic agents, stimulation and recording procedures, and criteria for neuronal identification by ortho- and antidromic responses to stimulation of ipsilateral lateroposterior (LP) and rostral intralaminar centrolateral (CL) nuclei as well as to stimulation of homotopic foci in the contralateral cortex can be found in the preceding article (Steriade et al., 1993a). Unless otherwise mentioned, the depicted neurons were recorded under urethane anesthesia.

To rule out the possibility that the slow rhythm is due to a peculiar action of urethane or other anesthetics, in four animals ketamine was initially administered (40 mg/kg, i.m.) and large bilateral electrolytic lesions were performed in the mesencephalic tegmentum, to reproduce Bremer's (1935) *cerveau isolé* (isolated forebrain) preparation displaying spontaneous spindles and slower oscillations in the absence of large doses of different anesthetics. Figure 1 in the preceding article (Steriade et al., 1993a) showed the presence of the slow oscillation in naturally sleeping cats and humans.

In six animals, extensive electrolytic or excitotoxic thalamic lesions, including the pulvinar (PUL)-LP complex, mediodorsal (MD), centrum medianum-parafascicular and CL-paracentral (PC) intralaminar nuclei, ventroposterior (VP), ventroanterior–ventrolateral (VA-VL) complex, as well as other thalamic nuclei, were made before recordings to determine whether the slow oscillation of cortical neurons recorded from areas 5 and 7 is dependent upon thalamic input sources. The chemical lesions were performed by injecting 0.1 μl of a saline solution containing 1% kainic acid at six different sites in the thalamus at anterior plane 10; the animals received, in addition to the usual anesthetics, benzodiazepine (Valium, 2.5 mg/kg). In the same preparations, the corpus callosum was cut with a blunt spatula, at the level of the recorded cortical area. Thus, those recorded cortical cells were deprived of their inputs from both the thalamus and contralateral cortex.

Statistical analyses were performed by using the Brain Wave Systems software. The study of rhythmicity and synchrony between simultaneously recorded cells were based on autocorrelograms, cross-correlograms, and interspike interval histograms (ISIHs). When correlations between spike discharges and electrocorticogram-electrothalamogram (ECoG-EThG) slow waves were to be analyzed, we performed spike-triggered averages (STAs). In the latter case, symmetrical periods of up to 15 sec around the first action potential of the spike train composing the slow cellular oscillation were extracted from slow waves and averaged.

Results

This study is based on the same neuronal sample as the preceding article (Steriade et al., 1993a). Out of 277 cortical cells, 23 were recorded extracellularly and 254 intracellularly in association suprasylvian areas 5 and 7 ($n = 233$), motor pericruciate areas 4 and 6 ($n = 25$), and visual areas 17 and 18 ($n = 19$). The resting membrane potential (V_m) was -70.7 ± 0.6 mV (mean $\pm$ SE), spike amplitude was 82.1 ± 0.9 mV, and apparent input resistance was 20.6 ± 0.7 MΩ. The recorded neurons belonged to two classes: regular-spiking (slow- and fast-adapting) and intrinsically bursting cells. The input–output organization of cells was defined by orthodromic and antidromic activation (see Fig. 5D), showing that many oscillating neurons were callosal or corticothalamic elements receiving synaptic projections from related thalamic nuclei and from homotopic cortical areas in the contralateral hemisphere.

Urethane and ketamine (the latter supplemented by nitrous oxide or xylazine) induced EEG patterns consisting of prevailing slow and delta rhythms, but spindling was also observed at different stages of anesthesia in 14 out of 50 animals. Under deep barbiturate anesthesia, EEG spindling largely prevailed over EEG delta waves.

Relations between the slow (<1 Hz) and delta (1–4 Hz) rhythms

The association of slow and delta oscillations in the same cortical cell was observed in 38% of neurons ($n = 105$) recorded from all three types of investigated cortical areas. Two patterns of delta activities are described below: (1) clocklike action potentials fired within the frequency range of 1–4 Hz and occurring *between* the depolarizing phases of the slow rhythm (interdepolarizations lulls), and (2) membrane oscillations within the same delta frequency superimposed on the depolarizing phase of the slow rhythm.

(1) The first pattern of combined (slow and delta) rhythmicities and the EEG correlates of these cellular activities were seen in 47 out of 105 cells displaying the slow and delta oscillations. Figure 1A shows that the association between the slow (0.16 Hz) and delta (1.3 Hz) cellular rhythms took place in parallel with enhanced amplitudes of ECoG and EThG slow waves, reflecting the increase in cortical and thalamic synchronization. From short-lasting slow depolarizations, giving occasionally rise to one or a few spikes and separated by long periods of neuronal silence, this cell developed to a state characterized by longer depolarizing envelopes and, between them, spectacularly rhythmic single action potentials at 1.3 Hz.

Further analysis of the slow rhythm in this neuron revealed that the amplitude of action potentials superimposed on the slowly recurring depolarizations was about 20% smaller than that seen during the lulls between the slow depolarizations (Fig. 1B). This betrays changes in membrane conductance, due to intrinsic and synaptic factors underlying this slow depolarizing event (see Steriade et al., 1993a). In addition to repetitive EPSPs summed into the long-lasting depolarizing component, isolated IPSPs were observed at a V_m more positive than -70 mV (see asterisk in Fig. 1B).

The two (slow and delta) cellular rhythmicities and their relations to the field potentials recorded from the cortex and thalamus were also detected by first- and second-order statistics and STAs.

The autocorrelograms (Fig. 2A,B) show multiple major peaks recurring every ≈ 6 sec, reflecting the slow rhythm at 0.16 Hz, as well as minor peaks every ≈ 0.75 sec (arrowheads), reflecting the delta rhythm at 1.3 Hz. The smaller amplitude of delta peaks, as compared to those reflecting the slow oscillation, is due to (1) the smaller number of action potentials contributing the thalamically generated delta rhythm, as compared to those building up the slow cortical oscillations, and (2) resetting of the delta oscillation in the cortex by the rhythmic occurrence of the slow rhythm.

The analysis of the interspike interval (ISIH) distribution (Fig. 2C) revealed two peaks: (1) an early major mode at ≈ 0.04–0.12 sec, reflecting the ≈ 10–20 Hz frequency of spike trains during the depolarizing envelopes, and (2) a late mode at ≈ 0.7–0.8 sec, reflecting the silence periods between the single action potentials recurring at delta frequency (Fig. 2C, arrowhead). That the early mode did not reflect firing at 10–20 Hz due to spindle input from the thalamus is indicated by the presence of similar discharge rates on the depolarizing envelopes in thalamically lesioned animals, in which spindling is abolished (see Figs. 10, 12).

Finally, we averaged ECoG and EThG waves triggered by the first action potential in the depolarizing envelopes (dotted line in Fig. 2D). The STA shows that each depolarizing envelope
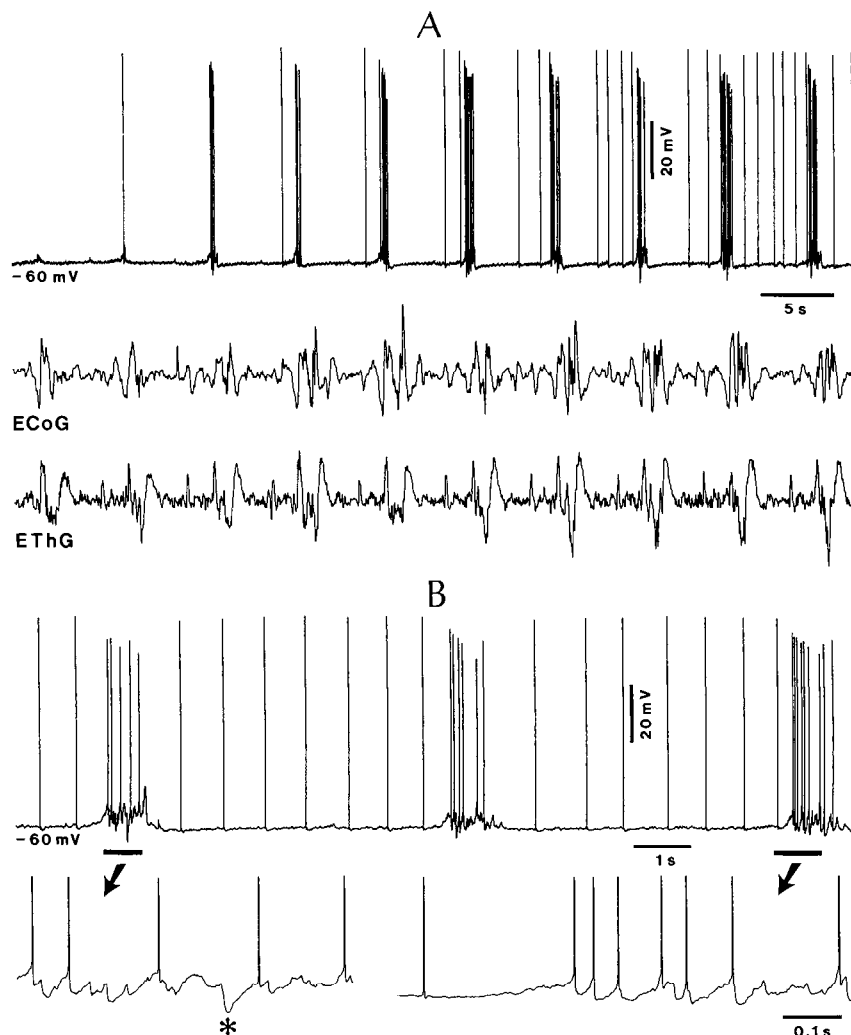
Figure 1. Slow (0.16 Hz) and delta (1.3 Hz) rhythms in regular-spiking, fast-adapting cell recorded at a depth of 0.6 mm in area 5. The neuron was synaptically driven from the LP and CL thalamic nuclei (at latencies of 3 and 2 msec, respectively) and from the contralateral area 5 (at a latency of 12 msec). *A*, Progressive buildup of both slow and delta oscillations with increasing EEG synchronization. Surface ECoG was recorded in area 5, 3 mm rostral to the impaled cell. EThG was recorded from the LP nucleus, through the same electrode that was used to drive the cell. Note the close relation between the slow cellular rhythm and the slow rhythm of ECoG and EThG wave complexes. *B*, Same cell, with fully developed slow and delta rhythms during later EEG-synchronized epoch. Periods marked by *horizontal bars* are expanded *below* (spikes are truncated) to show the details of repetitive spikes during the depolarizing envelopes and some IPSPs (*asterisk*). In this and following similar figures, resting V_m is indicated.

recurring with the slow rhythm (0.16 Hz) is coincident with a complex of EEG waves, starting with a sharp deflection and followed at ≈0.3–0.4 sec by a sequence of spindle waves at ≈10 Hz. Between the depolarizing envelopes, EEG delta waves are visible (arrowheads in middle trace of Fig. 2*D*), recurring at the same rhythm (1.3 Hz) as the stereotyped, periodic single action potentials depicted in Figure 1.

(2) The grouped delta events recurring with a slow rhythm were observed in 55% of the 105 cell sample. Phasic depolarizations and action potentials, occurring within a frequency range of 3–4 Hz, were superimposed on slow depolarizing envelopes recurring with the slow (0.3–0.4 Hz) rhythm (Fig. 3*A*). In a few cells (*n* = 5), we recorded similar events with QX-314–filled pipettes and observed that depolarizing waves, with an amplitude of ≈15 mV, a duration of 50–100 msec, and a frequency of 2–3 Hz, grouped in sequences repeating every 3–4 sec, survived the blockage of full Na⁺ spikes (data not shown).

In addition to intracellular recordings of regular-spiking neurons, as depicted in Figure 3*A*, we observed the same association of slow and delta rhythms in extracellular recordings. The discharge pattern of the neuron depicted in Figure 3*B* suggests its intrinsically bursting nature (see below intracellular recordings of similar bursting cells). The delta (3–4 Hz) oscillations of spike bursts, grouped in slowly recurring (0.3–0.4 Hz) sequences, were

closely related to similar rhythms in focal waves reflecting activities in a pool of neighboring cortical neurons.

While the aspect of focal waves illustrated in Figure 3*B* points to the summated activity of a neuronal group, synchronously displaying both delta and slow rhythms, this should not be taken as a general rule. With simultaneous extracellular recordings of two cells, both generally displayed the slow rhythm, but in less than half of such double recordings was the delta rhythm synchronously observed. The distribution of interspike intervals in the neuronal couple of Figure 4*A* shows that only cell *b* displayed a late mode (between 0.3 and 0.5 sec), thus suggesting that a delta rhythm (≈2.5 Hz) may be present. This was confirmed by autocorrelation analyses (Fig. 4*B*). Both cells, *a* and *b*, oscillated at 0.2 Hz, as seen from multiple peaks at ≈5 sec, but only cell *b* also exhibited multiple peaks reflecting a delta rhythmicity at 2.5 Hz (see inset). The two cells were synchronized in their slow oscillation (Fig. 4*C*), which was time-related with a similar rhythm of the surface EEG (Fig. 4*D*; compare Fig. 2*D*).

Relations between slow (<1 Hz) and spindle (7–14 Hz) rhythms

Combined spindle and slow rhythms were found in 26% of recorded neurons (*n* = 72). Both regular-spiking and intrinsically bursting neurons displayed the slow cortical rhythm, but they
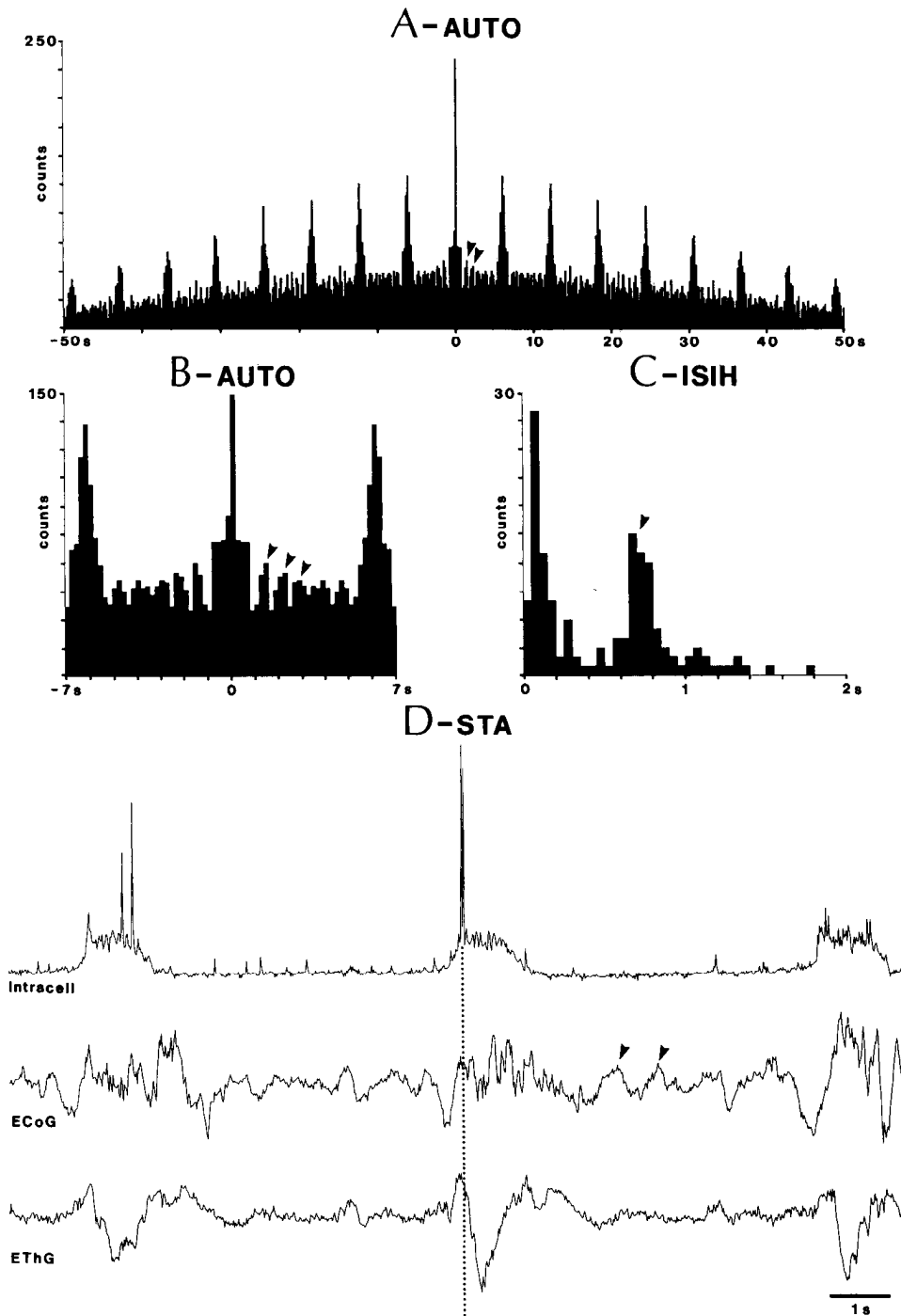
Figure 2. Analyses of slow and delta cellular rhythms related to activity patterns of ECoG and EThG (same cell as in Fig. 1). *A*, Autocorrelogram showing slow rhythm (0.16 Hz) as well as smaller peaks (*two arrowheads*) indicating delta rhythmicity (1.3 Hz) between depolarizing phases of slow rhythm (0.2 sec bin width and 100 sec window). *B*, Detail of *A* to show the delta peaks (*three arrowheads*). *C*, ISIH of cell firing during the analyzed epoch (50 msec bin). The first mode ($\approx$0.1 sec) reflects the $\approx$10 Hz repetitive discharges during the depolarizing envelopes recurring at the slow rhythm (0.16 Hz), while the second mode ($\approx$0.7–0.8 sec, *arrowhead*) reflects the delta rhythm (1.6 Hz) of single spikes between the slowly recurring depolarizing envelopes (see the original recordings in Fig. 1*B*). *D*, STA over a time period of 15 sec centered around the first action potential occurring during the slow rhythm of depolarizing envelopes (*dotted line*). The averaged intracellular trace ($n = 15$) is depicted with the averaged ipsilateral ECoG and ipsilateral EThG from the LP nucleus. Note three sequences of slow rhythm, spindle waves ($\approx$7–8 Hz) following the initial event of the slow rhythm, and delta waves ($\approx$1.3 Hz, two of them marked by *arrowheads*) between the slow rhythm.

had a differential propensity to follow the rhythmically synchronized spindle oscillations, known to be generated in the thalamus (see Steriade et al., 1990b).

(1) Regular-spiking cells ($n = 58$) exhibited the slow rhythm and also fully reflected the rhythm of thalamic spindles. The corticothalamic cell recipient of thalamocortical inputs depicted in Figure 5 (see *D* for physiological identification) oscillated with slowly recurring prolonged depolarizations, in close temporal relation with a similar rhythm of the EEG (Fig. 5*A*). Embryos of spindling were already visible at this stage of anesthesia on the top of some surface-positive EEG waves. A change in the EEG pattern (Fig. 5*B,C*) was associated with a diminished duration of cellular depolarizing envelopes and a reduction of the

superimposed discharges. At this point, steady hyperpolarizing currents blocked the majority of action potentials associated with the slow (0.2 Hz) depolarizations and revealed the spindle rhythm at 10–11 Hz. The amplitude of cellular spindle waves significantly increased toward the middle of the depolarizing envelopes when they reached $\approx$10 mV, each of them lasting for $\approx$40 msec (see inset in Fig. 5*C*).

(2) By contrast, intrinsically bursting neurons ($n = 14$), as identified by their burst responses to depolarizing current pulses (see Discussion), could not follow the spindle rhythmicity in its full extent. In spite of an EEG pattern demonstrating the clear presence of cortical spindles, grouped in slowly recurring sequences, the discharges of bursting neurons were only related
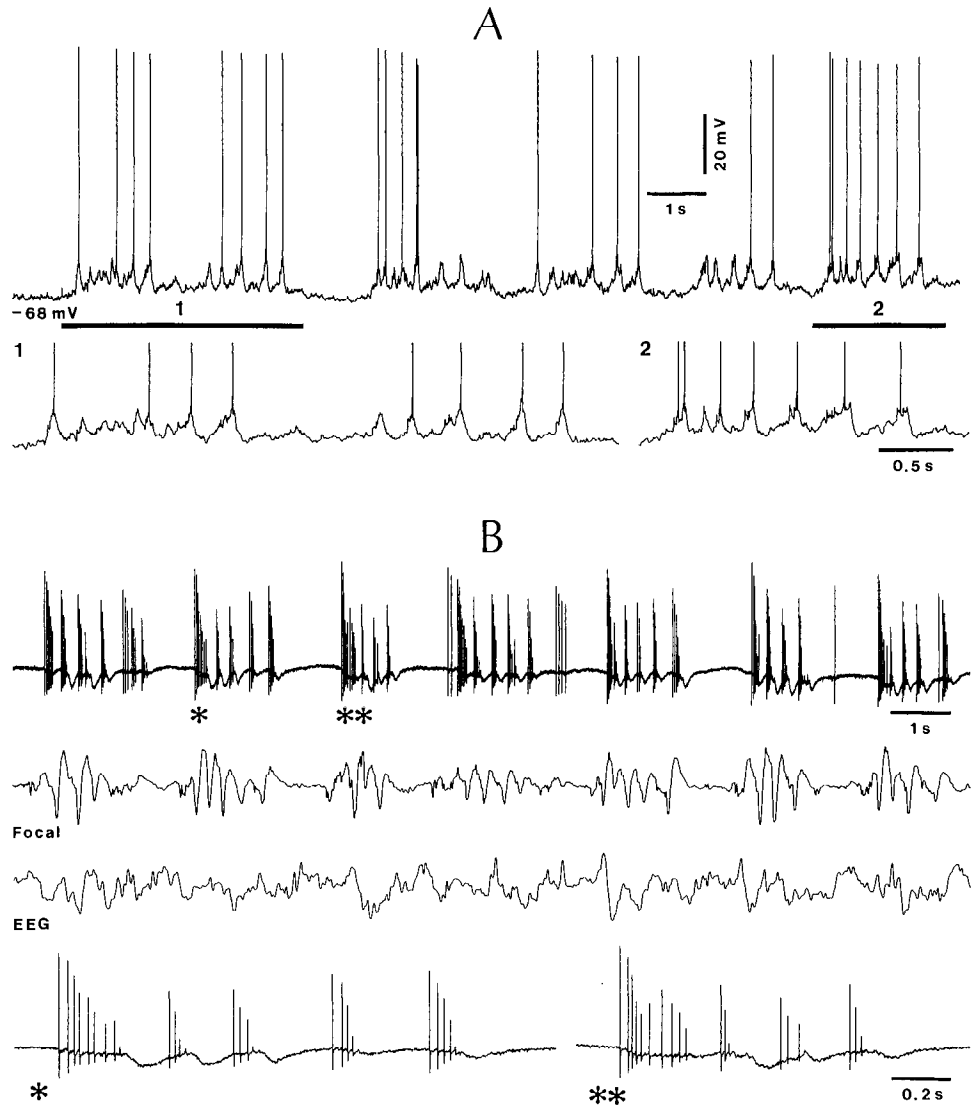
Figure 3. Delta (3–4 Hz) cellular oscillations grouped within sequences recurring with a slow (0.3–0.4 Hz) rhythm. *A*, Intracellular recording of a regular-spiking, slow-adapting neuron at a depth of 0.8 mm in area 5, driven synaptically from LP thalamic nucleus and backfired (3.5 msec latency) from the CL intralaminar thalamic nucleus. Parts marked by *horizontal bars (1, 2)* in the *upper trace* are expanded *below*. *B*, Extracellular recording of a bursting neuron at 0.6 mm in area 7, convergently excited by LP and CL thalamic nuclei. Below the cellular trace, focal waves recorded through the same micropipette and gross EEG waves recorded from the cortical surface are depicted. The sequence of spike bursts marked by *one* and *two asterisks* are expanded *below*.

to the slow rhythm, but did not follow the 7–14 Hz rhythm of spindles. During EEG spindle sequences, the neuron in Figure 6 oscillated with repetitive ($\approx$30 Hz) spikes eventually leading to well-formed spike bursts at >100 Hz, but the frequency of such groups of discharges did not exceed 2 Hz.

A similar aspect was seen in intrinsically bursting cells recorded under deep barbiturate anesthesia. Several EEG and cellular phenomena distinguished this type of anesthesia from those described until now (urethane and ketamine). First, spindling was overwhelming (Fig. 7A), even more so than in the isolated forebrain, a preparation characterized for its propensity to spindling (see below, Fig. 9). Between sequences of spindle waves recurring with a slow rhythm (0.1–0.2 Hz), waves at the upper range of delta or even higher were observed, but their amplitudes were not as high as those of spindles (Fig. 7A). Second, the thalamic and cortical synchrony of EEG spindle sequences was spectacular. This was seen between the thalamus and ipsilateral cortex, but also with the contralateral cortex (see the exception of a nonsynchronous spindle sequence in the contralateral cortex in Fig. 7A, open arrow). Third, under barbiturate anesthesia, we never recorded cellular activities within the frequency of delta waves, such as the stereotyped action

potentials illustrated in Figure 1. In these conditions, regular-spiking cells faithfully followed the frequency of thalamic spindles (see Fig. 6.20 in Steriade et al., 1990b). At variance, intrinsically bursting neurons (Fig. 7) oscillated at frequencies much lower (4–6 Hz) than the rhythm of the simultaneously recorded EEG spindle ($\approx$12–13 Hz). The intraburst frequency in these two cells was $\approx$150–200 Hz (see expanded records in Fig. 7A,B). The rhythm of cellular oscillation was lower than the frequency of EEG spindle waves even when the cells did not discharge spike bursts, but single spikes (Fig. 7A_2,B), and even when slight hyperpolarization blocked spike firing and only subthreshold spindle oscillations were recorded (see cellular spindle sequence at 6 Hz, extreme right in Fig. 7A_1, compared to EEG spindles at 12–13 Hz).

As mentioned above, the slow rhythm was predominant during urethane anesthesia, whereas spindle oscillations occurred more infrequently in this experimental condition. Administration of small doses (0.5–2 mg/kg, i.v.) of a short-acting barbiturate in a urethane-anesthetized animal produced an EEG change, from the slow rhythm (0.3 Hz) to sequences of fast spindles recurring with a rhythm of 0.6 Hz (Fig. 8). Correlatively, the intracellular recording showed that the prolonged
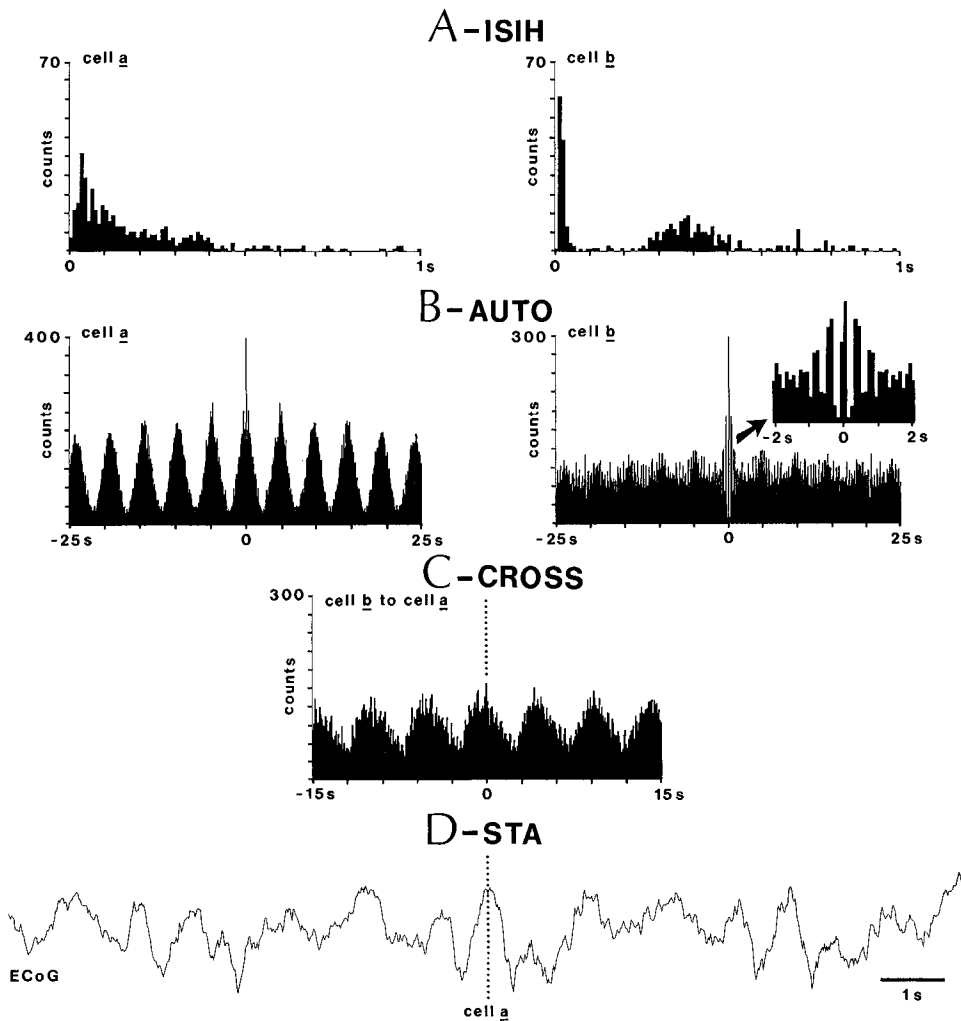
A – ISIH

B – AUTO

C – CROSS

D – STA

Figure 4. Slow and delta rhythms in two simultaneously (extracellularly) recorded neurons at 1.3 mm in motor area 4: single-spike discharging cell *a* and bursting cell *b*. *A*, ISIHs with 10 msec bins. Cell *b* displayed, in addition to the early mode of short intervals reflecting the intraburst intervals, a late mode between 0.3 and 0.5 sec reflecting the grouped spikes within the delta frequency ($\approx$2.5 Hz). *B*, Autocorrelograms (0.1 sec bin width and 50 sec window) showing the slow rhythm (0.2 Hz) in both cells. The delta rhythm (2.5 Hz) within the slowly (0.2 Hz) recurring discharge sequences in cell *b* is depicted in the expanded *inset* (*arrow*). *C*, Crosscorrelograms showing the synchrony between the two cells (cell *a* taken as reference; 0.1 sec bins and 30 sec window). *D*, STA between the initial action potential in the discharge train of cell *a* and ipsilateral ECoG.

($\approx$1–1.5 sec) depolarizing envelopes constituting the slow rhythm under urethane developed into faster recurring (0.6 Hz) depolarizations, with much shorter duration ($\approx$0.4 sec).

Intracellular recordings in isolated forebrain preparations

The possibility that urethane produces a slow rhythm that could not be otherwise detected, such as during natural EEG-synchronized sleep, was investigated by intracellular recordings of cortical cells in a brainstem-transected preparation that does not require large doses of anesthetics. It is known that full somatosensory deafferentation is produced by a cut rostral to the pontine site of trigeminal nerve's entrance. The best preparation exhibiting EEG synchronization with large-amplitude waves within the frequency range of different sleep oscillations is the animal with a transection at the low- or high-collicular level (Bremer, 1935). The EEG pattern depicted in Figure 9 is indicative of spindles ($\approx$9 Hz) and delta ($\approx$1–2 Hz) and slow ($\approx$0.3 Hz) rhythms, similarly to the bioelectrical activity recorded during natural sleep. Out of 18 recorded neurons in *cerveau isolé* preparations, 13 displayed the slow rhythm (Fig. 9), that is, a proportion similar to that found in deeply anesthetized animals.

The slow cortical rhythm survives extensive thalamic lesions

To determine whether or not the slow rhythm of cortical association neurons is critically dependent on the thalamus, we made extensive electrolytic or kainate-induced lesions of thalamic nuclei known to project to areas 5 and 7, that is, the PUL-LP complex, intralaminar CL-PC wing, and VA nucleus (see Jones, 1985). The chemical lesion depicted in Figure 10*A*, performed 2 d before the recording session, is a typical example for such experiments. We found a total loss of perikarya and their replacement by a massive gliosis in the PUL-LP, CL-PC, VA-VL and anteromedial–anteroventral (AM-AV) nuclear complexes, as well as $\approx$80% loss of cells in ventromedial (VM), VP complex, and MD nucleus (Fig. 10A_1–A_4), more than necessary to deprive areas 5 and 7 of their thalamic inputs completely. Since, as shown below, the slow rhythm was still recorded in the neocortex, in three animals we also made callosal sections in the commissural region connecting areas 5 and 7 of both hemispheres (Fig. 10*B*), in order to prevent the possibility that contralateral suprasylvian areas, driven from the thalamus, could induce the slow rhythm.

With recordings of both regular-spiking and intrinsically bursting cortical cells, we were able to demonstrate the presence of the slow rhythm in thalamically disconnected areas 5 and 7 cells ($n = 24$). (1) In experiments with only thalamic lesions (without callosal cuts), we could identify the recorded cells as projecting to, or receiving direct inputs from, contralateral area 5 or 7. Such neurons oscillated at 0.3–0.4 Hz, identically to those recorded in the intact brain. An example is illustrated in
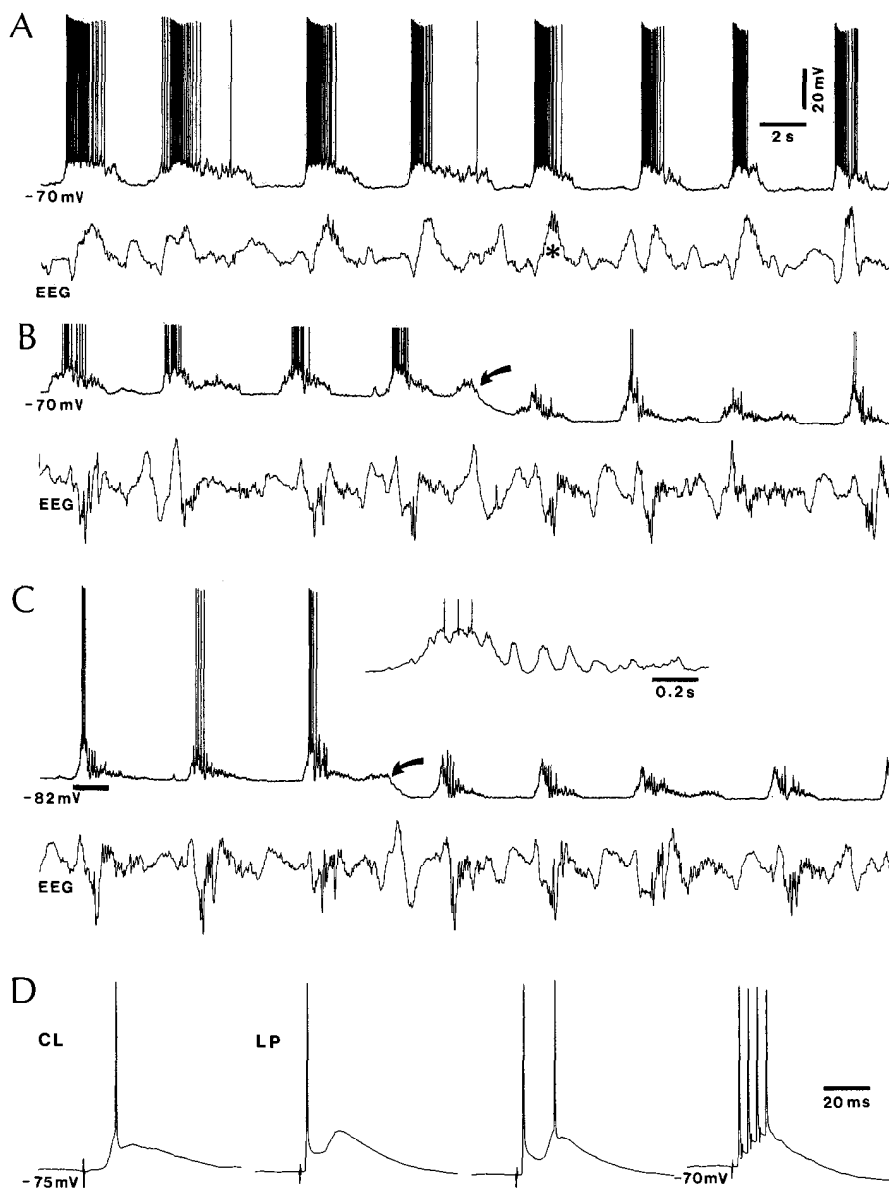
A

-70 mV

EEG

B

-70 mV

EEG

C

-82 mV

0.2 s

EEG

Figure 5. Slow rhythm and spindle oscillation: intracellular recording of regular-spiking, slow-adapting, corticothalamic cell, recorded at 1.5 mm in area 7. *A–C* show cellular activities during increasing EEG synchronization under urethane anesthesia. *Oblique arrows* in *B* and *C* indicate application of steady hyperpolarizing currents (−0.5 nA in *B*, and more −0.4 nA in *C*) to reveal sequences of cellular spindles (≈10–11 Hz) recurring with the slow rhythm (≈0.2 Hz). The intracellular spindle marked by *horizontal line* in *C* is expanded in *inset* (spikes truncated). *D*, Synaptic activation (7.5 msec latency) from CL thalamic nucleus; antidromic discharge (2.2. msec) followed by slow depolarization (peak at 18 msec), occasionally leading to spike discharge, in response to LP thalamic nucleus; and *faithful following of fast* (≈230 Hz) antidromic LP volleys.

D

CL   LP

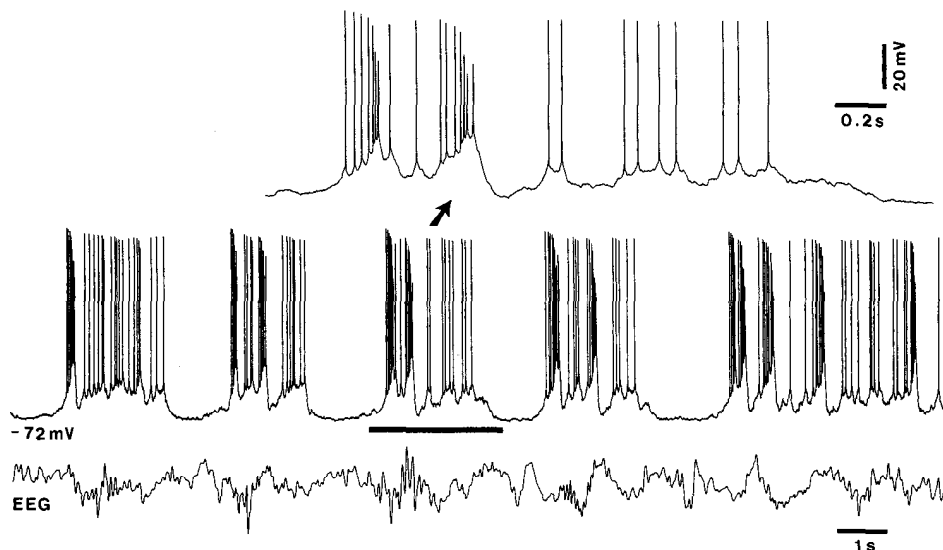-75 mV   -70mV

20 ms

Figure 6. Intrinsically bursting neuron does not follow the frequency of spindle oscillation: area 5 neuron at a depth of 1.3 mm, convergently driven from LP thalamic nucleus and contralateral cortex. Note EEG spindle waves (≈9 Hz) recurring with the slow rhythm (0.3 Hz). The burst sequences occurred in close time relation with the EEG slow rhythm, but the rhythm of cellular bursts was much slower (≈3–4 Hz) than that of spindles. Period marked by *horizontal line* is expanded *above*.
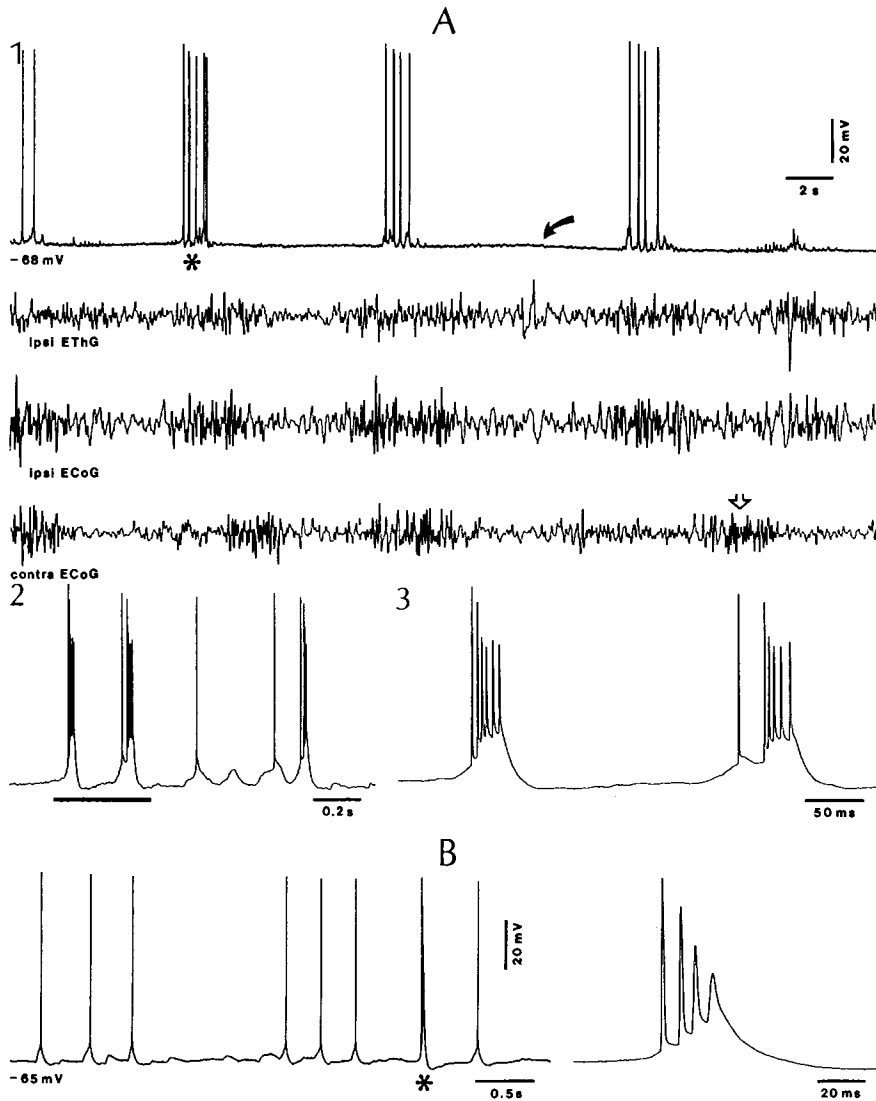
20 mV

0.2 s

-72 mV

EEG

1 s

Figure 7. Slow rhythm of barbiturate spindling and associated firing of intrinsically bursting neurons: recordings under deep (35 mg/kg) pentobarbital anesthesia. Two cells were recorded from area 5, at depths of 1 mm (*A*) and 1.5 mm (*B*). *A*, Simultaneous recordings of cellular spindling, ipsilateral EThG from CL intralaminar nucleus, and ipsilateral as well as contralateral ECoGs from area 5. Cellular spindle sequence marked by *asterisk* in *1* is expanded in *2*; part of the spindle in *2* marked by *horizontal line* is further expanded in *3* to show the pattern of spike bursts. Slight DC hyperpolarization in *1* is marked by *oblique arrow*. Open arrow on contralateral ECoG trace marks a spindle sequence that was not synchronous with the cell and ipsilateral EThG and ECoG spindling. *B*, A cellular spindle sequence in another cell; burst indicated by *asterisk* is expanded at *right*.

Figure 11*A*, with an intrinsically bursting cell firing stereotyped spike bursts at the onset of rhythmically recurring depolarizations. The bursts generally consisted of five or six action potentials, displaying one or two initial intervals of ≈10–12 msec, eventually leading to high-frequency (160–180 Hz) spikes. The callosally evoked spike bursts rode on a 30–40 msec EPSP (inset in Fig. 11*A*). (2) The slow cortical oscillation survived in animals having, in addition to massive thalamic destruction, callosal cuts disconnecting the right and left association suprasylvian cortices (Fig. 11*B*).

The physiological evidence that thalamocortical systems related to suprasylvian cortical neurons were out of function in these experiments using electrolytic or chemical lesions was provided by the absence of spindling in the cortical EEG. It is known that, after transections of corona radiata disconnecting the cortex from the thalamus (Steriade et al., 1987) or disconnection of thalamocortical cells from the thalamic pacemaking neurons of spindle oscillations (Steriade et al., 1985), cortical spindles are abolished, whereas slower sleep rhythms are preserved. This aspect was also observed in the present experiments with thalamic lesions (Fig. 12*A*). Moreover, administration of a short-acting barbiturate, well known for its potency in inducing

spindling, was not followed by cortical spindle oscillations in thalamically lesioned preparations; only slower EEG rhythms were present (Fig. 12*B*). At the cellular level, the effect of barbiturate administration was a change in the duration of rhythmic depolarizing envelopes and, consequently, an alteration in the frequency of the slow oscillation. Before barbiturate administration, the mean duration of cyclic depolarizations was >1 sec and the frequency of slow rhythm was ≈0.3 Hz, whereas 15–20 sec after thiamylal injection the mean duration of depolarizations was <0.5 sec and the frequency of the slow rhythm rose to ≈0.7 Hz (Fig. 12).

Modulation of the slow cortical rhythm by afferent drives: self-sustained changes after thalamic and cortical stimulation

Although the data presented above indicate that the thalamus is not involved in the genesis of the slow cortical rhythmicity, electrical stimulation of appropriate thalamic nuclei induced short- or long-lasting changes in target cortical neurons. As a rule, the slow rhythm was disrupted by thalamic single shocks, inducing long-lasting IPSPs in cortical cells, but this change did not outlast stimulus application (Fig. 13*A*). Much less commonly ($n = 3$), the slow rhythm (0.3–0.4 Hz) changed its fre-
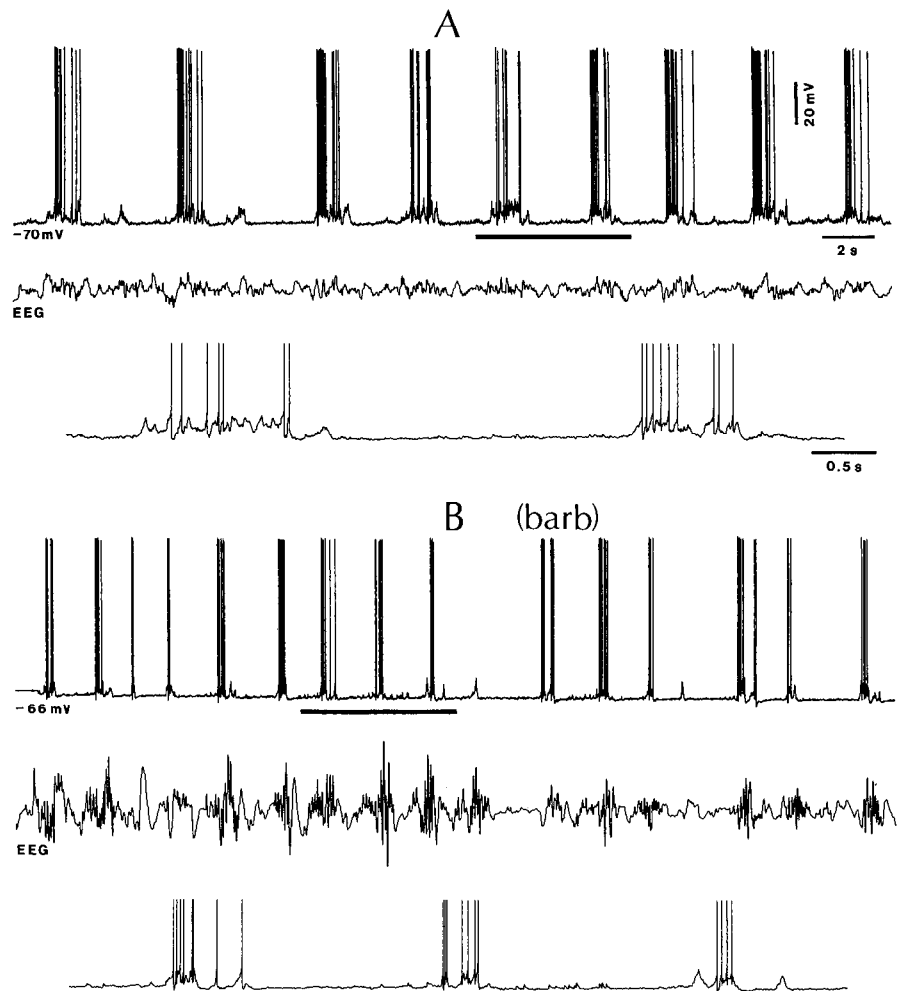
Figure 8. Effect of small dose of short-lasting barbiturate in urethane-anesthetized animal: regular-spiking cell in area 5b (depth 0.5 mm). *A,* Slow rhythm (≈0.3 Hz) of cellular activity during urethane anesthesia. Part indicated by *horizontal line* is expanded *below* (spikes truncated). *B,* Same cell after 2 mg/kg intravenous administration of a short-lasting barbiturate (thiamylal). Part indicated by *horizontal line* is expanded *below* (spikes truncated).

quency to a higher one, within the delta frequency range (1–2 Hz), after repeated trains of thalamic stimuli inducing incremental responses of the augmenting type. Importantly, such a change outlasted thalamic stimulation for 25–40 sec (Fig. 13*B*).

Dramatic changes in cortical rhythmicity, with persistent alterations of cellular activity after the cessation of stimuli, could be induced by repetitive shocks to the contralateral association cortex in thalamically lesioned animals. The intrinsically bursting, layer V cell, recorded from area 7 in an animal with an extensive thalamic lesion (Fig. 14*A*), oscillated at the slow rhythm (0.4 Hz). Stimulation of contralateral area 7 with trains of five shocks at 10 Hz induced augmenting responses, similar to those elicited by thalamic stimulation in a brain-intact preparation. This result is in line with previous data showing that cortical augmenting responses can be elicited by white matter stimulation even after destruction of appropriate thalamic nuclei (Morin and Steriade, 1981; Ferster and Lindström, 1983). The pattern of incremental corticocortical responses changed with the progressive repetition of pulse trains, displaying an increased number of action potentials within each evoked burst on a background of V_m depolarization by ≈7 mV (Fig. 14*B*). After the interruption of cortical stimulation, the neuron discharged *spontaneously* spike bursts at 10–12 Hz (very similar to those evoked in the last period of cortical stimulation), interrupted by long spike bursts recurring with the slow rhythm (0.4 Hz).

Discussion

The variety of cortical sleep oscillations

We have demonstrated that, during states mimicking natural EEG-synchronized sleep, the neocortical electrical activity is characterized by three major types of oscillations within the frequency range of ≈0.3 Hz, 1–4 Hz, and 7–14 Hz. This is valid for animals maintained under deep anesthesia as well as for deafferented, brainstem-transected, undrugged preparations. Parallel studies performed in this laboratory by means of multisite cellular recordings in the neocortex and thalamus of naturally sleeping cats and EEG recordings during human sleep have shown that this variety of oscillations also characterizes the normal behavioral state of quiescent sleep (see also Fig. 1 in Steriade et al., 1993a).

The interest of our findings mainly consists of revealing the diversity of sleep oscillations, with each of different rhythms arising from given intrinsic cellular properties or synaptic mechanisms, but all combined into patterns of activities generated by complex synaptic articulations in intracortical, intrathalamic, and corticothalamocortical networks. Until quite recently, it was assumed, on the basis of incomplete evidence, that the thalamus is the site of genesis of spindle oscillations while the cortex generates delta waves (Steriade et al., 1990b) and the cortical oscillation grouping EEG delta waves with a rhythm at ≈0.3
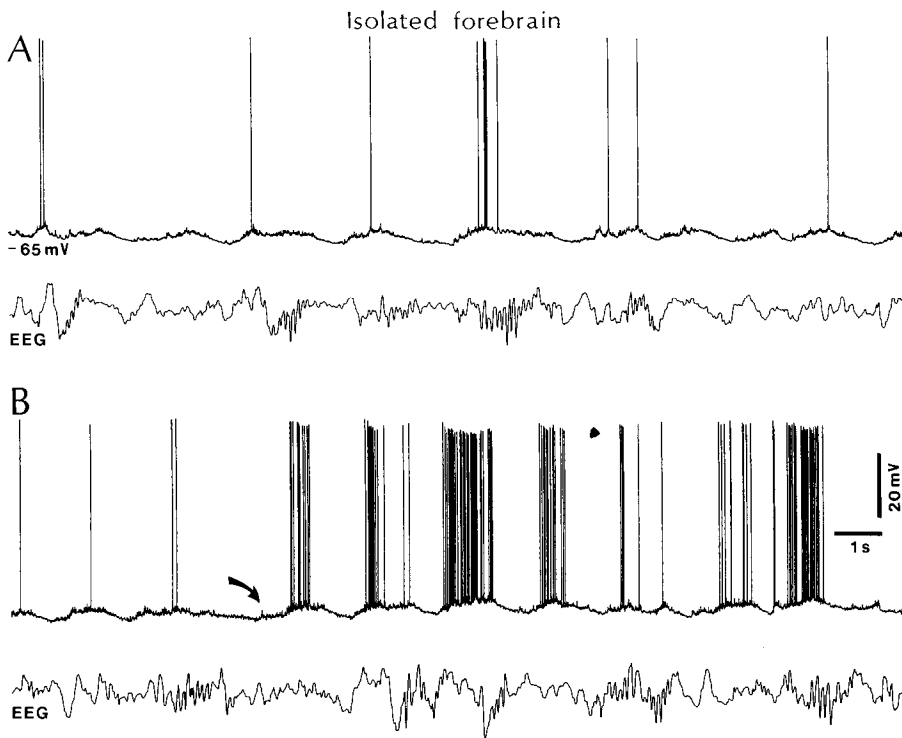
Isolated forebrain

A

-65 mV

EEG

B

EEG

Figure 9. The slow cortical rhythm is present in the undrugged *cerveau isolé* preparation: regular-spiking, slow-adapting cell recorded at a depth of 0.5 mm in area 7. The cellular depolarizing envelopes and the EEG sequences of spindle waves synchronously recurred with the slow rhythm ($\approx$0.4 Hz). *A* and *B* are continuous recordings; slight DC depolarization from resting V_m (−65 mV) was applied in *B* (*oblique arrow*) to show the pattern of neuronal discharges.

Hz was not known. The present set of experimental data provide evidence that, although the intrinsic electrophysiological properties are of fundamental importance for the propensity of single neurons to oscillate (Llinás, 1988), the detailed analysis of neuronal substrates underlying the rhythms distinguishing various states of vigilance can be achieved only by intracellular recordings in a preparation with preserved circuitry, the condition under which billions of elements are interacting as a unity to generate the global electrical activity of the brain.

Interaction between slow and delta oscillations

The common designation of "sleep delta waves" under the frequency range from 0.5 to 4 Hz, as generally used in clinical EEG and experimental studies of brain rhythms, conceals at least two rhythms with different sites of genesis and dissimilar neuronal mechanisms. The intrinsic cellular properties and synaptic mechanisms involved in the genesis of the slow neocortical rhythm (<1 Hz, mainly $\approx$0.3 Hz) are the topic of the preceding article (Steriade et al., 1993a). The assumption that the slow rhythm is generated within the cortex is substantiated by the present results showing the survival of this oscillation in thalamectomized preparations. The thalamic origin of delta (1–4 Hz) rhythm and the interaction between delta and slow rhythms through thalamocortical circuits are discussed below.

Although delta sleep activity was classically regarded as a rhythm arising in the cerebral cortex because laminar analyses of these waves found vertical sink–source relationships to EEG potentials at various cortical depths (Ball et al., 1977; Petsche et al., 1984), there is now accumulating evidence that delta activity also originates in the thalamus and is transferred to cortical neurons in different layers. Within the cortex, active excitatory–inhibitory synaptic processes and long-lasting intrinsic currents build up the delta waves, as reflected at the cortical surface. Earlier extracellular studies have reported spike bursts within the delta frequency range (2–4 Hz) in VL and dorsal

lateral geniculate (dLG) thalamic nuclei (Lamarre et al., 1971; McCarley et al., 1983). Some of these spike bursts could have been delta events. However, it is now known from intracellular studies that such slowly recurring spike bursts may well reflect spindles, not necessarily delta oscillations, because thalamocortical cells do not discharge postinhibitory rebound bursts after each IPSP related to the spindle frequency (7–14 Hz), but only one burst after two, three, or more IPSPs (Roy et al., 1984; Steriade and Llinás, 1988). Besides, at least in the case of VL thalamic nucleus, spike bursts at the same frequency as delta (1–2 Hz) may be the consequence of spike barrages with a similar frequency in afferent neurons recorded from deep cerebellar nuclei (Steriade et al., 1971).

That a stereotyped delta oscillation between 1 and 4 Hz is indeed generated in the thalamus was unambiguously demonstrated in recent intracellular studies of thalamocortical cells recorded from dLG and VP slices (McCormick and Pape, 1990a,b; Leresche et al., 1991; Soltesz et al., 1991) and from a variety of sensory, motor, associational, and intralaminar thalamic nuclei *in vivo* (Steriade et al., 1991; Curró Dossi et al., 1992; Nuñez et al., 1992a). McCormick and Pape (1990a) have proposed a model of delta oscillation resulting from the interplay between two membrane intrinsic currents present in thalamic cells: (1) a hyperpolarization-activated inward (anomalous) rectifier carried by Na$^+$ and K$^+$ (I_h) (Pape and McCormick, 1989), and (2) a transient Ca^{2+} current (I_t) underlying the low-threshold spike (LTS) giving rise to bursts of high-frequency, fast Na$^+$ action potentials (Jahnsen and Llinás, 1984a,b). According to this model, the hyperpolarization of thalamocortical cells activates the I_h, which depolarizes the membrane toward threshold for a Ca^{2+}-dependent LTS crowned by a burst of Na$^+$ fast spikes; this depolarization inactivates the I_h and the resulting hyperpolarizing overshoot again triggers the I_h, which depolarizes the membrane toward another LTS. The cycle could ideally repeat forever provided that the two processes of I_h–I_t activation–in-
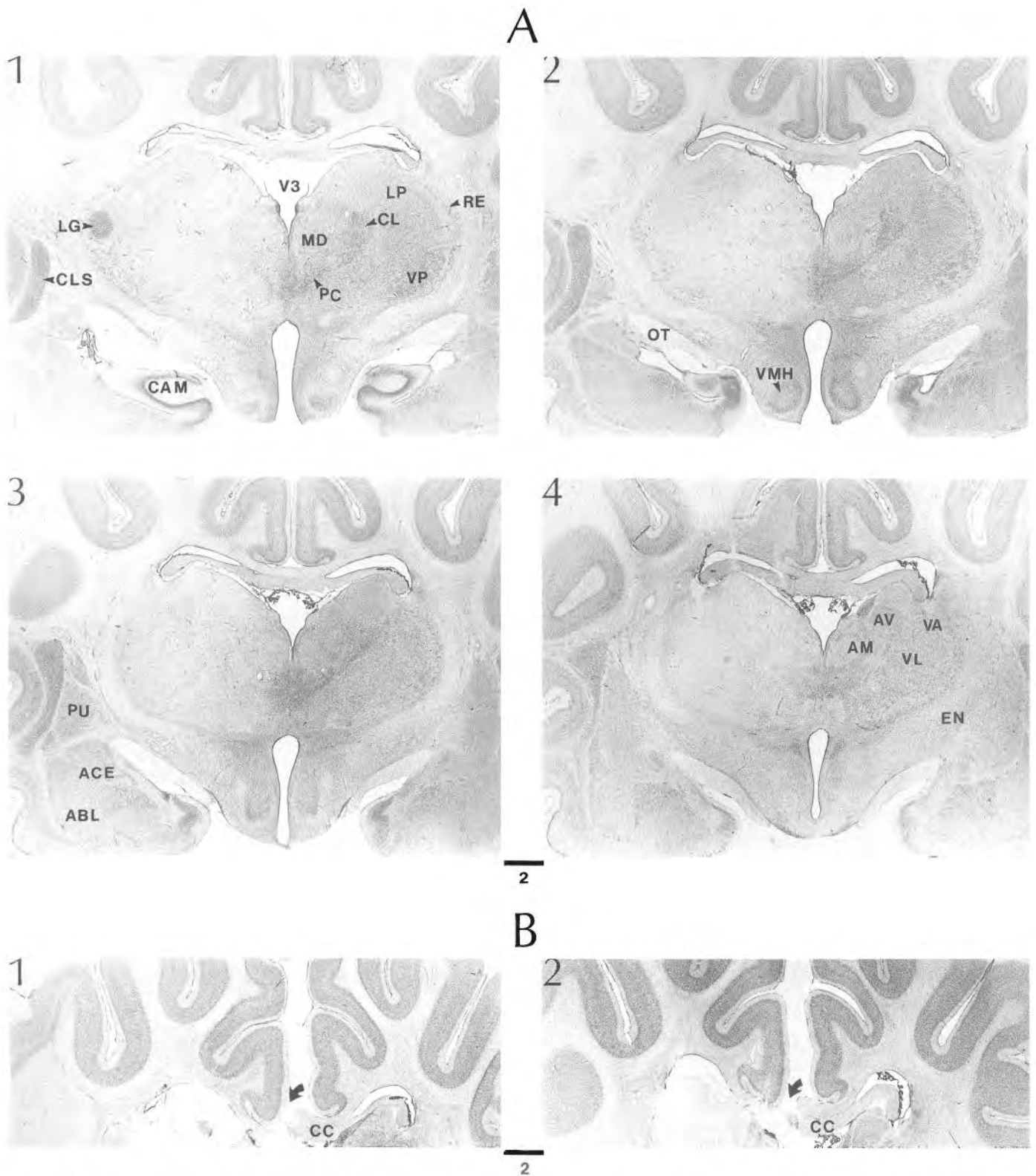
Figure 10. Thalamic lesions and callosal cuts. *A,* Extensive kainic lesion of thalamic perikarya, ipsilateral to recorded cortical neurons displaying the slow rhythm. *1–4,* Four frontal sections (from caudal to rostral). Note three penetrations of the Hamilton syringe through the corpus callosum in *section 4. ABL* and *ACE,* basolateral and centrolateral amygdaloid nuclei; *AM* and *AV,* anteromedial and anteroventral thalamic nuclei; *CAM,* corpus Ammoni; *CL,* centrolateral intralaminar thalamic nucleus; *CLS,* claustrum; *EN,* entopeduncular nucleus; *LG,* lateral geniculate nucleus; *LP,* lateroposterior thalamic nucleus; *MD,* mediodorsal thalamic nucleus; *OT,* optic tract; *PC,* paracentral intralaminar thalamic nucleus; *PU,* putamen; *RE,* reticular thalamic nucleus; *VA* and *VL,* ventroanterior and ventrolateral thalamic nuclei; *VMH,* ventromedial nucleus of hypothalamus; *V3,* third ventricle. *B,* Frontal sections showing callosal cuts (*arrows*) at two levels in a cat with extensive electrolytic thalamic lesion. *CC,* corpus callosum. *Horizontal bars* indicate millimeters.
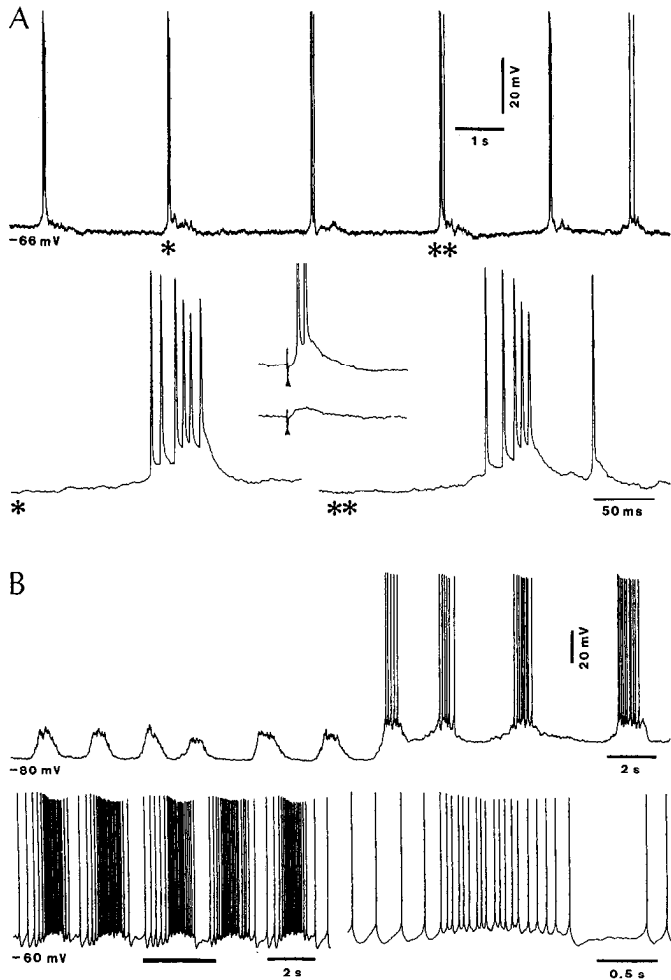
Figure 11. Slow (0.3–0.4 Hz) rhythms of suprasylvian cortical neurons after extensive lesions of thalamic inputs. *A*, Intrinsically bursting cell at 1.1 mm in area 5. Bursts marked by *one* and *two asterisks* are expanded *below*. *Inset*, Spike doublet and, *below*, EPSP elicited by stimulation of contralateral area 5 with decreasing stimulus strengths (*arrowheads*). *B*, Regular-spiking cell at 0.5 mm in area 7. In this animal, corpus callosum was also transected. Rhythmic depolarizing envelopes at the resting V_m (−80 mV) are seen, with action potentials upon DC depolarization (*right part in upper trace*), and further depolarization to −60 mV (*bottom trace*). Part marked by *horizontal bars on bottom trace* is expanded at *right* to show a period (≈0.5 sec) of silenced firing after the repetitive spikes riding on the depolarizing oscillation.

Figure 12. Slow cellular rhythm (0.3 Hz) of area 7 neuron in animal with extensive thalamic lesion and the effect of thiamylal (2.5 mg/kg, i.v.).

activation alternate with one another. The role of voltage-dependent currents in the genesis of thalamic delta oscillation is demonstrated by abolition of this rhythm after administration of I_h and I_t blockers, Cs^+ and Ni^{2+}, respectively (Leresche et al., 1990; McCormick and Pape, 1990a; Soltesz et al., 1991). It is also worth mentioning in this context that, although cortical cells also possess the I_h (Spain et al., 1991), at least in areas 5 and 7 they do not display the intrinsic delta oscillation, because the proportion of cortical association neurons having the I_t underlying the LTS is quite low (10%) and the level of hyperpolarization required to deinactivate this current is around −90 to −100 mV (Nuñez et al., 1993).

Thus, delta oscillation is generated by two currents of thalamocortical cells when their V_m is hyperpolarized by about 10–15 mV. This alteration occurs during natural slow-wave sleep (Hirsch et al., 1983), mainly because of the decrease in firing
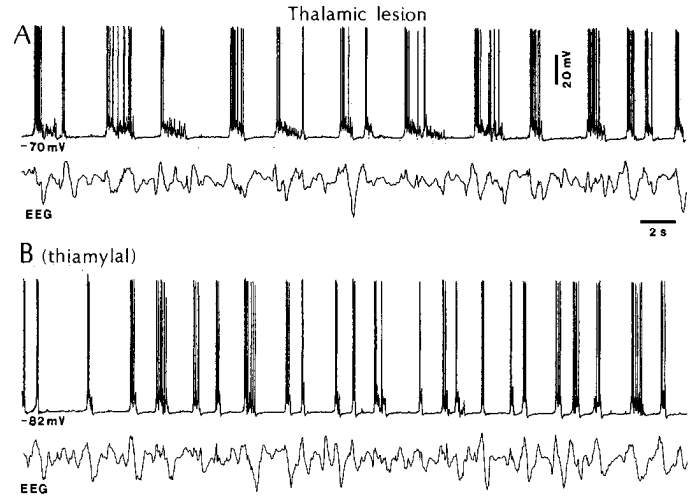
rates of activating cholinergic and monoaminergic brainstem neurons (reviewed in Steriade and McCarley, 1990). Indeed, the depolarization of thalamic cells by setting into action mesopontine cholinergic neurons (Curró Dossi et al., 1991) leads to blockage of rhythmically recurring LTSs within the frequency range of delta oscillation (Steriade et al., 1991). Another factor leading to the hyperpolarization of thalamic neurons during slow-wave sleep is the decreased firing rates of corticothalamic cells (Steriade, 1978). During waking, the cortical input produces a prolonged depolarization of thalamic cells resulting from a reduction in a resting K^+ conductance, I_{KL}, through the activation of glutamate metabotropic receptors (McCormick and van Krosigk, 1992). After removal of the powerful depolarizing impingement of cortical origin, thalamic neurons are hyperpolarized by about 10 mV and, consequently, spontaneous delta oscillations are seen in virtually all recorded neurons (Curró Dossi et al., 1992).

How are singly oscillating thalamic cells synchronized into neuronal ensembles, and how is it that a stereotyped, clocklike, intrinsic oscillation is transformed into polymorphous, irregular EEG delta waves?

(1) First, although delta is typically an intrinsic oscillation of single neurons, it cannot be reflected at the macroscopic level of the EEG unless thalamic neurons are synchronized (Steriade et al., 1991). This process is mainly achieved through long-range (reticular, RE) or short-range (local-circuit) GABAergic inhibitory thalamic neurons and, in some cases, through synaptic coupling between thalamocortical cells. Both inhibitory (RE and local-circuit) thalamic cellular types can effectively set the V_m of thalamocortical neurons at the required level for the genesis of the hyperpolarization-activated delta rhythm.

The role of RE neurons is indicated by the fact that potentiation and synchronization of thalamic delta rhythmicity may result from stimulation of cortical areas that are not directly related to the recorded thalamic neurons (Steriade et al., 1991). It is known that rostrolateral sectors of the RE nuclear complex are convergently afferented by multiple cortical areas and, in turn, project to widespread thalamic territories (Steriade et al., 1984; Jones, 1985).

As to local-circuit inhibitory thalamic cells, they may be powerfully driven by corticothalamic neurons receiving the rhyth-

Figure 13. Modification of slow cortical rhythm by thalamic stimulation. *A,* Regular-spiking, corticothalamic cell in area 5 (backfired from CL nucleus), displaying a slow rhythm (0.4 Hz) consisting of depolarizing–hyperpolarizing sequences. The rhythm was disrupted by 1/sec single-shock stimulation of LP thalamic nucleus (*right part in upper trace* and *left part in bottom trace*). Each LP stimulus gave rise to a long-lasting (≈0.5 sec) IPSP. After two LP stimuli separated by 3 sec, LP stimulation was interrupted and the slow rhythm resumed with the previous frequency at 0.4 Hz (*bottom trace*). *B,* Regular-spiking neuron in area 5, with slow depolarizing envelopes recurring at 0.4 Hz. LP thalamic repetitive stimulation [five-shock trains at 10 Hz, every 3 sec; averaged (*AVG*), augmenting cortical responses are depicted in *inset*] produced an increased frequency of the cortical rhythm; this effect outlasted thalamic stimulation as a self-sustained oscillation at 1.6 Hz. *Top* and *bottom traces* are continuous recordings.
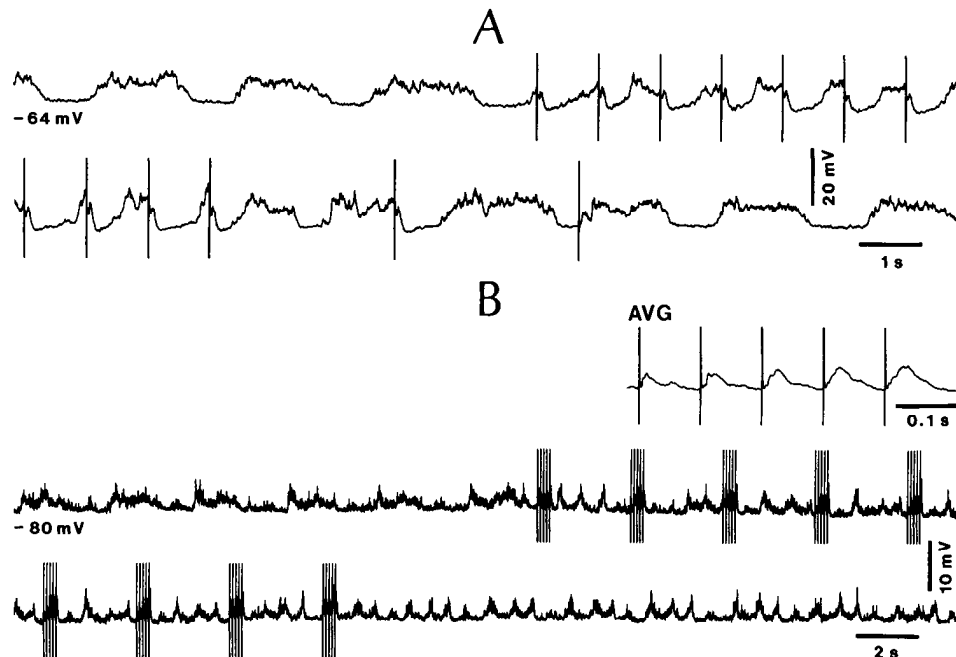
mic spike bursts building up the delta oscillation of thalamo-cortical cells. Since thalamocortical cells do not generally possess recurrent axonal collaterals (see Steriade et al., 1990b), local-circuit cells are not directly driven by thalamic relay cells located in the same nucleus. However, this morphological feature is possible when intranuclear recurrent axonal collaterals of cortically projecting thalamic cells are demonstrated. Of all thalamic nucleus so far investigated, this is seemingly the case of only dLG nucleus (Friedländer et al., 1981; Humphrey and Weller, 1988). In this case, however, no systematic electron microscopic studies have been performed and one may ask whether the collaterals were given off earlier in their route to the perigeniculate sector of the RE nucleus.

Nonetheless, electrophysiological evidence of delta synchrony in the dLG nucleus was recently provided in two intracellular studies, *in vitro* (Soltesz and Crunelli, 1992) and *in vivo* (Nuñez et al., 1992b). These experiments showed that, in addition to the intrinsically oscillating cells, other dLG neurons displayed the same delta frequency, but their rhythm was synaptically generated through coupling of thalamic relay cells by intranuclear axonal collaterals. Indeed, the rhythmic depolarizations of the synaptically induced delta rhythm consisted of grouped EPSPs and FPPs, developing into clocklike LTSs under slight hyperpolarization (Nuñez et al., 1992b). In the *in vitro* condition, the low-frequency, rhythmic EPSPs were abolished by TTX (Soltesz and Crunelli, 1992).

Thus, both long- and short-range circuits, possibly inhibitory as well as excitatory, can synchronize thalamic neurons. Synchronization within the frequency range of delta rhythm has recently been detected by multisite recordings in the RE and various dorsal thalamic nuclei of anesthetized or naturally sleeping animals (D. Contreras and M. Steriade, unpublished observations). However, the epochs during which synchronization was evident were rather limited in time. This probably explains why clocklike delta potentials, as illustrated in the present Fig-

ures 1 and 2, were seen in only a minority (17%) of cortical neurons. Also, the visible association at the cortical level between the slow and delta rhythms depends, on one hand, on the synchrony of thalamic neuronal pools exhibiting delta oscillation, and, on the other hand, on the recording sites in the cortical target areas. Future experiments, with multiple fine and coarse electrodes inserted in thalamic nuclei and related neocortical areas (as determined by ortho- and antidromic identification procedures), should quantitatively assess the association of slow and delta rhythms at single-cell and population levels in various thalamocortical systems and to determine the state dependency of this combined rhythmicity (e.g., its possible occurrence during late stages of natural sleep, as opposed to the presumed association between the slow rhythm and spindle oscillations in early sleep stages).

(2) Second, the thalamically generated delta oscillation is reflected on the EEG after intercalated excitatory and inhibitory processes in complex cortical networks. This passage probably accounts for the smoother, less regular aspect of EEG waves within delta frequencies. Thalamically generated events are transformed by multiple synaptic operations within the cortex, probably in a more complex way than that by which the signals of cortical origin undergo changes in the thalamus before being processed back to the cortex. For example, the single action potentials occurring within the delta frequency during the interdepolarization lulls of the slow rhythm are cyclically interrupted in some neurons (Fig. 1), probably because the slow cortical rhythm is imposed upon thalamic cells as a rhythmic depolarizing event (see Figs. 9, 10 in Steriade et al., 1993b) and this depolarization would bring thalamic relay cells out of the voltage range where delta rhythm is generated. As to the thalamic rhythms transmitted to cortex, the grouping of delta potentials within the frequency of slow oscillation (Fig. 3) is attributable to the rhythmic interruption of delta events by prolonged GABAergic synaptic processes and/or Ca^{2+}-dependent
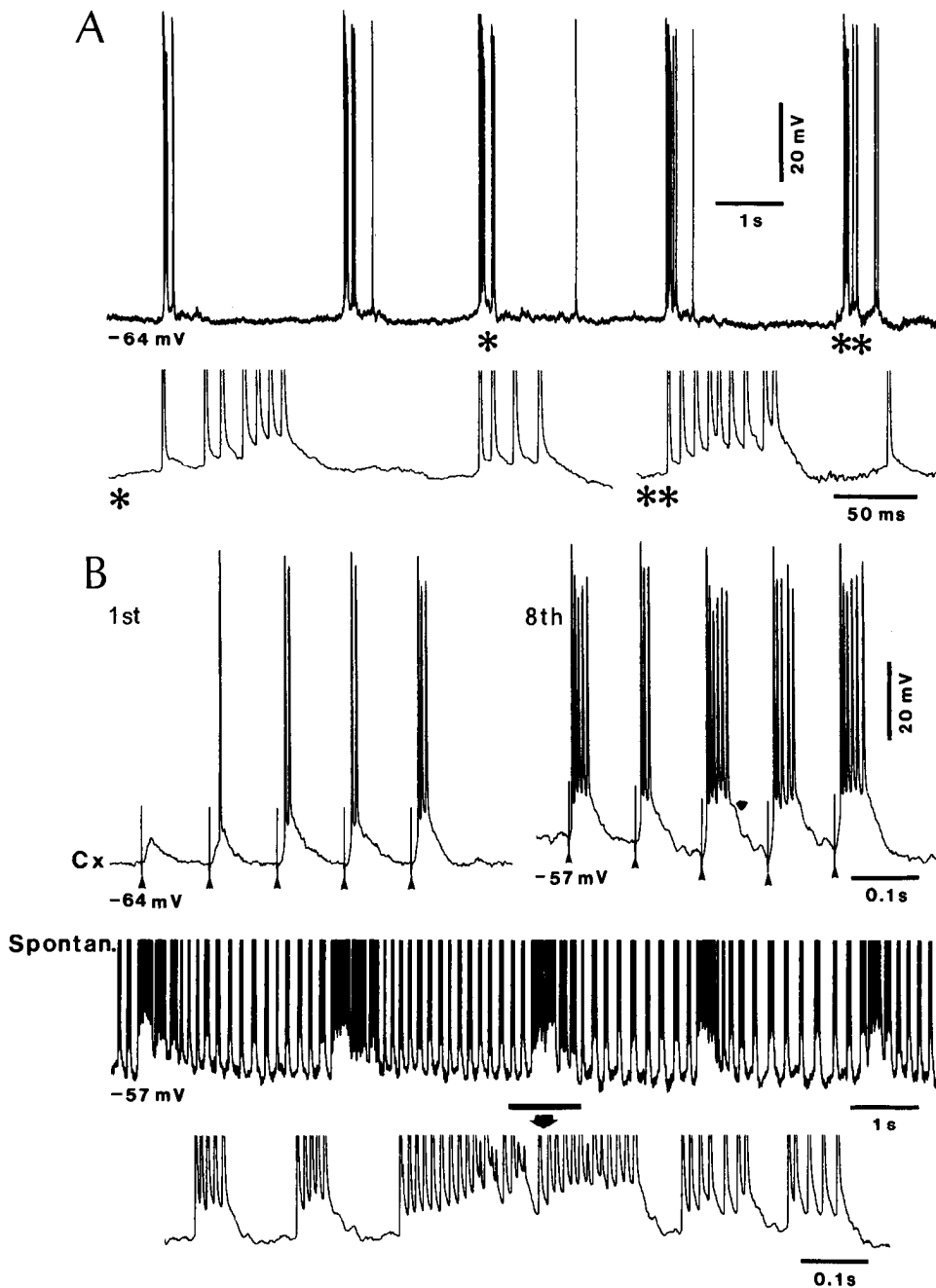
Figure 14. Self-sustained oscillation after repetitive cortical stimulation in a thalamically lesioned animal: intrinsically bursting neuron, recorded at 1.5 mm in area 7. A, Slow rhythm (0.4 Hz). Bursts marked by one and two asterisks are expanded below (spikes truncated). B, Responses of the same cell to repetitive stimulation (five-shock trains at 10 Hz, repeated every 3 sec) of the contralateral area 7. The augmenting responses to the first and eighth trains are illustrated. Spontaneous (Spontan.) activity is illustrated after 15 such cortical shock trains.

K$^+$ currents in cortical neurons (see evidence for this in Steriade et al., 1993a).

(3) Last, although we know that stereotyped delta oscillations are generated in the thalamus, we still need conclusive evidence of whether or not delta waves may also originate in the cortex, in the absence of the thalamus. If so, this would also explain the irregularity and polymorphism of EEG delta waves. Earlier experiments indicated that large thalamic lesions suppressed cortical spindles, but EEG delta waves were preserved in the cortex (Villablanca and Salinas-Zeballos, 1972). This was a major argument for the cortical origin of EEG delta rhythm. Total thalamectomy is, however, a heroic procedure that may leave intact some parts of the thalamus. Indeed, the anatomical study of those "athalamic" animals showed that "the thalamus was

almost completely removed" (Villablanca and Salinas-Zeballos, 1972, p 386). Morphological work during the past 15 years demonstrated that some thalamic nuclei, to only mention the VM and intralaminar CL-PC wing, have diffuse projections to the neocortical convexity (see reviews in Jones, 1985; Macchi and Bentivoglio, 1986). This might explain, in the version of the thalamic genesis of delta oscillation, the presence of EEG delta waves on some cortical fields. Accepting, however, the results of experiments with extensive thalamic lesions, leaving intact delta waves in the cortex, we have to take into serious consideration the possibility that at least some types of delta waves arise in the cortex after total thalamic destruction. Although this issue is not settled at the present time, we would like to suggest that the clocklike, stereotyped delta oscillation,

occurring during the interdepolarization lulls (Fig. 1), is generated by intrinsic properties of thalamic cells, whereas the cellular events within the delta frequency and superimposed upon the slow depolarizing envelopes (Fig. 3) may have a more complex origin, including their genesis within the cerebral cortex.

The slow cortical rhythm modulates the slow rhythm of thalamically generated spindle sequences

Spindles (7–14 Hz) are generated in the thalamus in the absence of the cerebral cortex (Morison and Bassett, 1945), but cortical volleys may reinforce this type of thalamic rhythmicity, "presumably by facilitation fed back" (Morison and Dempsey, 1943, p 307). This considerably important statement was generally neglected, in spite of similar ideas on reverberating thalamocorticothalamic circuits (Dusser de Barenne and McCulloch, 1938; Chang, 1950).

The pacemaking role of the RE thalamic nucleus in spindle genesis was demonstrated by absence of spindles in thalamic territories disconnected by lesions or naturally devoid of inputs from the RE nucleus (Steriade et al., 1985; Paré et al., 1987) and by preservation of spindle rhythmicity in the isolated RE nucleus, that is, deafferented from the dorsal thalamus and cerebral cortex (Steriade et al., 1987). These results from cat experiments are strengthened by abolition of spindling in thalamocortical systems after RE lesions in rats (Buzsáki et al., 1988). Recently, the role of RE neurons in promoting and synchronizing EEG spindles was confirmed by elicitation of spindling after chemical excitation of RE perikarya; the phenomenon was so impressive that spindle sequences protruded into the state of rapid eye movement sleep, when the EEG is usually desynchronized (Marini et al., 1992).

Spindle waves are grouped in sequences lasting for 1.5–3 sec and recurring periodically, every 5–10 sec. Although, with the benefit of hindsight, this slow (0.1–0.2 Hz) rhythm can be seen in early EEG recordings of animals and humans, it was only lately described (Steriade and Deschênes, 1984). As yet, we have no explanation about the intrinsic or synaptic origin of the slow rhythm separating the sequences of spindle waves (interspindle rhythm). Studies of cat dLG slices done by Crunelli's group (Leresche et al., 1991) have reported that sequences of "spindle-like" waves (so termed by those authors) recurred every ≈10 sec, even after TTX application, thus pointing to the intrinsic nature of this slow (0.1 Hz) rhythm. However, the frequency of those "spindles" was ≈2–2.5 Hz (at least three times lower than the frequency of bona fide spindles in a living animal) and the mean duration of a "spindle" sequence was 8.5 sec (three to four times longer than *in vivo*). To add to these dissimilarities, DC depolarization decreased the frequency of "spindles" and resulted into their transformation into the pacemaker oscillation of the delta type (Leresche et al., 1991), whereas *in vivo* experiments showed that the transformation of spindles into delta oscillation is brought about by hyperpolarization of thalamic cells with either DC current (Steriade et al., 1991; Nuñez et al., 1992a) or application of NMDA blockers (Buzsáki, 1991). Lastly, the so-called "spindles" in that *in vitro* study were depolarizing events, whereas all *in vivo* intracellular studies of thalamocortical neurons have described this oscillation as consisting of rhythmic (7–14 Hz) hyperpolarizing IPSPs, associated with a large increase in membrane conductance (Andersen and Sears, 1964; Maekawa and Purpura, 1967; Deschênes et al., 1984). These comparisons indicate that the conclusions about spindles

based on those *in vitro* data are at least questionable, especially when no sign of interneuronal cooperation is detected. While some cellular types oscillate by virtue of their intrinsic currents (see above, Interaction between slow and delta waves; and below, The role of intrinsically bursting cells in cortical oscillations), their rhythms should be synchronized to be reflected as EEG macropotentials.

All experimental evidence reviewed above showed that spindling is a typical network operation, driven and synchronized by the RE thalamic nucleus. Some intrinsic properties of RE and thalamic relay cells may, however, be decisive in shaping the pattern of spindles. For example, this may be the case for the termination of spindle sequences. McCormick (1992) has suggested that changes in I_h activation curve and kinetics, ascribed to an increase in intracellular Ca^{2+} concentration after Ca^{2+}-dependent LTSs (Hagiwara and Irisawa, 1989), may account for the depolarization terminating a spindle sequence. Other scenarios accounting for the same phenomenon include the desynchronization of RE synaptic network toward the end of a spindle sequence and/or the fact that spindle-related RE-cell rhythmic bursts end with a tonic tail (Domich et al., 1986; Steriade et al., 1986). Both these possibilities may contribute to a diminished efficacy of RE neurons in producing sharp IPSPs in target thalamocortical neurons. Still other factors accounting for the slow rhythm of thalamic spindle sequences might be similar or even slower oscillations of locus coeruleus (Akaike, 1982), rostral midbrain reticular (Oakson and Steriade, 1982), and mesopontine cholinergic (Steriade et al., 1990a) neurons.

Is the slow (0.1–0.2 Hz) interspindle thalamic rhythm *entirely* due to a similar rhythm (≈0.3 Hz) in corticothalamic neurons, as described in this series of articles? That this is not the case, although the cortical rhythm potently modulates the thalamic one, is indicated by a series of results.

(1) Both rhythms of spindle waves (7–14 Hz) and interspindle sequences (0.1–0.2 Hz) exist in the thalamus after bilateral decortication and high brainstem transection (Morison and Bassett, 1945). Also, the isolated RE thalamic nucleus, disconnected from dorsal thalamic as well as cortical inputs, still displays spindles as well as their rhythmic recurrence with a slow rhythm (Steriade et al., 1987).

(2) Conversely, after extensive thalamic lesions, resulting in complete disappearance of cortical EEG spindles, the slow rhythm of cortical neurons survived (see Figs. 10, 12).

(3) Intracellular recordings of cortical pyramidal tract neurons showed a close relationship between oscillations in membrane potential at 7–14 Hz and spontaneous or thalamically induced spindle waves recorded at the cortical surface (Jasper and Stefanis, 1965; Creutzfeldt et al., 1966). By contrast to the close time-relation between spindle oscillations in cortical cells and the same rhythm in cortical EEG, both dependent upon the thalamus, the depolarizing envelopes of the slow cortical rhythm consisted of EPSPs and IPSPs that sometimes appeared at 7–14 Hz, but were more commonly seen at lower (3–4 Hz) or higher (15–30 Hz) frequencies. Thus, the components of the slow cortical oscillation are different from those of the slow spindle rhythmicity. Pure spindling was only obtained under barbiturate anesthesia (Fig. 7).

(4) The final arguments pointing to the different sites of genesis and mechanisms of the slow cortical oscillation and the slow rhythm of spindle oscillation arise from the patterns of associated EEG wave complexes recurring at 0.1–0.3 Hz. The EEG

complex consisted of a positive–negative or negative–positive deflection at the surface, which was simultaneous with the onset of the depolarization and action potentials in the slow cellular rhythm, followed after ≈0.4 sec by a sequence of spindles at ≈10 Hz (Figs. 1*A*, 2*D*). This suggests that the slow rhythm of cortical neurons drives RE cells and, subsequently, dorsal thalamic neurons to trigger spindles in thalamocortical systems. This possibility is substantiated by data reported in the final article of this series (Steriade et al., 1993b). Besides, the slow cortical rhythm may appear in advance of full development of cortical spindles that can be seen later on, with increasing EEG synchrony (see Figs. 1*A*, 5). By no means would this aspect imply that, in the chronological order of sleep stages, the slow cortical rhythm is more precocious than spindling. It only indicates that the thalamic neuronal pools have to be synchronized before spindles are visible over the cortex, and this process of synchronization goes in parallel with that of oscillations generated by the cerebral cortex. In support of this assumption, a previous article showed that spindles are generated in the thalamus from the first postnatal day, but they are fully transferred to the cortex only by the eighth or ninth day (Domich et al., 1987), only with increased synchrony due to continuing synaptogenesis after birth.

To sum up, both the thalamus and cortex are endowed with mechanisms required to generate a slow oscillation. The mechanism(s) of thalamic slow interspindle rhythm still remains a mystery and should be investigated. Besides the long-term synaptic and/or intrinsic properties that should be investigated to this end, the possibility exists that the slow interspindle rhythmicity of cortically disconnected thalamic cells results from their special metabolic properties that could periodically interrupt their phases of activity by long-lasting lulls (see Pape, 1992). In natural conditions, when the thalamus and cerebral cortex interact through reciprocal projections, the slow rhythms of their neurons are synchronized and mutually reinforced.

The role of intrinsically bursting cells in cortical oscillations

Intrinsically bursting cortical cells have been initially described by Connors et al. (1982) and McCormick et al. (1985) in slices from sensorimotor cortex of rodents. Some of these neurons display rhythmic bursts in response to single volleys applied to the cortical slice or direct cellular stimulation (Agmon and Connors, 1989; Chagnac-Amitai and Connors, 1989b; Silva et al., 1991). Similar repetitive spike bursts, up to a frequency of 10 Hz, have been elicited by depolarizing current pulses in our *in vivo* study of cat association cortical neurons (see Fig. 4 in Nuñez et al., 1993). However, synaptic volleys from the thalamus are less efficient in driving intrinsically bursting cortical cells at high rates, as seen from their lower-frequency (2–6 Hz) bursts during EEG spindles at 10–13 Hz (Figs. 6, 7). In the experimental condition of completely or partially suppressed inhibition, the frequency of spike bursts may be higher (Chagnac-Amitai and Connors, 1989a,b).

The discharge patterns of intrinsic bursts in the present study on cat are very similar to those described in cortical slices of rodents. In our experiments, intraburst frequencies of action potentials were ≈150–250 Hz, the fully developed burst often followed the occurrence of one or two single spikes, and repetitive stimuli dramatically enhanced the number and frequency of bursting action potentials (see Fig. 14), much the same as reported in rat neocortical slices (see Fig. 10 in Chagnac-Amitai

and Connors, 1989b). The intracellularly stained bursting neurons in this study were pyramidal elements (see Fig. 10 in Steriade et al., 1993a), as also documented in rat sensorimotor slices (McCormick et al., 1985). While the intrinsically bursting cells of rat seem to be confined to layer V in both somatosensory and visual cortices (Chagnac-Amitai et al., 1990; Mason and Larkman, 1990), we also found such a cell in layer III of association area 5, but our sample of stained bursting cells is to small to draw definite conclusions.

Bursting neurons probably have a great impact on adjacent as well as distant, synaptically coupled, neurons. All intrinsically bursting cells investigated in our study were oscillating within the slow rhythm. They were strongly and consistently excited during the slow depolarizing envelopes described here (see Figs. 6, 14). The possibility exists that intrinsically bursting cells receive their inputs from each other, as suggested by Chagnac-Amitai and Connors (1989b) from data indicating that regular-spiking cells are only briefly excited during synchronous activity (see also Thomson et al., 1988). This is consistent with data illustrated in Figure 3*B* in which the slow oscillations of a bursting cell were closely time related with focal waves recorded through the same micropipette, reflecting summated PSPs in a pool of neurons, possibly of the same type. That intrinsically bursting cells may indeed form an interconnected network is suggested by our data showing self-sustained oscillation in such a neuron after prolonged stimulation of the homotopic area in the contralateral cortex (Fig. 14). In that recording, the thalamus was extensively lesioned and, thus, the prolonged oscillation with an almost paroxysmal pattern is attributable to intrinsic cortical circuits. Even more powerful synchronization is expected in a brain-intact preparation when spike bursts are transferred to thalamocortical cells, with obvious consequences for the spread of synchronous activity. Repetitive cortical volleys are indeed able to produce resonance phenomena in thalamic cells, with spontaneous spike bursts persisting with similar or identical intra- and interburst frequencies if compared to those elicited in the final stage of stimulation (see Fig. 7 in Steriade, 1991). In both amygdalo-hippocampal circuits (Steriade, 1964) and corticothalamic systems (Steriade et al., 1976), self-sustained activities, like those outlasting the stimulation period in Figure 14, may lead to paroxysmal events of the absence petit mal type or other forms of epilepsy. The role of thalamic neurons in the synchronization of the cortically generated slow oscillation is further documented in the next article.

References

Agmon A, Connors BW (1989) Repetitive burst-firing neurons in the deep layers of mouse somatosensory cortex. Neurosci Lett 99:137–141.

Akaike T (1982) Periodic bursting activities of locus coeruleus neurons in the rat. Brain Res 239:629–633.

Andersen P, Sears TA (1964) The role of inhibition in the phasing of spontaneous thalamo-cortical discharge. J Physiol (Lond) 173:459–480.

Ball GJ, Gloor P, Schaul N (1977) The cortical microphysiology of pathological delta waves in the electroencephalogram of cats. Electroencephalogr Clin Neurophysiol 43:346–361.

Bremer F (1935) Cerveau isolé and physiologie du sommeil. C R Soc Biol (Paris) 118:1235–1241.

Buzsáki G (1991) The thalamic clock: emergent network properties. Neuroscience 41:351–364.

Buzsáki G, Bickford RG, Ponomareff G, Thal LJ, Mandel R, Gage F

(1988) Nucleus basalis and thalamic control of neocortical activity in the freely moving rat. J Neurosci 8:4007–4026.

Chagnac-Amitai Y, Connors BW (1989a) Horizontal spread of synchronized activity in neocortex, and its control by GABA-mediated inhibition. J Neurophysiol 61:747–758.

Chagnac-Amitai Y, Connors BW (1989b) Synchronized excitation and inhibition driven by bursting neurons in neocortex. J Neurophysiol 62:1149–1162.

Chagnac-Amitai Y, Luhmann HJ, Connors BW (1990) Burst generating and regular spiking layer 5 pyramidal neurons of rat neocortex have different morphological features. J Comp Neurol 296:598–613.

Chang HT (1950) The repetitive discharges of corticothalamic reverberating circuit. J Neurophysiol 13:235–257.

Connors BW, Gutnick MJ, Prince DA (1982) Electrophysiological properties of neocortical neurons in vitro. J Neurophysiol 48:1302–1320.

Creutzfeldt OD, Watanabe S, Lux HD (1966) Relations between EEG phenomena and potentials of single cells. I. Evoked responses after thalamic and epicortical stimulation. Electroencephalogr Clin Neurophysiol 20:1–18.

Curró Dossi R, Paré D, Steriade M (1991) Short-lasting nicotinic and long-lasting muscarinic depolarizing responses of thalamocortical neurons to stimulation of mesopontine cholinergic nuclei. J Neurophysiol 65:393–406.

Curró Dossi R, Nuñez A, Steriade M (1992) Electrophysiology of a slow (0.5–4 Hz) intrinsic oscillation of cat thalamocortical neurones in vivo. J Physiol (Lond) 447:215–234.

Deschênes M, Paradis M, Roy JP, Steriade M (1984) Electrophysiology of neurons of lateral thalamic nuclei in cat: resting properties and burst discharges. J Neurophysiol 51:1196–1219.

Domich L, Oakson G, Steriade M (1986) Thalamic burst patterns in the naturally sleeping cat: a comparison between cortically-projecting and reticularis neurones. J Physiol (Lond) 379:429–450.

Domich L, Oakson G, Deschênes M, Steriade M (1987) Thalamic and cortical spindles during early ontogenesis in kittens. Dev Brain Res 31:140–142.

Dusser de Barenne JG, McCulloch WS (1938) The direct functional interrelation of sensory cortex and optic thalamus. J Neurophysiol 1:176–186.

Ferster D, Lindström S (1983) An intracellular analysis of geniculo-cortical connectivity in area 17 of the cat. J Physiol (Lond) 342:181–215.

Friedländer MJ, Lin CS, Stanford LR, Sherman SM (1981) Morphology of functionally identified neurons in lateral geniculate nucleus of the cat. J Neurophysiol 46:80–129.

Hagiwara N, Irisawa H (1989) Modulation by intracellular Ca^{2+} of the hyperpolarization activated inward current in rabbit sino-atrial node cells. J Physiol (Lond) 409:121–141.

Hirsch JC, Fourment A, Marc ME (1983) Sleep-related variations of membrane potential in the lateral geniculate body relay neurons of the cat. Brain Res 259:308–312.

Humphrey AL, Weller RE (1988) Structural correlates of functionally distinct X-cells in the lateral geniculate nucleus of the cat. J Comp Neurol 268:448–468.

Jahnsen H, Llinás R (1984a) Electrophysiological properties of guinea-pig thalamic neurones: an in vitro study. J Physiol (Lond) 349:205–226.

Jahnsen H, Llinás R (1984b) Ionic basis for the electroresponsiveness and oscillatory properties of guinea-pig thalamic neurones in vitro. J Physiol (Lond) 349:227–247.

Jasper HH, Stefanis C (1965) Intracellular oscillatory rhythms in pyramidal tract neurones in the cat. Electroencephalogr Clin Neurophysiol 18:541–553.

Jones EG (1985) The thalamus. New York: Plenum.

Lamarre Y, Filion M, Cordeau JP (1971) Neuronal discharges of the ventrolateral nucleus of the thalamus during sleep and wakefulness in the cat. I. Spontaneous activity. Exp Brain Res 12:480–498.

Leresche N, Jassik-Gerschenfeld D, Haby M, Soltesz I, Crunelli V (1990) Pacemaker-like and other types of spontaneous membrane potential oscillations of thalamocortical cells. Neurosci Lett 113:72–77.

Leresche N, Lightowler S, Soltesz I, Jassik-Gerschenfeld D, Crunelli V (1991) Low-frequency oscillatory activities intrinsic to rat and cat thalamocortical cells. J Physiol (Lond) 441:155–174.

Llinás RR (1988) The intrinsic electrophysiological properties of

mammalian neurons: a new insight into CNS function. Science 242:1654–1664.

Macchi G, Bentivoglio M (1986) The thalamic intralaminar nuclei and the cortex. In: Cerebral cortex, Vol 5, Sensory-motor areas and aspects of cortical connectivity (Jones EG, Peters A, eds), pp 355–401. New York: Plenum.

Maekawa K, Purpura DP (1967) Properties of spontaneous and evoked synaptic activities of thalamic ventrobasal neurons. J Neurophysiol 30:360–381.

Marini G, Macchi G, Mancia M (1992) Potentiation of EEG spindles by ibotenate microinjections into nucleus reticularis thalami of cats. Neuroscience 51:759–762.

Mason A, Larkman A (1990) Correlations between morphology and electrophysiology of pyramidal neurons in slices of rat visual cortex. II. Electrophysiology. J Neurosci 10:1415–1428.

McCarley RW, Benoit O, Barrionuevo G (1983) Lateral geniculate nucleus unitary discharge in sleep and waking: state-and rate-specific aspects. J Neurophysiol 50:798–818.

McCormick DA (1992) Neurotransmitter actions in the thalamus and cerebral cortex and their role in neuromodulation of thalamocortical activity. Prog Neurobiol 39:337–388.

McCormick DA, Pape HC (1990a) Properties of a hyperpolarization-activated cation current and its role in rhythmic oscillation in thalamic relay neurones. J Physiol (Lond) 431:291–318.

McCormick DA, Pape HC (1990b) Noradrenergic and serotonergic modulation of a hyperpolarization-activated cation current in thalamic relay cells. J Physiol (Lond) 431:319–342.

McCormick DA, von Krosigk M (1992) Corticothalamic activation modulates thalamic firing through metabotropic receptors. Proc Natl Acad Sci USA 89:2774–2778.

McCormick DA, Connors BW, Lighthall JW, Prince DA (1985) Comparative electrophysiology of pyramidal and sparsely spiny stellate neurons of the neocortex. J Neurophysiol 54:782–806.

Morin D, Steriade M (1981) Development from primary to augmenting responses in primary somatosensory cortex. Brain Res 205:49–66.

Morison RS, Bassett DL (1945) Electrical activity of the thalamus and basal ganglia in decorticate cats. J Neurophysiol 8:309–314.

Morison RS, Dempsey EW (1943) Mechanism of thalamocortical augmentation and repetition. Am J Physiol 138:297–308.

Nuñez A, Curró Dossi R, Contreras D, Steriade M (1992a) Intracellular evidence for incompatibility between spindle and delta oscillations in thalamocortical neurons of cat. Neuroscience 48:75–85.

Nuñez A, Amzica F, Steriade M (1992b) Intrinsic and synaptically generated delta (1–4 Hz) rhythms in dorsal lateral geniculate neurons and their modulation by light-induced fast (30–70 Hz) events. Neuroscience 51:269–284.

Nuñez A, Amzica F, Steriade M (1993) Electrophysiology of cat association cortical cells in vivo: intrinsic properties and synaptic responses. J Neurophysiol, in press.

Oakson G, Steriade M (1982) Slow rhythmic rate fluctuations of cat midbrain reticular neurons in synchronized sleep and waking. Brain Res 247:277–288.

Pape HC (1992) Adenosine promotes burst activity in guinea-pig geniculocortical neurones through two different ionic mechanisms. J Physiol (Lond) 447:729–753.

Pape HC, McCormick DA (1989) Noradrenaline and serotonine selectively modulate thalamic burst firing by enhancing a hyperpolarization-activated cation current. Nature 340:715–718.

Paré D, Steriade M, Deschênes M, Oakson G (1987) Physiological characteristics of anterior thalamic nuclei, a group devoid of inputs from reticular thalamic nucleus. J Neurophysiol 57:1669–1685.

Petsche H, Pockberger H, Rappelsberger P (1984) On the search for the sources of the electroencephalogram. Neuroscience 11:1–27.

Roy JP, Clercq M, Steriade M, Deschênes M (1984) Electrophysiology of neurons of the lateral thalamic nuclei in cat: mechanisms of long-lasting hyperpolarizations. J Neurophysiol 51:1220–1235.

Silva LR, Amitai Y, Connors BW (1991) Intrinsic oscillations of neocortex generated by layer 5 pyramidal neurons. Science 251:432–435.

Soltesz I, Crunelli V (1992) A role for low-frequency, rhythmic synaptic potentials in the synchronization of cat thalamocortical cells. J Physiol (Lond) 457:257–276.

Soltesz I, Lightowler S, Leresche N, Jassik-Gerschenfeld D, Pollard CE, Crunelli V (1991) Two inward currents and the transformation of

low-frequency oscillations of rat and cat thalamocortical cells. J Physiol (Lond) 441:175–197.

Spain WJ, Schwindt PC, Crill WE (1991) Post-inhibitory excitation and inhibition in layer V pyramidal neurones from cat sensorimotor cortex. J Physiol (Lond) 434:609–626.

Steriade M (1964) Development of evoked responses into self-sustained activity within amygdalo-hippocampal circuits. Electroencephalogr Clin Neurophysiol 16:221–236.

Steriade M (1978) Cortical long-axoned cells and putative interneurons during the sleep-waking cycle. Behav Brain Sci 1:465–514.

Steriade M (1991) Alertness, quiet sleep, dreaming. In: Cerebral cortex, Vol 9, Normal and altered states of function (Peters A, Jones EG, eds), pp 279–357. New York: Plenum.

Steriade M, Deschênes M (1984) The thalamus as a neuronal oscillator. Brain Res Rev 8:1–63.

Steriade M, Llinás RR (1988) The functional states of the thalamus and the associated neuronal interplay. Physiol Rev 68:649–672.

Steriade M, McCarley RW (1990) Brainstem control of wakefulness and sleep. New York: Plenum.

Steriade M, Apostol V, Oakson G (1971) Control of unitary activities in cerebellothalamic pathway during wakefulness and synchronized sleep. J Neurophysiol 34:389–413.

Steriade M, Oakson G, Diallo A (1976) Cortically elicited spike-wave afterdischarges in thalamic neurons. Electroencephalogr Clin Neurophysiol 41:641–644.

Steriade M, Parent A, Hada J (1984) Thalamic projections of nucleus reticularis thalami of cat: a study using retrograde transport of horseradish peroxidase and fluorescent tracers. J Comp Neurol 229:531–547.

Steriade M, Deschênes M, Domich L, Mulle C (1985) Abolition of spindle oscillations in thalamic neurons disconnected from nucleus reticularis thalami. J Neurophysiol 54:1473–1497.

Steriade M, Domich L, Oakson G (1986) Reticularis thalami neurons revisited: activity changes during shifts in states of vigilance. J Neurosci 6:68–81.

Steriade M, Domich L, Oakson G, Deschênes M (1987) The deafferented reticular thalamic nucleus generates spindle rhythmicity. J Neurophysiol 57:260–273.

Steriade M, Datta S, Paré D, Oakson G, Curró Dossi R (1990a) Neuronal activities in brainstem cholinergic nuclei related to tonic activation processes in thalamocortical systems. J Neurosci 10:2541–2559.

Steriade M, Jones EG, Llinás RR (1990b) Thalamic oscillations and signaling. New York: Wiley.

Steriade M, Curro Dossi R, Nuñez A (1991) Network modulation of a slow intrinsic oscillation of cat thalamocortical neurons implicated in sleep delta waves: cortically induced synchronization and brainstem cholinergic suppression. J Neurosci 11:3200–3217.

Steriade M, Nuñez A, Amzica F (1993a) A novel slow (<1 Hz) oscillation of neocortical neurons *in vivo*: depolarizing and hyperpolarizing components. J Neurosci 13:3252–3265.

Steriade M, Contreras D, Curró Dossi R, Nuñez A (1993b) The slow (<1 Hz) oscillation in reticular thalamic and thalamocortical neurons: scenario of sleep rhythm generation in interacting thalamic and neocortical networks. J Neurosci 13:3284–3299.

Thomson AM, Girdlestone D, West DC (1988) Voltage-dependent currents prolong single-axon postsynaptic potentials in layer III pyramidal neurons in rat neocortical slices. J Neurophysiol 60:1896–1907.

Villablanca J, Salinas-Zeballos ME (1972) Sleep-wakefulness EEG and behavioral studies of chronic cats without the thalamus: the "athalamic" cat. Arch Ital Biol 110:383–411.

GROUPING OF BRAIN RHYTHMS IN CORTICOTHALAMIC SYSTEMS

M. STERIADE*

Laboratory of Neurophysiology, Laval University, Faculty of Medicine, Quebec, Canada G1K 7P4

Abstract—Different brain rhythms, with both low-frequency and fast-frequency, are grouped within complex wave-sequences. Instead of dissecting various frequency bands of the major oscillations that characterize the brain electrical activity during states of vigilance, it is conceptually more rewarding to analyze their coalescence, which is due to neuronal interactions in corticothalamic systems. This concept of unified brain rhythms does not only include low-frequency sleep oscillations but also fast (beta and gamma) activities that are not exclusively confined to brain-activated states, since they also occur during slow-wave sleep. The major factor behind this coalescence is the cortically generated slow oscillation that, through corticocortical and corticothalamic drives, is effective in grouping other brain rhythms. The experimental evidence for unified oscillations derived from simultaneous intracellular recordings of cortical and thalamic neurons *in vivo*, while recent studies in humans using global methods provided congruent results of grouping different types of slow and fast oscillatory activities. Far from being epiphenomena, spontaneous brain rhythms have an important role in synaptic plasticity. The role of slow-wave sleep oscillation in consolidating memory traces acquired during wakefulness is being explored in both experimental animals and human subjects. Highly synchronized sleep oscillations may develop into seizures that are generated intracortically and lead to inhibition of thalamocortical neurons, via activation of thalamic reticular neurons, which may explain the obliteration of signals from the external world and unconsciousness during some paroxysmal states. © 2005 Published by Elsevier Ltd on behalf of IBRO.

Key words: neocortex, thalamus, grouped rhythms, states of vigilance, seizures.

Contents

*Correspondence to: M. Steriade, Department of Physiology, University of Montreal, Pavillon Paul-G. Desmarais, local 5115, 2960 Chemin de la Tour, Montreal, Canada H3C 3J7. Tel: +1-514-343-6370; fax: +1-514-343-2111.
E-mail address: mircea.steriade@phs.ulaval.ca (M. Steriade).
Abbreviations: ACh, acetylcholine; EEG, electroencephalogram; EPSP, excitatory postsynaptic potential; FRB, fast-rhythmic-bursting; IPSP, inhibitory postsynaptic potential; LG, lateral geniculate; LTS, low-threshold spike; MEG, magnetoencephalogram; PET, positron emission tomography; PGO, ponto-geniculo-occipital; PPT, pedunculopontine tegmental; PSW, polyspike wave; rCBF, regional cerebral blood flow; RE, thalamic reticular; SW, spike-wave; TC, thalamocortical.

I shall elaborate the concept that, instead of strictly defining the frequency bands that characterize various rhythms of the electroencephalogram (EEG) and even splitting them into sub-types, it is more rewarding and closer to the reality to analyze the major EEG oscillations as grouped within complex wave-sequences. The progress in analytical methods used in studies on experimental animals, such as simultaneous intracellular recordings of cortical and thalamic neurons, as well as the advance in more global methods used in human investigations, i.e. EEG and magnetoencephalogram (MEG), led to the description of a multitude of oscillations generated in the cerebral cortex and/or thalamus. This great variety in wave frequencies and patterns is due to different electrophysiological and connectivity features of cortical, thalamic reticular (RE), and thalamocortical (TC) neurons, which generate most brain rhythms.

Francis Crick once asked me: "why so many oscillations?" At least for slow-wave sleep, the question was justified because the three cardinal rhythms defining this state (spindles, delta, and slow oscillation) are all associated with prolonged hyperpolarizations of TC and cortical neurons, which are effective in inhibiting the transmission of afferent signals and, thus, each one of these oscillations predisposes to brain disconnection and falling asleep. In more recent years, the above question received a definite answer from analyses of the neuronal circuitry and transmitters in the corticothalamic system, which fully explained how different brain rhythms coalesce into complex wave-sequences. The idea of grouping brain rhythms originally stemmed from analysis of sleep rhythms, with frequencies less than 15 Hz (Fig. 1). However, further studies showed that waking-like oscillations (beta, 20–30 Hz; and gamma, 30–60 Hz) are coalesced with the depolarizing phase of the slow sleep oscillation (Fig. 2). This might be thought as the substratum of peculiar forms of mental activity occurring episodically during slow-wave sleep. Moreover, while most investigators consider beta and gamma rhythms as distinct oscillatory types, our intracellular recordings have
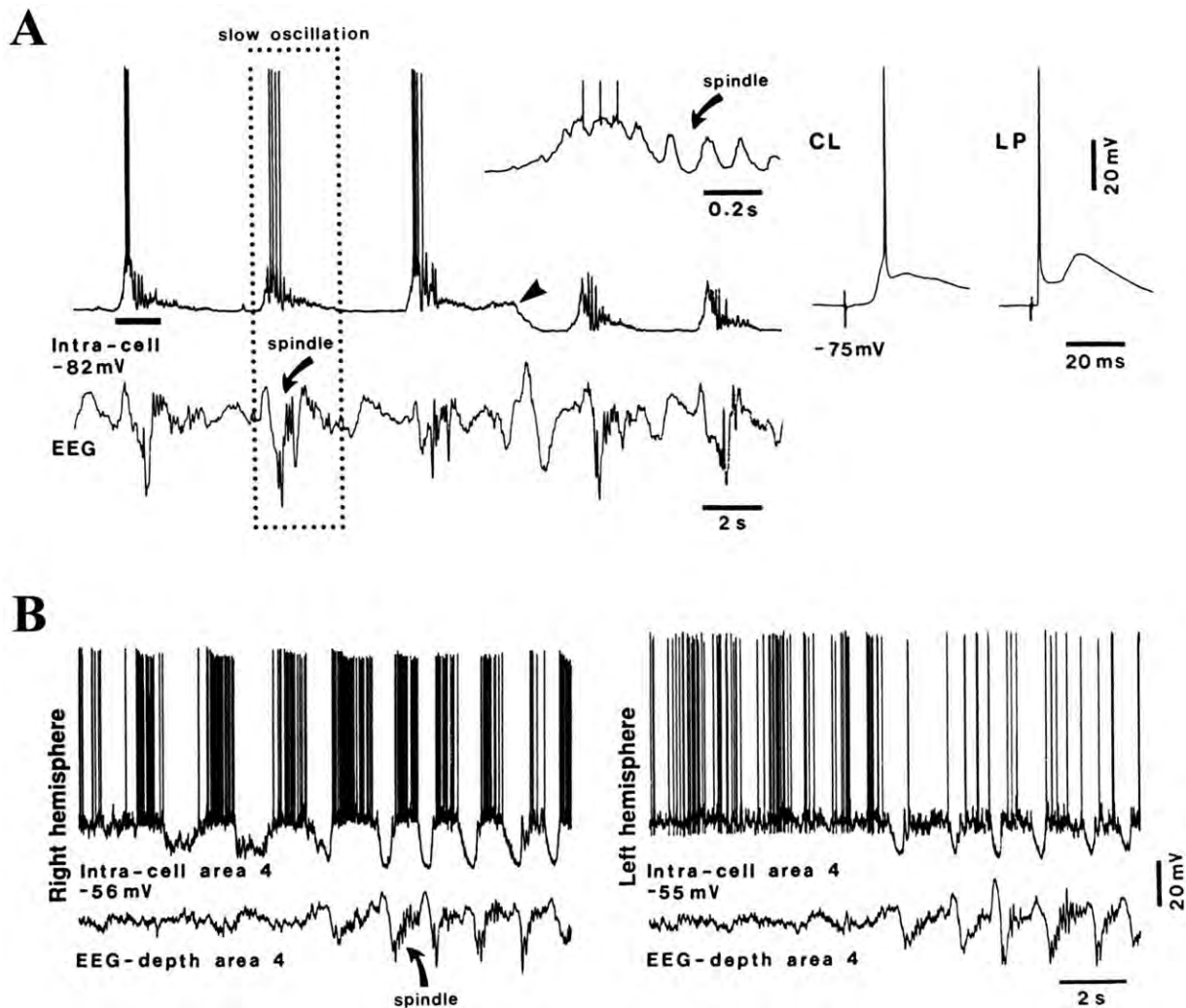
Fig. 1. The cortical slow oscillation groups thalamically generated spindles. (A) Intracellular recording in cat from cortical association area 7 (1.5 mm depth). Electrophysiological identification (at right) shows orthodromic response to stimulation of thalamic centrolateral (CL) intralaminar nucleus and antidromic response to stimulation of lateroposterior (LP) nucleus. Note slow oscillation of neuron and related EEG waves. One cycle of the slow oscillation is framed in dots. Part marked by horizontal bar below the intracellular trace (at left) is expanded above (right) to show spindles following the depolarizing envelope of the slow oscillation. (B) Dual simultaneous intracellular recordings from right and left cortical area 4 in cat. Note spindle associated with the slow oscillation and synchronization of EEG when both neurons synchronously displayed prolonged hyperpolarizations. Modified from Steriade et al. (1993d, 1994)

shown that beta activity transforms into gamma oscillation under slight membrane depolarization, and global EEG studies in humans support the idea that these two rhythms should be considered as grouped into one single entity since they occur in conjunction and fluctuate simultaneously during different mental activities (see *Slow oscillation and fast (beta/gamma) and ultra-fast rhythms*).

Thus, the variations in distinct oscillation frequencies are less important than the unified picture of brain oscillations, which was first revealed by performing *in vivo* intracellular recordings from formally identified long-axon and local-circuit neurons in the cortex or cortex and thalamus (Steriade et al., 1993b,e; Contreras and Steriade, 1995).

In this article, I will successively analyze (i) some aspects of the neuronal circuitry that are relevant to the generation and synchronization of low-frequency and fast rhythms; (ii) the coalescence of these rhythms investigated by intracellular recordings in animals, as well as congruent results from studies in humans on grouped brain oscillations; (iii) the role of spontaneously occurring rhythms in synaptic plasticity and memory consolidation, as resulting from animal and human studies; and (iv) the transformation of sleep oscillations into electrical seizures of the spike-wave (SW) type, suggesting possible neuronal substrates of unconsciousness during absence epilepsy.

Neuronal circuitry in the corticothalamic system

I use the term corticothalamic, instead of TC, because axons in the descending pathway are much more numerous than in the ascending projection (Jones, 1985; White, 1989). Besides, the slow sleep oscillation, which is the
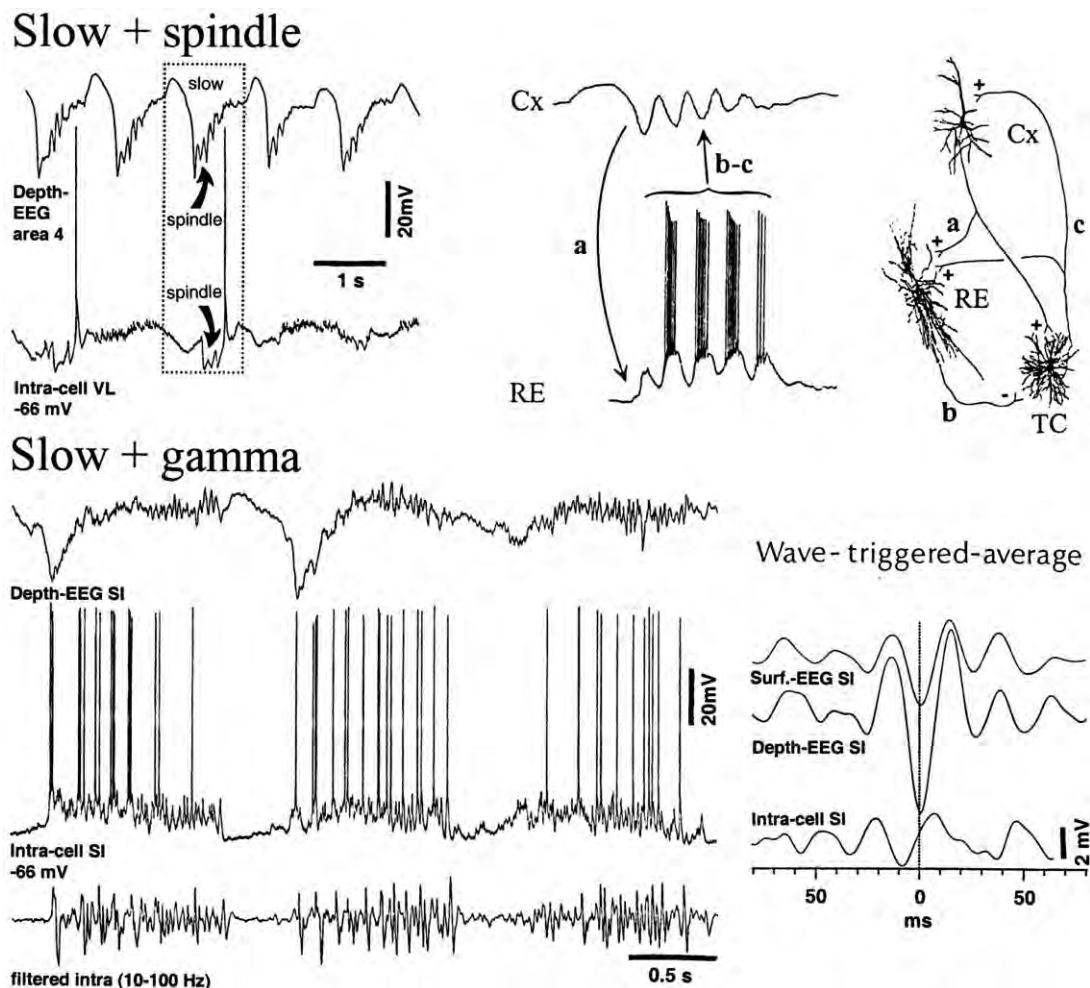
Fig. 2. Coalescence of slow oscillation with spindle and gamma rhythms. Intracellular recordings from cortical and thalamic neurons in cats. *Slow+spindle*, combined slow oscillation and spindle. Left: depth-EEG from cortical area 4 and intracellular recording of TC neuron from ventrolateral (VL) nucleus. The excitatory component (negative depth-EEG wave, downward deflection) of the slow cortical oscillation (0.9 Hz) is followed by a sequence of spindle waves at 10 Hz (arrows). One typical cycle of these two combined rhythms is indicated by dotted box; note IPSPs in VL neuron leading to a postinhibitory rebound. Right: top and bottom traces represent field potential from the depth of association cortical area 5 and intracellular recording from RE neuron. In neuronal circuits (far right), synaptic projections are indicated with small letters, corresponding to the arrows at left, which indicate the time sequence of the events. The depolarizing phase of the field slow oscillation (depth-negative, downward deflection) in the cortex (*Cx*) travels through the corticothalamic pathway (*a*) and triggers in the RE nucleus a spindle sequence that is transferred to TC cells of the dorsal thalamus (*b*) and thereafter back to the cortex (*c*), where it shapes the tail of the slow oscillatory cycle (see middle panel). *Slow+gamma*, fast activity (40 Hz) crowns the depolarizing phase of the slow oscillation. Three traces depict: depth-EEG waves from primary somatosensory cortex (S1), intracellular recording from S1 neuron, and filtered intracellular trace (between 10 and 100 Hz). Note fast waves (40 Hz) during the depolarizing phase of the slow sleep-like oscillation and absence of such fast waves during hyperpolarization. Modified from Steriade et al. (1993c, 1996b); Contreras and Steriade (1995); Timofeev and Steriade (1997).

main factor in the coalescence of brain rhythms, is generated intracortically, even in the absence of the thalamus (Steriade et al., 1993e; Sanchez-Vives and McCormick, 2000). Moreover, even though sleep spindles are generated within the thalamus, their near-simultaneous occurrence over widespread territories is produced by corticothalamic projections (Contreras et al., 1996a, 1997). Finally, fast-rhythmic-bursting (FRB) cortical cells are particularly well suited to generate coherent gamma rhythms in the corticothalamic system because some of them, located in deep cortical layers and projecting to the thalamus (Steriade et al., 1998a; Cardin et al., 2005), may synchronize cortical and thalamic generators of this oscillation. Thus, the cerebral

cortex has a prevalent role in the generation and synchronization of different brain rhythms.

Some of the main neuronal types and networks implicated in brain oscillations are (i) corticothalamic neurons, (ii) the recurrent inhibitory circuit between RE and TC neurons, and (iii) thalamically projecting brainstem cholinergic (and other neuromodulatory) projections.

Although all corticothalamic neurons are glutamatergic and thus excitatory, the effect of a synchronous cortical drive (an electrical volley or a spike-burst during natural states of vigilance) on RE neurons is excitatory and followed by rhythmic spike-bursts in the frequency range of spindles, whereas TC neurons simultaneously display bi-

phasic inhibitory postsynaptic potentials (IPSPs) leading to low-threshold spikes (LTSs) in isolation or crowned by fast action potentials (see Fig. 1 in Steriade, 2000). This contrasting effect on RE and TC neurons is due to the fact that excitatory postsynaptic currents (EPSCs) elicited in RE neurons by minimal stimulation of corticothalamic axons are 2.5 times larger than in TC neurons, and GluR4 receptor subunits in RE neurons outnumber those in TC neurons by 3.7 times (Golshani et al., 2001; Jones, 2002). These data are important in that they explain how, during the bursting mode of thalamic neurons (as is the case during slow-wave sleep and some seizures), the cortically elicited direct excitation of TC neurons is overwhelmed by the bisynaptic inhibition of these neurons, mediated by GABAergic RE neurons.

Another point in this complex circuitry, which can only be studied in intact-brain preparations (see Steriade, 2001), relates to the effects exerted on thalamic neurons by brainstem cholinergic cellular aggregates that are among the most important neuromodulatory systems in shifting the state of vigilance from the disconnected to the activated brain (Steriade and McCarley, 2005). The same neuron from the brainstem cholinergic pedunculopontine tegmental nucleus (PPT) may branch its axon to innervate both RE and TC neurons (Spreafico et al., 1993). At the TC level, PPT neurons produce direct depolarization with increase in input resistance, which explains the increased excitability in this gateway to the cerebral cortex (Curró Dossi et al., 1991). This effect is combined with, and strengthened by, the simultaneous inhibition produced by brainstem cholinergic neurons on GABAergic RE neurons (Hu et al., 1989), which leads to disinhibition of their targets, TC cells. These effects account for the suppression of thalamically generated slow-wave sleep rhythms (spindles and the clock-like component of delta waves; see below), which consist of long-lasting periods of hyperpolarizations, and account for the shift from the disconnected state of sleep to brain-active states.

Grouping of brain rhythms: evidence from intracellular recordings in animals and EEG studies in humans

Three rhythms (spindles, 7–15 Hz; delta, 1–4 Hz; slow oscillation, 0.5–1 Hz) define slow-wave sleep, and two rhythms (beta, 20–30 Hz; gamma, 30–60 Hz) occur in a sustained manner during the brain-active states of waking and REM sleep, though these fast oscillations are also episodically present during slow-wave sleep when they possibly underlie dreaming mentation during this disconnected behavioral state (see below).

The importance of the slow oscillation resides in the fact that it groups other brain rhythms, with both low- and fast-frequencies, within complex wave-sequences (Figs. 1 and 2). The slow oscillation was first described using intracellular recordings from different neuronal types in anesthetized cats and, in the same article (Steriade et al., 1993d), was also detected in EEG recordings during natural slow-wave sleep in humans in which cyclic groups of delta waves at 1–4 Hz recurred with a slow periodicity,

0.4–0.5 Hz. The grouping of these two oscillatory types is one of the arguments supporting the distinctness between delta and slow oscillations. Another argument came from human studies (Achermann and Borbély, 1997) showing that the typical decline in delta activity (1–4 Hz) from the first to the second sleep episode was not present at frequencies characteristic for the slow oscillation (range 0.55–0.95 Hz).

The cortical nature of the slow oscillation was demonstrated by its survival in the cerebral cortex after thalamectomy (Steriade et al., 1993e), its absence in the thalamus of decorticated animals (Timofeev and Steriade, 1996), and its presence in cortical slices maintained *in vitro* (Sanchez-Vives and McCormick, 2000). This rhythm was recorded in all major types of neocortical neurons, including pyramidal-shaped and local-circuit inhibitory neurons (Contreras and Steriade, 1995), and is made up by a prolonged depolarizing ("up") phase, followed by a long-lasting hyperpolarizing ("down") phase (Fig. 1). In intracellular recordings from cortical neurons of chronically-implanted, naturally sleeping animals, the slow oscillation with clear-cut hyperpolarizing phases appears from the very onset of slow-wave sleep and disappears in wakefulness and REM sleep when hyperpolarizations are erased and the activity of cortical neurons is tonically depolarized (Steriade et al., 2001; see also acute experiments, Steriade et al., 1993a). The depolarizing phase consists of non-*N*-methyl-D-aspartate-mediated excitatory postsynaptic potentials (EPSPs), fast prepotentials, a voltage-dependent persistent Na$^+$ current ($I_{Na(p)}$), and fast IPSPs reflecting the action of synaptically coupled GABAergic local-circuit cortical cells (Steriade et al., 1993d). The hyperpolarizing (silent) phase is *not* produced by GABAergic inhibitory interneurons but is due to disfacilitation (removal of synaptic, mainly excitatory, inputs) in intracortical and TC networks, and also to some K$^+$ currents (Contreras et al., 1996b; Timofeev et al., 2001). The disfacilitation factor may be explained by a progressive depletion of extracellular Ca^{2+} ([Ca^{2+}]$_{out}$) during the depolarizing phase of the slow oscillation (Massimini and Amzica, 2001), which would produce a decrease in synaptic efficacy and an avalanche reaction that would eventually lead to the functional disconnection of cortical networks.

Unlike "pure" rhythms within distinct frequency bands, generated in restricted neuronal circuits of extremely simplified experimental preparations, the living brain does not generally display separate oscillations during slow-wave sleep, but a coalescence of the slow oscillation with other sleep rhythms (spindles and delta) as well as with faster (beta and gamma) rhythms that are superimposed on the depolarizing phase of the slow oscillation (Fig. 2). Thus, such fast oscillations also appear, with lower incidence, during natural slow-wave sleep or anesthesia. Here, I briefly discuss the circuitry and neuronal mechanisms that account for the grouping of low-frequency and fast-frequency rhythms by the slow oscillation.

Slow oscillation and spindles: the K-complex

The thalamic generation of sleep spindles and the crucial role of RE GABAergic neurons are discussed in detail elsewhere (Steriade, 2003). Recent experimental

(Fuentealba et al., 2004) and modeling (Traub et al., 2005) studies support the notion that RE neurons are pacemakers of spindles. During the depolarizing phase of the slow oscillation, the synchronous firing of neocortical neurons impinges upon thalamic RE pacemaking neurons, thus creating conditions for formation of spindles, which are transferred to TC neurons and up to cortex, at which level spindles shape the tail of the slowly oscillatory cycle (see middle panel in *Slow+spindle* in Fig. 2). This connectivity explains why a cycle of the slow oscillation is followed by a brief sequence of spindles in TC neurons and in the cortical EEG (left panel in *Slow+spindle* in Fig. 2), as seen with intracellular recordings (Fig. 1) as well as with EEG recordings in human slow-wave sleep (Amzica and Steriade, 1997; Mölle et al., 2002; Fig. 3). The sequence of graphoelements consisting of an ample surface-positive transient, corresponding to the excitation in deeply lying cortical neurons, followed by a slower, surface-negative component and eventually a few spindle waves, represents the combination between the slow and spindle oscillations. It is termed the K-complex (Fig. 4) and is a reliable sign for stage 2 of human sleep, but it is apparent in all stages of slow-wave sleep (Niedermeyer, 2005). Spectral analysis shows the periodic recurrence of human K-complexes, with main peaks at 0.5–0.7 Hz (Fig. 4). The other frequency bands in this figure are between 1 and 4 Hz (delta band, with several ill-defined peaks) and between 12 and 15 Hz (the spindling range). The decomposition of the signal into three digitally filtered channels (Fig. 4) indicates that the S-lead reflects the slow oscillation, the Δ lead reflects the shape of the K-complex, and the σ lead faithfully reflects the spindle activity of the original signal. The laminar profile and intracellular substrates of the K-complex during cat sleep or anesthesia revealed that the surface-recorded, positive K-complexes reverse at a cortical depth of about 0.3 mm, and that the sharp depth-negative (surface-positive) wave of the K-complex is associated with cells' depolarizations, eventually leading to a spindle sequence (Amzica and Steriade, 1998). These investigations indicate that the K-complexes are the expression of the spontaneously occurring, cortically generated slow oscillation, though K-complexes can also be evoked by sensory stimuli during sleep.

Slow oscillation and delta waves

There are two components of delta waves. The cortical one survives thalamectomy (Villablanca, 1974; Steriade et al., 1993e). The thalamic component is generated through the interplay between two intrinsic currents of TC neurons, a hyperpolarization-activated cation current, I_H (Leresche et al., 1990, 1991; McCormick and Pape, 1990), and a low-threshold transient Ca^{2+} current, I_T (Llinás, 1988; Huguenard, 1996). Although arising from intrinsic properties of single TC neurons, the thalamic clock-like delta activity can be synchronized by corticothalamic volleys, which set into action RE neurons that, in turn, hyperpolarize TC neurons at the adequate membrane potential at which delta potentials are generated (Steriade et al., 1991). Thus, the synchronous discharges of cortical neurons during the depolarizing

phase of the slow oscillation excite RE neurons and the resulting hyperpolarization-activated delta potentials in TC cells are transferred back to cortex, where they shape the slowly oscillatory phase.

Slow oscillation and fast (beta/gamma) and ultra-fast rhythms

The unexpected association between a slow sleep rhythm and fast oscillations that are conventionally regarded as defining the electrical activity of brain-active states is explained by the voltage-dependency of fast oscillations. Indeed, long-axon and local-circuit cortical neurons generate beta and gamma rhythmicity at relatively depolarized values of the membrane potential (Llinás et al., 1991; Nuñez et al., 1992; Gray and McCormick, 1996; Steriade et al., 1996a). Thus, fast rhythms are sustained during the steady depolarization of cortical neurons during waking and REM sleep, selectively appear over the depolarizing phase of the slow sleep oscillation, and are absent during the hyperpolarizing phase of the slow oscillation (see Fig. 2). FRB neurons, located throughout cortical layers 2–6 and projecting to the thalamus (Steriade et al., 1998a; Cardin et al., 2005), are among the best candidates to generate and synchronize beta and gamma rhythms because they may link cortical and thalamic generators of these fast oscillations. That the thalamus and neocortex display coherent beta and gamma rhythms is demonstrated by cross-correlations between intracellularly recorded TC neurons and field potentials in the appropriate cortical area (Fig. 5A). At variance with the long-range synchrony of the slow sleep oscillation (see below), fast rhythms are synchronized over restricted cortical territories and within specific circuits between TC and neocortical areas (Fig. 5A–B).

Beta and gamma rhythms can interchangeably be termed *fast* because neurons may pass from beta to gamma oscillation in very short periods of time, 0.5–1 s, with slight depolarization (Steriade et al., 1996a). Studies in humans also showed that there is no precise cutoff between the beta and gamma bands, since these activities may fluctuate simultaneously, as shown by increased activities within both beta and gamma frequency bands (21–34 Hz) during semantic memory recall (Slotnick et al., 2002). Also, tasks demanding working memory are associated with phase synchrony of both beta (20 Hz) and gamma (30–40 Hz) cortical activities (Palva et al., 2005). These authors discussed the origin of fast activity in the cerebral cortex and considered that FRB neurons are key elements in reciprocal corticothalamic loops that generate fast rhythms, as demonstrated in experimental studies (Steriade et al., 1998a). The association between slow oscillation and fast rhythms has also been reported in human sleep (Mölle et al., 2002).

The synchronized fast rhythmic activity led to hypotheses postulating that linkages between spatially distributed oscillatory elements in the visual cortex may be the bases for "feature binding" and pattern recognition function (Singer, 1999; see the evaluation of this theory in Shadlen and Movshon, 1999). It should be noted that fast rhythms
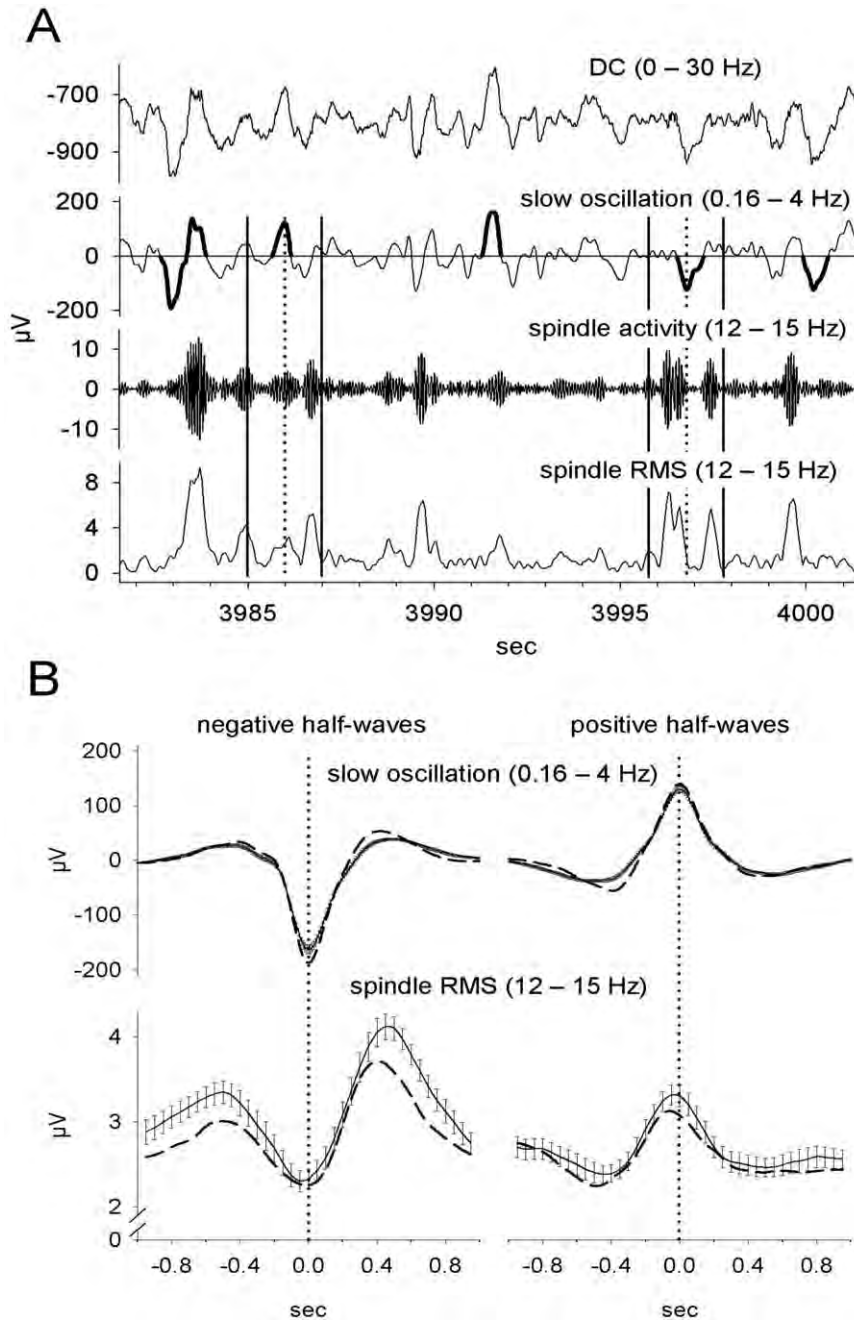
Fig. 3. Grouping of slow oscillation and spindle waves in human slow-wave sleep. (A) Analysis of slow oscillation-dependent changes in spindle activity. From top to bottom, DC-recorded (0–30 Hz) original EEG signal, slow oscillatory signal (0.16–4 Hz) with detected slow positive and negative half-waves indicated by a thick solid line, and spindle *rms* (root mean square) signal. For one positive and one negative half-wave each, the peak time used or for time-locked averaging and the ±1 s averaging interval are indicated by a dotted line and two sold vertical lines, respectively. (B) Grand means (across 13 subjects) of results from wave-triggered analysis of slow negative (left) and positive (right) half-waves. The mean±S.E.M. slow oscillation signal (top) and spindle *rms* signal (bottom) are shown. Dashed lines indicate mean values at Fz. Modified from and courtesy of Mölle et al. (2002).

are also present during the depolarizing phase of the slow oscillation during deep anesthesia and natural slow-wave sleep when consciousness is suspended. However, some studies have shown that fast rhythms are correlated with high cognitive and conscious processes in wakefulness and with dreaming mentation in REM sleep (Llinás and Ribary, 1993), and this aspect should be further explored.

Ultra-fast (or very fast) rhythms (80–200 Hz, up to 400 Hz), also called "ripples," are superimposed over the depolarizing phase of the slow oscillation in neocortex (Grenier et al., 2001). The synchronous occurrence of ripples over many cortical sites is explained by their strict relation with the depolarizing phase of the slow oscillation, and the fact that the slow oscillation is co-
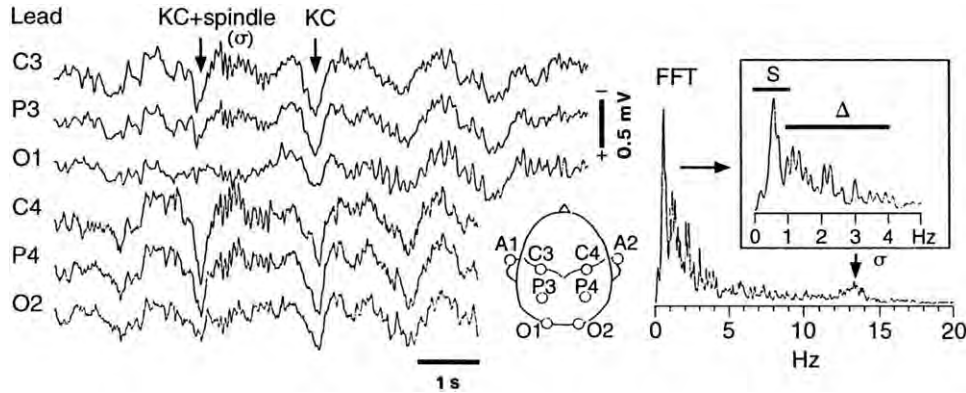
Fig. 4. Coalescence of slow oscillation and spindles in humans-the K-complex during natural sleep. Scalp monopolar recordings with respect to the contralateral ear are shown (see figurine). Traces show a short episode from a stage 3 slow-wave sleep. The two arrows point to two K-complexes, consisting of a surface-positive wave, followed (or not) by a sequence of spindle (sigma, σ) waves. Note the synchrony of K-complexes in all recorded sites. On the right, frequency decomposition of the electrical activity from C3 leads into three frequency bands: slow oscillation (S, 0–1 Hz), delta waves (Δ, 1–4 Hz), and spindles (σ, 12–15 Hz). Modified from Amzica and Steriade (1997).

herent in different, adjacent but also distant, cortical areas. The possible involvement of inhibition in the phase-locking of neurons during ripples was corroborated by the increased activity of fast-spiking neurons (representing local-circuit inhibitory cells) in relation with ripples. Ripples are also found in the perirhinal cortex and hippocampus, associated with bursts of sharp potentials during anesthesia, behavioral immobility and natural sleep (Chrobak and Buzsáki; 1996; Collins et al.,

1999). Surgically isolated stratum oriens neurons in the CA1 region of the hippocampus can generate ripples, as predicted by a model with axonal electrical coupling (Traub et al., 1999, 2003, 2005). Such ultra-fast oscillations are also observed preceding epileptiform bursts in children with seizures caused by cortical dysplasia (Traub et al., 2001) and in initiating spontaneously occurring electrical paroxysms in cats (Grenier et al., 2003).
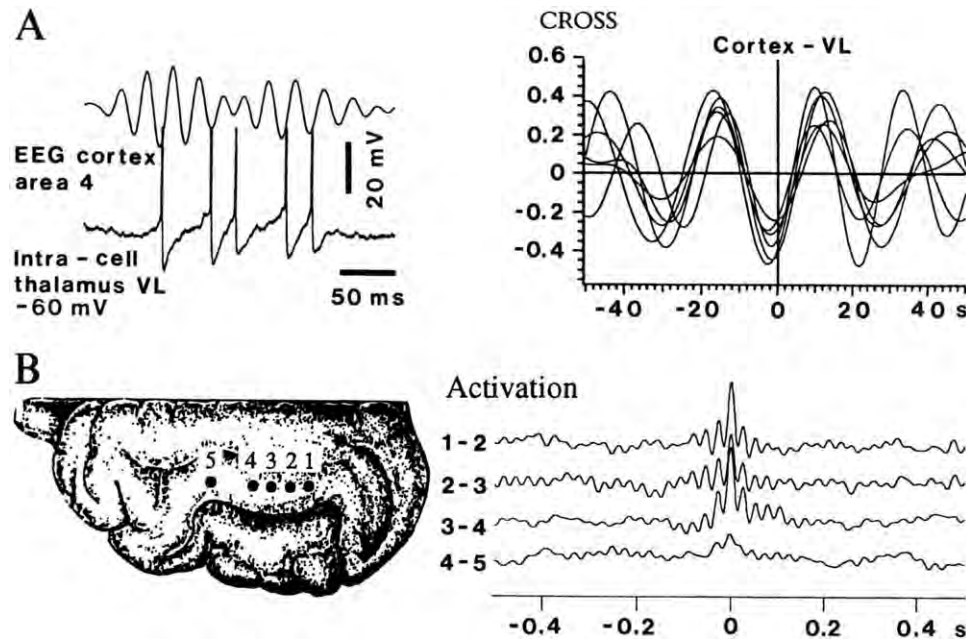

Fig. 5. Intracortical and corticothalamic synchronization of fast (gamma) rhythms, and their relation with the depolarizing phase of the slow sleep oscillation. (A) Short episode of activation in cat cerebral cortex, associated with coherent fast rhythms (~40 Hz) in EEG from motor cortex (area 4) and intracellularly recorded TC neuron from ventrolateral (VL) nucleus. Two traces represent simultaneous recordings of depth-EEG and intracellular activity of VL neuron (spikes truncated). Note close time-relations between action potentials of VL neuron and depth-negative waves in cortical EEG (reflecting summated excitatory events in a pool of neurons) at a frequency of about 40 Hz. Cross-correlations (CROSS) between action potentials and depth-EEG shows clear-cut relation, with opposition of phase, between intracellularly recorded VL neuron and EEG waves. (B) Synchronization of fast rhythms (35–40 Hz) among closely spaced leads in cortical areas 5 and 7 of cat. Distance between electrodes 1–2, 2–3 and 3–4: about 1.5 mm; between electrodes 4–5: about 3 mm. Cross-correlations between field potentials recorded from foci *1–2*, *2–3*, *3–4*, and *4–5* (see cortex figurine at left). Note decreased correlation with a slightly increased distance (*4–5*). Modified from Steriade et al. (1996a).

Traveling slow oscillation in humans and actions on distant subcortical structures

The slow oscillation (generally 0.5–1 Hz) was demonstrated during natural sleep of humans using EEG (Achermann and Borbély, 1997; Amzica and Steriade, 1997; Mölle et al., 2002; Marshall et al., 2003) and MEG (Simon et al., 2000) recordings.

The intracortical propagation of the slow sleep oscillation was studied in humans, using high-density (180) EEG leads (Massimini et al., 2004). The detection of slow oscillation on the multichannel EEG is depicted in Fig. 6. The slow oscillation originates in frontal regions and propagates in an anterior–posterior direction with a speed of 1.2–7 m/s, much faster than described in cortical slices (10–100 mm/s), where only pure neighbor-to-neighbor synaptic propagation could be observed (Compte et al., 2003). The anterior frontal origin of the slow sleep oscillation in the human study (Massimini et al., 2004) suggested a stronger need for sleep of this cortical region, as also indicated by very low cerebral blood flow values in this area (Maquet et al., 1997). Marked decreased of regional cerebral blood flow (rCBF) was also found during slow-wave sleep in the medial thalamus (Hofle et al., 1997) and significant covariation between the midbrain and the thalamus was reported in a positron emission tomography (PET) study on humans (Fiset et al., 1999). This covariation is explained by direct connections between the upper brainstem core and thalamus (see Steriade, 2003).

Rather than global changes in neocortex, rCBF measured with PET in humans showed major deactivation in heteromodal association areas during slow-wave sleep, while activity in primary and secondary sensory cortices was relatively preserved (Braun et al., 1997). The anterior frontal origin of the human slow oscillation and the suggestion that this may implicate a stronger need for sleep in this cortical region (Massimini et al., 2004) is congruent with the fact that the increase in slow-wave sleep activity after sleep deprivation is highest in anterior prefrontal regions (Finelli et al., 2000).

The cortically generated slow oscillation is reflected in subcortical structures. The discharge properties of both subthalamic and globus pallidus neurons are related to neocortical activity as these neurons fire spike-bursts with a periodicity that is coincident with the cortical slow oscillation and the oscillatory activity of those basal ganglia neurons is lost during cortical inactivation through pharmacological tools (Magill et al., 2000). The close relation between the slow oscillation recorded from striatal neurons and neocortical activity that generates this oscillation was also observed (Wilson and Kawaguchi, 1996; Mahon et al., 2001).

The basolateral nucleus of the amygdala complex and the perirhinal cortex display highly synchronous slow oscillation (Collins et al., 2001) and the hippocampus also reflects slow oscillatory cortical activity, as spike-bursts in deeply lying neocortical neurons trigger population events in the hippocampus associated with ultra-fast oscillations (Sirota et al., 2003).

Synaptic plasticity during and following brain rhythms

The question whether spontaneously occurring brain waves are epiphenomena with little or no functional significance may especially apply to the state of sleep that was considered to be associated with widespread inhibition throughout the cortex and subcortical structures (Pavlov, 1923), which would lead to abolition of cognitive and conscious events. However, the rich spontaneous firing of neocortical neurons, revealed by intracellular recordings during natural slow-wave sleep (Steriade et al., 2001), challenges the assumption that cortical neurons are inactive in this state. Although external signals are blocked at the thalamic level during slow-wave sleep, mainly because of TC neurons' inhibition during spindle waves, the intracortical dialogue is maintained (Timofeev et al., 1996) and the responsiveness of cortical neurons to callosal volleys is even increased during slow-wave sleep (Steriade et al., 1974). In humans too, this response is actually stronger in slow-wave sleep than in waking, but it abates much earlier (Massimini et al., 2005). That neocortex is active during slow-wave sleep suggests a reorganization/specification of neuronal circuits (Steriade et al., 1993b). This view is supported by studies using indicators of neuronal activities during slow-wave sleep in humans, revealing more marked changes in those neocortical areas that are implicated in memory tasks and decision-making during wakefulness (Maquet et al., 1997). In what follows, I shall discuss the role of low-frequency (spindle and slow) rhythms in synaptic plasticity. The fast rhythms, which are present in the background electrical activity during waking and REM sleep, also enhance the responsiveness of neocortical neurons (Steriade and Timofeev, 2003a). Then, spontaneous brain rhythms during different states of vigilance may lead to increased responsiveness and plastic changes in the strength of connections among neurons, a mechanism through which information is stored.

Experimental studies on animals

The experimental model of sleep spindles is the sequence of augmenting (or incremental) responses, defined as thalamically evoked cortical potentials that grow in size during the first stimuli at a frequency of 5–15 Hz, which mimics the initially waxing pattern of spindle waves. Similar incremental responses can be evoked in the thalamus by stimulating the cortex within the frequency of spindle waves. The cellular mechanisms of augmenting responses have been studied in slices maintained *in vitro* (Castro-Alamancos and Connors, 1996) and using simultaneous intracellular recordings from TC and related cortical neurons *in vivo* (Steriade et al., 1998b). In the intact brain, augmenting responses evoked by rhythmic (10 Hz) thalamic stimulation are characterized in cortical neurons by an increase in the secondary depolarization, at the expense of the primary EPSP. The secondary depolarization in neocortical neurons follows by 3 ms the postinhibitory spike-burst in simultaneously recorded TC neurons (Steriade et al., 1998b) (Fig. 7A). Another factor that may account for the
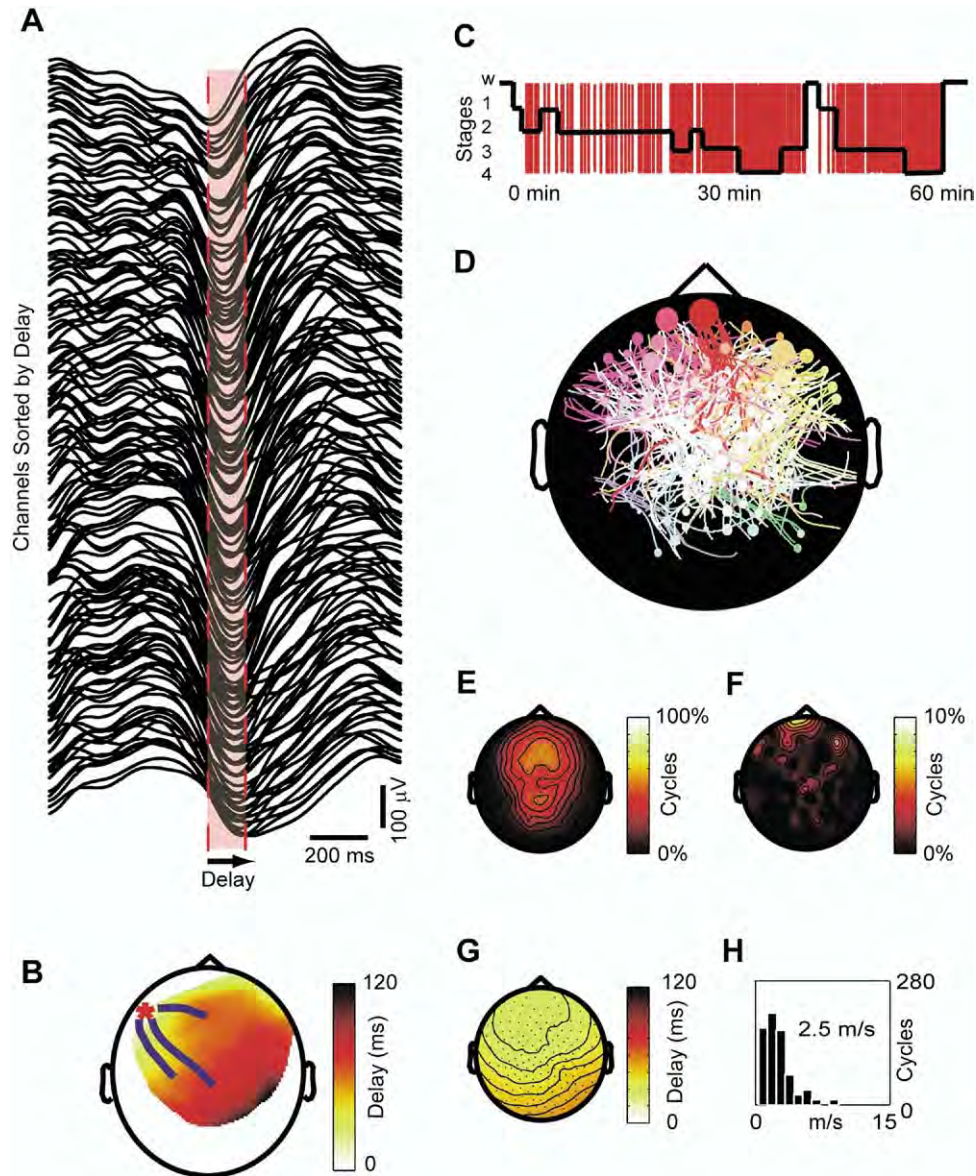
Fig. 6. The slow oscillation in human sleep as a traveling wave. (A) The signals recorded with 256-channel EEG during one cycle of the slow oscillation (SO) are ranked from top to bottom according to the delay of the negative peak of the SO. In this example, the delay from the negative peak at the top trace to the negative peak at the bottom trace is 120 ms. (B) Spatial distribution of the delays. The lines starting around the origin represent the streamlines calculated on the vector field of delays. The SO originates locally and propagates orderly to the rest of the scalp. Thus, each cycle of the slow oscillation behaves as a traveling wave. (C) Time of occurrence of SOs superimposed on the hypnogram. During 1 h of sleep several hundred cycles can be detected by means of an automated algorithm. (D) Coverage map. Superimposition of the streamlines describing the propagation of all the SOs detected for the first hour of sleep. The size of each dot is proportional to the number of cycles originating from each electrode. This representation shows that virtually any pattern of origin and propagation is possible although anterior electrodes tend to start more SOs and streamlines traveling in the antero-posterior direction are more numerous. (E) Probability of each EEG sensor being affected by a SO. Sensors in the fronto-central region had a 70% chance of being affected by a SO, while parietal and occipital electrodes detected few, or no, SOs. (F) Origin density map. The probability of each electrode being the origin of a SO is interpolated to obtain an origin density map. Foci with a higher origin density are detected in anterior regions of the scalp. (G) Average direction of propagation. Note the prevalent anterior–posterior direction of propagation of the SO. (H) Distribution of propagation speeds. Average speed was calculated for all the cycles traveling on the antero-posterior axis. On average, the SO sweeps over the cerebral cortex in the antero-posterior direction at a speed of 2.5 m/s. Modified from and courtesy of Massimini et al. (2004).

increased amplitude of the secondary depolarizing component during augmentation is the activation of local-circuit cortical interneurons, which would hyperpolarize pyramidal neurons and de-inactivate the Ca^{2+}-dependent LTS in these neurons, thus further enhancing augmented waves. The role of cortical inhibitory interneurons in augmenting

responses was also shown in a modeling study (Bazhenov et al., 1998).

Synaptic plasticity evoked by augmenting potentials in the projection pathway from thalamus to cortex is not only seen by progressively enhanced amplitudes of responses during the pulse-train but also by persistence of self-sus-
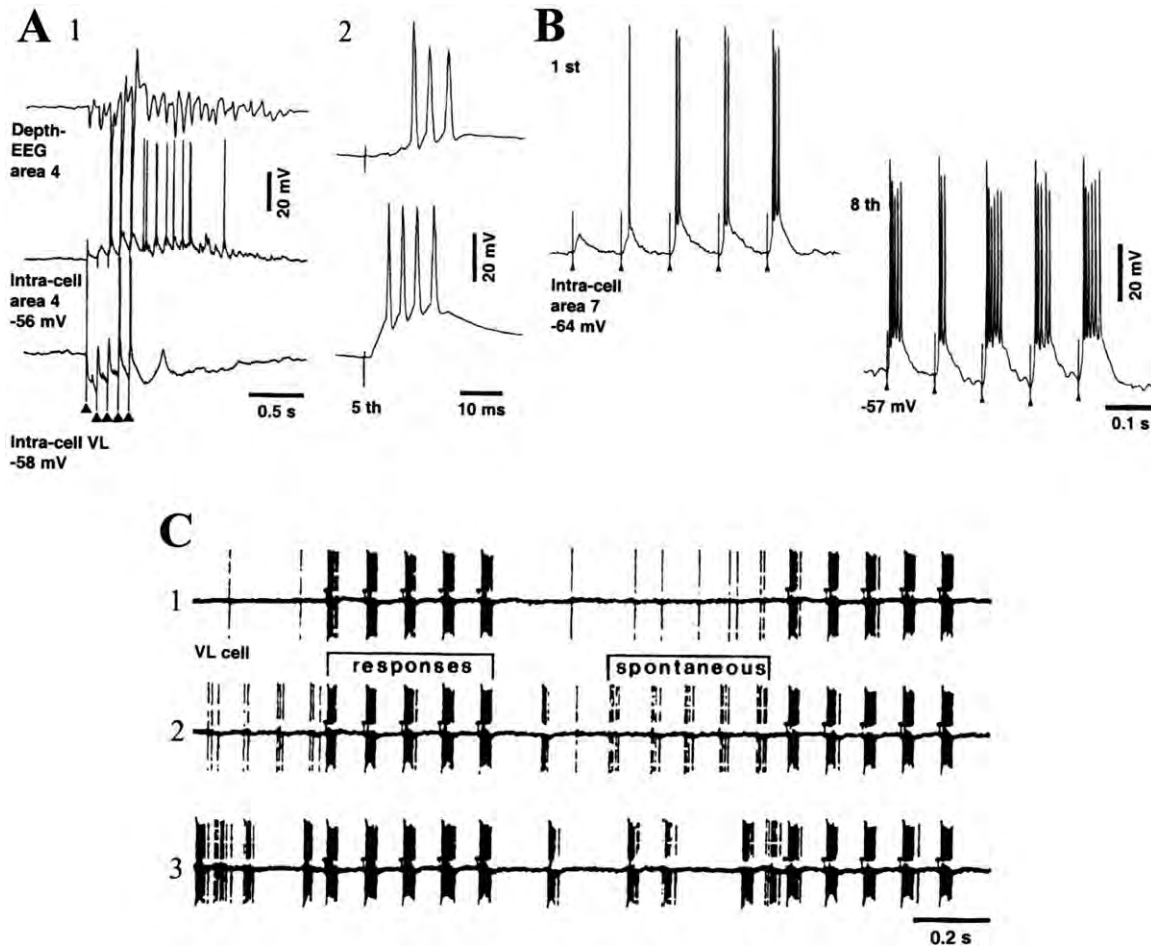
Fig. 7. Synaptic plasticity in TC and intracortical systems, and "memory" of electrical responses in corticothalamic system, induced by low-frequency stimuli mimicking sleep spindles. (A) Dual simultaneous intracellular recordings from cortical and TC neurons in cat (top trace is depth-EEG from area 4). *1*, Pulse-train (five stimuli at 10 Hz, arrowheads) applied to the thalamic ventrolateral (VL) nucleus produced augmenting responses in cortical neuron, whereas simultaneously recorded VL neuron displayed hyperpolarization. *2*, Expanded 5th response; the augmented response in cortical neuron followed the rebound spike-burst of VL neuron. Note self-sustained oscillatory activity at 10 Hz in cortical neuron after cessation of thalamic stimuli, despite persistent hyperpolarization in the VL neuron. (B) Intracellular responses of cat area 7 bursting cortical neuron to repetitive callosal stimulation (10 Hz). The thalamus ipsilateral to the recorded neuron was extensively lesioned using kainic acid. The intracortical augmenting responses to the 1st and 8th pulse-trains are illustrated. Note depolarization by about 7 mV and increased number of action potentials within bursts after repetitive stimulation. (C) Extracellular recording of VL neuron in brainstem-transected cat. Motor cortex stimulation with pulse-trains at 10 Hz (stimuli are marked by dots). In *1*, the pattern of responses in thalamic VL neuron in early stages of rhythmic pulse-trains. In *2–3*, responses at later stages of stimulation. Note appearance of spontaneous spike-bursts resembling the evoked ones, as a form of "memory" in the corticothalamic circuit. Modified from Steriade (1991); Steriade et al. (1993e); Steriade and Timeofeev (2001).

tained potentials, with the same pattern and frequency as those of responses during the prior stimulation period (Steriade et al., 1998b). Setting in action the feedback cortico-thalamic projections with pulse-trains at 10 Hz results in evoked responses but also, after protracted stimulation, in "spontaneously" occurring spike-bursts whose form and rhythmicity are similar to those of evoked responses, as if the repetition of volleys were imprinted in the "memory" of the corticothalamic network (Fig. 7C). Synaptic plasticity can take place not only in corticothalamic and the ascending TC pathway but also in the cortex of athalamic animals (Fig. 7B). That short- and medium-term (5–30 min) neuronal plasticity can occur inside cortical circuitry was also shown using callosal stimulation (Cissé et al., 2004). One of the mechanisms that may explain the increased neuro-

nal responsiveness to rhythmic and repeated pulse-trains at 10 Hz, simulating sleep spindles, is the activation of high-threshold Ca^{2+} currents and enhanced $[Ca^{2+}]_{in}$ that, in association with synaptic volleys reaching the neuron, may activate protein kinase A (Abel et al., 1997) and/or Ras/mitogen-activated protein kinase (Dolmetsch et al., 2001), which are involved in memory consolidation (see also the results by Cirelli et al., 2004, based on molecular correlates). The term memory consolidation, often used in both animal experiments and human studies, may not necessarily imply that the cellular phenomena revealed in experiments are the same as those underlying memory events in humans.

Thus, besides their role in cortical disconnection through inhibition of incoming messages in the thalamus, spindles are

also operational in important cerebral functions. During spindles, rhythmic and synchronized spike-bursts of thalamic neurons depolarize the dendrites of neocortical neurons, which is associated with massive Ca^{2+} entry (Yuste and Tank, 1996) that may provide an effective signal to efficiently activate Ca^{2+} calmodulin-dependent protein kinase II (CaMKII), which is implicated in synaptic plasticity of excitatory synapses in cortex and other sites in the nervous system (Soderling and Derkach, 2000; see also Sejnowski and Destexhe, 2000).

Similar phenomena, with Ca^{2+} entry in dendrites and somata of cortical neurons, may occur during the rhythmic spike-trains associated with oscillations in the slow (0.5–1 Hz) or delta (1–4 Hz) frequency bands, during later stages of slow-wave sleep. The hypothesis that the slow oscillation is responsible for the consolidation of memory traces acquired during the state of wakefulness (Steriade et al., 1993b) is supported by data showing that slow and delta (0.5–4 Hz) oscillations are implicated in cortical plasticity evoked by monocular deprivation in the developing visual cortex (Frank et al., 2001). In the latter study, microelectrode recording and optical imaging showed that the effects of monocular deprivation on cortical responses are increased by a 6 h slow-wave sleep period in the dark, and slow-wave sleep deprivation blocked this enhancement.

Synaptic plasticity has also been observed after testing with fast (20–60 Hz) pulse-trains. Stimulation of homotopic sites in the contralateral cortex with pulse-trains at 40 Hz induced prolonged facilitation of control response evoked by single callosal volleys, which lasted up to several minutes (Steriade and Timofeev, 2003a; Cissé et al., 2004). In some cases, a depolarization plateau lasted for 0.4–0.5 s after cessation of stimulation and gave rise to action potentials that closely mimicked the grouping and frequency of responses recorded during the prior period of stimulation. Spontaneous activity in the gamma frequency band (30–60 Hz) improves the coherent fluctuations in visual cortex excitability and thus may ensure more rapid and reliable transmission (Fries et al., 2001).

In the hippocampus too, neuronal synchrony associated with sharp potentials during slow-wave sleep may consolidate the information and transfer it to neocortical fields (Buzsáki, 1989). Dendritic recordings from CA1 hippocampal pyramidal neurons (Kamondi et al., 1998) suggested that sleep patterns are important for the preservation of experience-induced synaptic modifications in the limbic system (Buzsáki, 1998). Experiments on hippocampal "place cells" showed that, if a rat is confined to a place field, the firing rate of neurons is increased during subsequent slow-wave sleep, and an increased correlation is observed between cell pairs whose activities were related during waking behavior (Pavlides and Winson, 1989; Wilson and McNaughton, 1994).

Human studies on the role of sleep in memory, learning, and dreaming mentation

The above experimental data and ideas that low-frequency oscillations (spindles and slow oscillation) are associated with synaptic plasticity are supported by human studies demonstrating that the overnight improvement of discrimination tasks requires some steps, including those in early slow-wave sleep stages (Stickgold et al., 2000a,b). Also, procedural memory formation may be associated with oscillations during early sleep stages (Gais et al., 2000). After training on a declarative learning task, the density of human sleep spindles is significantly higher, compared with the non-learning control task (Gais et al., 2002). The early part of night sleep favors retention of declarative memories (which can be brought to conscious recollection), while the late part of sleep favors retention of non-declarative (procedural, unconscious) memories (Plihal and Born, 1997). During early night (stage 2 sleep), when sleep spindles prevail, these effects are due to the rhythmic bombardment of neocortical neurons by high-frequency spike-bursts of TC neurons, while the spike-trains of cortical neurons are associated with the slow oscillation throughout slow-wave sleep. The low frequencies (0.5–15 Hz) of spike-bursts and trains of single action potentials are the main factors behind synaptic consolidation of memory traces in the neocortex.

Experimental data showing that hippocampal neurons that increase firing rates during wakefulness also display enhanced discharge rates during subsequent sleep epochs (see above) are congruent with (i) the hypothesis that the higher the amount of synaptic potentiation in cortical circuits during waking, the higher the increase in slow-wave activity during subsequent sleep (Tononi and Cirelli, 2003), (ii) human data showing that learning activity increases the density of sleep spindles (Gais et al., 2002), and (iii) results indicating that simply sensory (auditory) stimulation during wakefulness produces increased power of sleep spindles, accompanied by increased coherence between frontal and temporal cortical regions (Cantero et al., 2002).

Acetylcholine (ACh) influences memory consolidation during human sleep. The memory for a declarative wordlist task was blocked after infusion of physostigmine (a cholinesterase inhibitor that increases cholinergic activation), without interfering with a consolidation of a non-declarative task (Gais and Born, 2004). Since physostigmine did not modify memory consolidation during wakefulness when cholinergic tone is maximal, it was predicted that a *low* cholinergic tone during slow-wave sleep is essential for consolidation of declarative memory. It was suggested that high levels of ACh, known to be present during both brain-activated states of waking and REM sleep (see Steriade and McCarley, 2005), may set favorable conditions for encoding new information in the hippocampus, whereas lower ACh levels, present during slow-wave sleep, facilitate consolidation of memory traces by allowing spread of activity from hippocampus to entorhinal cortex, with consequent neocortical involvement (Hasselmo, 1999; see also Buzsáki, 1996).

At variance with the commonly used notion of global brain processes in slow-wave sleep, two major findings were reported in humans subjects, namely: slow-wave sleep activity increases 2 h after a motor learning task and the enhancement (~27%) is expressed *locally*, in parietal association areas 40 and 7 that receive converging visual

and proprioceptive inputs relevant to spatial attention and skilled actions; and, changes in local slow-wave sleep activity are strongly correlated with improved performance in the task the next day after sleep (Huber et al., 2004).

The increased cortical activity that accounts for consolidation of memory traces during slow-wave sleep also explains the presence of dreaming mentation during this state. In contrast with the assumption that dreams exclusively occur in REM sleep, a series of studies, starting during the 1960s (Foulkes, 1962), has demonstrated the presence of dreaming mentation during slow-wave sleep. In slow-wave sleep dreaming is rational and repetitive, whereas during REM sleep the internally generated perceptions are vivid, thought becomes illogical, and the intensity of emotions is higher than during slow-wave sleep (Hobson et al., 2000). Awakenings from stages 3–4 of slow-wave sleep reported a recall incidence higher (45–65%) than in stage 2 (Pivik and Foulkes, 1968; Nielsen, 2000) but lower than in REM sleep when the recall may reach 90–95% (Cicogna et al., 2000). Then, the brain is never "empty" and mental activity is present during all stages of normal sleep.

Human studies using a sleep monitoring system, which distinguishes between waking and different sleep states, described the reports of subjects who awoke during all stages of the waking–sleep cycle (Hobson and Pace-Schott, 2002; Fosse et al., 2004). The results indicate reciprocal changes of thinking and hallucinations across sleep, with directed thinking (defined as continued mental effort as well as attempts to decide and plan) more frequent during slow-wave sleep and hallucinations (endogenous sensations) more frequent during REM sleep. The intensified hallucinations with transition from slow-wave sleep to REM sleep may reflect the progressive appearance of ponto-geniculo-occipital (PGO) waves, the "stuff dreaming is made of," which occur during slow-wave sleep well in advance of muscular atonia, the cardinal sign of REM sleep, and are further synchronized throughout the cortex during REM sleep (Steriade et al., 1989; Amzica and Steriade, 1996). The transitional period between EEG-synchronized (slow-wave) and EEG-activated (REM sleep) sleep, called pre-REM period, during which PGO waves appear over the background of a fully synchronized EEG, may have importance for dreaming. Thus, TC neurons are hyperpolarized during the pre-REM period, when the sleep EEG is still fully synchronized, whereas they are tonically depolarized by 7–10 mV during REM sleep (Hirsch et al., 1983). These two states (pre-REM and fully developed REM sleep) generate different PGO-related responses of TC neurons to brainstem inputs, which influence the signal-to-noise ratio in the visual channel, i.e. the ratio between the neuronal activities related to the PGO signal and the background firing of the same neuron. During pre-REM, the activity of lateral geniculate (LG) TC neurons starts with a short, high-frequency (300–500 Hz) spike-burst coinciding with the PGO wave, but during REM sleep the rate of LG-cells' spontaneous firing is 1.5- to three-fold higher than in pre-REM and the peak-to-peak amplitudes of PGO waves are two to three times lower

(Steriade et al., 1989). Thus, the greater signal-to-noise ratio in the LG-cortical channel during the pre-REM epoch than during REM sleep suggests that the vivid imagery associated with dreaming sleep may appear before fully developed REM sleep, during a period of apparent slow-wave sleep. The idea that PGO waves with greater amplitudes during the pre-REM stage may reflect more vivid imagery during that epoch than even during REM sleep (Steriade et al., 1989) corroborates earlier data showing that, after interrupting sleep immediately after the occurrence of the first PGO wave (in the pre-REM stage) and eliminating about 30 s of the slow-wave sleep stage that precedes REM sleep, the increased time of the REM sleep rebound was due to phasic events (PGO waves) rather than the loss of REM sleep per se (Dement et al., 1969). This observation fits in well with data on dream reports from the last epoch of EEG-synchronized sleep, which are indistinguishable from those obtained from REM sleep awakenings (Hobson, 1988; Hobson and Pace-Schott, 2002).

Transition from cortical sleep rhythms to electrical seizures

The synaptic plasticity that follows rhythmic brain stimulation within the frequency range of low-frequency sleep oscillations may take paroxysmal forms. This is especially seen with cortical FRB neurons that display a peculiar enhancement of rhythmic responses, with progressively grown depolarization and dramatically increased number of action potentials, which have an epileptiform aspect (Fig. 8). The changes in responsiveness of neocortical neurons, which lead to self-sustained oscillations of the paroxysmal type, are already initiated during rhythmic stimulation with pulse-trains at 10 Hz, within the frequency range of sleep spindles. Dual intracellular recordings from TC and cortical neurons (Fig. 9) show that (i) the cortical neuron exhibited progressively enhanced responsiveness, as seen from the increased number of action potentials, whereas the TC neuron remained hyperpolarized due to the action of GABAergic RE neurons set into action by thalamic stimulation; (ii) following cessation of rhythmic stimulation, self-sustained electrical seizure occurred in the EEG and intracellular activities, consisting of spike-wave (SW) complexes at about 2 Hz that lasted for 8 s; and (iii) during the stimulation period, "spontaneous" depolarizing events appeared between pulse-trains, with the same frequency as that used during pulse-trains (see asterisk in the expanded panel at bottom right in Fig. 9). The latter aspect is reminiscent of the "memory" in the corticothalamic system, which followed protracted stimulation (see above, Fig. 7C). Then, slow-wave sleep oscillations or their experimental model (augmenting responses) may lead to self-sustained paroxysms of the SW type.

In clinical studies too, although absences (loss of consciousness) can only be detected in the waking state, the electrographic correlates of such seizures with SW complexes at ~3 Hz preferentially occur during the early or late stages of slow-wave sleep. The relation between SW seizures and the EEG correlates of slow-
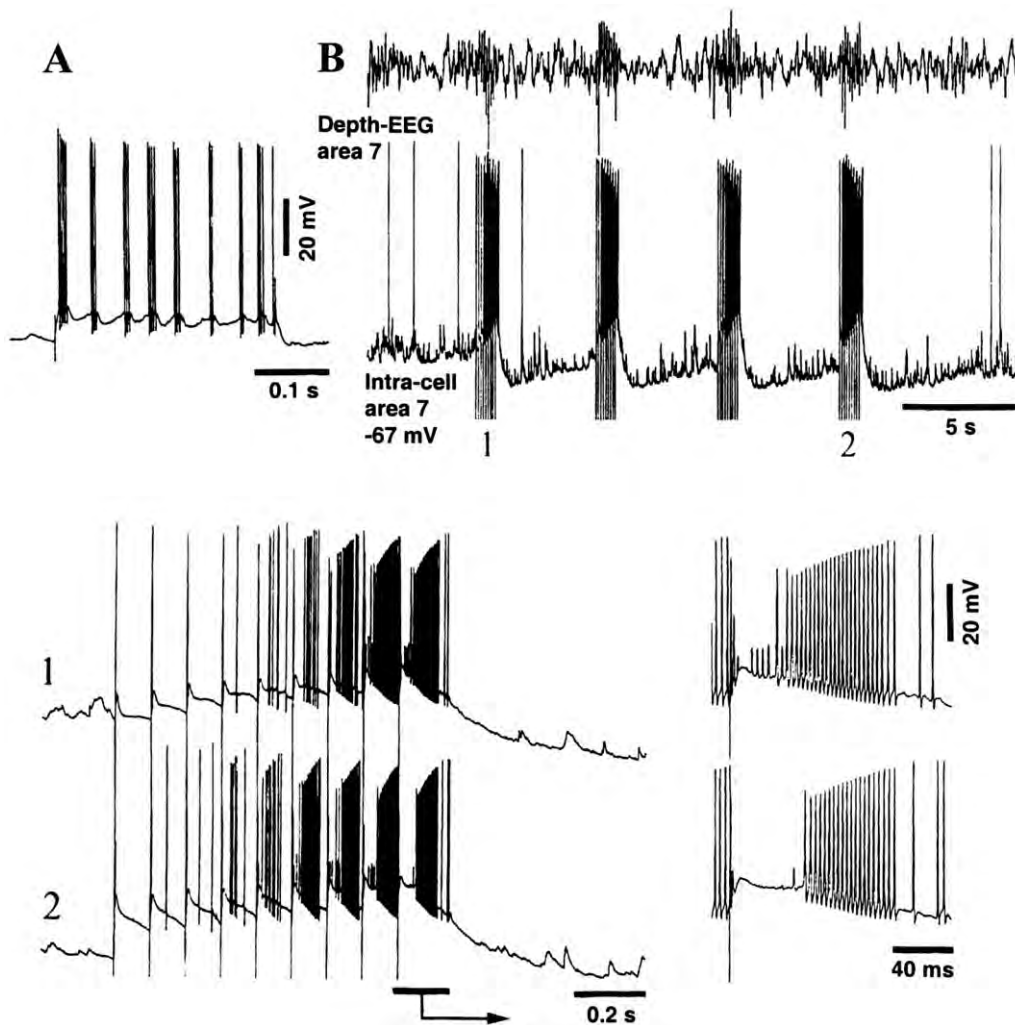
Fig. 8. Progressively growing, paroxysmal-like depolarization during cortically evoked augmenting responses in cortical FRB neuron from cat suprasylvian area 7. Close intracortical stimulation, in adjacent area 21. (A) Identification of FRB neuron by depolarizing current step (0.5 nA). (B) Responses of this FRB neuron to four pulse-trains, each consisting of nine pulses at 10 Hz applied to area 21. Responses to pulse-trains *1* and *2* (last) are expanded below, and responses to the last stimulus in these pulse-trains are further expanded at right (arrow). The neuron persistently depolarized during stimulation. At depolarized levels of the V_m, IPSPs evoked by area 21 stimuli shunted the early occurring spikes. Modified from Steriade and Timofeev (2003b).

wave sleep was repeatedly demonstrated (Kellaway and Frost, 1983; Kellaway, 1985; Shouse et al., 1996; Shouse, 2001). By contrast, SW seizures are decreased or totally absent during REM sleep (Frank, 1969). The occurrence of SW seizures is facilitated during transitional states, especially between waking and slow-wave sleep, during the state of drowsiness. This was observed in humans (Noachtar, 2001) and in behaving monkeys displaying tonic eye movements at the onset and the end of seizures, as in clinical absence seizures (Steriade, 1974; Fig. 10). SW seizures are reduced or abolished with transition from slow-wave sleep to spontaneous or sensory-elicited arousal as well as during repetitive brainstem reticular formation stimulation, and they are increased after administration of low doses of a cholinergic receptor antagonist (Danober et al., 1993, 1995).

The original assumption that SW seizures originate in the diencephalon and the conventional definition of these seizures as "suddenly generalized and bilaterally synchronous" have been challenged by recent experimental research that are also congruent with human studies. The deeply located source of SW (absence or petit-mal) seizures was ascribed to a "centrencephalic" system (Penfield and Rasmussen, 1950), based on experiments under barbiturate anesthesia reporting SW patterns evoked by stimulation of midline thalamic nuclei (Jasper and Droogleever-Fortuyn, 1949). The morphological substrate of the "centrencephalic" system was never demonstrated, since there are no bilateral projections of thalamic nuclei, and the experimental studies reported *responses* evoked by thalamic stimulation but no self-sustained activity, as it would be the case in bona fide seizures. On the other hand, SW seizures seem to be "suddenly generalized" only in EEG
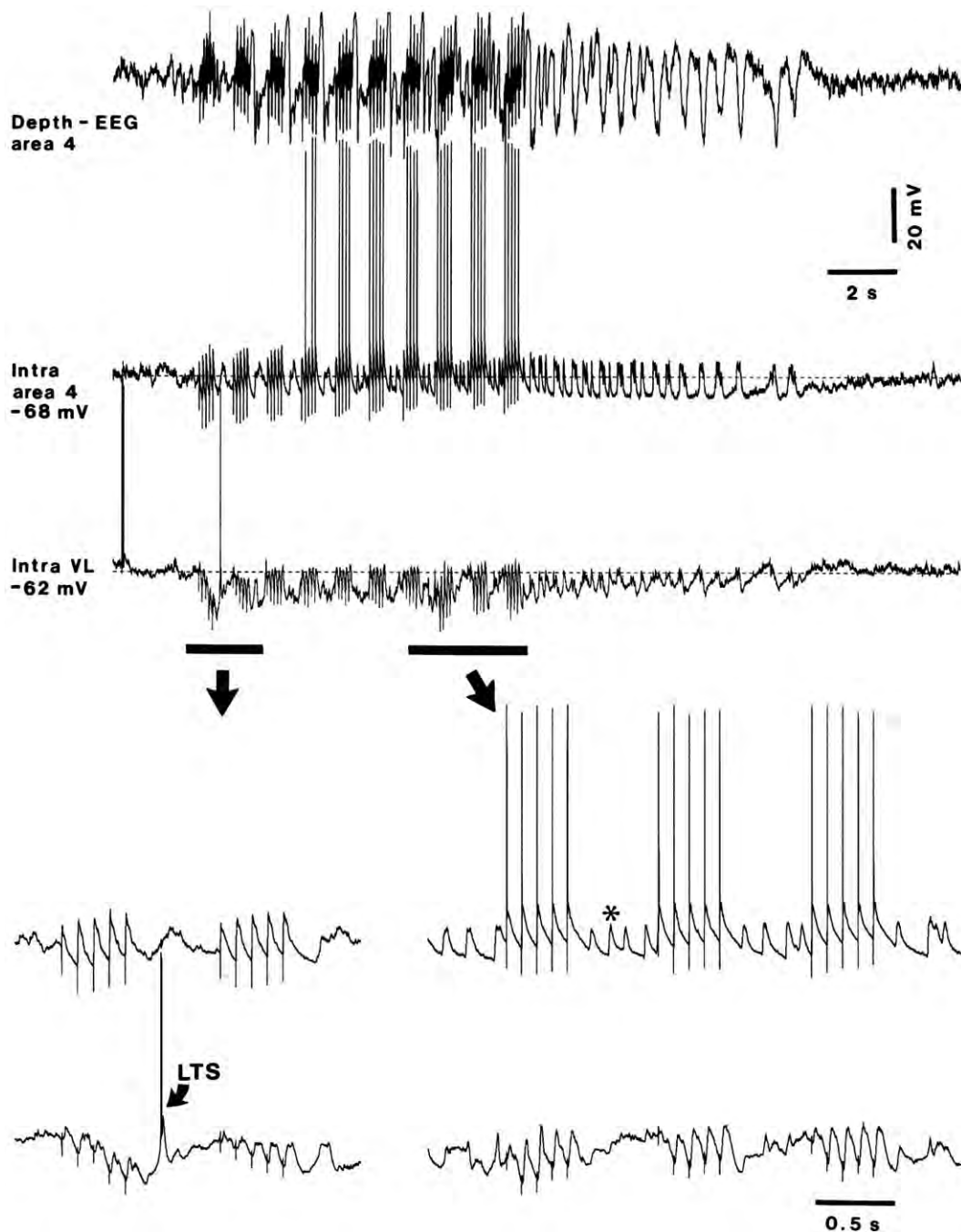
Fig. 9. Plastic changes in cortical responsiveness, leading to self-sustained paroxysmal oscillation, simultaneously with decreased low-threshold (LT)-type augmenting in TC neuron. Dual simultaneous intracellular recording from TC neuron in cat ventrolateral (VL) nucleus and cortical area 4 neuron, together with depth-EEG from area 4. Stimulation applied to cortex and consisting of pulse-trains at 10 Hz, repeated every second. Two parts, at the beginning and end of stimulation (marked by horizontal bars and arrows) are expanded below. Note that, although LT-type augmenting responses in TC neuron diminished from the second pulse-train, cortical augmenting responses were progressively enhanced and, after finishing the stimulation period, a self-sustained oscillation at ~2 Hz ensued, lasting for ~8 s. Also note, in cortical neuronal recording, depolarizing events with the similar frequency (10 Hz) as that used in pulse-trains, occurring between pulse-trains (asterisk in bottom right panel). Modified from Steriade and Timofeev (2003b).

recordings and, even at this macroscopic level, clinical studies have reported that the "spike" of SW complexes propagates from one hemisphere to another with time-lags as short as 12–25 ms (Lemieux and Blume, 1986; Kobayashi et al., 1994), too short to be estimated by simple

visual inspection. Indeed, experimental studies using neuronal and field potential recordings from cortex or cortex and thalamus, have shown that spontaneously occurring SW seizures are initiated in one cortical focus, are transferred to neurons in another cortical area with latencies
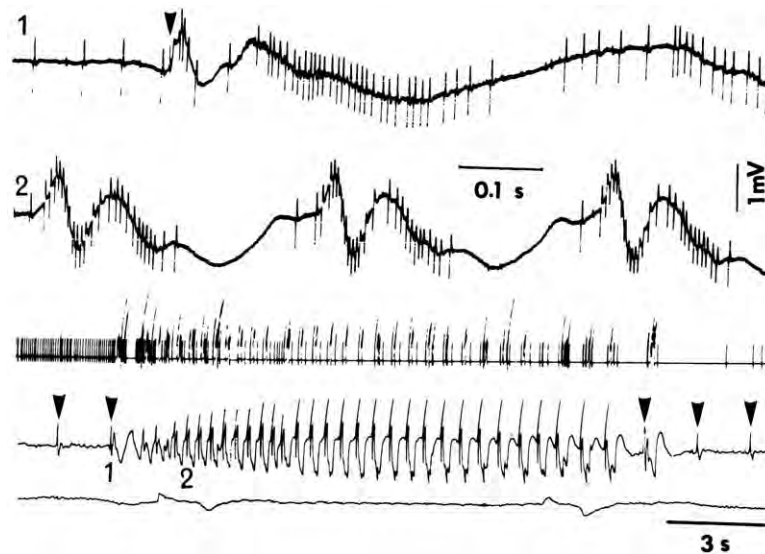
Fig. 10. SW seizures in chronically-implanted *Macaca mulatta*. Neuronal activity during seizure with SW complexes at 3 Hz during drowsiness in the behaving monkey. Single neuron recorded from the arm area in the precentral gyrus (area 4). The top oscilloscopic trace indicates the corresponding part (marked by horizontal bar) in the below-depicted ink-written record (the three traces represent: unit spikes used to deflect a pen of the EEG machine; each deflection exceeding the common level representing a group of high-frequency spikes; focal slow EEG waves, simultaneously recorded by the same microelectrode; and eye movements, EOG). Arrowheads indicate stimuli applied to the appropriate thalamic nucleus for neuronal identification. When the experimenter observed increased amplitude of the evoked field potential (second stimulus), stimuli were interrupted and the seizure developed in the absence of any stimulus. Note spike-bursts over the depth-negative (upward in this case) field potential of the SW complexes (the EEG "spike") and silent firing during the late part of the depth-positive "wave" component of SW complexes. Also note tonic eye movements at the onset and end of the SW seizure. Modified from Steriade (1974).

ranging from 20 to 100 ms, and finally to the thalamus after several seconds (Steriade and Amzica, 1994; Neckelmann et al., 1998; Meeren et al., 2002). That some SW seizures are locally generated and result from multiple, independent cortical foci has been reported in human studies since the late 1930s (Jasper and Hawkes, 1938).

The independence of cortically generated SW seizures, with typical SW and polyspike wave (PSW) complexes at ~3 Hz, on the thalamic circuitry was demonstrated in acutely prepared athalamic cats (Steriade and Contreras, 1998) and athalamic behaving monkeys displaying impairment of awareness during SW bursts (Marcus et al., 1968). These studies, using global methods of recordings, are corroborated by intracellular studies showing inhibition of TC neurons during cortically generated SW/PSW seizures (Fig. 11). This inhibition (Steriade and Contreras, 1995) was also found in genetic models of absence seizures (Crunelli and Leresche, 2002) and is due to the fact that, at each paroxysmal depolarizing shift in neocortical neurons, thalamic GABAergic RE neurons are excited and, consequently, they impose IPSPs on TC neurons that, because of their repetitive nature and increased membrane conductance, do not succeed in de-inactivating the transient Ca^{2+} current responsible for spike-bursts. Thus, during cortically generated SW seizures, TC neurons are steadily hyperpolarized and silent (Fig. 11A). The inhibition of TC neurons during cortically generated SW seizures is further demonstrated during brief epochs when SW/PSW complexes stop and TC neurons are disinhibited, thus recovering their capacity to fire single action potentials (Fig. 11, B2).

To sum up, two major types of thalamic neurons, RE and TC, behave differently during cortically generated SW/PSW seizures. RE neurons are excited by each corticofugal drive during SW/PSW complexes (Steriade and Contreras, 1995; Slaght et al., 2002) and, then, these GABAergic thalamic neurons participate actively during cortically generated SW seizures. This conclusion is also drawn from the increase in the ionic current that underlies spike-bursts of RE cells in SW seizures (Tsakiridou et al., 1995; Avanzini et al., 1999) and the fact that the Cd^{2+}-induced blockage of RE-cells' spike-bursts leads to a decrease in the ipsilateral SW activity (Avanzini et al., 1992). On the contrary, the opposite occurs in TC cells that are inhibited during cortically generated SW/PSW seizures (Fig. 11). The inhibition of thalamic relay cells may explain the unconsciousness during absence seizures, due to the blockage of signals from the external world in their route to the cerebral cortex.

CONCLUSIONS

The living brain, with intact connections between neocortex, thalamus, and various modulatory systems, displays low-frequency and fast rhythms grouped within complex wave-sequences. Some of these oscillations can be generated by interplay between intrinsic neuronal properties, but the coalescence of various rhythms and their synchronization is due to network operations in corticothalamic systems. The tendency to analyze distinct, precise frequency bands of EEG activities, in isolation from others, will hopefully be replaced by the concept of unified brain
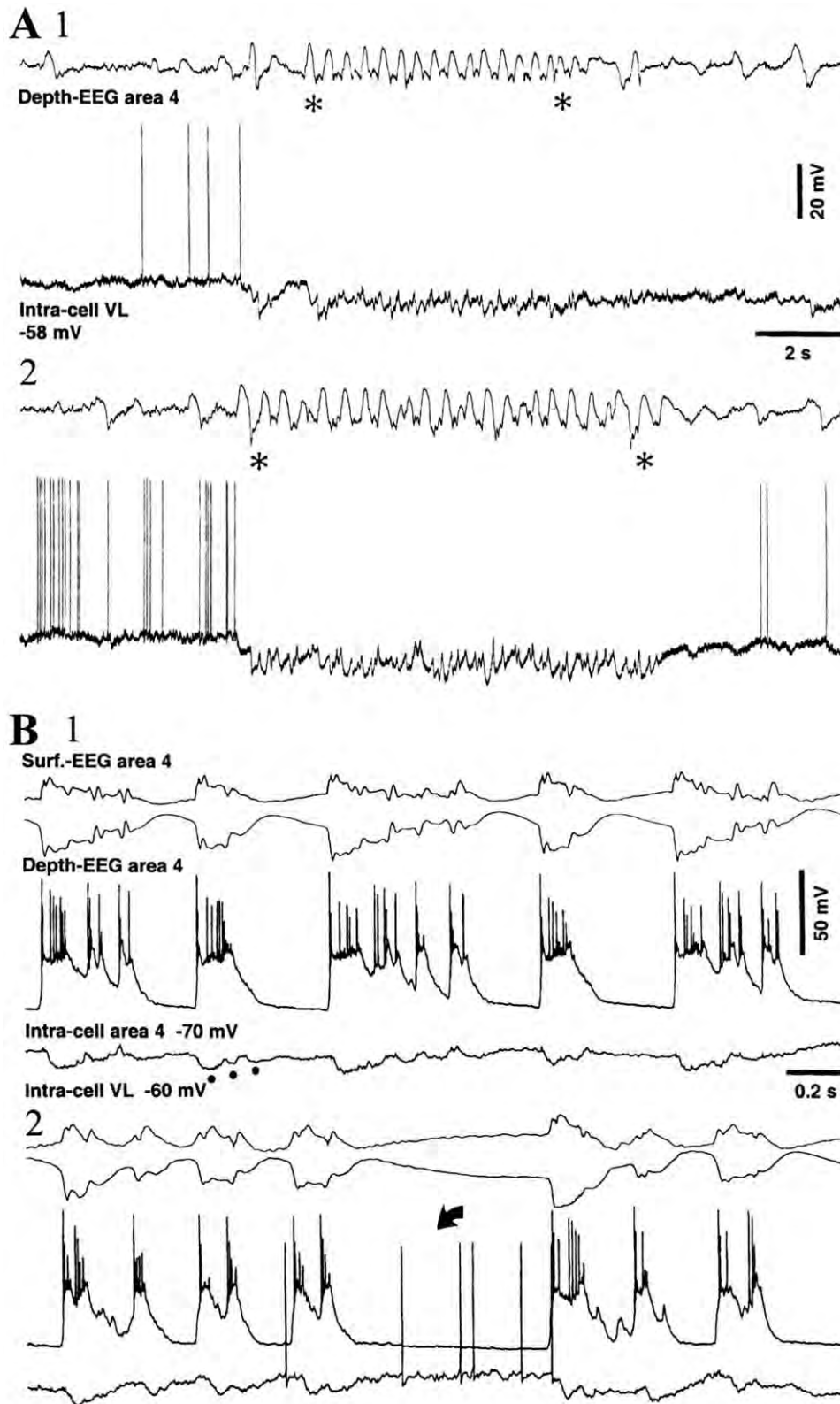
Fig. 11. TC neurons are inhibited during cortically generated SW seizure, and display phasic IPSPs but not spike-bursts. (A) Depth-EEG from cortical area 4 and intracellular recording of TC neuron from ventrolateral (VL) nucleus of cat. Note hyperpolarization and phasic IPSPs in VL neuron throughout cortically generated SW seizure (between asterisks); also note increased hyperpolarization and IPSPs in thalamic neuron with increased duration of the cortical seizure. (B) Dual intracellular recordings from area 4 cortical neuron and TC neuron from VL nucleus, together with surface- and depth-EEG from cortical area 4. The SW and PSW seizure developed, without discontinuity, from sleep-like EEG patterns. Note paroxysmal depolarizing shifts (PDSs) in cortical neuron, and phasic IPSPs (see three dots below the intracellular VL trace) related to cortical PDSs. Also note that, during a brief period of quiescence in cortical SW/PSW seizure (arrow in 2), the hyperpolarization of TC neuron was removed, the TC cell was disinhibited, and the neuron fired single action potentials. Modified from Steriade and Contreras (1995) and Lytton et al. (1997).

rhythms based on basic cellular mechanisms that underlie generation of brain waves. For example, the separation between "lower-frequency" and "faster" EEG spindles can be avoided by considering longer hyperpolarization-rebound sequences of some thalamic neurons in the former case, without splitting an oscillation generated by identical basic mechanisms, regardless of its wide frequency range. Similarly, fast rhythms are voltage-dependent, during either brain-active or brain-disconnected states, and the transition from beta to gamma oscillation operates in very short time periods under slight neuronal depolarization, which does not necessarily require their separate analysis. Clinical investigators have already begun to use the knowledge obtained in cellular studies on experimental animals.

REFERENCES

Abel T, Nguyen PV, Barad M, Deuel TA, Kandel ER, Bourtchouladze R (1997) Genetic demonstration of a role for PKA in the late phase of LTP and in hippocampus-based long-term memory. Cell 88: 615–626.

Achermann P, Borbély A (1997) Low-frequency (<1 Hz) oscillations in the human sleep EEG. Neuroscience 81:213–222.

Amzica F, Steriade M (1996) Progressive cortical synchronization of ponto-geniculo-occipital potentials during rapid eye movement sleep. Neuroscience 72:309–314.

Amzica F, Steriade M (1997) The K-complex: its slow (<1 Hz) rhythmicity and relation to delta waves. Neurology 49:952–959.

Amzica F, Steriade M (1998) Cellular substrates and laminar profile of sleep K-complex. Neuroscience 82:671–686.

Avanzini G, De Curtis M, Marescaux C, Panzica F, Spreafico R, Vergnes M (1992) Role of thalamic reticular nucleus in the generation of rhythmic thalamo-cortical activities subserving spike and waves. J Neural Transm 35(Suppl):85–95.

Avanzini G, De Curtis M, Pape HC, Spreafico R (1999) Intrinsic properties of reticular thalamic neurons relevant to genetically determined spike-wave generation. In: Jasper's basic mechanisms of the epilepsies, 3rd edition (Delgado-Escueta AV, Wilson WA, Olsen RW, Porter RJ, eds), pp 297–309. Philadelphia: Lippincott-Williams & Wilkins.

Bazhenov M, Timofeev I, Steriade M, Sejnowski TJ (1998) Computational models of thalamocortical augmenting responses. J Neurosci 18:6444–6465.

Braun AR, Balkin TJ, Wesensten NJ, Carson RE, Varga M, Baldwin P, Selbie S, Belenky G, Herscovitch P (1997) Regional cerebral blood flow throughout the sleep-wake cycle. Brain 120:1173–1197.

Buzsáki G (1989) Two-stage model of memory trace formation: a role for "noisy" brain states. Neuroscience 31:551–570.

Buzsáki G (1996) The hippocampo-neocortical dialogue. Cereb Cortex 6:81–92.

Buzsáki G (1998) Memory consolidation during sleep: a neurophysiological perspective. J Sleep Res 7(Suppl 1):17–23.

Cantero JL, Atienza M, Salas RM, Dominguez-Marin E (2002) Effects of prolonged waking-auditory stimulation on electroencephalogram synchronization and cortical coherence during subsequent slow-wave sleep. J Neurosci 22:4702–4708.

Cardin JA, Palmer LA, Contreras D (2005) Stimulus-dependent gamma (30–50 Hz) oscillations in simple and complex fast rhythmic bursting cells in primary visual cortex. J Neurosci 25: 5339–5350.

Castro-Alamancos MA, Connors BW (1996) Cellular mechanisms of the augmenting response: short-term plasticity in a thalamocortical pathway. J Neurosci 16:7742–7756.

Chrobak JJ, Buzsáki G (1996) High-frequency oscillations in the output networks of the hippocampal-entorhinal axis of the freely behaving rat. J Neurosci 16:3056–3066.

Cicogna P, Natale V, Occhionero M, Bosinelli M (2000) Slow wave sleep and REM sleep mentation. Sleep Res Online 3:67–72.

Cirelli C, Gutierrez CM, Tononi G (2004) Extensive and divergent effects of sleep and wakefulness on brain gene expression. Neuron 41:35–43.

Cissé Y, Crochet S, Timofeev I, Steriade M (2004) Synaptic enhancement induced through callosal pathways in cat association cortex. J Neurophysiol 92:3221–3232.

Collins DR, Lang EJ, Paré D (1999) Spontaneous activity of the perirhinal cortex in behaving cats. Neuroscience 89:1025–1039.

Collins DR, Pelletier JG, Paré D (2001) Slow and fast (gamma) neuronal oscillations in the perirhinal cortex and lateral amygdala. J Neurophysiol 85:1661–1672.

Compte A, Sanchez-Vives MV, McCormick DA, Wang XJ (2003) Cellular and network mechanisms of slow oscillatory activity (<1 Hz) and wave propagations in a cortical network model. J Neurophysiol 89:2707–2725.

Contreras D, Steriade M (1995) Cellular basis of EEG slow rhythms: a study of dynamic corticothalamic relationships. J Neurosci 15: 604–622.

Contreras D, Destexhe A, Sejnowski TJ, Steriade M (1996a) Control of spatiotemporal coherence of a thalamic oscillation by corticothalamic feedback. Science 274:771–774.

Contreras D, Timofeev I, Steriade M (1996b) Mechanisms of long-lasting hyperpolarizations underlying slow sleep oscillations in cat corticothalamic networks. J Physiol (Lond) 494:251–264.

Contreras D, Destexhe A, Sejnowski TJ, Steriade M (1997) Spatiotemporal patterns of spindle oscillations in cortex and thalamus. J Neurosci 17:1179–1196.

Crunelli V, Leresche N (2002) Childhood absence epilepsy: genes, channels, neurons and networks. Nat Rev Neurosci 3:371–382.

Curró Dossi R, Paré D, Steriade M (1991) Short-lasting nicotinic and long-lasting muscarinic depolarizing responses of thalamocortical neurons to stimulation of mesopontine cholinergic nuclei. J Neurophysiol 65:393–406.

Danober L, Depaulis A, Marescaux C, Vergnes M (1993) Effects of cholinergic drugs on genetic absence seizures in rats. Eur J Pharmacol 234:263–268.

Danober L, Depaulis A, Vergnes M, Marescaux C (1995) Mesopontine cholinergic control over generalized non-convulsive seizures in a genetic model of absence epilepsy in the rat. Neuroscience 69: 1183–1193.

Dement WC, Ferguson J, Cohen H, Barchas J (1969) Non-chemical methods and data using a biochemical model: the REM quanta. In: Psychochemical research in man: methods, strategy and theory (Mandell A, Mandell MP, eds), pp 275–325. New York: Academic Press.

Dolmetsch RE, Pajvani U, Fife K, Spotts JM, Greenberg ME (2001) Signaling to the nucleus by an L-type calcium channel-calmodulin complex through the MAP kinase pathway. Science 294:333–339.

Finelli LA, Baumann H, Borbely A, Achermann P (2000) Dual electroencephalogram markers of human sleep homeostasis: correlation between theta activity in waking and slow-wave activity in sleep. Neuroscience 101:523–529.

Fiset P, Paus T, Daloze T, Plourde G, Meuret P, Bonhomme V, Hajj-Ali N, Backman SB, Evans AC (1999) Brain mechanisms of propofol-induced loss of consciousness in humans: a positron emission tomography study. J Neurosci 19:5506–5513.

Fosse R, Stickgold R, Hobson JA (2004) Thinking and hallucinating: reciprocal changes in sleep. Psychophysiology 41:298–305.

Foulkes D (1962) Dream reports from different stages of sleep. J Abnorm Soc Psychol 65:14–25.

Frank G (1969) A study of the inter-relations of spike discharge density and sleep stages in epileptic patients. Electroencephalogr Clin Neurophysiol 26:238

Frank MG, Issa NP, Stryker MP (2001) Sleep enhances plasticity in the developing visual cortex. Neuron 30:275–287.

Fries P, Reynolds JH, Rorie AE, Desimone R (2001) Modulation of oscillatory neuronal synchronization by selective visual attention. Science 291:1560–1563.

Fuentealba P, Timofeev I, Steriade M (2004) Prolonged hyperpolarizing potentials precede spindle oscillations in the thalamic reticular nucleus. Proc Natl Acad Sci U S A 101:9816–9821.

Gais S, Born J (2004) Low acetylcholine during slow-wave sleep is critical for declarative memory consolidation. Proc Natl Acad Sci U S A 101:2140–2144.

Gais S, Plihal W, Wagner U, Born J (2000) Early sleep triggers memory for early visual discrimination skills. Nat Neurosci 3:1335–1339.

Gais S, Mölle M, Helms K, Born J (2002) Learning-dependent increases in sleep density. J Neurosci 22:6830–6834.

Golshani P, Liu XB, Jones EG (2001) Differences in quantal amplitude reflect GluR4-subunit number at corticothalamic synapses on two populations of thalamic neurons. Proc Natl Acad Sci U S A 98:4172–4177.

Gray CM, McCormick DA (1996) Chattering cells: superficial pyramidal neurons contributing to the generation of synchronous oscillations in the visual cortex. Science 274:109–113.

Grenier F, Timofeev I, Steriade M (2001) Focal synchronization of ripples (80–200 Hz) in neocortex and their neuronal correlates. J Neurophysiol 86:1884–1898.

Grenier F, Timofeev I, Steriade M (2003) Neocortical very fast oscillations (ripples, 80–200 Hz) during seizures: intracellular correlates. J Neurophysiol 89:841–852.

Hasselmo ME (1999) Neuromodulation: acetylcholine and memory consolidation. Trends Cogn Sci 3:351–359.

Hirsch JC, Fourment A, Marc ME (1983) Sleep-related variations of membrane potential in the lateral geniculate body relay neurons of the cat. Brain Res 259:308–312.

Hobson JA (1988) The dreaming brain. New York: Basic Books.

Hobson JA, Pace-Schott EF (2002) The cognitive neuroscience of sleep: neuronal systems, consciousness and learning. Nat Rev Neurosci 3:679–693.

Hobson JA, Pace-Schott E, Stickgold R (2000) Dreaming and the brain: toward a cognitive neuroscience of conscious states. Brain Behav Sci 23:793–842.

Hofle N, Paus T, Reutens D, Fiset P, Gotman J, Evans AC, Jones BE (1997) Regional cerebral blood flow changes as a function of delta and spindle activity during slow wave sleep in humans. J Neurosci 17:4800–4808.

Hu B, Steriade M, Deschênes M (1989) The effects of peribrachial stimulation on reticular thalamic neurons: the blockage of spindle waves. Neuroscience 31:1–12.

Huber R, Ghilardi MF, Massimini M, Tononi G (2004) Local sleep and learning. Nature 430:78–81.

Huguenard JR (1996) Low-threshold calcium currents in central nervous system neurons. Annu Rev Physiol 58:329–348.

Jasper HH, Droogleever-Fortuyn J (1949) Experimental studies on the functional anatomy of petit-mal epilepsy. Res Publ Ass Nerv Ment Dis 26:272–298.

Jasper HH, Hawkes WA (1938) Electroencephalography. IV. Localization of seizure waves in epilepsy. Arch Neurol (Chic) 39:885–901.

Jones EG (1985) The thalamus. New York: Plenum.

Jones EG (2002) Thalamic circuitry and thalamocortical synchrony. Phil Trans R Soc Lond B 357:1659–1673.

Kamondi A, Acsády L, Buzsáki G (1998) Dendritic spikes are enhanced by cooperative network activity in the intact hippocampus. J Neurosci 18:3919–3928.

Kellaway P (1985) Sleep and epilepsy. Epilepsia 26(Suppl 1):15–30.

Kellaway P, Frost JD Jr (1983) Biorhythmic modulation of epileptic events. In: Recent advances in epilepsy, Vol. 1 (Pedley TA, Meldrum BS, eds), pp 139–154. London: Churchill-Livingstone.

Kobayashi K, Nishibayashi N, Ohtsuka Y, Oka E, Ohtahara S (1994) Epilepsy with electrical status epilepticus during slow sleep and secondary bilateral synchrony. Epilepsia 35:1097–1103.

Lemieux JF, Blume WT (1986) Topographical evolution of spike-wave complexes. Brain Res 373:275–287.

Leresche N, Jassik-Gerschenfeld D, Haby M, Soltesz I, Crunelli V (1990) Pacemaker-like and other types of spontaneous membrane potential oscillations of thalamocortical cells. Neurosci Lett 113:72–77.

Leresche N, Lightowler S, Soltesz I, Jassik-Gerschenfeld D, Crunelli V (1991) Low-frequency oscillatory activities intrinsic to rat and cat thalamocortical cells. J Physiol (Lond) 441:155–174.

Llinás RR (1988) The intrinsic electrophysiological properties of mammalian neurons: insights into central nervous system function. Science 242:1654–1664.

Llinás RR, Ribary U (1993) Coherent 40-Hz oscillation characterizes dream state in humans. Proc Natl Acad Sci U S A 90:2078–2081.

Llinás RR, Grace AA, Yarom Y (1991) In vitro neurons in mammalian cortical layer 4 exhibit intrinsic oscillatory activity in the 10- to 50-Hz frequency range. Proc Natl Acad Sci U S A 88:897–901.

Lytton WW, Contreras D, Destexhe A, Steriade M (1997) Dynamic interactions determine partial thalamic quiescence in a computer network model of spike-wave seizures. J Neurophysiol 77:1679–1696.

Magill PJ, Bolam P, Bevan MD (2000) Relationship of activity in the subthalamic nucleus-globus pallidus network to cortical EEG. J Neurosci 20:820–833.

Mahon S, Deniau JM, Charpier S (2001) Relationship between EEG potentials and intracellular activity of striatal and cortico-striatal neurons: an in vivo study under different anesthetics. Cereb Cortex 11:360–373.

Maquet P, Degueldre C, Delfiore G, Aerts J, Péters JP, Luxen A, Franck G (1997) Functional neuroanatomy of human slow wave sleep. J Neurosci 17:2807–2812.

Marcus EM, Watson CW, Simon SA (1968) Behavioral correlates of acute bilateral symmetrical epileptogenic foci in monkey cerebral cortex. Brain Res 9:370–373.

Marshall L, Mölle M, Born J (2003) Spindle and slow wave rhythms at slow wave sleep transitions are linked to strong shifts in the cortical direct current potential. Neuroscience 121:1047–1053.

Massimini M, Amzica F (2001) Extracellular calcium fluctuations and intracellular potentials in the cortex during the slow sleep oscillation. J Neurophysiol 85:1346–1350.

Massimini M, Huber R, Ferrarelli F, Tononi G (2004) The sleep slow oscillation as a traveling wave. J Neurosci 24:6862–6870.

Massimini M, Ferrarelli F, Huber R, Esser SK, Singh H, Tononi G (2005) Breakdown of cortical effective connectivity during sleep. Science 309:2228–2232.

McCormick DA, Pape HC (1990) Properties of a hyperpolarization-activated cation current and its role in rhythmic oscillation in thalamic relay neurones. J Physiol (Lond) 431:291–318.

Meeren HKM, Pijn JPM, van Luijtelaar EJLM, Coenen AML, Lopes da Silva FH (2002) Cortical focus drives widespread corticothalamic networks during spontaneous absence seizures in rats. J Neurosci 22:1480–1495.

Mölle M, Marshall L, Gais S, Born J (2002) Grouping of spindle activity during slow oscillations in human non-REM sleep. J Neurosci 22:10941–10947.

Neckelmann D, Amzica F, Steriade M (1998) Spike-wave complexes and fast components of cortically generated seizures. III. Synchronizing mechanisms. J Neurophysiol 80:1480–1494.

Niedermeyer E (2005) Sleep and EEG. In: Electroencephalography: basic principles, clinical applications and related fields, 5th edition (Niedermeyer E, Lopes da Silva FH, eds), pp 193–208. Philadelphia: Lippincott Williams & Wilkins.

Nielsen T (2000) Cognition in REM and NREM sleep. Brain Behav Sci 23:851–866.

Noachtar S (2001) Generalized epilepsy and sleep. In: Epilepsy and sleep (Dinner DS, Lüders HO, eds), pp 75–83. San Diego: Academic Press.

Nuñez A, Amzica F, Steriade M (1992) Voltage-dependent fast (20–40 Hz) oscillations in long-axoned neocortical neurons. Neuroscience 51:7–10.

Palva JM, Palva S, Kaila K (2005) Phase synchrony among neuronal oscillations in the human cortex. J Neurosci 25:3962–3972.

Pavlides C, Winson J (1989) Influences of hippocampal place cell firing in the awake state on the activity of these cells during subsequent sleep episodes. J Neurosci 9:2907–2918.

Pavlov IP (1923) "Innere Hemmung" der bedingten Reflexe und der Schlaf: ein und derselbe Prozess. Skand Arch Physiol 44:42–58.

Penfield W, Rasmussen T (1950) The cerebral cortex of man. A clinical study of localization of function.New York: Macmillan Co.

Pivik T, Foulkes D (1968) NREM mentation: relation to personality, orientation time and time of night. J Consult Clin Psychol 32:144–151.

Plihal W, Born J (1997) Effects of early and late nocturnal sleep on declarative and procedural memory. J Cogn Neurosci 9:534–547.

Sanchez-Vives MV, McCormick DA (2000) Cellular and network mechanisms of rhythmic recurrent activity in neocortex. Nat Neurosci 3:1027–1034.

Sejnowski TJ, Destexhe A (2000) Why do we sleep? Brain Res 886:208–223.

Shadlen MN, Movshon JA (1999) Synchrony unbound: a critical evaluation of the temporal binding hypothesis. Neuron 24:67–77.

Shouse MN (2001) Physiology underlying relationship of epilepsy and sleep. In: Epilepsy and sleep (Dinner DS, Lüders HO, eds), pp 43–62. San Diego: Academic Press.

Shouse MN, Martins da Silva A, Sammaritano M (1996) Circadian rhythm, sleep, and epilepsy. J Clin Neurophysiol 13:32–50.

Simon NR, Mandshanden I, Lopes da Silva FH (2000) A MEG study of sleep. Brain Res 860:64–76.

Singer W (1999) Neuronal synchrony: a versatile code for the definition of relations? Neuron 24:49–65.

Sirota A, Csicsvari J, Buhl D, Buzsáki G (2003) Communication between neocortex and hippocampus during sleep in rodents. Proc Natl Acad Sci U S A 100:2065–2069.

Slaght SJ, Leresche N, Deniau JM, Crunelli V, Charpier S (2002) Activity of thalamic reticular neurons during spontaneous genetically determined spike and wave discharges. J Neurosci 22:2323–2334.

Slotnick SD, Moo LR, Kraut MA, Lesser RP, Hart J Jr (2002) Interactions between thalamic and cortical rhythms during semantic memory recall in human. Proc Natl Acad Sci U S A 99:6440–6443.

Soderling TR, Derkach VA (2000) Postsynaptic protein phosphorylation and LTP. Trends Neurosci 23:75–80.

Spreafico R, Amadeo A, Angoscini P, Panzica P, Battaglia G (1993) Branching projections from mesopontine nuclei to the nucleus reticularis and related thalamic nuclei: a double labelling study in the rat. J Comp Neurol 336:481–492.

Steriade M (1974) Interneuronal epileptic discharges related to spike-and-wave cortical seizures in behaving monkeys. Electroencephalogr Clin Neurophysiol 37:247–263.

Steriade M (1991) Alertness, quiet sleep, dreaming. In: Cerebral cortex, Vol. 9, Normal and altered states of function (Peters A, Jones EG, eds), pp 279–357. New York: Plenum.

Steriade M (2000) Corticothalamic resonance, states of vigilance, and mentation. Neuroscience 101:243–276.

Steriade M (2001) The intact and sliced brain. Cambridge, MA: MIT Press.

Steriade M (2003) Neuronal substrates of sleep and epilepsy. Cambridge: Cambridge University Press.

Steriade M, Amzica F (1994) Dynamic coupling among neocortical neurons during evoked and spontaneous spike-wave seizure activity. J Neurophysiol 72:2051–2069.

Steriade M, Contreras D (1995) Relations between cortical and thalamic cellular events during transition from sleep pattern to paroxysmal activity. J Neurosci 15:623–642.

Steriade M, Contreras D (1998) Spike-wave complexes and fast runs of cortically generated seizures. I. Role of neocortex and thalamus. J Neurophysiol 80:1439–1455.

Steriade M, McCarley RW (2005) Brain control of wakefulness and sleep. New York: Springer-Kluwer-Plenum.

Steriade M, Timofeev I (2001) Corticothalamic operations through prevalent inhibition of thalamocortical neurons. Thal Rel Syst 1:225–236.

Steriade M, Timofeev I (2003a) Neuronal plasticity in thalamocortical networks during sleep and waking oscillations. Neuron 37:563–576.

Steriade M, Timofeev I (2003b) Neuronal plasticity during sleep oscillations in corticothalamic systems. In: Sleep and brain plasticity (Maquet P, Stickgold R, Smith CS, eds), pp 271–291. Oxford: Oxford University Press.

Steriade M, Deschênes M, Wyzinski P, Hallé JP (1974) Input-output organization of the motor cortex during sleep and waking. In: Basic sleep mechanisms (Petre-Quadens O, Schlag J, eds), pp 144–200. New York: Academic.

Steriade M, Paré D, Bouhassira D, Deschênes M, Oakson G (1989) Phasic activation of lateral geniculate and perigeniculate neurons during sleep with ponto-geniculo-occipital spikes. J Neurosci 9:2215–2229.

Steriade M, Curró Dossi R, Nuñez A (1991) Network modulation of a slow intrinsic oscillation of cat thalamocortical neurons implicated in sleep delta waves: cortical potentiation and brainstem cholinergic suppression. J Neurosci 11:3200–3217.

Steriade M, Amzica F, Nuñez A (1993a) Cholinergic and noradrenergic modulation of the slow (~0.3 Hz) oscillation in neocortical cells. J Neurophysiol 70:1384–1400.

Steriade M, Contreras D, Curró Dossi R, Nuñez A (1993b) The slow (<1 Hz) oscillation in reticular thalamic and thalamocortical neurons: scenario of sleep rhythm generation in interacting thalamic and neocortical networks. J Neurosci 13:3284–3299.

Steriade M, McCormick DA, Sejnowski TJ (1993c) Thalamocortical oscillation in the sleeping and aroused brain. Science 262:679–685.

Steriade M, Nuñez A, Amzica F (1993d) A novel slow (<1 Hz) oscillation of neocortical neurons in vivo: depolarizing and hyperpolarizing components. J Neurosci 13:3252–3265.

Steriade M, Nuñez A, Amzica F (1993e) Intracellular analysis of relations between the slow (<1 Hz) neocortical oscillation and other sleep rhythms. J Neurosci 13:3266–3283.

Steriade M, Contreras D, Amzica F (1994) Synchronized sleep oscillations and their paroxysmal developments. Trends Neurosci 17:199–208.

Steriade M, Amzica F, Contreras D (1996a) Synchronization of fast (30–40 Hz) spontaneous cortical rhythms during brain activation. J Neurosci 16:392–417.

Steriade M, Contreras D, Amzica F, Timofeev I (1996b) Synchronization of fast (30–40 Hz) spontaneous oscillations in intrathalamic and thalamocortical networks. J Neurosci 16:2788–2808.

Steriade M, Timofeev I, Dürmüller N, Grenier F (1998a) Dynamic properties of corticothalamic neurons and local cortical interneurons generating fast rhythmic (30–40 Hz) spike bursts. J Neurophysiol 79:483–490.

Steriade M, Timofeev I, Grenier F, Dürmüller N (1998b) Role of thalamic and cortical neurons in augmenting responses: dual intracellular recordings *in vivo*. J Neurosci 18:6425–6443.

Steriade M, Timofeev I, Grenier F (2001) Natural waking and sleep states: a view from inside neocortical neurons. J Neurophysiol 85:1969–1985.

Stickgold R, James L, Hobson JA (2000a) Visual discrimination learning requires sleep after training. Nat Neurosci 3:1237–1238.

Stickgold R, Whitbee D, Schirmer B, Patel V, Hobson JA (2000b) Visual discrimination improvement. A multi-step process occurring during sleep. J Cogn Neurosci 12:246–254.

Timofeev I, Steriade M (1996) Low-frequency rhythms in the thalamus of intact-cortex and decorticated cats. J Neurophysiol 76:4152–4168.

Timofeev I, Steriade M (1997) Fast (mainly 30–100 Hz) oscillations in the cat cerebellothalamic pathway and their synchronization with cortical potentials. J Physiol (Lond) 504:153–168.

Timofeev I, Contreras D, Steriade M (1996) Synaptic responsiveness of cortical and thalamic neurons during various phases of slow oscillation in cat. J Physiol (Lond) 494:265–278.

Timofeev I, Grenier F, Steriade M (2001) Disfacilitation and active inhibition in the neocortex during the natural sleep-wake cycle: an intracellular study. Proc Natl Acad Sci U S A 98:1924–1929.

Tononi G, Cirelli C (2003) Sleep and synaptic homeostasis. Brain Res Bull 62:143–150.

Traub RD, Schmitz D, Jefferys JGR, Draguhn A (1999) High-frequency population oscillations are predicted to occur in hippocampal pyramidal networks interconnected by axoaxonal gap junctions. Neuroscience 92:1370–1374.

Traub RD, Whittington MA, Buhl EH, LeBeau FN, Bibbig A, Boyd S, Cross H, Baldeweg TA (2001) A possible role of gap junctions in generation of very fast EEG oscillations preceding the onset of, or perhaps initiating, seizures. Epilepsia 42: 153–170.

Traub RD, Cunningham MO, Gloveli T, LeBeau FEN, Bibbig A, Buhl EH, Whittington MA (2003) GABA-enhanced collective behavior in neuronal axons underlies persistent gamma-frequency oscillation. Proc Natl Acad Sci U S A 100:11047–11052.

Traub RD, Contreras D, Cunningham MO, Murray H, LeBeau FE, Roopun A, Bibbig A, Wilent WB, Higley MJ, Whittington MA (2005) Single column thalamocortical network model exhibiting gamma oscillations, sleep spindles, and epileptogenic bursts. J Neurophysiol 93:2194–2232.

Tsakiridou E, Bertollini L, de Curtis M, Avanzini G, Pape HC (1995) Selective increase in T-type calcium conductance of reticular thalamic neurons in a rat model of absence epilepsy. J Neurosci 15:3110–3117.

Villablanca J (1974) Role of the thalamus in sleep control: sleep-wakefulness studies in chronic diencephalic and athalamic cats. In: Basic sleep mechanisms (Petre-Quadens O, Schlag J, eds), pp 51–81. New York: Academic Press.

White EL (1989) Cortical circuits: synaptic organization of the cerebral cortex. Boston: Birkhäuser.

Wilson CJ, Kawaguchi Y (1996) The origin of two-state spontaneous membrane potential fluctuations of neostriatal spiny neurons. J Neurosci 16:2397–2410.

Wilson MA, McNaughton BL (1994) Reactivation of hippocampal ensemble memories during sleep. Science 265:676–679.

Yuste R, Tank DW (1996) Dendritic integration in mammalian neurons, a century after Cajal. Neuron 16:701–716.

EEG 90606

Report of IFCN Committee on Basic Mechanisms

Basic mechanisms of cerebral rhythmic activities [1]

M. Steriade (Canada), P. Gloor (Canada), R.R. Llinás (U.S.A.), F.H. Lopes da Silva (The Netherlands) and M.-M. Mesulam (U.S.A.)

1. Synchronizing and desynchronizing neuronal networks

Various wave patterns of the electroencephalogram (EEG), related to distinct behavioral states, are usually referred to as *synchronized* or *desynchronized* activities. The first term implies the occurrence of high-amplitude oscillations with relatively slow frequencies, and the second term indicates a replacement of synchronized rhythms by lower-amplitude and relatively faster waves. While this dichotomy may appear as an oversimplification, since an increased frequency of EEG waves may be associated with their increased amplitudes in peculiar behavioral conditions, the above terms have some heuristic values.

1.1. Synchronization

Synchronization is a state in which two or more oscillators display the same frequency because of some forms of co-interaction. There is no necessity in deciding between the two parts of the

---

Correspondence to: Prof. M. Steriade, MD, DSc, Laboratoire de Neurophysiologie, Faculté de Médecine, Université Laval, Quebec G1K 7P4 (Canada).

alternative, whether the intrinsic properties of single neurons are essential for the genesis of brain waves with different frequencies or whether such rhythms basically emerge from synaptic interactions in large neuronal pools. Both these factors should be eclectically considered.

Some central single neurons display spontaneous oscillations in vitro, even after blockage of synaptic transmission. Other types of neurons can be led to an oscillatory state by injecting intracellular currents in particular bathing conditions, due to their special ionic conductances. The intrinsic electrophysiological properties of thalamic, neocortical and allocortical neurons allow them to oscillate within different frequency spectra, and much of the patterning of basic EEG rhythms requires special sodium, calcium and potassium conductances, other than the conventional ones generating the action potentials (see Section 2). There is now ample evidence that, under imposed experimental conditions, isolated neurons can display oscillations, usually within a frequency band of 1–20 Hz.

In the intact brain, however, the intrinsic properties of single cells are subject to controlling influences from synchronizing pacemakers or driving forces within given neuronal networks that unite single elements into ensembles. Indeed, the notion of EEG synchronization supposes the co-activation of a large number of neurons, the summed synaptic events of which become sufficiently large to be recorded with gross electrodes within the brain or over the scalp. The role of synaptic networks in the genesis of various EEG

rhythms is emphasized by frequency differences between various oscillations generated within various neuronal ensembles, in spite of essentially similar intrinsic electrophysiological properties and ionic conductances of their constituent single neurons (Steriade et al. 1990b). Also, some EEG oscillations are absent in thalamocortical systems in the absence of the rhythm-pacemaker, despite the fact that single neurons within those systems preserve their intrinsic properties (see Section 3.2).

The synchronizing systems can be viewed as multiple devices with equal properties of rhythmicity and mutual influences within a series of interconnected structures or as a single pacemaker. *(a)* The multiple synchronizing systems are probably those generating theta waves which originate in a series of synaptically coupled stations of the limbic system (see Section 3.4). In the
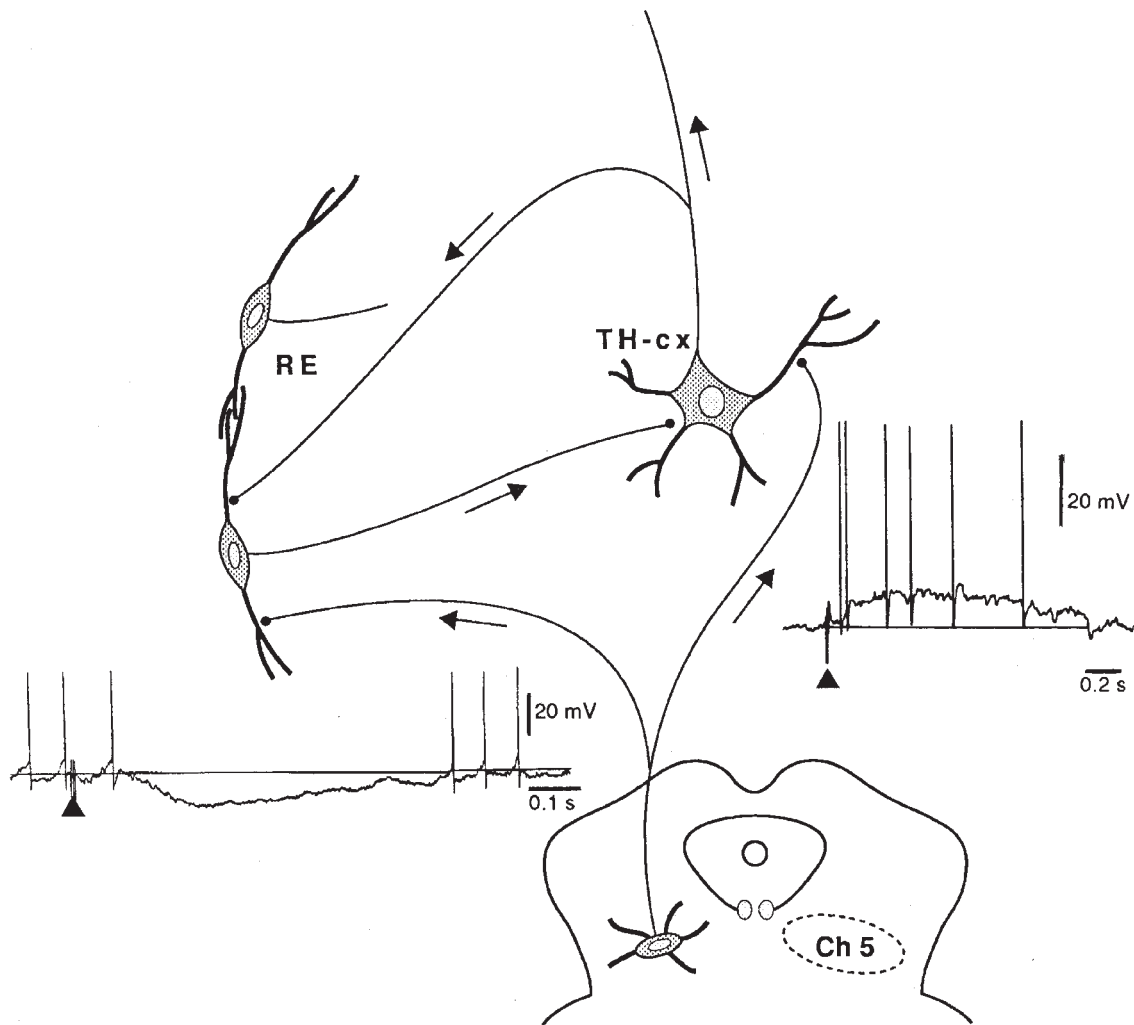
Fig. 1. Recurrent inhibitory loop of thalamocortical (TH-cx) and reticular thalamic (RE) neurons, and modulation of TH-cx and RE cells by mesopontine cholinergic afferents (only the Ch5 group of pedunculopontine tegmental neurons is depicted). In insets, Ch5 stimulation (brief pulse-train, arrowhead) induces a depolarization of TH-cx neurons and a hyperpolarization of RE neurons. Intracellular recordings from studies by Currό Dossi et al. (1990, TH-cx) and Hu et al. (1989a, RE). The direct excitation of TH-cx cells is accompanied by their disinhibition (through inhibition of GABAergic RE cells). These effects are effective in disrupting synchronized spindle oscillations in TH-cx systems, the thalamic part of the EEG desynchronization process (see also Section 3.2).

case of distributed systems, each endowed with pacemaker faculties, the starting point of rhythmic activity may change from time to time according to activity in afferent pathways, but distinctly in such synchronizing systems lesioning any part does not prevent rhythmicity in others. *(b)* For some types of brain oscillations, such as spindles, the pacemaker is located within the reticular thalamic nucleus, consisting of chemically homogenous neurons that establish the necessary connections to secure spread of rhythmicity toward virtually all cortically projecting thalamic nuclei. The criteria for determining a cell group as a unique pacemaker are loss of oscillations in target structures disconnected from the pacemaker and presence of oscillations in the pacemaker disconnected from its inputs (see Section 3.2).

1.2. Desynchronization

Blockage of spindles and slow waves occurs upon awakening from the state of EEG-synchronized sleep as well as during rapid eye movement (REM) or EEG-desynchronized sleep. The EEG-synchronized activity is replaced by low-amplitude and fast waves in the thalamocortical circuit. The similar pattern of EEG activity and the similarly enhanced synaptic excitability of thalamic and neocortical cells during waking and REM sleep, two states that were initially regarded as the two poles of the waking-sleep cycle, indicate that both these EEG-desynchronized states are *activated* at the electrophysiological level of central neurons, despite great differences in their mental content and the fact that central motor commands are blocked because of the hyperpolarization of spinal motoneurons during REM sleep.

The EEG desynchronization during both waking and REM sleep concerns widespread thalamic and cortical territories and reflects diffuse excitability changes. In states of focussed attention, however, synchronized focal oscillations with fast frequencies may develop in quite circumscribed neocortical areas (see Section 3.5). On the other hand, the hippocampus, entorhinal cortex and related subsystems display synchronized theta waves during various forms of waking activities and during REM sleep (see Section 3.4), at a time when

large regions of the neocortical mantle display desynchronized waves.

The mechanisms that underly the blockage of synchronized spindles and slow waves with transition from EEG-synchronized sleep to either waking or REM sleep do basically depend upon cholinergic projections arising in the brain-stem and basal forebrain. The long-standing hypothesis of a cholinergic activating system was recently substantiated by much experimental evidence. Morphological studies combining retrograde tracing techniques with choline acetyltransferase immunohistochemistry have revealed the brain-stem projections to the thalamus and the basal forebrain projections to the cerebral cortex as well as the thalamus (see Sections 2.4 and 4.1). Electrophysiological studies have indicated that the desynchronizing brain-stem–thalamic network involves a synaptic decoupling in the thalamic generator of spindle oscillations, in addition to direct excitation of thalamic relay neurons (Fig. 1). Acetylcholine is the neurotransmitter responsible for this action, by switching the burst firing mode and the depressed responsiveness of thalamic and neocortical neurons during EEG-synchronized sleep toward a tonic firing mode associated with enhanced transfer function of externally or internally generated messages during waking and REM sleep (see Section 4.2). Another neuromodulator, norepinephrine, acts in conjunction with acetylcholine during wakefulness, but is not operational during the other brain-activated state (REM sleep) because of the virtual silence of locus coeruleus neurons.

2. Intrinsic electrophysiological properties of neurons in the thalamocortical circuit and in related brain-stem nuclei

In the last 5–10 years, intracellular recording from neurons in the thalamus and cortex have revealed specialized electrophysiological properties which endow them with oscillatory properties. This research has been performed initially in in vitro mammalian slices as well as in the in vivo condition, most particularly, in the guinea pig and cat (Steriade and Llinás 1988). Because in the in

vitro studies the ionic milieu of the cell can be directly controlled by the use of ion channel blockers, such investigations have revealed that neurons at thalamic and cortical levels are endowed with many electroresponsive ionic conductances.

2.1. Thalamocortical neurons

In the thalamus, intracellular studies have demonstrated that most of the neurons which project to the cerebral cortex behave, electrophysiologically, in an almost uniform fashion. In addition to the sodium and potassium conductances which generate the fast action potentials, the cells demonstrate a high-threshold dendritic calcium spike which regulates the duration of the normal spike afterhyperpolarization. This calcium conductance may be blocked by either cadmium or cobalt, in which case the duration of the afterhyperpolarization is reduced since the calcium-dependent potassium conductance is not activated (Jahnsen and Llinás 1984a,b).

Another conductance well represented in these neurons is that which generates the low-threshold calcium spike, which was initially described in the inferior olivary cells (Llinás and Yarom 1981) and which generates the rebound spike of thalamic neurons (Llinás and Jahnsen 1982; Fig. 2). These channels allow inward calcium movement and are inactive at rest but de-inactivated upon membrane hyperpolarization. De-inactivation reaches a maximum at about -85 mV and is time-dependent. Also present in the thalamus is an early potassium conductance similar to that found in invertebrates and known as the A current. Finally, a non-inactivating sodium conductance (Llinás and Sugimori 1980; Stafstrom et al. 1984a) may be observed in thalamic neurons. Taking together, these conductances lead thalamic neurons to oscillate at either 10 Hz, if allowed to come to an equilibrium state upon the non-inactivating sodium conductance, or at 6 Hz if hyperpolarizing potentials are generated by inhibitory means (cf., Steriade and Llinás 1988). These two intrinsic rhythms allow the cells to either oscillate or resonate in reciprocal thalamocortical loops at these two main frequencies.
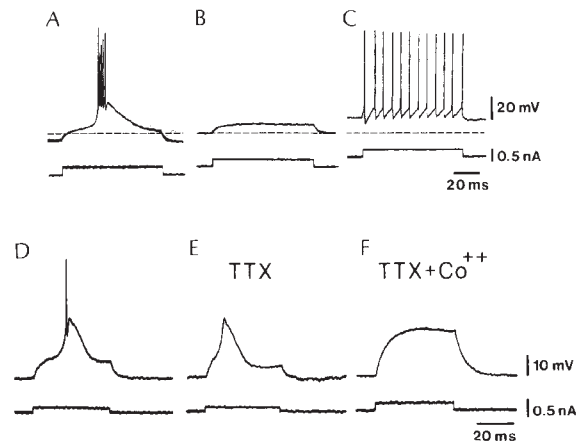

Fig. 2. Two firing levels in thalamic neurons and ionic conductance for low-threshold spike (LTS) in in vitro studies of guinea-pig thalamus. A: cell was directly excited while being hyperpolarized by a constant current injection. Depolarizing current pulse induces an LTS that triggers a burst of fast action potentials. B: same current pulse produces a sub-threshold depolarization if superimposed on a slightly depolarized membrane potential level. C: after further depolarization by direct current, pulse produces a train of action potentials. D: LTS generated by direct stimulation from a slightly hyperpolarized neuron. E: blockage of sodium conductance by tetradotoxin (TTX) removes fast spike but leaves LTS unmodified. F: addition of cobalt to the bath abolishes LTS even when current pulse is increased in amplitude by 2.5 times, demonstrating that LTS is generated by a low-threshold calcium conductance. (Modified from Llinás and Jahnsen 1982.)

In addition to the oscillatory properties, the thalamic neurons are also capable of functioning as relay elements (Steriade and Llinás 1988). Thus, depolarization of the membrane from resting level generates repetitive activity of the neuron which resembles that in other cells of the neural axis. Thalamic neurons are, thus, capable of 2 distinct forms of activity, namely: *(a)* a burst-like event that occurs when the membrane potential is negative to -70 mV (Deschênes et al. 1984; Jahnsen and Llinás 1984a,b) and underlies the burst response observed during spindling and during the late stage of EEG-synchronized sleep when ponto-geniculo-occipital (PGO) waves appear and herald REM sleep; *(b)* when the cell depolarizes from -60 mV the cells are capable of tonic repetitive activity and may serve as relay elements (Deschênes et al. 1984; Jahnsen and Llinás 1984a,b). These 2 types of thalamic activity repre-

sent intrinsic electrophysiological states which co-exist with different functional states of the brain such as the sleep-wakefulness cycle (Steriade and Llinás 1988).

2.2. Reticular thalamic neurons

Another element in the thalamocortical circuit is the neurons of the reticular thalamic nucleus. These neurons, that use GABA, a powerful inhibitory transmitter, are similar to the cortically projecting thalamic cells but, in addition to the conductances described above, they possess powerful sodium-dependent dendritic spiking properties and a second rebound excitation produced by a calcium entry located most probably at dendritic level (Llinás and Geijo-Barrientos 1988). These properties allow the reticular thalamic neurons to oscillate easily, in fact, more readily than the thalamic neurons themselves, especially during the light sleep state with EEG synchronization (Steriade et al. 1986). In this respect, the synaptic organization in the circuit between thalamocortical and reticular thalamic cells becomes oscillatory since the neurons of the reticular nucleus generate powerful inhibitory postsynaptic potentials (IPSPs) in thalamocortical neurons, which produce rebound excitation which returns to the reticular thalamic neurons (Steriade and Llinás 1988). Moreover, since the thalamic neurons give collaterals to the reticular thalamic nucleus on their way to the cortex, and the cortical pyramidal cells also give collaterals as they return to the thalamus, a second oscillatory system includes a thalamocortical pathway.

2.3. Neocortical neurons

While the cortical neurons demonstrate the rebound calcium conductance (Grace and Llinás 1984; Stafstrom et al. 1984b; McCormick et al. 1985) observed in thalamic neurons, this conductance is not as sizable as in the thalamic cells. Nevertheless, cortical neurons have sufficient low-threshold spiking to be able to respond very specifically to given thalamic input at given frequencies. In addition to a rebound calcium spiking, the cortical cells possess an inactivating sodium conductance and are capable of repetitive firing. The cells also demonstrate anomalous rectification as well as a powerful delay rectification (Connors et al. 1982; Stafstrom et al. 1984a; McCormick et al. 1985).

2.4. Brain-stem neurons with thalamic projections

Another set of neurons that is important in the functional organization of the thalamocortical system is located in the brain-stem, namely, in the pedunculopontine tegmental (PPT) and laterodorsal tegmental (LDT) nuclei. Neurons of these nuclei provide the major cholinergic input to the thalamus (Mesulam et al. 1983; Hallanger et al. 1987; Paré et al. 1988; Steriade et al. 1988; see also Section 4.1) and have recently been investigated in brain slices (Leonard and Llinás 1988, 1990; Kang and Kitai 1990). Three types of neurons have been identified electrophysiologically, one of which has low-threshold calcium spikes, one has a strong transient potassium conductance (A-conductance), and one has both (Leonard and Llinás 1990). The latter two types of neurons have been demonstrated to project to the thalamus by intracellular recordings and dye injection of PPT neurons retrogradely labeled with fluorescent microspheres injected into the thalamus. In addition, the type of neuron having the A-conductance has been shown to be cholinergic by combining intracellular recording, dye injection and histochemical labeling methods. Thus, the use of a combination of 3 different techniques reveals that cholinergic and other thalamically projecting neurons of PPT and LDT nuclei have the necessary electrophysiological characteristics to generate functional events of the sleep-wake cycle, such as PGO waves (see also Section 4.2).

3. Phenomenology, mechanisms, and behavioral connotations of various EEG rhythms in normal and pathological conditions

3.1. Alpha waves

The alpha rhythm has a frequency range of 8–13 Hz, occurs during wakefulness particularly
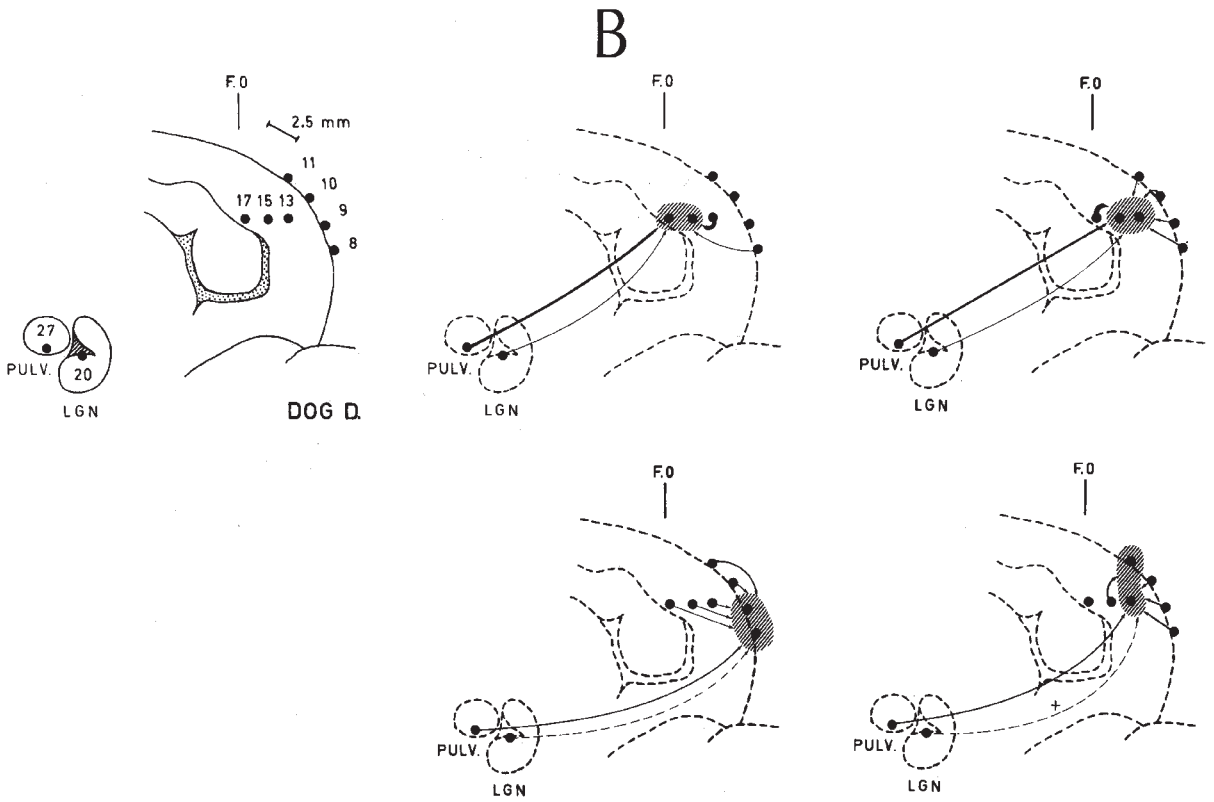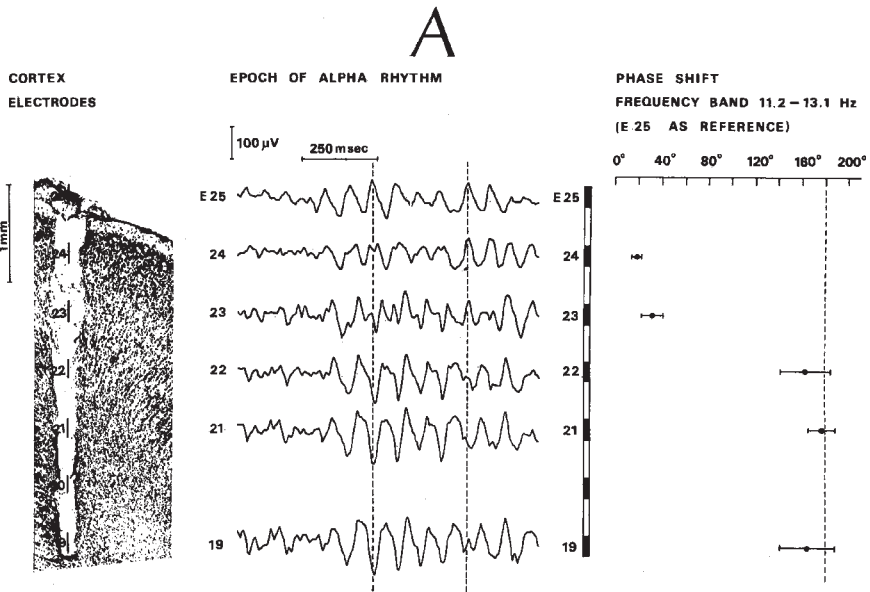
over the occipital cortex, appears at eyes closure and disappears at eyes opening. Several alpha rhythms differing in frequency components may coexist in the occipital cortex.

In order to study experimentally the mechanisms of generation of the alpha rhythm, it is important to have available animal models of this EEG activity. Two types of experimental models have been used in this context. *(a)* Recordings by way of chronically indwelling electrodes in experimental animals in the awake state under conditions as close as possible to those known to be necessary for the occurrence of the alpha rhythm in man. This has been studied particularly in cat (Lanoir and Cordeau 1970; Rougeul et al. 1974), dog (Storm van Leeuwen et al. 1967; Lopes da Silva et al. 1973a), and monkey (Jurko and Andry 1967). *(b)* In view of the apparent similarity between sequences of alpha waves and spindles under barbiturate anesthesia, the latter have been assumed to provide an acceptable experimental animal model of alpha rhythmic activity (Andersen and Andersson 1968). However, there are a number of essential differences between both types of phenomena, concerning spectra and topographic distribution (Lopes da Silva et al. 1973b).

Moreover, barbiturate-induced or natural sleep spindling appears during unconsciousness and is associated with blockade of synaptic transmission through the thalamus (see Section 3.2), whereas alpha waves may increase during attention tasks (Creutzfeldt et al. 1969; Ray and Cole 1985). Furthermore, alpha waves are mainly distributed along cortico-cortical pathways (see below, this section), whereas spindle waves are generated in the thalamus and exclusively distributed to neocortex along thalamocortical axons (see Section 3.2). Nevertheless it is possible that parts of the neuronal elements and networks responsible for the generation of spindles, also account for the genesis of alpha rhythms. The main differences between both types of phenomena pertain mainly to dynamics of the two types of rhythmic activities.

Experimentally a number of features of alpha rhythms recorded from the awake animal have been established, particularly using the dog as the experimental model: *(a)* alpha rhythms of the same peak frequency, bandwidth and reactivity can be recorded from the visual cortex as well as from the visual thalamus, namely, lateral geniculate and pulvinar nuclei (Lopes da Silva et al.

Fig. 3. Alpha rhythm in dog. A, left: photomicrograph of a section of the lateral gyrus (visual cortex). The electrode bundle consisted of 7 wires with a bare tip of 0.15 mm, as indicated by the bars at the side of the electrode numbers. Middle: an epoch of alpha activity recorded simultaneously from 6 sites corresponding to those shown at left, against a common frontal cranial reference (negativity upwards). Note that there is a polarity change between the most superficial sites (E25, 24) and the deepest sites (E22, 21, 19). At E23 a transition type of wave form can be seen. Right: phase shift between the most superficial site (E25) and deeper lying sites computed using spectral analysis based on the average of a number of epochs within the frequency band 11.2–13.1 Hz. The mean values of the phase shift and the corresponding standard deviations are indicated. Note the gradual increase in phase shift as a function of cortical depth down to electrode site E23 and the jump in phase of about 180° (broken line) at the level of E22. This indicates that the neuronal generators of the cortical alpha rhythm are at the level of the large pyramidal cells at about 1.1 mm below the surface of the visual cortex. B: schematic view of the relationship between thalamic and cortical alpha rhythmic activity. The lines indicate the amount of influence that a thalamic signal has on the coherence between a pair of cortical signals (shaded area) recorded during alpha rhythm in the awake dog. This was measured by partializing the intercortical coherence on the thalamic signals recorded from the LGN (lateral geniculate nucleus) and the PULV (pulvinar nucleus) or other cortical signals. This computation of "partial coherence functions" permits to perform a sort of "theoretical thalamic deafferentation." On the left-hand side the position of the cortical and thalamic electrodes is depicted, with the electrode sites numbered (frontal plane 0 is given by F0). Each scheme on the right-hand side represents the result of a partialization – the width of the lines indicates the amount of influence of a third signal on the coherence between a pair. Note that the influence of PULV is much larger than that of the LGN; the influence of the cortical site 13 is also large but that of site 8 is small. On the 2nd row can be seen that the influence of the thalamic sites on the coherence between pairs involving the visual cortex is much smaller, even negligible, for the LGN (broken lines). These results indicate that the PULV, but not the LGN, has a widespread influence on cortico-cortical domains of alpha activity over the mesial occipital cortex, but much less over the lateral gyrus. Nevertheless, the residual cortico-cortical coherences are still large (not shown) indicating that intracortical factors play also a significant role for the establishment of cortical domains of alpha activity. (A modified from Lopes da Silva and Storm van Leeuwen 1977; and B from Lopes da Silva et al. 1980.)

A

CORTEX ELECTRODES

EPOCH OF ALPHA RHYTHM

PHASE SHIFT FREQUENCY BAND 11.2 – 13.1 Hz (E 25 AS REFERENCE)

B

DOG D.

1973a); *(b)* alpha rhythms of the visual cortex are generated by an equivalent dipole layer centered at the level of the somata and basal dendrites of pyramidal neurons of layers IV and V (Fig. 3A; Lopes da Silva and Storm van Leeuwen 1977); *(c)* cortical alpha rhythms appear to be generated in relatively small cortical areas which act as epicenters; from these, alpha activity spreads around in different directions up to distances of 4 mm with an apparent velocity of propagation over the cortical surface of about 0.33/msec (Lopes da Silva and Storm van Leeuwen 1977); *(d)* coherences between alpha rhythms simultaneously recorded in thalamus and cortex are in most cases significantly different from zero (largest value for the squared coherence was found to be 0.56 at 12.1 Hz, 95% confidence limits 0.75–0.32; Lopes da Silva et al. 1973a); *(e)* coherences between alpha rhythms recorded between electrodes placed in the cortex at relatively small distances (2 mm) are usually large (> 0.81 squared coherence) and decrease with distance (Lopes da Silva and Storm van Leeuwen 1977); *(f)* the above mentioned studies have revealed that intracortical coherences are in general larger than any thalamocortical coherence measured in the same animal. Furthermore it was found that the alpha rhythms of the lateral geniculate nucleus influence the coherence between cortical alpha rhythms only moderately, whereas those of the pulvinar may have a much stronger influence on the same activity (Lopes da Silva et al. 1980; Fig. 3B).

These findings led to the general conclusion that there are thalamocortical and cortico-cortical systems which interact in the generation of cortical alpha rhythms.

Theoretically, a model of alpha rhythm generation and propagation in a cortical network has suggested that the influence of the excitatory and inhibitory intracortical connections in the networks generating an alpha rhythm falls off exponentially with characteristic distances of the same order of magnitude as a cortical module or column (Van Rotterdam et al. 1982).

These experimental and theoretical studies provide a basis for an understanding of alpha rhythms as EEG signals generated by well defined neuronal networks. At the macroscopic level the dynamics of these neuronal networks are becoming understood. However, the precise cellular mechanisms of alpha rhythms are still little known (Steriade and Llinás 1988). In particular the role of intrinsic membrane properties of single neurons and the neuronal ensembles involved in the generation of oscillations characteristic of alpha activity is still unclear. The main difficulty for these types of studies lies in the fact that the conditions under which intrinsic properties may be best studied, i.e., in vitro, are not compatible with those necessary for the occurrence of alpha rhythms in the awake animal. Nevertheless, some of the findings pertaining to the generation of spindle rhythmicity (see Section 3.2) may serve as a working hypothesis to be tested in relation to the generation of alpha rhythms, namely that the thalamic reticular nucleus appears to play an essential role in pacemaking synchronized oscillations in the thalamus (Steriade and Deschênes 1984). As yet, there is no evidence of such a synchronizing device in the neocortex, if alpha waves are mainly cortical in origin.

3.2. Spindle oscillations

Spindle waves are the epitome of EEG synchronization during the early stage of sleep. In the cat, the species of choice for studying this type of oscillations at the intracellular level, spindles represent the electrographic landmark of the transition from waking to sleep.

Spindles are defined as waxing and waning waves between 7 and 14 Hz, grouped in sequences that last for 1.5–2 sec and that recur periodically with a slow rhythm of 0.1–0.2 Hz. Both these rhythms (7–14 Hz and 0.1–0.2 Hz) can be seen over widespread cortical territories in animals sleeping naturally or in barbiturate sleep (Steriade and Deschênes 1984).

Two main theories have been elaborated to explain the thalamic genesis of spindle oscillations.

3.2.1. The hypothesis of an intranuclear recurrent inhibitory circuit

The theory elaborated by Andersen and his colleagues (see Andersen and Andersson 1968)

postulated that spindles originate in feedback inhibitory loops, disseminated in virtually all thalamic nuclei and involving thalamocortical neurons, their presumed local axonal collaterals, and intrinsic inhibitory cells (or interneurons). Each thalamic nucleus was thought to be endowed with oscillatory properties and no particular nucleus was regarded as playing the role of a pacemaker. The spread and synchronization of oscillations were ascribed to "distributor" neurons linking various thalamic nuclei.

This theory was refuted on the basis of following evidence. *(a)* The intranuclear recurrent collaterals of thalamocortical axons are absent, as demonstrated by intracellular injections with horseradish peroxidase (HRP) in various relay, associational and intralaminar nuclei, including the ventrobasal complex in which Andersen's experiments have been conducted (Yen and Jones 1983; Steriade and Deschênes 1984; Jones 1985). *(b)* There is little, if any, cross-talk between various thalamic nuclei (Jones 1985). It is, therefore, necessary to postulate a synchronizing nucleus with the required projections to virtually all thalamic nuclei. The only such structure is the reticular (RE) thalamic nucleus. *(c)* The hypothesis that each thalamic nucleus is endowed with the property of generating spindle oscillations was disproved by experiments showing that, after disconnection from the RE thalamic nucleus, spindles are absent in all remaining thalamic territories (see below, Section 3.2.2).

3.2.2. The reticular thalamic nucleus generates spindle rhythms

The RE nucleus is a peripheral sheet of GABAergic neurons covering the rostral, lateral and ventral surfaces of the thalamus. The hypothesis that RE nucleus generates spindling oscillations was substantiated by the following experimental evidence.

(a) Intracellularly, spindle oscillations are associated with a slowly growing and decaying depolarization with superimposed spike barrages in RE neurons, whereas the reverse image is seen in their targets, the thalamocortical neurons, which simultaneously display rhythmic long-lasting (100–150 msec) hyperpolarizations that occasion-
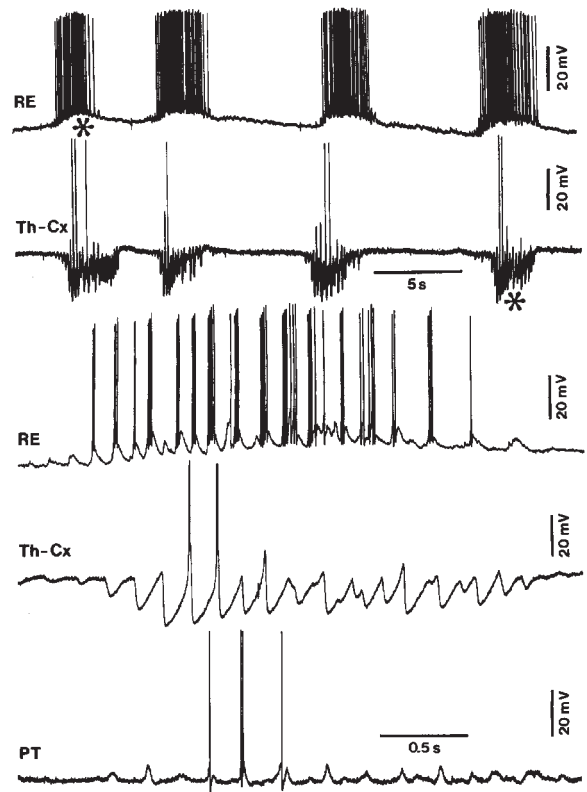
Fig. 4. Intracellular aspects of spindling oscillatory activities in reticular thalamic (RE), thalamocortical (Th-Cx; recorded from ventrolateral nucleus), and pyramidal tract (PT; recorded from motor cortex) neurons of cats under barbiturate anesthesia. Resting membrane potentials over −55 mV. The spindle sequences marked by asterisks in top traces of RE and Th-Cx neurons are depicted below at higher speed. Note in top traces the slow rhythm of spindle sequences, recurring every 5–10 sec. The spindle oscillations of GABAergic RE neurons are superimposed on a slowly growing and decaying depolarization, whereas spindles of Th-Cx cells are characterized by rhythmic hyperpolarizations that, occasionally, deinactivate a low-threshold rebound spike. See also text. (Modified from Steriade and Deschênes 1988.)

ally de-inactivate a rebound spike burst (Steriade and Deschênes 1988; Fig. 4). The burst, an intrinsic property of thalamic cells (see Section 2), is transferred along thalamocortical axons and triggers excitatory postsynaptic potentials (EPSPs) and spikes, within the frequency range of spindle waves, in neocortical neurons. These are the cellular bases of EEG spindles. The suggestion that opposite activity patterns in GABAergic RE neu-

rons and their targets reflect a causal relation was tested and confirmed.

(b) After disconnection of cortically projecting thalamic nuclei from their RE inputs (by transections and chemical lesions of RE perikarya), spindling is abolished in thalamocortical neurons (Steriade et al. 1985). Instead of rhythmic long-lasting hyperpolarizations that underly spindle oscillations in thalamocortical neurons with intact connections, RE-deprived thalamocortical cells display inhibitory postsynaptic potentials (IPSPs) with short duration and without any rhythmicity; such chloride-dependent IPSPs are generated by GABAergic interneurons, intrinsic to each thalamic nucleus. The absence of spindle oscillations was also observed (without any experimental manipulation) in anterior thalamic nuclei (Paré et al. 1987), the only major group of dorsal thalamic nuclei that are naturally devoid of connections with the RE nucleus (Steriade et al. 1984). Importantly, spindles are absent in anterior thalamic neurons despite their having intrinsic electrophysiological properties similar to those of other thalamic neurons (Paré et al. 1987). This indicates that the afferents from RE nucleus are crucial for generating the spindle-related hyperpolarizations in thalamocortical neurons.

(c) The hypothesis that RE neurons are pacemakers of spindle oscillations was finally supported by presence of focal spindles and associated rhythmic spike barrages in RE neurons disconnected from their major input sources, the thalamus and cerebral cortex (Steriade et al. 1987a).

3.2.3. Mechanisms of spindle blockage upon arousal

In addition to the intrinsic properties of thalamic neurons and the synaptic networks that necessarily include the RE thalamic nucleus, the third factor behind spindle appearance is a dampened activity in cholinergic brain-stem-thalamic projections, as it occurs during the transition from waking to EEG-synchronized sleep. This assumption is supported by two lines of evidence discussed below.

(a) Brain-stem reticular neurons with antidromically identified thalamic projections reliably decrease their firing rates, up to virtual neuronal silence, 1 sec before the first spindle sequence during wake-to-sleep transition (Steriade 1984). Since brain-stem reticular neurons exert direct excitatory actions upon thalamocortical neurons (Steriade and Glenn 1982), this sudden withdrawal of facilitatory impulses produces hyperpolarizations (by disfacilitation) in pools of thalamic neurons that may lead to rebound excitation. In turn, the postinhibitory rebounds in thalamofugal axons (which collateralize into the RE nucleus) efficiently drive RE neurons, and an avalanche process throughout the dendrodendritic network of the RE nuclear complex eventually results in synchronizing virtually all thalamocortical systems within spindle frequencies (see Section 3.2.2). In addition to this action mediated by thalamocortical neurons, the drop in activity of brain-stem–thalamic cholinergic neurons at sleep onset directly influences the RE pacemaker and sets it into motion, because acetylcholine is a powerful inhibitor of GABAergic RE cells (see below, *b*).

(b) Natural arousal or the artificial condition which mimicks it, namely, the electrical stimulation of brain-stem–thalamic projections, lead to blockage of spindles in thalamocortical systems and to replacement of the oscillatory mode of sleep by a tonic discharge mode with increased transfer function (Steriade and Llinás 1988). The blockage of spindle-related cyclic hyperpolarizations in thalamocortical neurons by brain-stem reticular stimulation (Purpura et al. 1966; Singer 1973) depends upon the obliteration of spindles at their very site of genesis, the RE thalamic nucleus. Stimulation of peribrachial cholinergic area of the pedunculopontine tegmental nucleus induces in RE neurons a hyperpolarization with increased membrane conductance (Hu et al. 1989a; see Fig. 1), probably to potassium ions (McCormick and Prince 1986a). This brain-stem-elicited inhibition of RE neurons produces a synaptic decoupling in the pacemaker of spindle oscillations. An additional factor in the disruption of spindle oscillations upon arousal is the action exerted by basal forebrain neurons. Besides their projections to the cerebral cortex, basal forebrain neurons project to the RE thalamic nucleus (Levey et al. 1987; Steriade et al. 1987b; Parent et al. 1988). This projection is partially cholinergic, but GABAergic

neurons of the basal forebrain also contribute to it (Asanuma and Porter 1990). Both acetylcholine and GABA are powerful inhibitors of GABAergic RE cells. Therefore, any increased activity of basal forebrain neurons (as it occurs upon arousal) would inhibit the genesis of spindles, and any lesion of basal forebrain neurons would lead to an increased incidence of spindling (Buzsaki et al. 1988).

3.3. Slow waves

This section summarizes evidence on slow (or delta) waves during natural sleep, but especially on pathological slow waves.

Slow waves between 0.5 and 4 Hz prevail during the deep stage of normal EEG-synchronized sleep when they are indented by faster spindle waves. It is probable that the site of genesis of slow waves is different from that of spindle oscillations since, in experimental animal studies, spindles are abolished while slow waves persist in the cerebral cortex of athalamic cats (Villablanca 1974). As yet, there is no systematic intracellular analysis of cortical slow waves.

3.3.1. Generators of delta activity

Stratigraphic studies of cats' association cortex (Calvet et al. 1964) and current-source-density analyses of rabbit's visual cortex (Petsche et al. 1984) indicate that slow waves around 4 Hz are generated between layers II–III and layer V.

Ball et al. (1977) studied the extracellular microphysiology of cortical polymorphic delta waves produced by lesions of the subcortical white matter, the thalamus or the mesencephalic reticular formation. It was found that the spatio-temporal average of these cortical delta waves exhibits a dipolar profile across cortical layers. This demonstrates that the main current flow underlying polymorphic delta activity within the cortex is vertical, especially since tangential recording of delta activity over distances of cortex comparable to its thickness did not show any evidence for a significant tangential component of current flow underlying delta waves.

These findings indicate that delta waves are generated by vertically arranged dipolar genera-

tors lying parallel to each other. The most likely candidates are the pyramidal neurons of the cerebral cortex. The fact that the delta waves are generated by pyramidal neurons is suggested also by the observation of Ball et al. (1977) that a statistical relationship exists between the firing probability of single cortical neurons and the surface-positive phases of cortical delta activity, while surface-negative deflections were associated with a diminution in firing probability. Delta waves thus reflect sequences of excitatory and inhibitory processes of cortical neurons.

In addition of being the result of synaptic activity, slow waves may also reflect intrinsic properties of cortical neurons, such as a long-lasting (200–500 msec) calcium-mediated potassium conductance (Connors et al. 1982), that is markedly attenuated by acetylcholine (Krnjević et al. 1971; McCormick et al. 1986b). It was hypothesized that the suppression of slow (delta) waves upon arousal results from the action of cortically projecting basal forebrain cholinergic neurons (Buzsaki et al. 1988).

Atropine-induced delta activity, both at the macrophysiological and extracellular microphysiological scale, is very similar to that produced by white matter, thalamic or reticular formation lesions (Schaul et al. 1978). Since partial cortical deafferentation seems to be a likely candidate as a factor involved in the production of polymorphic delta activity, one may suspect that in the case of brain lesions cholinergic deafferentation may play a role in the production of cortical delta activity. Recent reports showed that whenever the discharge rate of presumably cholinergic cortically projecting basal forebrain neurons decreased, large slow waves appeared in the cortical EEG (Detari and Vanderwolf 1987), and chemical lesions of basal forebrain cholinergic perikarya with subsequent decrease in acetylcholinesterase-positive fibers in the cortex resulted in a dramatic increase in delta activity in the ipsilateral cortex (Buzsaki et al. 1988).

3.3.2. Polymorphic and other delta activity due to metabolic disturbances

The underlying fundamental mechanisms leading to slow wave activity in metabolic derange-

ments remain unknown. The only experimental work reporting single cell recordings related to metabolically induced delta activity was carried out in acute anoxia and hypoglycemia (Creutzfeldt et al. 1961; Creutzfeldt and Meisch 1963). Changes in single-cell activity are correlated with delta wave activity, the single-cell discharges becoming more grouped in time. Action potentials of cortical neurons occur in relation to extracellular negativity of the slow wave at the site of unit recording within the depth of the cortex. This deep negativity corresponds to a surface-positive phase of the slow wave which may be preceded by a slight negative hump. There are thus similarities between the extracellular microphysiology of metabolically induced delta waves and those seen with cerebral structural lesions.

We now turn to pathological slow waves, especially in human studies. Pathological slow waves can be divided into the following 2 categories: *theta activity* in the frequency range of 4.5–7 Hz (this type of pathological activity should not be confused with the normal theta activity seen in the subprimate hippocampus which occurs during activated behavioral states; see Section 3.4); and *delta activity* with a frequency of below 4.5 Hz.

3.3.3. Pathological waves within theta frequency range

Nothing very precise is known about the underlying pathophysiological mechanism of theta waves. Three major types can be distinguished.

(a) A first type of theta rhythm probably represents a slowing down of the alpha activity. There exists a relationship between the EEG frequency and the rate of cerebral blood flow and oxygen uptake in cortical grey matter: the slower the frequency, the greater the reduction in cerebral blood flow (Ingvar et al. 1965, 1976). Such slowing of the background activity is seen in mild to moderate hypoxia, cerebrovascular disease, dementias, and in mild degrees of metabolic encephalopathies, for instance renal or hepatic (Saunders and Westmoreland 1979). It is also seen in epileptic patients, where it sometimes may be due to anticonvulsant medication (Saunders and Westmoreland 1979).

(b) A second type of theta activity, particularly that which occurs intermittently and with frontotemporal predominance, is often attributed to disturbances in deep midline structures (Gloor 1976).

(c) Localized theta activity may merely represent the mildest form of polymorphic delta activity (see below).

3.3.4. Pathological delta activity

3.3.4.1. Classification. On the basis of purely morphological criteria 2 major types of delta activity can be distinguished: *(a)* continuous, polymorphic delta activity; and *(b)* intermittent, often paroxysmal monomorphic delta activity.

3.3.4.2. Definitions. Polymorphic delta activity is usually continuous or occurs in long trains. It is characterized by a marked irregularity of wave form. There is usually one predominant frequency, which may, however, vary over a certain range. This form of delta activity may occur in a localized fashion or it may be unilateral or truly generalized, with or without asymmetry. *Intermittent monomorphic delta activity* normally occurs in bilaterally synchronous paroxysmal bursts with frontal predominance (so-called frontally predominant intermittent rhythmic delta activity or FIRDA) (Goldensohn 1979) but it may sometimes predominate posteriorly and occasionally may occur unilaterally or even focally, although the latter is rare. The wave form of this type of delta activity is smooth with a very strong predominance of a single frequency.

3.3.4.3. Pathological substrate of polymorphic delta activity. Both metabolic and structural pathology can give rise to polymorphic delta activity. In the case of generalized and symmetrical polymorphic delta activity, the cause is usually a diffuse encephalopathy, either metabolic or structural, in the latter case most likely a diffuse white matter encephalopathy (Gloor et al. 1968; Saunders and Westmoreland 1979; see below). Localized delta activity is usually attributed to a localized lesion in which some destruction of cerebral tissue has taken place (Hess 1976; Goldensohn 1979) but it should be recognized that such polymorphic delta activity may also occur in a localized fashion in patients with partial epilepsy (Marshall et al. 1988). Sometimes such slow wave

activity in epileptics is postictal, but there is also in many a more enduring slow wave disturbance.

The important role of subcortical white matter pathology in the genesis of polymorphic delta activity has been demonstrated most conclusively in animal experiments (Gloor et al. 1977). There are many instances from human pathology which support this experimentally derived notion of the pathogenetic importance of subcortical white matter pathology in the genesis of polymorphic delta activity (Goldensohn 1979).

Other structural lesions that can produce either localized, lateralized or bilateral delta activity are lesions of the thalamus and lesions of the mid-brain reticular formation. If bilateral they produce bilateral generalized polymorphic delta activity. These effects of thalamic and brain-stem lesions have also been demonstrated in experimental animals (Gloor et al. 1977) and are supported by clinical observations (Schaul et al. 1981a).

By contrast, localized lesions of the cortical gray matter do not produce polymorphic delta activity, not even on the fringes of the lesion. They only depress the amplitude of the cortical background activity (Gloor et al. 1977). This is in line with the observation of absence or paucity of polymorphic delta activity in extraparenchymatous lesions that merely compress the brain, such as meningiomas or subdural hematomas (Goldensohn 1979).

Vasogenic edema per se, often considered by clinicians to be a major factor in producing polymorphic delta activity (Hess 1976), does not induce slow waves, unless the edema is massive and leads to pressure on, or distortion of, deep midline structures. The delta waves then are probably produced because of interference with thalamic or brain-stem reticular mechanisms (Gloor et al. 1977).

These findings suggest that a common denominator favoring the appearance of either localized or generalized polymorphic delta activity as a consequence of structural brain pathology is a partial deafferentation of the cerebral cortex (Stein 1965; Gloor et al. 1977). Total deafferentation of the cortex does not seem to produce polymorphic delta activity (Gloor et al. 1977).

3.3.4.4. Intermittent monomorphic delta activity.
Traditionally this type of paroxysmal, usually bilaterally, synchronous and frontally predominant delta activity (FIRDA), has been attributed to lesions or disturbances in deep midline structures in the region of the third ventricle or in the upper midbrain (see Gloor 1976).

There exists no known experimental model of intermittent monomorphic delta activity. Clinico-pathological studies in humans demonstrate that this type of intermittent monomorphic delta disturbance is non-specific and may be encountered in a great variety of cerebral pathologies, some structural, some metabolic, most commonly, but not exclusively, some diffuse encephalopathy (Gloor 1976; Schaul et al. 1981b; Fariello et al. 1982). There is no close association of this abnormality with structural lesions located in deep midline structures (Schaul et al. 1981a) although undoubtedly some patients (but by no means the majority) with such lesions do show intermittent monomorphic delta activity. However, lesions in other parts of the brain are also at times associated with this EEG pattern (Gloor 1976; Fariello et al. 1982). The most common structural pathology associated with the appearance of bilaterally synchronous slow wave activity is diffuse gray matter disease involving both cortical and subcortical structures (Gloor et al. 1968).

Nothing is known about the behavior of single cells nor of the involvement of neurotransmitters or neuromodulators in the genesis of intermittent monomorphic delta activity.

3.3.5. Requirements for future research
Obviously most of the questions concerning the pathophysiology of slow waves in the EEG remain unanswered. Adequate animal models especially for the various forms of theta activity and for intermittent monomorphic delta activity, that are sufficiently similar to their human counterparts, are presently unavailable and must be developed. Furthermore, the cellular mechanisms of the various forms of pathological slow wave activity must be studied, not only extracellularly (which so far has only been done for polymorphic delta activity), but also intracellularly. The latter is the single

most urgent requirement in this field. Once the intracellular electrophysiological correlates of pathological delta activity have been established, the search can begin for the factors that underlie these changes. These may include disturbances in the regulation of various ionic membrane currents, improper regulation of transmitter release, re-uptake or inactivation, abnormal regulation of peptidergic and other neuromodulator mechanisms, activity of false transmitters under pathological conditions, abnormal second messenger mechanisms, and so on. Once these basic mechanisms are understood, it is to be expected that the clinical electroencephalographer will then be able to use the analysis of pathological slow wave activity in a much more effective and sophisticated way for purposes of diagnosis and patient management than is presently possible.

3.4. Theta waves

According to the current human EEG nomenclature, the theta rhythm is an activity within the frequency range of 4–7 Hz. It dominates the EEG activity recorded from the hippocampus of most mammals, but especially in rodents. However, in lower mammals the hippocampal EEG has a wider frequency range and may extend from 3–4 Hz up to 10–12 Hz. Therefore, it has become current practice to name this EEG activity rhythmic slow activity (RSA), in order to avoid the term theta rhythm that does not cover the entire frequency range within which the hippocampal EEG of lower animals may fall.

A controversial point is whether hippocampal RSA occurs not only in lower mammals but also in humans. Single cases have been reported in which hippocampal RSA was observed in man, but Halgren et al. (1985) were not able to find RSA in human recordings. However, using spectral analysis, Arnolds et al. (1980) were able to demonstrate a peak corresponding to the frequency of RSA in the hippocampus of epileptic patients. This RSA presented a dominant low frequency (about 3–4 Hz) which was modulated with behavior in a similar way as in lower mammals. The relative difficulty of demonstrating RSA in the human hippocampus may be related to the de-

crease in RSA amplitude and regularity in higher primates (Crowne and Radcliffe 1975).

3.4.1. Septal "pacemaker": input pathways and topographic distribution

RSA is commonly associated with the hippocampal formation, since it is most conspicuous in this structure. However, RSA with the same general characteristics as that of the hippocampus has also been found in other cortical limbic areas, namely in the entorhinal and the cingular cortices. It is generally agreed that the RSA of the hippocampus and the other limbic areas is dependent on an intact septal area that will act as a pacemaker of the RSA.

It has long been known that the hippocampal RSA is modulated by ascending fibers from the brain-stem (Torii 1961; Yokota and Fujimori 1964; Anchel and Lindsley 1972). This has in particular been clarified in the studies of Vertes (1980, 1981, 1982).

The experimental evidence for the notion that the neuronal population of the septal area forms the pacemaker of RSA is based on the following findings. Destruction of the medial septum results in the disappearance of the RSA from the hippocampus and other limbic cortical areas (Petsche et al. 1962; Vinogradova et al. 1980). Several investigators using quantitative methods demonstrated that a population of medial septal/diagonal band neurons discharges in phase with the hippocampal RSA (Apostol and Creutzfeldt 1974; Assaf and Miller 1978; Gaztelu and Buño 1982). In the study of Gaztelu and Buño (1982) in the rat, about 56% of the total septal population showed a tight phase locking to the hippocampal RSA. The neurons, the activity of which show the highest correlation with the hippocampal RSA, are most densely concentrated within the dorsal part of the vertical limb of the diagonal band and the ventral part of the medial septal nucleus (Wilson et al. 1976; Assaf and Miller 1978; Gaztelu and Buño 1982). In the same region, McLennan and Miller (1976) were able to record bursting cells at the frequency of the RSA after fimbria cuts that isolated the medial septum from the hippocampus. However, we should note that the hippocampal neurons need not be considered just as passive followers of

the rhythmic septal pacemaker. The local networks may also contribute to the RSA. Recently, Konopacki et al. (1987) showed that in hippocampal slices in vitro, application of the cholinergic agonist carbachol (50 μM) produced theta-like rhythmical wave forms. This shows that hippocampal neurons are capable of producing synchronized rhythmic activity when isolated from septal inputs. The same group of investigators demonstrated that in this preparation both the CA1 field and the dentate gyrus can independently generate carbachol-induced RSA activity. Furthermore, theta-like activity in hippocampal slices has been shown to be due to muscarinic receptor activation suggesting that this type of theta activity is most likely caused by cholinergic inputs arising from the septum and diagonal band (Konopacki et al. 1988).

3.4.2. Cellular mechanisms of generation

In the hippocampal formation, a clear dipole field profile of RSA was obtained in the CA1 field with null amplitude at the proximal parts of the apical pyramidal dendrites (type I profile of Winson 1976a,b) and an amplitude maximum near the hippocampal fissure (Green et al. 1960; Artemenko 1972; Bland et al. 1975). However, in freely moving rats, a different RSA depth profile was found, the so-called type II profile of Winson (1974). In these cases, there is a gradual phase shift up to 180° in the stratum radiatum and an amplitude maximum at the molecular layer of the upper blade of the dentate gyrus.

It is of importance to be able to relate intracellularly recorded membrane potential fluctuations to the extracellular RSA. Recently, some intracellular data relevant for this discussion became available. Leung and Yim (1986), in urethane-anesthetized rats, made intracellular recordings from CA1 pyramidal cells and found oscillations of the membrane potential in the frequency range of the RSA (intracellular theta rhythm), phase-locked with the extracellular RSA. By means of current injection of acetate ions they were able to invert the phase relationship between the intracellular and extracellular rhythmic activity as well as that of the IPSPs.

However, such an interpretation is still controversial. Namely, Nunez et al. (1987) reported that intracellular RSA activity in identified CA1-CA3 pyramidal cells in rats, curarized and anesthetized with urethane, reflects EPSPs and slow calcium-mediated spikes. Moreover, these authors showed that during the RSA most of the CA1 pyramidal cells undergo a sustained depolarization of up to 20 mV above the resting level. In about 25% of the CA1 cells analyzed, the membrane potential oscillated in close relation to the extracellularly recorded RSA. Using small hyperpolarizing pulses, Nunez et al. (1987) calculated that there is a mean conductance decrease of about 30% during the sustained depolarization. In some CA1 cells, depolarizing waves were also found during the RSA that strongly resembled slow calcium-mediated dendritic spikes observed in vitro. According to these data, the hippocampal RSA is correlated with sustained depolarization and periodic transmembrane potential oscillations. This may be caused by cholinergic stimulation, since acetylcholine blocks the hyperpolarizing M current (Halliwell and Adams 1982) and also blocks the tonic release of GABA from local interneurons (Hounsgaard 1978; Ben-Ari et al. 1981). This would explain the decrease in membrane conductance found. Nunez et al. (1987) concluded that IPSPs are not essential in the generation of the RSA. In this respect, it is important to note that also glutamate may play a role in mediating the rhythmic septal inputs (Puil and Carlen 1984). It may be concluded that two major excitatory synaptic influences contribute to the intracellular RSA: an acetylcholine-mediated sustained depolarization of septal origin, and glutamate-mediated EPSPs. Such an interpretation is compatible with the observation that there are at least two types of RSA with different sensitivity to anticholinergic drugs.

It is becoming clear that RSA is not a uniform phenomenon, and that different cellular mechanisms underlie different aspects of the hippocampal RSA. The precise mechanism by which the septal inputs modulate hippocampal membrane potentials underlying the RSA is still a matter of discussion. A possibility is that the septal inputs induce disinhibition by shutting off a tonic inhibition from the local interneurons (Krnjević and

Ropert 1982). To clarify this question, experimental evidence that septal fibers indeed inhibit hippocampal interneurons is necessary (Krnjević et al. 1988).

Concerning the RSA of the entorhinal cortex, a clear dipole profile was obtained in freely moving animals, with two amplitude maxima, one superficial in layer II–I and the other deep in layer III (Mitchell and Ranck 1980; Alonso and García-Austt 1987a,b; Boeijinga and Lopes da Silva 1988).

As to the RSA of the cingulate cortex, there is evidence that the RSA may be locally generated, but this is still controversial. In rats, under urethane anesthesia, depth profiles in the cingulate cortex show a phase reversal during the RSA in layers V and VI (Feenstra and Holsheimer 1979). However, in other studies such a phase reversal was not encountered (Bland and Whishaw 1976; Leung and Borst 1987). Nevertheless, Leung and Borst (1987) showed that cingulate cortex units fire at the RSA frequency in phase with the local RSA. This is in agreement with the anatomical evidence that the cingulate cortex receives projections from the area of the septal RSA pacemaker.

3.4.3. Behavioral correlates and pharmacological aspects

The relationship between the RSA and behavior has been a subject of controversy over the last two decades. Vanderwolf and Robinson (1981) have emphasized the relationship between the RSA in the hippocampus and what they termed "voluntary or type 1" movements, and between irregular electrical activity and more "automatic or type 2" movements.

An interesting new aspect of RSA is its relationship with the phenomenon of long-term synaptic potentiation (LTP). Such a relationship was recently demonstrated both for synapses of the Schaffer commissural fibers on CA1 neurons in hippocampal slices (Larson et al. 1986; Rose and Dunwiddie 1986; Larson and Lynch 1988) and for synapses of the perforant path fibers on the granular cells of the dentate gyrus in vivo (Greenstein et al. 1988; Pavlides et al. 1988). In the CA1 field, LTP induction is optimal when the time interval between stimuli is approximately 200 msec which

corresponds to the frequency band of the spontaneously occurring RSA in the hippocampus. In the dentate gyrus, a significant potentiation of synaptic efficacy, as measured by the field synaptic potential slope and the population spike, can only be obtained when the tetanic pattern consists of a priming pulse followed by a 100 Hz train of 6 pulses at 200 msec interval. It appears that brief high-frequency bursts elicit a weak N-methyl-D-aspartate (NMDA) receptor response which is amplified when the bursts are delivered in a pattern within the frequency range of the RSA. The hypothesis is that the amplification occurs because at this RSA frequency there is a suppression of IPSPs (Larson and Lynch 1988) and hence a prolongation of the depolarization. This would favor an enhanced influx of calcium ions resulting in an amplification of LTP, and this implies that during the RSA-mode LTP phenomena are facilitated. There is evidence that RSA may cause a steady-state depolarization of the dendrites of pyramidal cells (Lopes da Silva et al. 1985; Nunez et al. 1987). These findings are compatible with the interpretation that RSA may facilitate the establishment of LTP.

3.5. Beta waves

Fast (over 30 Hz) EEG potentials during epochs of increased alertness, also called beta waves, have been studied in cats in experimental conditions that may be qualified as "hunting" situations (Fig. 5; Bouyer et al. 1981, 1987; Rougeul-Buser et al. 1983).

(a) If the animal is in a position of expectancy, waiting for an unseen mouse to come out through a hole, the EEG rhythms are around 14 Hz and are localized over the anterior limb zone of the primary somatosensory cortex. Such rhythms related to blockage of motor activity have been initially termed the "sensorimotor rhythm" (Roth et al. 1967) and are homologous to a similar rhythm that appears over the central sulcus in humans. While such oscillations may superficially resemble spindles, the behavioral context of these two distinct types of rhythms (waking or sleep) is quite different. Besides, the 14 Hz oscillations during waking immobility are recorded over a very

restricted cortical region, whereas spindles appear diffusely over the neocortical mantle.

(b) When the cat is watching a visible but unseizable mouse, high-frequency (35–45 Hz) oscillations appear in two cortical foci, the motor and the parietal association areas (Rougeul-Buser et al. 1983; Bouyer et al. 1987). Similar fast rhythms have been observed in monkey (Rougeul et al. 1979). Both the 14 Hz and the 35–45 Hz rhythms are accompanied by fluctuations in activity of ventrobasal and adjacent thalamic neurons (Rougeul-Buser et al. 1983; Delagrange et al. 1987). The dependence of fast (35–45 Hz) oscillations upon the dopaminergic system was suggested by their suppression after lesions of the ventral tegmental area (Montaron et al. 1982). The origin(s) and cellular bases of these rhythms remain to be elucidated.

Beta activity (36–44 Hz) was also reported to occur in humans while performing a reaction-time motor task (Sheer 1988). It was hypothesized that the 40 Hz activity is an index of the focused arousal in motor programming and that it represents an optimal periodicity for maximal synaptic transmission in cortical circuits.

Fast (40 Hz) oscillations have been found in the visual cortex in response to moving light bars (Gray and Singer 1989; Gray et al. 1989).
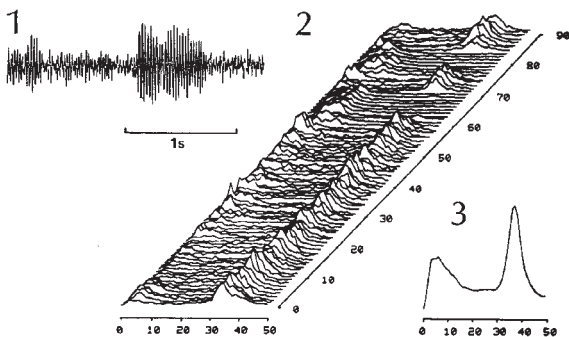

Fig. 5. Fast (beta) rhythms during focused attention in the cat. 1: sample of ECoG activity recorded from the precruciate cortex (rhythms at 40 Hz). 2: evolutive spectra established from a 90 min record taken from cortical area 5a; each line corresponds to a spectral analysis of a 1 min record (1–50 Hz); successive minutes are lines up as the y axis. 3: spectrum averaged over 90 min; low frequency (5 Hz) peak corresponds to movement artifacts; beta rhythms are visible as the 35–40 Hz. (Modified from Bouyer et al. 1987.)

4. Brain-stem core modulatory systems and their synaptic effects on thalamic and cortical targets

We shall focus on cholinergic and noradrenergic systems because the actions of acetylcholine (ACh) and noradrenaline (NA) are better understood than those of transmitters used by other brain-stem regulatory systems.

4.1. Central cholinergic pathways

Cholinergic pathways occupy a pivotal position in the ascending reticular activating system and play an important role in modulating the cortical EEG as well as its behavioral correlates in the realms of arousal and attention. This cholinergic influence of the reticular activating system is exerted along two ascending pathways: one originates in the basal forebrain and projects to the cerebral cortex, the other originates in the pontomesencephalic reticular formation and projects to the thalamic nuclei. The following description summarizes the salient anatomical features related to these cholinergic systems (Mesulam 1988; Wainer and Mesulam 1990; Fig. 6).

4.1.1. The cholinergic innervation from the basal forebrain

Cholinergic cells in the medial septal nucleus (Ch1 cell group) and the vertical limb nucleus of the diagonal band (Ch2) provide the major source of cholinergic input to the hippocampus, cholinergic neurons in the horizontal limb nucleus of the diagonal band (Ch3) provide the major cholinergic input to the olfactory bulb, and the cholinergic neurons of the nucleus basalis of Meynert (Ch4) provide the major cholinergic input for the amygdala and all neocortical regions. Each of the nuclei containing the Ch groups also contains non-cholinergic neurons. The Ch nomenclature was introduced to designate only the cholinergic constituents of these regions. In the brain of rodents, the cerebral cortex contains cholinergic interneurons that can account for up to 30% of the cortical cholinergic presynaptic markers. Such neurons have not been reported in other adult mammalian brains. This special feature of the
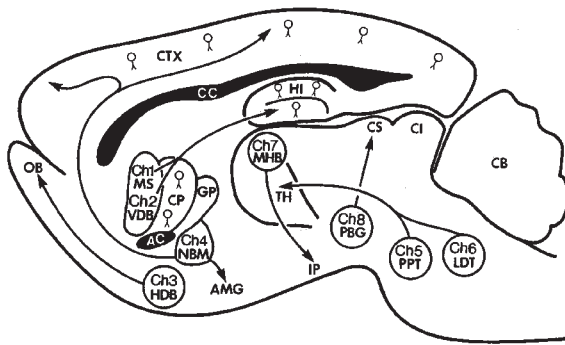
Fig. 6. Schematic illustration of major ascending cholinergic pathways in the rat brain. Ch1-Ch8 designations identify cholinergic neurons contained within the various forebrain and brain-stem nuclei illustrated. Abbreviations: AC, anterior commissure; AMG, amygdala; CB, cerebellum; CC, corpus callosum; CI, inferior colliculus; CP, caudate putamen; CS, superior colliculus; CTX, cortex; GP, globus pallidus; HDB, nucleus of the horizontal limb of the diagonal band of Broca; HI, hippocampus; IP, interpeduncular nucleus; LDT, laterodorsal tegmental nucleus; MHB, medial habenular nucleus; MS, medial septal nucleus; NBM, nucleus basalis of Meynert; OB, olfactory bulb; PBG, parabigeminal nucleus; PPT, pedunculopontine tegmental nucleus; TH, thalamus; VDB, nucleus of the vertical limb of the diagonal band of Broca. Cholinergic neurons are shown schematically in CTX, HI, and CP. (From Wainer and Mesulam 1990.)

rodent brain should be kept in mind in interpreting experimental observations.

In the primate brain, the most highly developed cholinergic cell group is Ch4. Projections from Ch4 are topographically organized. The anteromedial subsector (Ch4am) is the major source of cholinergic input for medially situated cortical areas, the anterolateral subsector (Ch4al) for the amygdala and frontoparietal operculum, the intermediate sector (Ch4i) for frontoparietal and occipitotemporal lateral cortex, and the posterior subsector (Ch4p) for the superior temporal gyrus and the temporal pole. There is considerable overlap in this organization and the topography is not as precise as in thalamocortical projections. The Ch4 complex projects to all cortical areas, but receives reciprocal projections from only a very limited set of limbic and paralimbic areas. This organization suggests that Ch4 is in a position to act as a cholinergic relay for rapidly modulating the activation of all neocortical regions according

to the prevailing limbic state as encoded by limbic and paralimbic areas.

Although all regions of the cerebral cortex receive cholinergic input, there are major regional differences. Presynaptic cholinergic markers (e.g., choline acetyltransferase) show regional variations that are as high as seven-fold. Limbic and paralimbic areas of the forebrain contain the highest concentrations of presynaptic cholinergic markers. The less differentiated non-isocortical sectors in each of the major paralimbic areas display greater cholinergic innervation than immediately adjacent isocortical regions within the same paralimbic region. Association and primary sensorimotor areas contain a significantly less intense cholinergic input than limbic and paralimbic areas. These variations in regional cholinergic innervation may explain why systemically injected cholinoactive agents appear to have marked effects on mood and memory, behaviors that are closely linked with the limbic system.

The vast majority of cortical cholinergic receptors are of the M1 muscarinic type. The distribution of M1 receptors is generally (but not entirely) consistent with regional variations in presynaptic cholinergic markers in that all limbic and paralimbic areas show high densities of this receptor type (Mash and Mesulam 1988). The regional distribution of M2 receptors in the monkey brain shows a rather unexpected pattern. This type of receptor shows peak intensity in all primary sensory and motor areas. It is not known if these regional variations of M2 receptors reflect changes merely in postsynaptic specialization or if they indicate that primary sensorimotor areas receive a somewhat different type of presynaptic cholinergic input. In the latter case, it is conceivable that these parts of the cortex receive a higher proportion of their direct cholinergic input from the pontomesencephalic cholinergic cell groups (Ch5-Ch6). This is merely a speculation not yet based on available fact. Recent experiments show that cholinergic transmission in primary sensory areas is directly involved in modulating the rapid responses to sensory stimulation (Sato et al. 1987). In high order association cortex, cholinergic innervation also mediates the responses to motiva-

tionally relevant sensory cues (Rigdon and Pirch 1984).

The low voltage fast EEG activity induced by the systemic administration of cholinergic agonists appears to be mediated by the ascending projections from the Ch4 complex (Stewart et al. 1984; Buzsaki et al. 1988). These projections are also thought to play an important role in regulating cortical blood flow (Iadecola et al. 1983). The hypothesized role of the basal forebrain in maintaining non-REM sleep (Szymusiak and McGinty 1986) may be due to the cortical projections of GABAergic neurons in that region.

4.1.2. Rostral brain-stem cholinergic neurons

The pontomesencephalic reticular formation contains two constellations of cholinergic neurons, one centered around the pedunculopontine nucleus (Ch5) and the other around the laterodorsal tegmental nucleus (Ch6; see Fig. 6). There is no strict delineation between these two groups of cholinergic cells. With respect to thalamopetal projections in rat, the Ch5 neurons are more closely associated with the sensory relay nuclei, whereas the Ch6 neurons are more closely associated with the limbic nuclei (Hallanger et al. 1987). The Ch5 and Ch6 cell groups collectively provide the vast majority of cholinergic input for all thalamic nuclei in cat (Steriade et al. 1988). Lesser cholinergic afferents of the thalamus also originate in Ch1-Ch4, especially for the reticular and mediodorsal thalamic nucleus (Hallanger et al. 1987; Steriade et al. 1987b; Parent et al. 1988). There seems to be a direct cholinergic projection from the Ch5-6 nuclei to Ch4 but the exact organization of this and whether there is a reciprocal projection from Ch4 back to Ch5-6 remains to be determined (Semba et al. 1988).

The cholinergic reticulothalamic projection from Ch5-Ch6 is one of the most important constituents of the ascending reticular activating system. Electrical stimulation in the Ch5-Ch6 region causes an activation of thalamocortical neurons and an enhancement of their response to afferent stimulation (see Fig. 1 and Section 4.2). These neurons also provide the cholinergic innervation for brain-stem regions involved in regulating REM sleep (Mitani et al. 1988). In addition to par-

ticipating in ascending reticular activating pathways, the Ch5 and Ch6 groups have extensive interconnections with extrapyramidal and limbic structures (Mikol et al. 1984; Satoh and Fibiger 1986).

Additional cholinergic cells are found within the medial habenular nucleus. These neurons, designated Ch7, are thought to constitute the origin of the cholinergic habenulo-interpeduncular projection. There are also cholinergic neurons in the parabigeminal nucleus. These neurons, designated Ch8, provide the major cholinergic input of the superior colliculus.

4.1.3. The cholinergic innervation of the striatum

Another major forebrain structure with a heavy cholinergic input is the striatum. Anatomical experiments show that the vast majority of striatal cholinergic innervation is intrinsic and that it originates from cholinergic interneurons. These cholinergic interneurons belong to the class of large aspiny cells. The caudate and probably the putamen also receive a lesser cholinergic input from the Ch4 cell group (Arikuni and Kubota 1984).

4.1.4. Some functional interpretations

Anatomical experiments show that cholinergic pathways are ubiquitous but not without internal organization. Activating the cholinergic neurons in the pontomesencephalic reticular formation appears to promote the transthalamic passage of corticopetal impulses (see details in Section 4.2). Some of these neurons may also provide important relays for extrapyramidal motor outflow. The cholinergic projection from the basal forebrain to the cerebral cortex acts as one of the most powerful excitatory neuromodulators of cortical neurons and enhances their responses to both motivationally relevant and neutral sensory stimuli. Thus, the net effect of cholinergic activation along these two ascending pathways is to augment the impact of extrapersonal sensory experience upon the organism and, perhaps, also to increase the readiness for motor responses.

The ascending projections from the basal forebrain and pontomesencephalic cholinergic neurons are arranged in such a way that a relatively

small group of cells (under a restricted set of descending neural controls) can rapidly influence the information processing state throughout the cerebral cortex. This is in keeping with the behavioral affiliations (for example arousal, vigilance, motivation, mood and memory) that have been attributed to ascending cholinergic pathways (Mesulam 1987). This type of asymmetry in neural feedback also applies to the widespread corticopetal projections from the nucleus locus coeruleus, the ventral tegmental area, and the brain-stem raphe nuclei. The transmitters associated with these pathways (norepinephrine, dopamine and serotonin) have also been implicated in state functions such as motivation, sleep and mood. The Ch1-Ch6 neurons, the ventral tegmental area, the brain-stem raphe nuclei, and the nucleus locus coeruleus are thus ideally suited for modulating, regulating and shifting behavioral states in the brain.

4.2. Effects of cholinergic systems upon thalamic and cortical neurons

Congruent data related to the physiological actions of cholinergic systems have been obtained in intracellular recordings of thalamic cells by stimulating the synaptic pathways arising in the brain-stem reticular core in vivo and by studying the effects of iontophoretically applied cholinomimetic substances on intracellularly recorded thalamic and neocortical neurons in vivo and in vitro.

Acetylcholine application in vitro induces in cat's lateral geniculate (LG) and medial geniculate (MG) neurons a fast nicotinic depolarization associated with an increase in membrane conductance, followed by a slow hyperpolarization and a slow depolarization caused by activation of muscarinic receptors and associated, respectively, with an increased and a decreased potassium conductance (McCormick and Prince 1987).

The nicotinic depolarization was also detected in in vivo recordings of LG relay neurons after stimulation of the Ch5 brain-stem group (Hu et al. 1989b). This nicotinic event underlies the phasic excitation of LG and other thalamic neurons, associated with the PGO sharp waves that occur during dreaming episodes of REM sleep (Hu et al. 1989c; Steriade et al. 1989).

In addition to short-term effects, stimulation of

Fig. 7. Schematic diagram of ascending cholinergic actions upon thalamocortical (relay) neurons, reticular thalamic (RE) GABAergic neurons, and pyramidal-shaped neurons of the cerebral cortex. Direction of axons is indicated by arrows. Acetylcholine (ACh) is released in the thalamus by peribrachial (PB) neurons of the pedunculopontine nucleus and by laterodorsal dorsal tegmental (LDT) neurons (Ch5-Ch6 cell groups). In the cortex, ACh is mostly released by nucleus basalis (NB) neurons. In relay and RE thalamic cells as well as in cortical pyramidal neurons, EEG-synchronized sleep (S) is characterized by rhythmic inhibitory periods and bursts of action potentials within the frequency range of spindle oscillations. Spindles are generated by RE neurons which impose rhythmic inhibitory postsynaptic potentials (IPSPs) onto thalamic relay cells; the IPSPs are followed by rebound spike bursts transmitted to cortical cells (see Fig. 4 in Section 3.2). The information transfer of thalamocortical cells is dramatically reduced during the oscillatory mode of S. In cortical cells, the activity evoked by prethalamic afferents is further reduced due to a relatively uninhibited M-current and slow afterhyperpolarization current (I_{ahp}) which underlie spike frequency adaptation. Upon transition from sleep (S) to waking (W), the cholinergic PB/LDT neurons increase their rates of spontaneous discharges, about 20 sec before the time 0 of W (defined as the most precocious change from EEG synchronization to EEG desynchronization). An increased activity during the shift from S to W is also seen in NB cells. (Note that no change in firing rate from S to W is seen in neurons recorded from specific prethalamic relays.) Increased activity of cholinergic PB/LDT and NB neurons disrupts rhythm generation in the thalamus by depolarizing relay neurons (through a decrease in potassium conductance, g_K). As well, cortical pyramidal cells are activated through a decrease in M-current and I_{ahp}. Thus, relay thalamic cells and pyramidal cortical cells are depolarized by cholinergic afferents originating in PB/LDT and NB, respectively. There is, in addition, an excitatory action on cortical pyramidal cells by non-cholinergic thalamocortical cells (increase in cationic permeability). The hyperpolarization of RE cells by PB/LDT cholinergic cells as well as by NB cholinergic and GABAergic cells underlies the blockage of spindle generation in the pacemaking RE neurons. Although PB/LDT cholinergic afferents hyperpolarize RE thalamic cells by an increase in g_K, these neurons are brought upon arousal toward single-spike firing, with increased discharge rates, because they are subject to excitatory influences from both relay thalamic and cortico-RE neurons using excitatory amino acids (glu). Scheme of changes in ionic conductances is modified from McCormick (1990), from in vitro data on RE thalamic, relay thalamic, and cortical pyramidal neurons (McCormick and Prince 1986a,b, 1987). Data related to the S-W behavior of various types of depicted neurons are from chronic experiments on PB/LDT (Steriade et al. 1990a), RE thalamic (Steriade et al. 1986), thalamocortical and cortical pyramidal cells (see details in monograph by Steriade et al. 1990b).
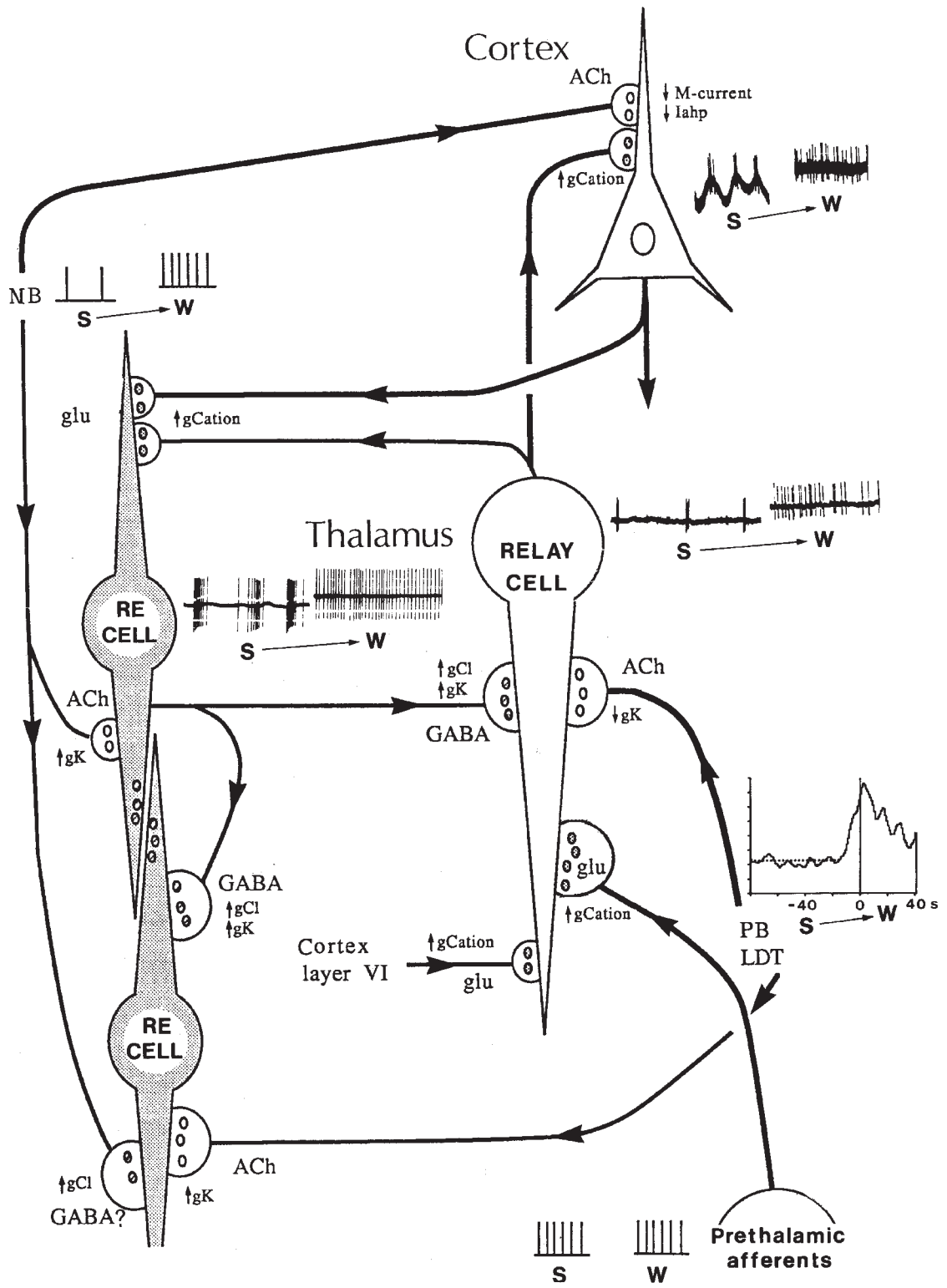
brain-stem cholinergic nuclei elicits a prolonged (20 sec) depolarization which is associated with increase in apparent input resistance, has a similar time-course as the EEG desynchronizing reaction, and is abolished after administration of scopolamine, a muscarinic blocker (Curró Dossi et al. 1990). This prolonged excitation of thalamocortical cells is due to the suppression of various potassium currents (see McCormick 1990; Fig. 7). The long-lasting muscarinic excitation of thalamocortical neurons is accompanied by a prolonged enhancement of synaptic responsiveness in thalamocortical neurons of limbic (anterior) nuclei (Paré et al. 1990), that may underly plastic neuronal changes at the thalamic level.

By contrast to the cholinergic excitation of thalamocortical neurons, acetylcholine application hyperpolarizes RE thalamic neurons in vitro by increasing a potassium conductance, an effect probably mediated by M2 subclass of muscarinic receptors (McCormick and Prince 1986a; Fig. 7). The results of intracellular recordings of RE neurons in vivo are consistent with these data: stimulation of the Ch5 group at the midbrain-pontine junction induces a hyperpolarization of RE thalamic cells, associated with increased membrane conductance, an effect which is blocked by scopolamine (Hu et al. 1989a). As discussed in Section 3.2.3, the cholinergic inhibition of RE thalamic nucleus, the spindle pacemaker, accounts for the disruption of spindle oscillations upon arousal and represents a major part of the EEG desynchronizing reaction.

The action of acetylcholine on neocortical neurons was elucidated by intracellular recordings in vivo and in vitro (Krnjević et al. 1971; McCormick and Prince 1986b). Similarly to the effects on thalamocortical neurons, the acetylcholine-induced depolarization of cortical cells is due to a reduction in potassium conductance and is associated with a rise in membrane resistance (Fig. 7). As is the case of thalamocortical neurons, the excitatory action of acetylcholine on cortical cells is highly susceptible to depression by barbiturates.

Thus, mesopontine cholinergic reticular neurons are operational in shifting the state of thalamocortical neurons from EEG-synchronized sleep to wakefulness and REM sleep. Indeed,

Ch5-Ch6 (pedunculopontine and laterodorsal tegmental) neurons with identified thalamic projections increase their rates of spontaneous discharges as a precursor sign of the transition from sleep to arousal (Steriade et al. 1990a; Fig. 7). The cholinergic depolarization of thalamocortical neurons transforms their bursting firing (due to their hyperpolarization during slow-wave sleep) into tonic repetitive firing associated with an increased readiness to integrate afferent informations (Fig. 7). Finally, the release of acetylcholine by cortically projecting basal forebrain neurons blocks the potassium-mediated long-lasting hyperpolarizations underlying slow (delta) waves and contributes to the enhanced responsiveness of neocortical cells (Fig. 7).

4.3. Noradrenergic pathways and actions

The noradrenergic system arising in locus coeruleus has a direct access to neocortex and hippocampus and projects as well to the thalamus but less densely than the brain-stem cholinergic system (DeLima and Singer 1987). Most of the ascending noradrenergic fibers enter the thalamus via the mammillothalamic tract, while other fibers ascend along the zona incerta and radiate within the internal and external medullary laminae. The corticopetal fibers leave the main bundle at rostral hypothalamic level and distribute from the frontal lobe to the entire length of the hemisphere (Morrison et al. 1981). Marked laminar variations are seen in the striate and extrastriate visual cortices in primates (Morrison and Foote 1986). This stands in contrast with the more homogenous distribution of noradrenergic fibers throughout the neocortex in lower mammals.

In addition to the effects of noradrenaline on hippocampal neurons (that are beyond the scope of this article), these actions have been best studied in thalamic neurons in vitro. However, systematic intracellular studies of thalamic and cortical cell responses to stimulation of synaptic noradrenergic projections are still lacking. The effect of noradrenaline on thalamic neurons in vitro consists of a slow depolarization caused by blockage of a resting potassium conductance (McCormick and Prince 1988), quite similarly to the actions of

acetylcholine. This similarity was recently confirmed in neocortical cells of humans studied in vitro (McCormick and Williamson 1989). Extracellular studies of cortical neurons have reported that noradrenaline could inhibit their spontaneous discharges while simultaneously enhancing neuronal responses to specific synaptic inputs, thus leading to an increased signal-to-noise ratio (Foote et al. 1983).

In sum, both cholinergic and noradrenergic systems are good candidates for depolarizing thalamocortical neurons and, thus, for shifting their functional mode from the bursting firing associated with diminished transfer function, as is the case of EEG-synchronized sleep, to a tonic discharge pattern associated with enhanced responsiveness, as is the case during wakefulness. The cholinergic system also accounts for a similar process during transition from EEG-synchronized sleep to EEG-desynchronized sleep (see Section 1).

References

Alonso, A. and García-Austt, E. Neuronal sources of theta rhythm in the entorhinal cortex of the rat. I. Laminar distribution of theta field potentials. Exp. Brain Res., 1987a, 67: 493–501.

Alonso, A. and García-Austt, E. Neuronal sources of theta rhythm in the entorhinal cortex of the rat. II. Phase relations between unit discharges and theta field potentials. Exp. Brain Res., 1987b, 67: 502–509.

Anchel, H. and Lindsley, D.B. Differentiation of two reticulohypothalamic systems regulating hippocampal activity. Electroenceph. clin. Neurophysiol., 1972, 32: 209–226.

Andersen, P. and Andersson, S.A. Physiological Basis of the Alpha Rhythm. Appleton-Century-Crofts, New York, 1968.

Apostol, G. and Creutzfeldt, O.D. Cross-correlation between the activity of septal units and hippocampal EEG during arousal. Brain Res., 1974, 67: 65–75.

Arikuni, T. and Kubota, K. Substantia innominata projection to caudate nucleus in macaque monkeys. Brain Res., 1984, 302: 184–189.

Arnolds, D.E.A.T., Lopes da Silva, F.H., Aitink, J.W., Kamp, A. and Boeijinga, P. The spectral properties of hippocampal EEG related to behaviour in man. Electroenceph. clin. Neurophysiol., 1980, 50: 324–328.

Artemenko, D.P. Role of hippocampal neurons in theta-wave generation. Neirofiziologhia, 1972, 4: 531–539. (In Russian.)

Asanuma, C. and Porter, L.L. Light and electron microscopic evidence for a GABAergic projection from the caudal basal forebrain to the thalamic reticular nucleus in rats. J. Comp. Neurol., 1990, in press.

Assaf, S.Y. and Miller, J.J. The role of a raphe serotonin system in the control of septal unit activity and hippocampal desynchronization. Neuroscience, 1978, 3: 539–550.

Ball, C.J., Gloor, P. and Schaul, N. The cortical electromicrophysiology of pathological delta waves in the electroencephalogram of cats. Electroenceph. clin. Neurophysiol., 1977, 43: 346–361.

Ben-Ari, Y., Krnjević, K., Reinhardt, W. and Ropert, N. Intracellular observations on disinhibitory action of acetylcholine in hippocampus. Neuroscience, 1981, 6: 2445–2463.

Bland, B.H. and Whishaw, I.Q. Generators and topography of hippocampal theta (RSA) in the anaesthetized and freely moving rat. Brain Res., 1976, 118: 259–280.

Bland, B.H., Andersen, P. and Ganes, T. Two generators of hippocampal theta activity in rabbits. Brain Res., 1975, 94: 199–218.

Boeijinga, P.H. and Lopes da Silva, F.H. Differential distribution of beta and theta EEG activity in the entorhinal cortex of the cat. Brain Res., 1988, 448: 272–286.

Bouyer, J.J., Montaron, M.F. and Rougeul, A. Fast fronto-parietal rhythms during combined focused attentive behaviour and immobility in cat: cortical and thalamic localizations. Electroenceph. clin. Neurophysiol., 1981, 51: 244–252.

Bouyer, J.J., Montaron, M.F., Vahnée, J.M., Albert, M.P. and Rougeul, A. Anatomical localization of cortical beta rhythms in cat. Neuroscience, 1987, 22: 863–869.

Buzsaki, G., Bickford, R.G., Ponomareff, G., Thal, L.G., Mandel, R. and Gage, F.G. Nucleus basalis and thalamic control of neocortical activity in the freely moving rat. J. Neurosci., 1988, 8: 4007–4026.

Calvet, J., Calvet, M.C. and Scherrer, J. Etude stratigraphique corticale de l'activité EEG spontanée. Electroenceph. clin. Neurophysiol., 1964, 17: 109–125.

Connors, B., Gutnick, M.J. and Prince, D.A. Electrophysiological properties of neocortical neurons in vitro. J. Neurophysiol., 1982, 48: 1302–1320.

Creutzfeldt, O. and Meisch, J.J. Changes of cortical neuronal activity and EEG during hypoglycemia. In: R. Hernandez-Péon (Ed.), The Physiological Basis of Mental Activity. Electroenceph. clin. Neurophysiol., Suppl. 24. Elsevier, Amsterdam, 1963: 158–171.

Creutzfeldt, O., Bark, J. and Fromm, G.H. Alterations in activity of cortical neurons during anaesthesia compared with hypoxia. In: H. Gastaut and J.S. Meyer (Eds.), Cerebral Anoxia and the Electroencephalogram. Thomas, Springfield, IL, 1961: 35–45.

Creutzfeldt, O., Grunewald, G., Simonova, O. and Schmitz, H. Changes of the basic rhythms of the EEG during performance of mental and visuo-motor tasks. In: C.R. Evans and T.B. Mulholland (Eds.), Attention in Neurophysiology. Butterworth, London, 1969: 148–168.

Crowne, D.P. and Radcliffe, D.D. Some characteristics and functional relations of the electrical activity of the primate

hippocampus and hypotheses of hippocampal function. In: R.L. Isaacson and K.H. Pribram (Eds.), The Hippocampus, Vol. 2. Plenum, New York, 1975: 185–203.

Curró Dossi, R., Paré, D. and Steriade, M. Short- and long-lasting depolarizing responses of thalamocortical neurons to stimulation of mesopontine cholinergic nuclei. J. Neurophysiol., 1990, in press.

Delagrange, P., Tadjer, D., Rougeul, A. and Buser, P. Activité unitaire de neurones du noyau ventral postérieur du thalamus pour divers degrés de vigilance chez le chat normal. C.R. Acad. Sci. (Paris), 1987, 305: 149–155.

DeLima, A.D. and Singer, W. The brainstem projection to the lateral geniculate nucleus in the cat: identification of cholinergic and monoaminergic elements. J. Comp. Neurol., 1987, 259: 92–121.

Deschênes, M., Paradis, M., Roy, J.P. and Steriade, M. Electrophysiology of neurons of lateral thalamic nuclei in cat: resting properties and burst discharges. J. Neurophysiol., 1984, 51: 1196–1219.

Detari, L. and Vanderwolf, C.H. Activity of cortically projecting and other basal forebrain neurons during large slow waves and cortical activation in anesthetized cat. Brain Res., 1987, 437: 1–8.

Fariello, R.G., Orrison, W., Blanco, G. and Reyes, P.F. Neuroradiological correlates of frontally predominant intermittent rhythmic delta activity (FIRDA). Electroenceph. clin. Neurophysiol., 1982, 54: 194–202.

Feenstra, B.W.A. and Holsheimer, J. Dipole-like neuronal sources of theta rhythm in dorsal hippocampus, dentate gyrus and cingulate cortex of the urethane-anesthetized rat. Electroenceph. clin. Neurophysiol., 1979, 47: 532–538.

Foote, S.L., Bloom, F.E. and Aston-Jones, G. Nucleus locus ceruleus: new evidence of anatomical and physiological specificity. Physiol. Rev., 1983, 63: 844–914.

Gaztelu, J.M. and Buño, W. Septo-hippocampal relationships during EEG theta rhythm. Electroenceph. clin. Neurophysiol., 1982, 54: 375–387.

Gloor, P. Generalized and widespread bilateral paroxysmal abnormalities. In: A. Rémond (Ed.), Handbook of Electroencephalography and Clinical Neurophysiology, Vol. 11, Part B. Elsevier, Amsterdam, 1976: 11B52–11B87.

Gloor, P., Kalabay, O. and Giard, N. The electroencephalogram in diffuse encephalopathies: electroencephalographic correlates of grey and white matter lesions. Brain, 1968, 91: 779–802.

Gloor, P., Ball, G. and Schaul, N. Brain lesions that produce delta waves in the EEG. Neurology, 1977, 27: 326–333.

Goldensohn, E.S. Use of the EEG for evaluation of focal intracranial lesions. In: D.W. Klass and D.D. Daly (Eds.), Current Practice of Electroencephalography. Raven Press, New York, 1979: 307–341.

Grace, A.A. and Llinás, R. Electrophysiology and morphology of four classes of prefrontal neocortical neurons studies in vitro. Soc. Neurosci. Abst., 1984, 10: 739.

Gray, C.M. and Singer, W. Stimulus-specific neuronal oscillations in orientation columns of cat visual cortex. Proc. Nat. Acad. Sci. (U.S.A.), 1989, 86: 1698–1702.

Gray, C.M., König, P., Engel, A.K. and Singer, W. Oscillatory responses in cat visual cortex exhibit inter-columnar synchronization which reflects global stimulus properties. Nature, 1989, 338: 334–337.

Green, J.D., Maxwell, D.S., Schindler, W.J. and Stumpf, C. Rabbit EEG "theta" rhythm: its anatomical source and relation to activity in single neurons. J. Neurophysiol., 1960, 23: 403–420.

Greenstein, Y.J., Pavlides, C. and Winson, J. Long-term potentiation in the dentate gyrus is preferentially induced at theta rhythm periodicity. Brain Res., 1988, 438: 331–334.

Halgren, E., Smith, M.E. and Stapleton, J.M. Hippocampal field-potentials evoked by repeated vs. nonrepeated words. In: G. Buzsaki and C.H. Vanderwolf (Eds.), Electrical Activity of the Archicortex. Akademiai Kiadó, Budapest, 1985: 67–81.

Hallanger, A.E., Levey, A.I., Lee, H.J., Rye, D.B. and Wainer, B.H. The origins of cholinergic and other subcortical afferents to the thalamus in the rat. J. Comp. Neurol., 1982, 262: 105–124.

Halliwell, J.C. and Adams, P.R. Voltage-clamp analysis of muscarinic excitation in neurons. Brain Res., 1982, 250: 71–92.

Hess, R. Localized abnormalities. In: A. Rémond (Ed.), Handbook of Electroencephalography and Clinical Neurophysiology, Vol. 11, Part B. Elsevier, Amsterdam, 1976: 11B88–11B116.

Hounsgaard, J. Presynaptic inhibitory action of acetylcholine in area CA1 of the hippocampus. Exp. Neurol., 1978, 62: 787–797.

Hu, B., Steriade, M. and Deschênes, M. The effects of brainstem peribrachial stimulation on reticular thalamic neurons: the blockage of spindle waves. Neuroscience, 1989a, 31: 1–12.

Hu, B., Steriade, M. and Deschênes, M. The effects of brainstem peribrachial stimulation on neurons of the lateral geniculate nucleus. Neuroscience, 1989b, 31: 13–24.

Hu, B., Steriade, M. and Deschênes, M. The cellular mechanisms of thalamic ponto-geniculo-occipital (PGO) waves. Neuroscience, 1989c, 31: 25–35.

Iadecola, C., Mraovitch, S., Meeley, M.P. and Reis, D.J. Lesions of the basal forebrain in rat selectively impair vasodilation elicited from cerebellar fastigial nucleus. Brain Res., 1983, 279: 41–52.

Ingvar, D.H., Baldy-Moulinier, M., Sulg, I. and Horman, S. Regional cerebral blood flow related to EEG. Acta Neurol. Scand., 1965, Suppl. 14: 179–182.

Ingvar, D.H., Sjölund, B. and Ardo, A. Correlation between ECG frequency, cerebral oxygen uptake and blood flow. Electroenceph. clin. Neurophysiol., 1976, 41: 268–276.

Jahnsen, H. and Llinás, R. Electrophysiological properties of guinea-pig thalamic neurones: an in vitro study. J. Physiol. (Lond.), 1984a, 349: 205–226.

Jahnsen, H. and Llinás, R. Ionic basis for the electroresponsiveness and oscillatory properties of guinea-pig thalamic neurons in vitro. J. Physiol. (Lond.), 1984b, 349: 227–247.

Jones, E.G. The Thalamus. Plenum, New York, 1985.

Jurko, M.F. and Andy, O.J. Comparative EEG frequencies in rhesus, stumptail, and cynomolgus monkeys. Electroenceph. clin. Neurophysiol., 1967, 23: 270–272.

Kang, Y.N. and Kitai, S.T. Electrophysiological properties of pedunculopontine neurons and their postsynaptic responses following stimulation of substantia nigra reticulata. Brain Res., 1990, in press.

Konopacki, J., Bland, B.H., MacIver, M. and Roth, S.H. Cholinergic theta rhythm in transected hippocampal slices: independent CA$_1$ and dentate generators. Brain Res., 1987, 436: 21–22.

Konopacki, J., Bland, B.H. and Roth, S.H. Evidence that activation of in vitro hippocampal theta rhythm only involves muscarinic receptors. Brain Res., 1988, 455: 110–114.

Krnjević, K. and Ropert, N. Electrophysiological and pharmacological characteristics of facilitation of hippocampal population spikes by stimulation of the medial septum. Neuroscience, 1982, 7: 2165–2183.

Krnjević, K., Pumain, R. and Renaud, L. The mechanism of excitation by acetylcholine in the cerebral cortex. J. Physiol. (Lond.), 1971, 215: 247–268.

Krnjević, K., Ropert, N. and Caullo, J. Septohippocampal disinhibition. Brain Res., 1988, 438: 182–192.

Lanoir, J. and Cordeau, J.P. Rythmes et fuseaux spontanés de l'aire visuelle du chat au cours des différents stades de la veille et du sommeil. J. Physiol. (Paris), 1970, 62 (Suppl. 3): 399–400.

Larson, J. and Lynch, G. Role of N-methyl-D-aspartate receptors in the induction of synaptic potentiation by burst stimulation patterned after the hippocampal theta rhythm. Brain Res., 1988, 441: 111–118.

Larson, J., Wong, D. and Lynch, G. Patterned stimulation at the theta frequency is optimal for the induction of hippocampal long-term potentiation. Brain Res., 1986, 368: 347–350.

Leonard, C.S. and Llinás, R. Electrophysiology of thalamic projecting cholinergic brainstem neurons and their inhibition by ACh. Soc. Neurosci. Abst., 1988, 14: 297.

Leonard, C.S. and Llinás, R. Electrophysiology of mammalian pedunculopontine and laterodorsal tegmental neurons in vitro: implications for the control of REM sleep. In: M. Steriade and D. Biesold (Eds.), Brain Cholinergic Systems. Oxford Univ. Press, Oxford, 1990: 205–223.

Leung, L.-W.S. and Borst, J.G.G. Electrical activity of the cingulate cortex. I. Generating mechanisms and relations to behavior. Brain Res., 1987, 407: 68–80.

Leung, L.-W.S. and Yim, C.Y. Intracellular records of theta rhythm in hippocampal CA1 cells of the rat. Brain Res., 1986, 367: 323–327.

Levey, A.I., Hallanger, A.E. and Wainer, B.H. Cholinergic nucleus basalis neurons may influence the cortex via the thalamus. Neurosci. Lett., 1987, 74: 7–13.

Llinás, R. and Geijo-Barrientos, E. In vitro studies of mammalian thalamic and reticularis thalami neurons. In: M. Bentivoglio and R. Spreafico (Eds.), Cellular Thalamic Mechanisms. Elsevier, Amsterdam, 1988: 23–33.

Llinás, R. and Jahnsen, H. Electrophysiology of mammalian thalamic neurons. Nature, 1982, 297: 406–408.

Llinás, R. and Sugimori, M. Electrophysiological properties of in vitro Purkinje cell somata in mammalian cerebellar slices. J. Physiol. (Lond.), 1980, 305: 197–213.

Llinás, R. and Yarom, Y. Electrophysiology of mammalian inferior olivary neurones in vitro. J. Physiol. (Lond.), 1981, 315: 549–567.

Lopes da Silva, F.H. and Storm van Leeuwen, W. The cortical source of alpha rhythm. Neurosci. Lett., 1977, 6: 237–241.

Lopes da Silva, F.H., Van Rotterdam, A., Storm van Leeuwen, W. and Tielen, A.M. Dynamic characteristics of visual evoked potentials in the dog. II. Beta frequency selectivity in evoked potentials and background activity. Electroenceph. clin. Neurophysiol., 1970, 29: 260–268.

Lopes da Silva, F.H., Van Lierop, T.H.M.T., Schrijer, C.F.M. and Storm van Leeuwen, W. Organization of thalamic and cortical alpha rhythm: spectra and coherences. Electroenceph. clin. Neurophysiol., 1973a, 35: 627–639.

Lopes da Silva, F.H., Van Lierop, T.H.M.T., Schrijer, D.F.M. and Storm van Leeuwen, W. Essential differences between alpha rhythms and barbiturate spindles: spectra and thalamo-cortical coherences. Electroenceph. clin. Neurophysiol., 1973b, 38: 93–96.

Lopes da Silva, F.H., Groenewegen, H.J., Holsheimer, J., Room, P., Witter, M.P., Van Groen, Th. and Wadman, W.J. The hippocampus as a set of partially overlapping segments with a topographically organized system of inputs and outputs: the gain-setting system and the ventral striatum as a motor interface. In: G. Buzsaki and C.H. Vanderwolf (Eds.), Electrical Activity of the Archicortex. Akademiai Kiadó, Budapest, 1985: 83–106.

Lopes da Silva, F.H., Vos, J.E., Mooibroek, J. and Van Rotterdam, A. Relative contributions of intracortical and thalamo-cortical processes in the generation of alpha rhythms, revealed by partial coherence analyses. Electroenceph. clin. Neurophysiol., 1980, 50: 449–456.

Marshall, D.W., Boey, R.L. and Morse, M.W. Focal and/or lateralized polymorphic delta activity. Association with either normal or modified computed tomographic scans. Arch. Neurol., 1988, 45: 33–35.

Mash, D.C. and Mesulam, M.M. Distribution of muscarine receptor subtypes within architectonic subregions of the primate cerebral cortex. J. Comp. Neurol., 1988, 278: 265–274.

McCormick, D.A. Cellular mechanisms of cholinergic control of neocortical and thalamic neurons. In: M. Steriade and D. Biesold (Eds.), Brain Cholinergic Systems. Oxford Univ. Press, Oxford, 1990: 236–264.

McCormick, D.A. and Prince, D.A. Acetylcholine induces burst firing in thalamic reticular neurones by activating a potassium conductance. Nature, 1986a, 319: 402–405.

McCormick, D.A. and Prince, D.A. Mechanisms of action of acetylcholine in the guinea-pig cerebral cortex in vitro. J. Physiol. (Lond.), 1986b, 375: 169–194.

McCormick, D.A. and Prince, D.A. Actions of acetylcholine in

the guinea-pig and cat medial and lateral geniculate nuclei, in vitro. J. Physiol. (Lond.), 1987, 392: 147–165.

McCormick, D.A. and Prince, D.A. Noradrenergic modulation of firing pattern in guinea-pig and cat thalamic neurones in vitro. J. Neurophysiol., 1988, 59: 978–996.

McCormick, D.A. and Williamson, A. Convergence and divergence of neurotransmitter action in human cerebral cortex. Proc. Nat. Acad. Sci. (U.S.A.), 1989, 86: 8098–8102.

McCormick, D.A., Connors, B.W., Lighthall, J.W. and Prince, D.A. Comparative electrophysiology of pyramidal and sparsely spiny stellate neurons of the neocortex. J. Neurophysiol., 1985, 54: 782–806.

McLennan, H. and Miller, J.J. Frequency-related inhibitory mechanisms controlling rhythmical activity in the septal area. J. Physiol. (Lond.), 1976, 254: 827–841.

Mesulam, M.-M. Asymmetry of neural feedback and behavioral states. Science, 1987, 237: 537–538.

Mesulam, M.-M. Central cholinergic pathways: neuroanatomy and some behavioral implications. In: M. Avoli, T.A. Reader, R.W. Dykes and P. Gloor (Eds.), Neurotransmitters and Cortical Function. Plenum, New York, 1988: 237–260.

Mesulam, M., Mufson, E.J., Wainer, B.H. and Levey, A.I. Central cholinergic pathways in the rat: an overview based on an alternative nomenclature. Neuroscience, 1983, 10: 1185–1201.

Mikol, J., Ménini, M., Brion, S. and Guicharnaud, L. Connections of the laterodorsal nucleus of the thalamus in the monkey. Study of efferents. Rev. Neurol., 1984, 140: 615–624.

Mitani, A., Ito, K., Hallanger, A.E., Wainer, B.H., Kataoka, K. and McCarley, R.W. Cholinergic projections from the laterodorsal and pedunculopontine tegmental nuclei to the pontine gigantocellular tegmental field in the cat. Brain Res., 1988, 451: 397–402.

Mitchell, S.J. and Ranck, Jr., J.B. Generation of theta rhythm in medial entorhinal cortex of freely moving rat. Brain Res., 1980, 189: 49–66.

Montaron, M.F., Bouyer, J.J., Rougeul, A. and Buser, P. Ventral mesencephalic tegmentum (VMT) controls electrocortical beta rhythms and associated attentive behaviour in the cat. Behav. Brain Res., 1982, 6: 129–145.

Morrison, J.H. and Foote, S.L. Noradrenergic and serotonergic innervation of cortical, thalamic, and tectal visual structures in Old and New World monkeys. J. Comp. Neurol., 1986, 243: 117–138.

Morrison, J.H., Molliver, M.E., Grzanna, M.E. and Coyle, J.T. The intracortical trajectory of the coeruleo-cortical projection in the rat: a tangentially organized cortical afferent. Neuroscience, 1981, 6: 139–158.

Nunez, A., García-Austt, E. and Buño, Jr., W. Intracellular theta rhythm generation in identified hippocampal pyramids. Brain Res., 1987, 416: 289–300.

Paré, D., Steriade, M., Deschênes, M. and Oakson, G. Physiological properties of anterior thalamic nuclei, a group devoid of inputs from the reticular thalamic nucleus. J. Neurophysiol., 1987, 57: 1669–1685.

Paré, D., Parent, A., Smith, Y. and Steriade, M. Projections of

upper brainstem cholinergic and non-cholinergic neurons to the cat intralaminar and reticular thalamic nuclei. Neuroscience, 1988, 25: 69–86.

Paré, D., Steriade, M., Deschênes, M. and Bouhassira, D. Prolonged enhancement in synaptic efficacy of anterior thalamic neurons by stimulating a brainstem cholinergic nucleus. J. Neurosci., 1990, 10: 20–33.

Parent, A., Paré, D., Smith, Y. and Steriade, M. Basal forebrain cholinergic and noncholinergic projections to the thalamus and brainstem in cats and monkeys. J. Comp. Neurol., 1988, 277: 281–301.

Pavlides, C., Greenstein, Y.J., Goudman, M. and Winson, J. Long-term potentiation in the dentate gyrus is induced preferentially on the positive phase of theta-rhythm. Brain Res., 1988, 439: 383–387.

Petsche, H., Stumpf, C. and Gogolak, G. The significance of the rabbit's septum as a relay station between the midbrain and the hippocampus. The control of hippocampus arousal activity by septum cells. Electroenceph. clin. Neurophysiol., 1962, 14: 202–211.

Petsche, H., Pockberger, H. and Rappelsberger, P. On the search for the sources of the electroencephalogram. Neuroscience, 1984, 11: 1–27.

Puil, E. and Carlen, P.L. Attenuation of glutamic-action excitatory postsynaptic potentials, and spikes by intracellular QX-222 in hippocampal neurons. Neuroscience, 1984, 11: 389–398.

Purpura, D.P., McMurtry, J.G. and Maekawa, K. Synaptic events in ventro-lateral thalamic neurons during suppression of recruiting responses by brain stem reticular stimulation. Brain Res., 1966, 1: 63–76.

Ray, W.J. and Cole, H.W. EEG alpha activity reflects attentional demands and beta activity reflects emotional and cognitive processes. Science, 1985, 228: 750–752.

Rigdon, G.C. and Pirch, J.H. Microinjection of procaine or GABA into the nucleus basalis magnocellularis affects cue-elicited unit responses in the rat frontal cortex. Exp. Neurol., 1984, 85: 283–296.

Rose, G.M. and Dunwiddie, T.V. Induction of hippocampal long-term potentiation using physiologically patterned stimulation. Neurosci. Lett., 1986, 69: 244–248.

Roth, S.R., Sterman, M.B. and Clemente, C.D. Comparison of EEG correlates of reinforcement, internal inhibition and sleep. Electroenceph. clin. Neurophysiol., 1967, 23: 509–520.

Rotterdam, A. Van, Lopes da Silva, F.H., Van der Ende, J., Viergever, M.A. and Hermans, A.J. A model of the spatial-temporal characteristics of the alpha rhythm. Bull. Math. Biol., 1982, 44: 283–305.

Rougeul, A., Corvisier, J. and Letalle, A. Rythmes electrocorticaux caractéristiques de l'installation du sommeil naturel chez le chat. Leurs rapports avec le comportement moteur. Electroenceph. clin. Neurophysiol., 1974, 37: 41–57.

Rougeul, A., Bouyer, J.J., Dedet, L. and Debray, O. Fast somatoparietal rhythms during combined focal attention and immobility in baboon and squirrel monkey. Electroenceph. clin. Neurophysiol., 1979, 46: 310–319.

Rougeul-Buser, A., Bouyer, J.J., Montaron, M.F. and Buser, P. Patterns of activities in the ventrobasal thalamus and somatic cortex SI during behavioral immobility in the awake cat: focal waking rhythms. Exp. Brain Res., 1983, Suppl. 7: 69–87.

Sato, H., Hata, Y., Hagihara, K. and Tsumoto, T. Effects of cholinergic depletion on neuron activities in the cat visual cortex. J. Neurophysiol., 1987, 58: 781–794.

Satoh, K. and Fibiger, H.C. Cholinergic neurons of the laterodorsal tegmental nucleus: efferent and afferent connections. J. Comp. Neurol., 1986, 253: 277–302.

Saunders, M.G. and Westmoreland, B.F. The EEG in evaluation of disorders affecting the brain diffusely. In: D.W. Klass and D.D. Daly (Eds.), Current Practice of Clinical Electroencephalography. Raven Press, New York, 1979: 343–379.

Schaul, N., Gloor, P., Ball, G. and Gotman, J. The electromicrophysiology of delta waves induced by systemic atropine. Brain Res., 1978, 143: 475–486.

Schaul, N., Gloor, P. and Gotman, J. The EEG in deep midline lesions. Neurology, 1981a, 31: 157–167.

Schaul, N., Lueders, H. and Sachdev, K. Generalized bilaterally synchronous bursts of slow waves in the EEG. Arch. Neurol., 1981b, 38: 690–692.

Semba, K., Reiner, P.B., McGeer, E.G. and Fibiger, H.C. Brainstem afferents to the magnocellular basal forebrain studied by axonal transport, immunohistochemistry and electrophysiology in the rat. J. Comp. Neurol., 1988, 267: 433–453.

Sheer, D.E. A working cognitive model of attention to fit in the brain and in the clinic. In: D.E. Sheer and K. Pribram (Eds.), Attention: Cognition, Brain Function, and Clinical Application. Academic Press, New York, 1988.

Singer, W. The effect of mesencephalic reticular stimulation on intracellular potentials of cat lateral geniculate nucleus. Brain Res., 1973, 61: 35–54.

Stafstrom, C.E., Schwindt, P.C., Flatman, J.A. and Crill, W.E. Properties of subthreshold response and action potential recorded in layer V neurons from cat sensorimotor cortex in vitro. J. Neurophysiol., 1984a, 52: 244–263.

Stafstrom, C.E., Schwindt, P.C. and Crill, W.E. Repetitive firing in layer V neurons from cat neocortex in vitro. J. Neurophysiol., 1984b, 52: 264–277.

Stein, J. An explanation of the origin of delta waves in the electroencephalogram in man. Acta Univ. Carol. Med. (Prague), 1965, XIX: 133 pp.

Steriade, M. The excitatory-inhibitory response sequence in thalamic and neocortical cells: state-related changes and regulatory systems. In: G.M. Edelman, W.E. Gall and W.M. Cowan (Eds.), Dynamic Aspects of Neocortical Function. Wiley, New York, 1984: 107–157.

Steriade, M. and Deschênes, M. The thalamus as a neuronal oscillator. Brain Res. Rev., 1984, 8: 1–63.

Steriade, M. and Deschênes, M. Intrathalamic and brainstem-thalamic networks involved in resting and alert states. In: M. Bentivoglio and R. Spreafico (Eds.), Cellular Thalamic Mechanisms. Elsevier, Amsterdam, 1988: 37–62.

Steriade, M. and Glenn, L.L. The neocortical and caudate projections of intralaminar thalamic neurons and their synaptic excitation from the midbrain core. J. Neurophysiol., 1982, 48: 352–371.

Steriade, M. and Llinás, R. The functional states of the thalamus and the associated neuronal interplay. Physiol. Rev., 1988, 68: 649–742.

Steriade, M., Parent, A. and Hada, J. Thalamic projections of nucleus reticularis thalami of cat: a study using retrograde transport of horseradish peroxidase and double fluorescent tracers. J. Comp. Neurol., 1984, 229: 531–547.

Steriade, M., Deschênes, M., Domich, L. and Mulle, C. Abolition of spindle oscillations in thalamic neurons disconnected from nucleus reticularis thalami. J. Neurophysiol., 1985, 54: 1473–1497.

Steriade, M., Domich, L. and Oakson, G. Reticularis thalami neurons revisited: activity changes during shifts in states of vigilance. J. Neurosci., 1986, 6: 68–81.

Steriade, M., Domich, L., Oakson, G. and Deschênes, M. The deafferented reticular thalamic nucleus generates spindle rhythmicity. J. Neurophysiol., 1987a, 57: 260–273.

Steriade, M., Parent, A., Paré, D. and Smith, Y. Cholinergic and non-cholinergic neurons of cat basal forebrain project to reticular and mediodorsal thalamic nuclei. Brain Res., 1987b, 408: 272–276.

Steriade, M., Paré, D., Parent, A. and Smith, Y. Projections of cholinergic and non-cholinergic neurons of the brainstem core to relay and associational thalamic nuclei in the cat and macaque monkey. Neuroscience, 1988, 25: 47–67.

Steriade, M., Paré, D., Bouhassira, D., Deschênes, M. and Oakson, G. Phasic activation of lateral geniculate and perigeniculate thalamic neurons during sleep with pontogeniculo-occipital waves. J. Neurosci., 1989, 9: 2215–2229.

Steriade, M., Datta, S., Paré, D., Oakson, G. and Currô Dossi, R. Neuronal activities in brain-stem cholinergic nuclei related to tonic activation processes in thalamocortical neurons. J. Neurosci., 1990a, 10: 2527–2545.

Steriade, M., Jones, E.G. and Llinás, R.R. Thalamic Oscillations and Signaling. Wiley Interscience, New York, 1990b: 431 pp.

Stewart, D.J., MacFabe, D.F. and Vanderwolf, C.H. Cholinergic activation of the electrocorticogram: role of the substantia innominata and effects of atropine and quinuclidinyl benzylate. Brain Res., 1984, 322: 219–232.

Storm van Leeuwen, W., Kamp, A., Kok, M.L., De Quartel, F.W., Lopes da Silva, F.H. and Tielen, A.M. Relations entre les activités électriques cérébrales du chien, son comportement et sa direction d'attention. Actual. Neurophysiol. (Paris), 1967, 7: 167–186.

Szymusiak, R. and McGinty, D. Sleep suppression following kainic acid-induced lesions of the basal forebrain. Exp. Neurol., 1986, 94: 598–614.

Torii, S. Two types of pattern of hippocampal electrical activity induced by stimulation of hypothalamus and surrounding parts of rabbit's brain. Jpn. J. Physiol., 1961, 11: 147–157.

Vanderwolf, C.H. and Robinson, T.E. Reticulo-cortical activity and behavior: a critique of the arousal theory and a new synthesis. Brain Behav. Sci., 1981, 4: 459–514.

Vertes, R.P. Brain stem activation of the hippocampus: a role

for the magnocellular reticular formation and the MLF. Electroenceph. clin. Neurophysiol., 1980, 50: 48–58.

Vertes, R.P. An analysis of ascending brain stem systems involved in hippocampal synchronization and desynchronization. J. Neurophysiol., 1981, 46: 1140–1159.

Vertes, R.P. Brain stem generation of the hippocampal EEG. Prog. Neurobiol., 1982, 19: 159–186.

Villablanca, J. Role of the thalamus in sleep control: sleep-wakefulness studies in chronic diencephalic and athalamic cats. In: O. Petre-Quadens and J.D. Schlag (Eds.), Basic Sleep Mechanisms. Academic Press, New York, 1974: 51–78.

Vinogradova, O.S., Brazhnik, E.S., Karanov, A.N. and Zhadina, S.D. Analysis of neuronal activity in rabbit's septum with various conditions of deafferentiation. Brain Res., 1980, 187: 354–368.

Wainer, B.H. and Mesulam, M.-M. Ascending cholinergic pathways in the rat brain. In: M. Steriade and D. Biesold (Eds.), Brain Cholinergic Systems. Oxford Univ. Press, Oxford, 1990: 65–119.

Wilson, C.L., Motter, B.C. and Lindsley, D.B. Influences of hypothalamic stimulation upon septal and hippocampal electrical activity in the cat. Brain Res., 1976, 107: 55–68.

Winson, J. Patterns of hippocampal theta rhythm in the freely moving rat. Electroenceph. clin. Neurophysiol., 1974, 36: 291–301.

Yen, C.T. and Jones, E.G. Intracellular staining of physiologically identified neurons and axons in the somatosensory thalamus of the cat. Brain Res., 1983, 280: 148–154.

Yokota, T. and Fujimori, B. Effects of brain stem stimulation upon hippocampal electrical activity, somatomotor reflexes and autonomic functions. Electroenceph. clin. Neurophysiol., 1964, 16: 375–382.